AD NUMBER
ADB023566
LIMITATION CHANGES

TO:

Approved for public release; distribution is unlimited.

FROM:

Distribution authorized to U.S. Gov't. agencies only; Test and Evaluation; AUG 1977. Other requests shall be referred to Army Materials Research and Mechnics Center, Attn: AMXMR-PL, Watertown, MA 02172.

AUTHORITY
AMMRC per DTIC form 55 dtd Jul 1978

THIS REPORT HAS BEEN DELIMITED
AND CLEARED FOR PUBLIC RELEASE
UNDER DOD DIRECTIVE 5200.20 AND
NO RESTRICTIONS ARE IMPOSED UPON
ITS USE AND DISCLOSURE.

DISTRIBUTION STATEMENT A

APPROVED FOR PUBLIC RELEASE;
DISTRIBUTION UNLIMITED.

AD

ADB023566

AMMRC CTR 77-20

BRITTLE MATERIALS DESIGN, HIGH TEMPERATURE GAS TURBINE

W Bols-331

Technical Report By:

Arthur F. McLean, Ford Motor Company, Dearborn, Michigan 48121
Eugene A. Fisher, Ford Motor Company, Dearborn, Michigan 48121

August, 1977

Interim Report Number 11, July 1, 1976 to December 31, 1976

Contract Number DAAG 46-71-C-0162

Distribution limited to U.S. Government agencies only; Test Evaluation data; August, 1977. Other requests for this document must be referred to the Director, Army Materials and Mechanics Research Center, ATTN: AMXMR-PL, Watertown, Massachusetts 02172.

Prepared for

ARMY MATERIALS AND MECHANICS RESEARCH CENTER
Watertown, Massachusetts 02172

DDC FILE COPY

See 1473

AMMRC CTR 77-20

BRITTLE MATERIALS DESIGN, HIGH TEMPERATURE GAS TURBINE

Technical Report By:

Arthur F. McLean, Ford Motor Company, Dearborn, Michigan 48121
Eugene A. Fisher, Ford Motor Company, Dearborn, Michigan 48121

August, 1977

Interim Report Number 11, July 1, 1976 to December 31, 1976

Contract Number DAAG 46-71-C-0162

Agency Accession Number DA OD 4733

Prepared for:

ARMY MATERIALS AND MECHANICS RESEARCH CENTER
Watertown, Massachusetts 02172

ABSTRACT

The demonstration of uncooled brittle materials in structural applications at 2500°F is the objective of the "Brittle Materials Design, High Temperature Gas Turbine" program. Ford Motor Company, the contractor, is utilizing a small vehicular gas turbine comprising an entire ceramic hot flow path including the highly stressed turbine rotors. Westinghouse, the subcontractor, originally planned to evaluate ceramic first stage stator vanes in an actual 30 MW test turbine engine; however, this objective was revised to demonstrate ceramic stator vanes in a static test rig. Both companies had in-house research programs in this area prior to this contract.

In the stationary gas turbine project, the test of ceramic stator vanes in a static rig for 100 cycles up to temperatures of 2500°F has been completed. This accomplishment meets the revised objectives for the stationary turbine project and, therefore, this project was completed. The report of the last six months progress will be included in the final report for the project and published separately.

Fabrication of duo-density silicon nitride turbine rotors continued during this reporting period. Due to persistent bonding problems between the hot pressed materials in the three-piece design, the fabrication concept was altered to a simplified two-piece design with the only bond being between hot-pressed Si_3N_4 and reaction bonded Si_3N_4. This change was also made possible by the results of a hot pressing parametric study, which showed that good strength and density could be achieved at reduced hot pressing pressures. Ten two-piece rotors were fabricated, and of these, three are being prepared for testing.

The injection molding of duo-density rotor blade rings has been improved by the addition of a solid state automatic control system which was installed on the injection molding machine. A problem of unmelted inclusions was discovered and solved by the use of material extrusion and increased nozzle temperature during molding. Microfocus X-ray equipment has been evaluated and found advantageous for blade ring flaw detection

Fabrication of turbine inlet nose cones and stators was resumed on a limited basis. A silicon metal powder/organic system yielding 2.7 g/cc density reaction bonded silicon nitride material was utilized for the first time for injection molding of these components. Two additional test fixtures were built for use in pre-engine test evaluations of ceramic stators. One of these fixtures, the stator vane mechanical load test fixture, serves a two-fold purpose (1) as an NDE tool to evaluate material and processing variations, and (2) as a screening tool to qualify stator vanes for subsequent engine testing. The other rig, the stator outer shroud pressure test fixture, evaluates the stator outer shroud quality before subsequent engine testing In the testing area, the primary emphasis was placed on the utilization of these new fixtures to enhance the qualification of stationary ceramic flow path components. The initial evaluation of the best quality 2.7 g/cc density Si_3N_4 components is underway. In addition, a review of past weight gain data for 2.55 g/cc density stators, tested at 1930°F, was completed.

In order to select the best method of processing Si_3N_4 powder, the optimum MgO content and the best hot pressing parameters consistent with the hub forming portion of the duo-density rotor process, a parametric processing study was conducted. Strength at two elevated temperatures, along with the Weibull slope, were obtained for a number of hot pressed Si_3N_4 materials. A major concern with the three-piece approach to the duo-density rotor has been the degree of bonding and the resultant strength of the bond between the two regions of hot pressed Si_3N_4. Test bars were cut from six duo-density rotors such that the hot pressed to hot pressed bond could be positioned within the zone of maximum stress. Test results showed a strength variation at different locations, being higher at the center region and lower at the leading and trailing edges. Strength measurements were performed on Refel reaction silicon carbide, the material used for ceramic combustors. Statistical bend strength distributions were measured at room temperature and at five elevated temperatures. In addition, tensile strength was measured at room temperature.

ii

Previous results obtained from nitriding of large loads of silicon metal powder shapes, such as molded stators and rotor blade rings, have shown that the nitriding reaction was not under control. A technique was developed which allows the furnace to control the nitriding dependent upon the nitrogen gas consumption rate, resulting in improved material structure. The task on developing high strength, stable sintered Sialon materials was terminated as a result of funding reductions; the results of this work are summarized. Work was undertaken to evaluate the use of hot isostatic pressing to further densify reaction sintered Si_3N_4 performs, using glass encapsulation. Additives were evaluated and some densification and strengthening were obtained. As yet, attempts to densify complex shaped parts were not successful.

Work on analytical codes resulted in the development of relationships for computing time-dependent reliability of ceramics in the presence of delayed fracture or static fatigue. These equations are derived from the subcritical crack growth model and combined with Weibull strength statistics to determine failure probabilities.

FOREWORD

This report is the eleventh semi-annual technical report of the "Brittle Materials" Design, High Temperature Gas Turbine" program initiated by the Advanced Research Projects Agency, ARPA Order Number 1849, and Contract Number DAAG-46-71-C-0162. This is an incrementally-funded six year program.

Since this is an iterative design and materials development program, design concepts and materials selection and/or properties presented in this report will probably not be those finally utilized. Thus all design and property data contained in the semi-annual reports must be considered tentative, and the reports should be considered to be illustrative of the design, materials, processing, and NDE techniques being developed for brittle materials.

This report covers the period of FY7T (the transition quarter during which the Federal government fiscal year changed) and the first quarter of FY77. Starting with the first quarter of FY77, ERDA became a participant in this program along with ARPA. The next interim report, which will cover the first full reporting period under the sponsorship of both agencies, will be organized such that work sponsored by each agency will be separately reported.

The principal investigator of this program is Mr. A. F. McLean, Ford Motor Company, and the technical monitor is Dr. E. S. Wright, AMMRC. The authors would like to acknowledge the valuable contributions in the performance of this work by the following people:

Ford Motor Company

N. Arnon, R. J. Baer, R. R. Baker, H. D. Blair, J H. Buechel, D. J. Cassidy, J. C. Caverly, D. A. Davis, G. C. DeBell, A. Ezis, W. A. Fate, M. U. Goodyear, J. W. Grant, D. L. Hartsock, P. H. Havstad, J. A. Herman, R. A. Jeryan, C. F. Johnson, K. H. Kinsman, C. A. Knapp, J. G. LaFord, I. A. Mangels, W. E. Meyer, M. E. Milberg, T. G. Mohr, P. F. Nicholls, A. Paluszny, G. Peitsch, J. R. Secord, L. R. Swank, W. Trela, J. C. Uy, T. J. Whalen, R. M. Williams, W. Wu

Army Material and Mechanics Research Center

G. E. Gazza, E. M. Lenoe, R. N. Katz, D. R. Messier, H. Priest

iv

TABLE OF CONTENTS

LIST OF ILLUSTRATIONS

LIST OF ILLUSTRATIONS

vii

LIST OF ILLUSTRATIONS

LIST OF TABLES

LIST OF TABLES

1.   INTRODUCTION

As stipulated by the Advanced Research Projects Agency of the Department of Defense at the outset of this program, its major purpose is to demonstrate that brittle materials can be successfully utilized in demanding high temperature structural applications. ARPA's major program goal is to prove by a practical demonstration that efforts in ceramic design, materials, fabrication, testing and evaluation can by drawn together and developed to establish the usefulness of brittle materials for engineering applications.

The gas turbine engine, utilizing uncooled ceramic components in the hot flow path, was chosen as the vehicle for this demonstration. The progress of the gas turbine engine has been and continues to be closely related to the development of materials capable of withstanding the engine's environment at high operating temperature. Since the early days of the jet engine, new metals have been developed which have allowed a gradual increase in operating temperatures. Today's nickel-chrome superalloys are in use, without cooling, at turbine inlet gas temperatures of 1800°F to 1900°F. However, there is considerable incentive to further increase turbine inlet temperature in order to improve specific air and fuel consumptions. The use of ceramics in the gas turbine engine promises to make a major step in increasing turbine inlet temperature to 2500°F. Such an engine offers significant advances in efficiency, power per unit weight, cost, exhaust emissions, materials utilization and fuel utilization. Successful application of ceramics to the gas turbine would therefore not only have military significance, but would also greatly influence our national concerns of air pollution, utilization of material resources, and the energy crisis.

At the program beginning, the application of ceramics was planned for two gas turbine engines of greatly different size. One was a small vehicular turbine of about 200 HP (contractor Ford) and the other was a large stationary turbine of about 30 MW (subcontractor Westinghouse). In the vehicular turbine project, the plan was to develop an entire ceramic hot flow path including the highly stressed turbine rotors. In the stationary turbine project, the engine is so large that plans were confined to the development of ceramic first stage stator vanes, and design studies of ceramic rotors. The anticipated difficulties in applying ceramics to a large stationary turbine engine have been substantiated to the extent that the scope of work for the stationary turbine project was revised to demonstrate ceramic stator vanes in a static test rig rather than the formidable task of testing in an actual 30 MW test turbine engine (8).

It should be noted that both the contractor and sub-contractor had in-house research programs in this area prior to initiation of this program. Silicon nitride and silicon carbide had been selected as the primary material candidates. Preliminary design concepts were in existence and, in the case of the vehicular engine, hardware had been built and testing had been initiated.

At the outset, the program was considered to be both highly innovative and risky. However, it showed promise of large scale financial and technological payoff as well as stimulation of the pertinent technical communities. This reporting period is in the sixth year of the program and major accomplishments have been achieved. In the vehicular turbine project, the first 100 hour durability demonstration of stationary ceramic hot flow path components (a nose cone and stator, two shrouds and a spacer) was carried out in an engine completely coupled with a control system and producing power. In addition, a partially bladed ceramic turbine rotor has been tested in an experimental high temperature gas turbine engine up to a speed of 52,800 rpm and turbine inlet temperature of 2650°F before subsequent failure. In the stationary turbine project ceramic stator vanes have been tested in a static test rig for 100 cycles at temperatures up to 2500°F. This latter accomplishment meets the revised objectives for the stationary turbine project and therefore this project was completed.

The focus of the FY77 vehicular turbine project is to confirm, via hot spin testing of ceramic turbine rotors, the correlation between analytically-predicted rotor reliability and experimental results. This is a new interim goal, preceding a 200 hour test.

This is the 11th semi-annual report of progress. The format is different than most previous reports in that the stationary turbine project has been completed while the vehicular turbine project is continu-

1

ing. The report of the last six months progress on the stationary turbine project will be included in the final report for that project and published separately (44). This and future interim reports will cover the progress and accomplishments on the vehicular turbine project.

Note: Numbers in parantheses refer to references listed in Section 6.0

2. SUMMARY

The principal objective of the Vehicular Turbine Project is to develop ceramic components and demonstrate them in a 200-HP size high temperature vehicular gas turbine engine. The entire hot flow path will comprise uncooled ceramic parts. The objective is to demonstrate that these parts can survive 200 hours of operation over a representative duty cycle at turbine inlet temperatures of up to 2500°F. Successful completion of this program objective will not only demonstrate that ceramics are viable structural engineering materials, but will also represent a significant breakthrough by removing the temperature barrier which has for so long held back more widespread use of the small gas turbine engine.

Development of the small vehicular regenerative gas turbine engine using superalloy materials has been motivated by its potentially superior characteristics when compared with the piston engine. These include:

— Continuous combustion with inherently low exhaust emissions

— Multi-fuel capability

— Simple machine - fewer moving parts

— Potentially very reliable and durable

— Low maintenance

— Smooth, vibration-free production of power

— Low oil consumption

— Good cold starting capabilities

— Rapid warm-up time

With such impressive potential, the small gas turbine engine using superalloys has been under investigation by every major on-highway and off-highway vehicle manufacturer in the world.

In addition, the small gas turbine engine without exhaust heat recovery (i.e., non-regenerative) is an existing, proven type of power plant widely used for auxiliary power generation, emergency standby and continuous power for generator sets, pump and compressor drives, air supply units, industrial power plants, aircraft turboprops, helicopter engines, aircraft jet engines, marine engines, small portable power plants, total energy systems, and hydrofoil craft engines. While this variety of applications of the small gas turbine using superalloys is impressive, more widespread use of this type engine has been hampered by two major barriers, efficiency and cost. This is particularly so in the case of high volume automotive applications.

Since the gas turbine is a heat engine, efficiency is directly related to cycle temperature. In current small gas turbines, maximum temperature is limited not by combustion, which at stoichiometric fuel/air ratios could produce temperatures well in excess of 3500°F, but by the capabilities of the hot component materials. Today, nickel-chrome superalloys are used in small gas turbines where blade cooling is impractical, and this limits maximum turbine inlet gas temperature to about 1800°F. At this temperature limit, and considering state-of-the-art component efficiencies, the potential overall efficiency of the small regenerative gas turbine is not significantly better than that of the gasoline engine and not as good as the Diesel. On the other hand a ceramic gas turbine engine operating at 2500°F will have fuel economies superior to the Diesel at significant weight savings.

The other major barrier is cost and this too is strongly related to the hot component materials. Nickel-chrome superalloys, and more significantly cobalt based superalloys which meet typical tur-

3

bine engine specifications, contain strategic materials not found in this country and cost well over $5/lb. This is an excessive cost with respect to high volume applications such as trucks or automobiles.

High temperature ceramics such as silicon nitride or silicon carbide, on the other hand, are made from readily available and vastly abundant raw materials and show promise of significantly reduced cost compared to superalloys, probably by at least an order of magnitude.

Thus, successful application of ceramics to the small turbine engine, with an associated quantum jump to 2500°F would not only offer all of the attributes listed earlier, but in addition would offer superior fuel economy and less weight at competitive cost with the piston engine.

2.1 VEHICULAR TURBINE PROJECT PLAN

The vehicular turbine project is organized to design and develop an entire ceramic hot flow path for a high temperature, vehicular gas turbine engine. Figure 2.1 shows a schematic of this regenerative engine. Air is induced through an intake silencer and filter into a radial compressor, and then is compressed and ducted through one side of each of two rotary regenerators. The hot compressed air is then supplied to a combustion chamber where fuel is added and combustion takes place.

The hot gas discharging from the combustor is then directed into the turbine stages by a turbine inlet nose cone. The gas then passes through the turbine stages which comprise two turbine stators, each having stationary airfoil blades which direct the gas onto each corresponding turbine rotor. In passing through the turbine, the gas expands and generates work to drive the compressor and supply useful power. The expanded turbine exhaust gas is then ducted through the hot side of each of the two regenerators which, to conserve fuel, transfer much of the exhaust heat back into the compressed air.

The hot flow path components, subject to peak cycle temperature and made out of superalloys in today's gas turbine, are the combustor, the turbine inlet nose cone, the turbine stators, the turbine tip shrouds, and the turbine rotors. These are areas where the use of ceramics could result in the greatest benefits, therefore these components have been selected for application in the vehicular turbine project.

Successful development of the entire ceramic flow path, as demonstrated in a high temperature vehicular gas turbine engine, will involve a complex iterative development. Figure 2.2 shows a block diagram flow chart, including the feedback loops, of the major factors involved, and serves to illustrate the magnitude of this complex and comprehensive iterative development program. Of particular importance is the inter-relationship of design, materials development, ceramic processes, component rig testing, engine testing, non-destructive evaluation and failure analysis.
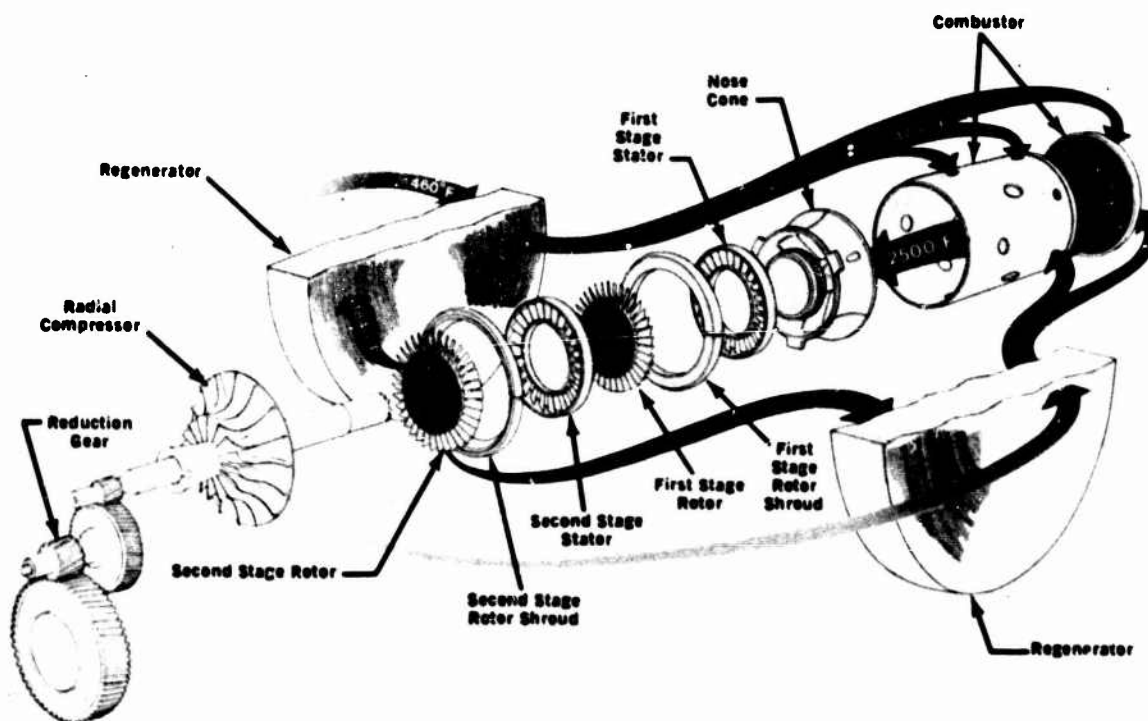
Figure 2.1 — Schematic View of the Vehicular Gas Turbine Engine Flowpath

5

One cannot divorce the development of ceramic materials from processes for making parts; no more so can one isolate the design of those parts from how they are made or from what they are made. Likewise, the design of mountings and attachments between metal and ceramic parts within the engine are equally important. Innovation in the control of the environment of critical engine components is another link in the chain. Each of these factors has a relationship with the others, and to obtain success in any one may involve compromises in the others.

Testing plays an important role during the iterative development since it provides a positive, objective way of evaluating the various combinations of factors involved. If successful, the test yields the credibility to move on to the next link in the development chain. If unsuccessful the test flags a warning and prompts feedback to earlier developments to seek out and solve the problem which has resulted in failure. Finally, all of the links in the chain are evaluated by a complete engine test, by which means the ultimate objective of the program will be demonstrated. It is important then to recognize that this is a systems development program — no single area is independent, but each one feeds into the total iterative system.
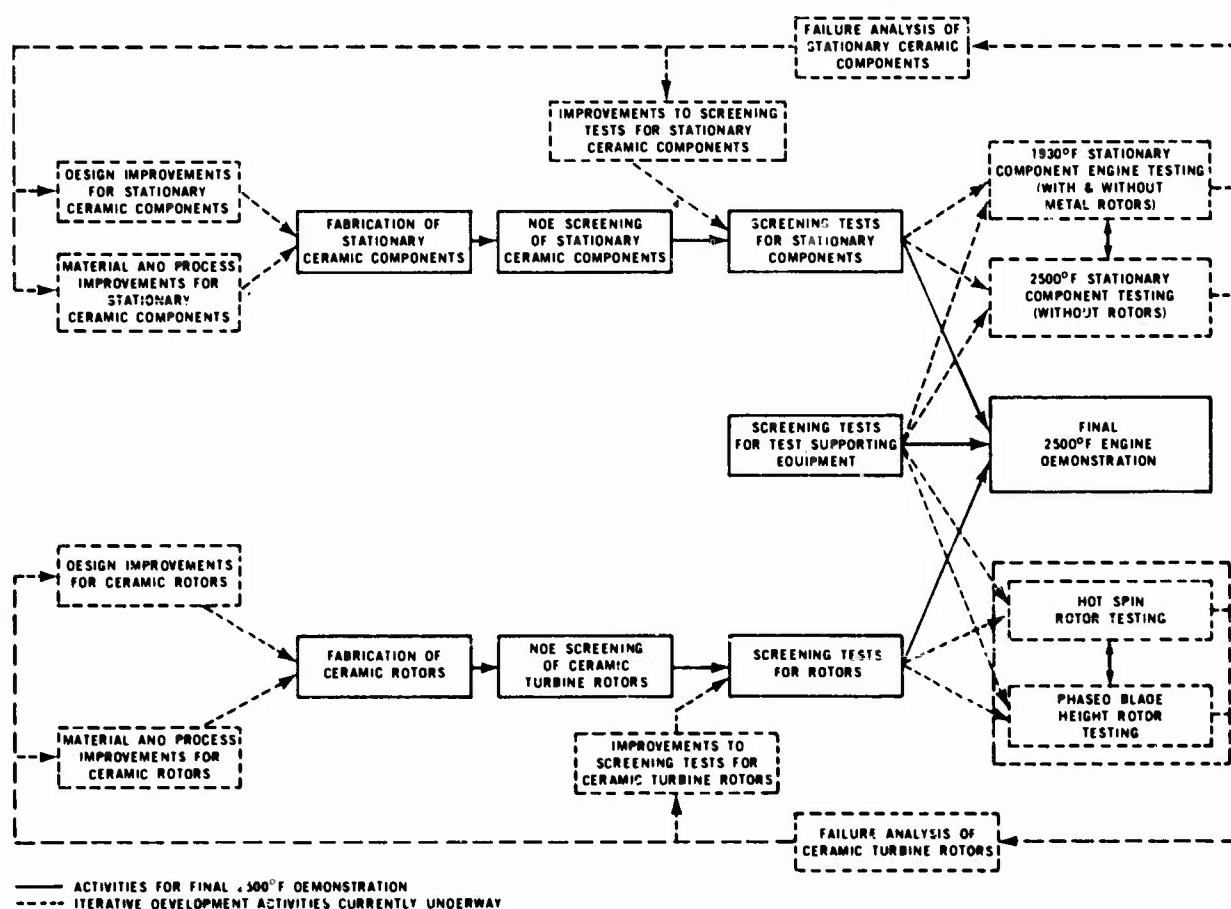
Figure 2.2 — ARPA/ERDA/Ford Ceramic Turbine Program — Major Project and Development Loops

2.2 CUMULATIVE PROGRAM SUMMARY

To meet the program objectives, the work has been divided into two major tasks:

1. Ceramic Component Development

2. Materials Technology

The progress and present status in each of these is summarized in Section 2.2.1 and 2.2.2.

2.2.1 CERAMIC COMPONENT DEVELOPMENT

Two categories of ceramic components are under development: rotating parts (i.e., ceramic rotors), and stationary parts (i.e., ceramic stators, rotor tip shrouds, nose cones, and combustors). In this iterative development, each component will pass through various phases comprising design and analysis, materials and fabrication, and testing. In order to assist the reader, those items are italicized which describe significant milestones which were achieved in the evaluation of ceramic components.

CERAMIC ROTORS

The development of the ceramic turbine rotors is by far the most difficult task in the ARPA program. This is because of:

● The very complex shape of the turbine rotor forcing the development of new and unique fabrication capabilities.

● The high centrifugal stresses associated with high maximum rotor speeds.

● The high thermal stresses and associated thermal fatigue resulting from both steady state and transient high temperature gradients from the rotor rim to the rotor hub.

● The hostile environment associated with the products of combustion from the combustor.

● The high temperature of the uncooled blades resulting from turbine inlet gas temperatures of 2500°F.

Progress and Status

● Fully dense Si_3N_4 first and second stage integral rotors were designed and analyzed [1,2,3,4].

● A method of attaching rotors was conceived and designed [1,2].

● The following approaches for making integral rotors were investigated but discontinued:

— Direct hot pressing of an integral Si_3N_4 rotor [1].

— Ultrasonic machining of a rotor from a hot pressed Si_3N_4 billet [1,2,3].

— Hot pressing an assembly of individually hot pressed Si_3N_4 blades [1,2].

— Pseudo-isostatic hot pressing of an injection molded Si_3N_4 preform [1,2,3].

— Hot pressing using coinformable tooling of preformed Si_3N_4 blades and hub [2,3,4].

— Fabrication of a dense SiC blade ring by chemical vapor desposition [1,2,3,4].

— Electric discharge machining of a rotor from a hot pressed SiC billet [2,3,4].

- A "duo-density" Si_3N_4 ceramic rotor was conceived and designed (3).

- Tooling to injection mold Si_3N_4 blade rings was designed and procured (3).

- Several hundred hot press bonding of duo-density rotors have been carried out (10). These have progressed from rotors with flat-sided hubs to fully-contoured hubs made simultaneously with the hot press bonding operation. Prior severe blade ring distortion problems have been solved by using a double blade fill to support the blade ring during bonding. In addition, the diffusion bond has been improved as evidenced by microstructural examination. Experiments were conducted using magnesium nitrate instead of magnesium oxide as a densification aid. Excellent bonding and density were achieved but strength was deficient. Successful modifications were made to the graphite wedge system to reduce blade ring cracking and tearing problems. Problems which remain are occasional blade ring and rim cracking (4,5,6,7,8).

- Over 110 cold spin tests resulted in blade failures over a range of speeds, some of which exceeded full speed requirements of the new Design D′ blading. However, an improvement in consistency is required if a reasonable yield from the blade ring fabrication process is to be achieved. This emphasizes the need for three-dimensional blade stress analysis as well as development of a higher strength, better quality blade material. Cold spin testing of rotor hubs of hot pressed Si_3N_4 showed a characteristic failure speed of 115,965 rpm with a Weibull rpm slope of 17.66 (7). Several hot pressed hubs, made by the hot press bonding process, were cold spun to destruction, and showed results consistent with hot pressed hubs fabricated separately (8). A high speed motion picture study (3000 frames/sec) was conducted of a turbine rotor failure in the cold spin pit (8).

- A three dimensional model of the rotor blade along with heat transfer coefficients has been generated for thermal and stress analysis (5,6,8).

- Development of better quality blade rings continues. X-ray radiography of green parts has proved effective in detecting major flaws. Slip cast Si_3N_4 test bars having a density of 2.7 gm/cc show four point MOR of 40,000 psi. Processes to slip cast a rotor blade ring have been investigated as have methods of achieving 2.7 gm/cc density with injection molded material (6,7,8).

- *Thermal shock testing simulating the engine light-off condition was conducted on rotor blade rings for approximately 2,500 cycles without damage (5,6).*

- A technique to evaluate probability of failure using Weibull's theories was developed and applied to ceramic rotors (5).

- A test rig was designed and built to simulate the engine for hot spin testing of ceramic rotors (3,4,5). A set of low quality duo-density rotors was spin tested to 20% speed and 1950°F for a short time before failure, believed due to an axial rub (7).

- A revised rotor design (Design D) was conceived, using common rotors at first and second stage locations (7).

- A lower stress version of the Design D rotor, designated Design D′, has been designed using radially stacked blade sections. Blade centrifugal stresses were reduced from 21,000 psi in Design D to 13,180 psi in Design D′ (8).

- The rotor test rig was rebuilt and testing initiated to evaluate the rotor attachment mechanism and the curvic coupling mounting design. Hot-pressed Si_3N_4 rotor hubs were subjected to 10 operating cycles from 900 to 1950°F, during a 3-3/4 hour test, without damage (8).

- Design codes for ceramics were refined to include nonlinear thermal properties of materials and to allow for the specification of the MOR-strength and Weibull "m" requirements for a given failure at a specified loading and reliability level (9,10).

- Rotor hubs were successfully densified and press bonded at both 2% and 3-1/2% MgO levels, resulting in reduction of MgO migration into the blade ring and improved high temperature strength over previous pressings with 5% MgO (9).

- A design C duo-density rotor with a few obviously flawed blades removed was cold spin tested after static oxidation at 1900°F for 200 hours. A single half-blade failure occurred at 53,710 rpm, which corrects to 68,000 rpm or 105% speed for the present shorter bladed Design D' configuration. The results of a number of spin tests of slip cast Si_3N_4 blade segments were combined to yield a median failure speed of 64,000 rpm (9).

- Over five hundred blade rings, previous to Design D, were injection molded for press bonding experiments, cold spin tests, and hot tests (9).

- New tooling to injection mold the lower stressed Design D' rotor blade rings was received and trial moldings to establish molding parameters were initiated (9).

- Progress has been made in several aspects of the press-bonding step of duo-density rotor fabrication. A problem of excessive deflection of the graphite support structure beneath the rotor assembly, permitting bending and subsequent blade fracture, was solved by the substitution of high modulus hot pressed SiC for the low modulus graphite. Increasing the rate of pressure application also improved the quality of the hub sections (9).

- A new hot spin test rig, designed to improve the turn-around-time in testing turbine rotors, has been constructed, and is currently in the shakedown testing phase. Using gas burners instead of a gas turbine combustion system, this rig simulates the engine environment and was designed to be quickly rebuilt following rotor failures (9).

- In the program to engine evaluate ceramic rotors having reduced blade length (and less risk of catastrophic failure), two duo-density Si_3N_4 rotors with the blades shortened to 10% of the design length were selected and cold spun to 64,000 rpm (9). These rotors were then hot tested in an engine for 45 minutes at 32,000 rpm and 2000°F turbine inlet temperature without failure (10).

- The aerodynamic design of an increased efficiency turbine, designated Design E, was initiated. Flowpath optimization, a one dimensional stress analysis, and preliminary detailed blade section definition were completed for both the first and second stage turbine stators and rotors (9).

- A process has been developed to slip cast turbine rotor blade rings (9).

- 3-D stress and reliability analyses were performed on preliminary blade configurations for the increased efficiency Design E turbine rotors (10).

- 500 Design D' blade rings have been injection molded which will nitride to 2.7 g/cc density (10).

- A new fabrication approach, called the 3 piece concept, to make duo-density silicon nitride turbine rotors, was conceived and demonstrated that a significant reduction of applied loads during hot press bonding could be achieved, generally eliminating blade and rim cracking (10).

- Good correlation was demonstrated between predicted cold burst speed and actual spin test results on nine rotor hubs spun to destruction (10).

- Six available duo-density turbine rotors of imperfect quality were used to check out the hot spin rigs by hot spin testing to failure, with failure speeds ranging from 12,000 rpm to 35,300 rpm at rotor rim temperatures ranging from 1780° to 2250°F, (corresponding to equivalent estimated blade tip temperatures in an engine of 1930°F to 2400°F) (10).

- A duo-density rotor with flawed blades removed achieved 52,800 rpm in the modified design engine with ceramic stationary flowpath prior to an unscheduled dynamometer shutdown. A maximum

turbine inlet temperature of 2650°F was observed during this run. Post inspection showed all ceramic parts to be crack free. The rotor failed during a subsequent run at 50,000 rpm and 2300°F T.I.T. (10).

● Since the Weibull probabilistic method is being used in the design of ceramic turbine rotors, an investigation of various estimation techniques to obtain Weibull parameters from test data was carried out. The method selected and used in this program is the "Maximum Likelihood Estimator" (MLE) method. Confidence intervals in estimating Weibull parameters using the MLE method were computed to vary significantly with the number of samples tested *.

● An analytical method was prepared, based on the Wiederhorn-Evans approach (11), to predict the time-to-failure of complex, multiaxially-stressed ceramic components such as the ceramic turbine rotor *.

● Effort to design improved efficiency ceramic turbine stages (Design E) led to the consideration of a 3-stage turbine versus the current 2-stage design. It was shown that, for the same overall level of efficiency, a three stage turbine would have a significantly higher reliability and could operate at 50,000 rpm maximum speed rather than the 64,000 rpm required to obtain the same power output from a two stage turbine. Alternately, for equal levels of overall reliability, the 3-stage design can be expected to be 3-5 percentage points better in aerodynamic efficiency. Further work on improved efficiency Design E turbine stages was terminated as a result of reductions in the overall program *.

● An automatic control system utilizing solid state logic elements was designed, built and applied to the injection molding of ceramic turbine components, particularly rotor blade rings. The objective was to consistently control such parameters as molding material temperature, die temperature and various sequencing times. The desired setting of each parameter was varied systematically to optimize the molding process for rotor blade rings based on visual and X-ray inspection. In addition to using optimized molding parameters, it was found necessary to clamp the die accurately to avoid blade root cracks, and to pre-extrude the starting material to avoid unmelted inclusions. A quantity of Design D' rotor blade rings was molded in the 2.7 g/cc density Si_3N_4 material system utilizing these improvements for subsequent processing *.

● A parametric study of processing hot pressed Si_3N_4 (HPSN) involving Si_3N_4 powder quality, hot pressing additive, powder milling conditions, and hot pressing conditions, was initiated in an effort to improve the expected reliability of duo-density Si_3N_4 turbine rotors. Sixty HPSN billets were made and used to establish Weibull strength data at 1600°F and 2200°F which is representative of the maximum operating temperatures at the rotor bore and bond respectively *.

● Test bars cut from three-piece duo-density Si_3N_4 rotors showed low strength in the bond between the HPSN hub and the HPSN bonding ring. Failures of this bond in spin tests also confirmed its lack of strength. In parallel, parametric studies on hot pressing Si_3N_4 showed that flat sided HPSN discs could be made at pressures as low as 500 psi. As a result, an improved two-piece, duo-density Si_3N_4 rotor with a simplified hub profile was considered; this would eliminate the troublesome hub/bonding ring bond and facilitate low hot pressing pressures which should minimize blade ring damage. Ten such two-piece, duo-density Si_3N_4 rotors were hot press bonded at pressures from 500 to 1500 psi using a 3-1/2 w/o MgO additive material for the hub. Three of these had no rim cracks and only minor blade cracking, and have been selected for finish machining and subsequent spin testing *.

● Development of the hot spin rig continued and resulted in improvements in the failure detector system, temperature measuring system, and burst absorption capability. To check out the latter, a bladeless rotor was accelerated to 64,840 rpm and the temperature gradient increased until failure occurred. The attachment bolt fractured as designed, the ceramic fiber insulation and stainless steel backing absorbed the failure, and the rotor shaft was only slightly scored at the bearing journal. This damage was quickly repaired to demonstrate a relatively fast turn-around time *.

Note: Refer to this report for items noted *.

- Finite element models of a duo-density Si_3N_4 rotor tested in the hot spin rig were made and will be used to calculate temperatures and stresses in the rotor for a given operating speed and rim temperature *.

- A number of lubricants have been investigated for the rotor ceramic-to-metal curvic coupling including Nickel Ease, Molykote, Electrofilm, Borkote, and Molydisulfide. A problem of limited life at the 1400°F operating temperature resulted in the development of a 1/4 mil thick gold coating on the contacting surfaces of the curvic teeth. Such a coupling has been tested through four complete thermal cycles with no significant deterioration, and will be used in the next engine test of a ceramic rotor *.

CERAMIC STATORS, ROTOR SHROUDS, NOSE CONES, AND COMBUSTORS

While development of the ceramic turbine rotor is the most difficult task, development of the stationary ceramic flow path components is also vitally necessary to meet the objective of running an uncooled 2500°F vehicular turbine engine. In addition, success in designing, fabricating, and testing these ceramic components will have an important impact on the many current applications of the small gas turbine where the use of stationary ceramics alone can be extremely beneficial. The progress and status of these developments is summarized, taking each component in turn.

Progress and Status

Ceramic Stator

- Early Design A first stage stators incorporating the turbine tip shrouds had been designed, made by assembling individual injection molded reaction bonded Si_3N_4 vanes, and tested, revealing short time thermal stress vane failures at the vane root [1].

- Investigation of a number of modified designs led to Design B, with the rotor shroud separated from the stator. Short time thermal stress vane failures at the vane root were eliminated [1].

- In the fabrication of stators, the starting silicon powder, the molding mixture, and the nitriding cycle were optimized for 2.2 gm/cc density reaction bonded Si_3N_4 [2,3].

- Engine and thermal shock testing of first stage Design B stators revealed a longer term vane cracking problem at the vane mid-span. This led to modification of the vane chord, designated the Design C configuration, which solved the vane mid-span cracking problem [3].

- A remaining problem in first and second stage Design B stators was cracking of outer shrouds, believed due to the notch effect between adjacent vanes. To solve this, a one-piece first stage stator (Design C) was designed and tooling was procured [4,5].

- The Design B second stage stator could not be made in one piece due to vane overlap, so an "inverted channel" design was investigated to eliminate notches at the outer diameter. However, engine testing showed that axial cracking of the outer shroud remained a problem [3,4,5,6].

- *A 50 hour duty-cycle engine test of the hot flow path components to 1930°F was completed. The assembled first stage Design C stator was in excellent condition; 8 out of 33 vanes in the second stage inverted channel stator had developed fine cracks [6].*

- *A 100 hour duty-cycle engine test of the hot flow path components (without a second stage stator) to 1930°F was completed. The reaction bonded silicon nitride (2.55 g/cc density) one piece first stage Design C stator successfully survived this test [7].*

- Improvements in materials and processing resulted in the fabrication of flaw free one piece stators of 2.55 gm/cc density [8].

Note: Refer to this report for items noted *.

- A test was devised for mechanically loading stator vanes to failure which provided useful information for material and process development [8].

- *Thermal shock testing of 2.7 gm/cc density stator vanes revealed no detectable cracking and negligible strength degradation after 9000 cycles of heating to 2700°F and cooling in the thermal shock rig [8].*

- Processing of 2.55 gm/cc density injection molded stators continued. Consistently high weight gains (61-62%) have been obtained using the Brew all-metal furnace employing a slow, gradual rate-of-rise cycle, 4% H_2-96% N_2 gas under static pressure, and Si_3N_4 setters and muffles [9].

- *An injection molded stator of 2.55 gm/cc density Si_3N_4 survived static testing (no rotors) for 175 hours at 1930°F steady state. Weight gain of the stator was less than 1%, and this stabilized after 10 hours of testing. The stator is in excellent condition [9].*

- *Testing of stators up to 2500°F in the Flow Path Qualification Test Rig was initiated with over eight hours of testing accumulated at 2500°F [9].*

- *A reaction bonded silicon carbide stator successfully accumulated 147 hours of testing at 1930°F and remains crack free [10].*

- *Over nine hours of testing of a silicon nitride stator were accumulated without incident in the modified engine configuration to a maximum turbine inlet temperature of 2650°F [10].*

- As a result of funding reductions in the over all program, a short-term attempt to fabricate stationary ceramic components was made and the best available parts were selected for testing. Attempts to injection mold one-piece stators in the 2.7 g/cc density Si_3N_4 material system were made and a variety of molding parameters were examined. A number of stators were processed with good vane quality but questionable outer shroud quality.*

- Three 2.7 g/cc density Si_3N_4 stators passed mechanical loading tests in the stator vane and outer shroud loading fixtures though one was categorized poor due to visual fillet cracks. This latter one failed the 10-light qualification test. The other two stators passed the 10-light qualification test*.

- A review was made of earlier durability testing of 2.55 g/cc density Si_3N_4 stators at 1930°F. The weight gain was a measure of incipient failure. For example, the failures of six 2.55 g/cc density Si_3N_4 stators were associated with weight gains in excess of 1.9%. This wide variation of weight gain is thought to be due to the variation in open porosity caused during the nitriding cycle. It is expected that this problem will be considerably lessened for higher density 2.7 g/cc density Si_3N_4 having good quality microstructure *.

Ceramic Rotor Shrouds

- Separate first and second stage ceramic rotor shrouds, which are essentially split rings, evolved in the stator change from Design A to Design B [1].

- As a result of rig and engine testing, rotor shrouds made of cold pressed, reaction sintered Si_3N_4 were modified to have flat rather than conical side faces [2].

- Because of occasional cracking, cold pressing was replaced with slip casting for making higher density rotor shrouds, resulting in a 2-3 fold increase in strength [3].

Note: Refer to this report for items noted *.

- Slip casting of rotor shrouds solved the cracking problem but revealed a dimensional change problem as a function of operating time. This was solved by incorporation of nitriding aids, heat treatment cycles, and other changes in the fabrication process which reduced instability to acceptable levels (4,5,6).

- A 50 hour duty cycle engine test of the hot flow path components to 1930°F was completed, after which both first and second stage rotor shrouds were in excellent condition (6).

- A 100 hour duty cycle engine test of the hot flow path components to 1930°F was completed, after which both first and second stage rotor shrouds were in excellent condition (7).

- Further testing of rotor shrouds to 245 hours and over 100 lights showed them to remain crack free and in excellent condition (7).

- Over nine hours of testing slip cast Si_3N_4 rotor tip shrouds were accumulated without incident in the modified engine configuration used for testing a ceramic turbine rotor up to a maximum turbine inlet temperature of 2650°F *.

Ceramic Combustors

- Combustor tubes made of slip cast Si_3N_4 and various grades of recrystalized SiC (Crystar) cracked during lights off tests in the combustor rig (4).

- A thick-walled, reaction bonded silicon carbide (REFEL) combustor successfully completed the 200 hour duty cycle test. A total of 26 hours and 40 minutes was accumulated at a turbine inlet temperature of 2500°F (10). This combustor was also successfully tested in an engine (8).

- Three thin-walled, reaction bonded silicon carbide (REFEL) combustors were successfully qualified over a 10 hour portion of the ARPA duty cycle (10).

Ceramic Nose Cones (with integral transition ducts)

- Early Design A nose cones had been designed, made from injection molded reaction sintered Si_3N_4, and tested (1).

- The nose cone was modified to Design B to accommodate the Design B first stage stator. Several Design B nose cones were made and tested in rigs and engines (2).

- Voids in molding nose cones were minimized by preferentially heating the tooling during molding (5).

- Circumferential cracking and axial cracking problems led to pre-slotted, scalloped nose cones designated Design C (3,4,5,6).

- A 50 hour duty cycle engine test of the hot flow path components to 1930°F was completed, after which the Design C nose cone was in excellent condition (7).

- A 100 hour duty cycle engine test of the hot flow path components to 1930°F was completed, after which the Design C nose cone was in excellent condition (7).

- Further testing of the 2.2 g/cc density nose cone to 221 hours showed it to remain crack free and in excellent condition (7).

- Improvements in materials and processing resulted in the fabrication of flaw free nose cones of 2.55 gm/cc density (8).

Note: Refer to this report for items noted *.

13

- Processing of 2.55 gm/cc density injection molded nose cones continued. Consistently high weight gains (61-62%) have been obtained using the Brew all-metal furnace employing a slow, gradual rate-of-rise cycle, 4% H_2-96% N_2 gas under static pressure, and Si_3N_4 setters and muffles (9).

- *Testing of nose cones up to 2500°F in the Flow Poth Qualification Test Rig wos initioted with over eight hours of testing accumuloted ot 2500°F (9).*

- *Over nine hours of testing o silicon nitride nose cone were occumulated withou! incident in the modified engine configurotion to o moximum turbine inlet temperature of 2650°F (10).*

- As a result of funding reductions in the overall program, a short-term attempt to fabricate stationary ceramic components was made and the best available parts were selected for testing. A number of Design D nose cones were injection molded in the 2.7 g/cc density Si_3N_4 material system using an automated molding control system, primarily developed to make high quality rotor blade rings. Nose cones were processed through nitriding and appeared visually good except for fine cracks between the strut and inner nose.*

- Three 2.7 g/cc density Si_3N_4 nose cones successfully passed the 10-light qualification test. One of these has accumulated 10 hours of testing at 1930°F *.

Note: Refer to this report for items noted *.

2.2.2 MATERIALS TECHNOLOGY

Materials technology forms the basis for component development including component design, component fabrication, material quality in the component as-made, and evaluation by testing. There are three major categories under materials technology — materials engineering data, materials science, and non-destructive evaluation. Progress and present status in each of these areas is summarized below:

Materials Engineering Data

● Techniques were developed and applied for correlating the strength of simple ceramic spin disks with bend test specimens using Weibull probability theories [5].

● Elastic property data as a function of temperature was determined for various grades of silicon nitride and silicon carbide [2,3,4,5,6,7,9].

● The flexural strength vs. temperature of several grades of SiC and Si_3N_4 was determined [3,4,5,6,9,10].

● The compressive strength vs. temperature of hot pressed SiC and hot pressed Si_3N_4 was determined [4].

● Creep in bending at several conditions of stress and temperature was determined for various grades of reaction sintered silicon nitride [4,5,6,9].

● The specific heat vs. temperature of 2.2 gm/cc density reaction sintered Si_3N_4 was measured, as were thermal conductivity and thermal diffusivity vs. temperature for both 2.2 gm/cc and 2.7 gm/cc density reaction sintered Si_3N_4 [4].

● Stress-rupture data was obtained for reaction sintered silicon nitride under several conditions of load and temperature [6,9,10].

● A group of 31 2.7 gm/cc density injection molded Si_3N_4 test bars, made using the best current nitriding cycle and an atmosphere of 4% H_2, 96% N_2, resulted in a Weibull characteristic strength of 44.3 ksi and an m value of 6.8. Additional material development work is aimed at obtaining a higher m value [9].

● The effects of surface finish and post machining heat treatment on the room temperature strength of hot pressed silicon nitride were determined [10].

● The variation in MOR strength of hot pressed silicon nitride was determined from rotor-to-rotor, within one rotor, and as a function of initial material preparation [10].

● Room and elevated temperature flexure strengths of injection molded reaction sintered silicon nitride of 2.7 g/cc density were determined [10].

● No time dependent failures were observed for 2.7 g/cc density injection molded reaction sintered silicon nitride during stress-rupture testing for up to 200 hours at stresses of 20-30 ksi and temperatures of 1900-2200°F [10].

● A simple, practical approach, based on the Wiederhorn-Evans [11] theory, was derived to predict the life of a ceramic under load. The only material measurements required are two sets of strength values at two stress rates. For a given material, this would comprise a statistical number of bend tests (preferably > 30) at each of two stress rates for each temperature. Stress-reliability-lifetime design diagrams can then be readily constructed. Comparison of predicted lifetimes using this method agrees reasonably well with limited published experimental stress rupture data *.

Note: Refer to this report for items noted *.

- Weibull MOR strength parameters were measured for "Refel" reaction bonded SiC at room temperature and five elevated temperatures. In addition, room temperature Weibull strength parameters in tension were measured but, using probablistic methods, did not correlate with the MOR strength data within a 90% confidence band. Suspected parasitic stresses in the tensile test and/or differences in specimen surface quality are being investigated *.

Materials Science

- A technique was developed and applied to perform quantitative x-ray diffraction analysis of the phases in silicon nitride (2).

- An etching technique was developed and used for the study of the microstructure of several types of reaction sintered silicon nitride (2).

- The relationship of some processing parameters upon the properties of reaction sintered Si_3N_4 were evaluated (3,4,5,6,10).

- The oxidation behavior of 2.2 gm/cc density Si_3N_4 was determined at several different temperatures. The effect of oxidation was found to be reduced when the density of reaction sintered Si_3N_4 increased (3,7).

- The relationship of impurities to strength and creep of reaction sintered silicon nitride was studied, and material was developed having considerably improved creep resistance (4,5,6,9).

- Fractography and slow crack growth studies were performed on reaction sintered SiC (5) and hot pressed Si_3N_4 (6,7).

- The development of sintered Sialon-type materials was initiated (7). The effects of yttria additives were being studied, especially in relation to the formation of glassy phases (8,10).

- A higher density (2.7 gm/cc) molded Si_3N_4 has been developed which will be used for component fabrication. Four point bend strengths of 43 ksi at room temperature were measured (8).

- An experimental study showed that high pressures did not facilitate nitriding of relatively dense silicon compacts. A parallel theoretical study showed that to store sufficient nitrogen within the pores and avoid diffusion, an impractically high pressure would be needed (8).

- Three techniques to improve the oxidation resistance of 2.7 gm/cc density injection molded Si_3N_4 were evaluated (9).

- Nitriding exotherms, resulting in localized silicon temperatures in excess of 1420°C, produced silicon "melt out" with resulting large porosity and lower strength. Eliminating these exotherms by controlling furnace temperature appears to be the key to uniform microstructure, fine porosity and higher strengths (10).

- Work on yttria-containing Sialons showed that melting occurred at about 1200°C whether or not the glassy phase was crystallized. A number of further experiments were conducted to prepare single phase sialons from either the $Si_3N_4/Al_2O_3/AlN$ or $Si_3N_4/Al_2O_3/AlN/SiO_2$ material systems. Further work on Sialons was terminated as a result of reductions in the overall program *.

- Use of a programmed temperature/time nitriding cycle resulted in variations of the microstructure of reaction sintered Si_3N_4, depending on furnace load. To correct this, a control system was designed and built to control the furnace temperature/time cycle automatically to maintain a reasona-

Note: Refer to this report for items noted *.

16

bly steady consumption of nitrogen (i.e. nitriding rate). Use of this automatic control was shown to produce 2.7 g/cc density Si_3N_4 with consistent, high quality microstructure over a wide range of furnace load.*

- A fabrication technique for turbine components of reaction bonded SiC has been under development by molding a thermoset polymer filled with SiC particles, pyrolyzing the polymer to carbon, then reaction bonding the structure by the infiltration of molten silicon *.

Non-Destructive Evaluation

- Ultrasonic C-scan techniques were developed and applied to the measurement of internal flaws in turbine ceramics [1,2,3,4].

- Sonic velocity measurements were utilized as a means of quality determination of hot pressed Si_3N_4 [2,3,5,9].

- A computer-aided-ultrasonic system was used to enhance the sensitivity of defect analysis in hot pressed Si_3N_4 [3,4,6].

- Acoustic emission was applied for the detection of crack propagation and the onset of catastrophic failure in ceramic materials [1,2,5,6].

- A method was developed and applied for the detection of small surface cracks in hot pressed Si_3N_4 combining laser scanning with acoustic emission [4].

- X-ray radiography was applied for the detection of internal defects in turbine ceramic components [2,3,4,5]. Hidden flaws in as-molded stators and rotor blade rings were located by x-ray radiography [5,6,7]. Such NDE of as-molded parts has been used to develop processes to make flaw-free components [8].

- A dye penetrant has been used to detect surface cracks in components made of the 2.55 gm/cc density Si_3N_4 [8].

- A state-of-the-art summary of NDE methods as applied to the ceramic turbine programs was compiled [6].

- 500 injection molded blade rings were examined, most of them in detail using 30X magnification and X-ray radiography NDE techniques [10].

- A blade bend test was applied to a number of rotor blade rings to assess their quality in terms of characteristic failure load and Weibull modulus. A distinct difference was demonstrated between blade rings nitrided in 100% N_2 and those nitrided in a 96% N_2/4% H_2 mixture, with the latter being approximately 30-40% stronger *.

- Two test fixtures were designed, built and applied for the mechanical loading of stators either to failure or to a pre-determined proof load. One fixture simultaneously loads each stator vane, and the other pressure loads the stator outer shroud. Testing to a proof load, while not a direct method of detecting flaws, can be considered a form of NDE. From testing several stators in these fixtures, a marked improvement in failure load was shown for 2.7 g/cc density Si_3N_4 stators as compared to stators made from earlier 2.55 g/cc density material. In addition, low-load vane failures could be directly related to fillet cracks *.

- A number of NDE techniques were reviewed for possible application to ceramic turbine components including Microfocus x-ray, infrared thermography, x-ray tomography, an electrostatic method, and holosonics *.

Note: Refer to this report for items noted *.

2.3 FUTURE PLANS

Section 2.2 of this report summarizes the progress made in ceramic component development and materials technology over the contract period. Significant accomplishments have been realized in terms of design, materials, fabrication and testing on both the statinary ceramic components and the ceramic turbine rotors; for both these areas, iterative development is well underway. Nonetheless, further iterations are required, particurlarly in the area of ceramic turbine rotors, to meet the program objective and demonstrate that such ceramic components can survive 200 hours of testing at temperatures up to 2500°F.

Finite element analytical techniques based on sub-critical crack growth will be developed and applied to the duo-density Si_3N_4 turbine rotor using estimated material time-dependent properties. These analyses should enable assessments of rotor lifetime reliability to be made for various operating conditions and may also influence the procedures for testing ceramic turbine rotors.

In line with the ERDA work tasks, a continued, concentrated effort in the next reporting period will be made on improved quality turbine rotors. Fabrication development of two piece, duo-density Si_3N_4 rotors will be emphasized, using the thicker hub, to eliminate problems of the three-piece rotors and to minimize blade ring damage. Tooling and procedures for finish diamond grinding the hub profile will be developed, and finish machining of improved quality rotors will be initiated. During the next 6 months and in accordance with the ARPA work tasks, testing of ceramic rotors will be performed in both the hot spin test rig and the modified engine. The major testing objective for final year 1977 is to test six duo-density Si_3N_4 rotors in the hot spin test rig at a fixed speed and temperature to assess their lifetime reliability, and establish correlation with analytical predictions.

In the area of stationary ceramic components, both 1930°F and 2500°F durability testing will be conducted using best-quality-available components made of 2.7 g/cc reaction sintered Si_3N_4.

3. PROGRESS ON CERAMIC COMPONENT DEVELOPMENT

3.1 DUO-DENSITY SILICON NITRIDE CERAMIC ROTOR DEVELOPMENT

SUMMARY

A study was performed which showed that, for equal levels of overall turbine reliability, a significant increase in turbine efficiency could be realized with a three-stage turbine versus a two-stage turbine. A method of analysis has been prepared for the prediction of turbine rotor failure reliability using the speed and temperature operating conditions experienced in the hot spin test rig.

Experience with injection molding of ceramic turbine components has indicated the need for very accurate control of molding parameters. An automatic solid state control system has been incorporated into the injection molding machine. Improved correlation between molding parameters and resulting flaws has been achieved through the use of a higher power microscope with improved part illumination, and higher resolution of rim voids by oblique x-ray techniques. An instrumentation probe was added to the molding die to monitor die movement relative to an established norm. Unmelted injection molding material inclusions in the molded parts were discovered and were eliminated by extruding the material several times prior to injection molding and by increasing injection nozzle temperature.

Forty-six turbine rotors of the three-piece concept were fabricated during this reporting period. Blade and rim cracking were minimal; however, lack of complete bonding between the hot pressed hub and the hot pressed bond ring persisted despite several modifications to the fabrication process intended to correct this problem. The fabrication concept was changed to a two-piece design involving hot pressing and simultaneous bonding of a simplified, flatter hub to a reaction bonded blade ring. Ten duo-density rotors were fabricated, and of these, three rotors are being prepared for testing to evaluate two-piece rotor fabrication quality.

A new tool for non-destructive evaluation of ceramic turbine components was investigated. The Magnaflux MXK-100M Microfocus x-ray tube is lightweight, small, and is particularly advantageous because of its small focal spot diameter. Using this equipment, a technique of panoramic x-ray of the rim of ceramic blade rings has been demonstrated.

Development of the hot spin test rig for evaluation of ceramic turbine rotors continued. The failure detector system was modified to incorporate platinum wire to correct an oxidation problem experienced with the chromel wire previously used. The turbine rotor temperature measuring system was improved by the addition of a bracket to support the pyrometer, which allows accurate repetition of temperature measurements at specific radii. Turn-around time of the test rig after a rotor burst was reduced by modification of the bearing and shaft labyrinth seal system. Burst of a rotor hub at 64,840 rpm resulted in minimal damage to the test rig components which was quickly repaired. Continuation of development of an interface material for the Curvic coupling rotor mounting system produced a successful demonstration of the capability of gold plating of the Curvic teeth to survive four simulated engine thermal cycles without significant deterioration.

3.1.1.   DESIGN AND ANALYSIS

Introduction

During this reporting period, studies were conducted on a Design E turbine and on the analysis of rotor spin test results.

Design E Three-Stage Vs. Two-Stage Study

Introduction

In the two previous reports (9) and (10), the analysis of a high-efficiency turbine with estimated near-future material properties, designated design E, was presented. In its final configuration this turbine was estimated to be about 7-1/2 percentage points higher in total-to-total efficiency than the current D' design. In order to determine if increased efficiency levels of this magnitude could be achieved without compromising mechanical reliability levels based on current material properties, a study was performed during this reporting period to investigate the relative advantage of replacing the current two-stage design with a three-stage design.

Generally speaking, in adding a stage to a turbine, one anticipates a gain in aerodynamic efficiency to be realized for the same blade speed and pressure ratio. Alternatively, the speed may be reduced, the efficiency level maintained, and the reliability increased because of the lower stress levels associated with the reduced speed. The latter, however, will be counteracted to some degree by the reduction in reliability due to the addition of a third rotating component.

The primary objectives of this study were to establish if a three-stage turbine design would have a clear-cut advantage over a two-stage design in either of two directions; (1) increased aerodynamic efficiency at current reliability levels; or (2) increased rotor reliability at current (two stage) efficiency levels.

To establish quantitatively the relative efficiency/reliability advantages of the three-stage turbine, various flow path configurations of both two and three-stage turbines were analyzed in terms of aerodynamic efficiency and mechanical reliability. Simplified stress models of disks and blades were used for all configurations. The disks considered were equal in thickness to those currently fabricated. In the efficiency analysis, various aerodynamic quantities were investigated to assure that the final configurations were reasonably optimum subject to common constraints.

Aerodynamic Efficiency Analysis

The conditions assumed in the efficiency calculations are summarized in Table 3.1. Free-vortex designs were used rather than non-free-vortex helically stacked designs because of the ease of scanning different configurations with free-vortex techniques. Helically stacked non-free-vortex turbines as currently designed (8) are generally one percentage point or less lower in efficiency than the equivalent free-vortex designs. The existing Ford Turbine Aerodynamic Analysis computer program, based on a modified version of the Ainley-Mathieson (12, 13) method of turbine performance evaluation, was used for the efficiency calculations. The design analysis condition was selected at the 70% of Nmax level (about 30% power) as it was felt that this was an appropriate middle range condition to assure reasonable low and high power performance. The lower limit of rotational speed variation for the three-stage turbine of 81.6% of current (52,452< N max<64,240 rpm) was selected to give the same average stage isentropic velocity ratio as the current two-stage turbine. Rotational speed and flow path configuration were found to have a significant effect on efficiency. Of the three different basic flow path configurations studied as shown in Figure 3.1, the constant tip (flow path C) is almost 3 percentage points higher than the constant hub (flow path A) at the same rotational speed. Both these results are due to similar variations in mean blade speed. The remaining quantities shown on Table 3.1, weight flow, stage work split, annulus area, and stage exit swirl all had generally small effects on efficiency.

TABLE 3.1

TURBINE AERODYNAMIC EFFICIENCY STUDY

Constant Parameters and Conditions

- Free Vortex Design Turbines
- Negligible Stator Leakage
- Solidity, Trailing Edge Thickness, Tip Clearance, Number of Blades

Turbine Inlet Conditions

- Design Condition: 70% Speed (1840°F Regenerator Inlet)
- $T_7 = 2715°R$ $W = 0.916$ lb/sec
- $P_7 = 32.7$ psia $PR_{7-9} = 2.21$

Varied Parameters:

- Rotational Speed: Nmax Varied From 100% to 81.6%.
- Flow Path Geometry
- Weight Flow
- Stage Work Split
- Annulus Areas
- Degree of Reaction: Stage Exit Swirl
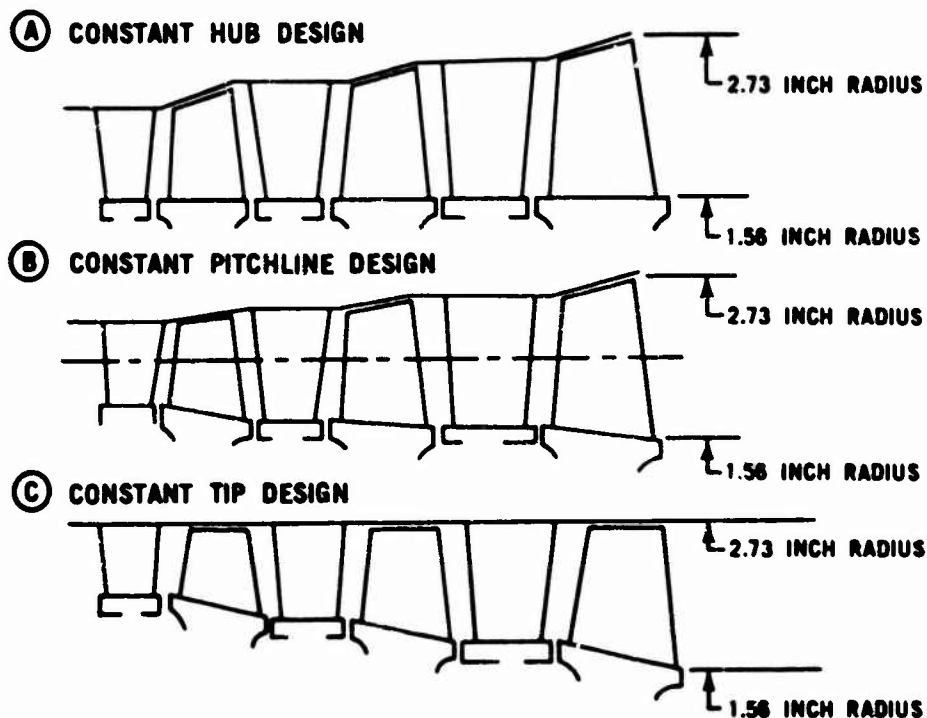
Figure 3.1 — Preliminary Three Stage Flowpath Configurations

The incremental total-to-total efficiency levels for the various configurations and rotational speeds are shown in Figure 3.2 as a function of mean turbine blade speed squared. The mean blade speed is calculated as the product of the arithmetic average blade radius and the rotational speed. The points on the left represent reduced blade speed due to reduced radius (constant hub design) and/or reduced rotational speed, while those on the right represent higher mean blade radius (i.e. constant tip design) and/or higher rotational speed. The relatively good correlation, in spite of the variety of configurations and speeds used, indicates that for the given gas conditions mean overall blade speed is the major factor of efficiency and, whether one varies blade speed by radius changes or by rotational speed, the effect will be the same.

As would be expected, the two-stage turbines can be seen to have significantly lower efficiencies than the three-stage for the speed range considered.
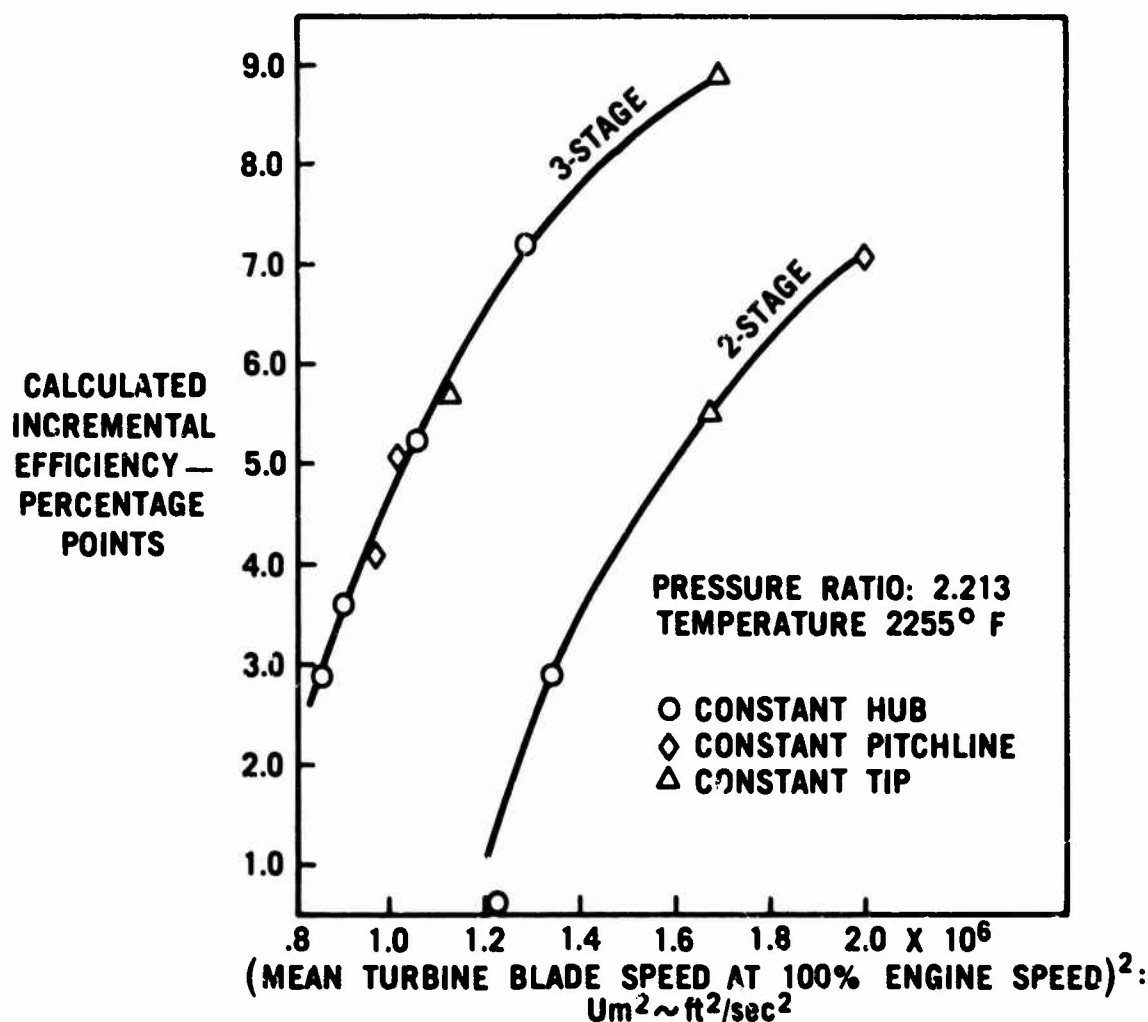
Figure 3.2 — Comparative Turbine Efficiency at 70 Percent Speed

Stress and Reliability Analysis

Simplified stress models were constructed of both the blading and the disks in order to estimate the relative fast fracture mechanical reliability of the various two and three-stage turbine configurations studied. The construction of the models was particularly oriented towards evaluating the effects of those measures which increase aerodynamic efficiency by increasing blade speed (i.e. hub and tip diameters and rotational speed). The assumptions used in the stress models are summarized in Table 3.2 and Figure 3.3 which schematically shows the simplified model used. All stress analysis was done at the appropriate 100% speed level (N max).

TABLE 3.2

TURBINE ROTOR STRESS ANALYSIS AND RELIABILITY MODEL

Disk Model

- D' First Stage Axisymmetric Finite Element Model

- Diameter Varied 3.1 Inches to 4.2 Inches

- Max Hub Thickness Maintained

- Common Temperature Boundary - All Stages

- Common Blade Number

- Speed 52,452 RPM to 64,240 RPM

- Material: Silicon Nitride - Duo-Density With Bond Ring

Blade Model

- One Dimensional Model

- Tip Diameter Varied

- Taper Ratio and Root Area Common to all Stages

- Blade Temperature Constant With Radius
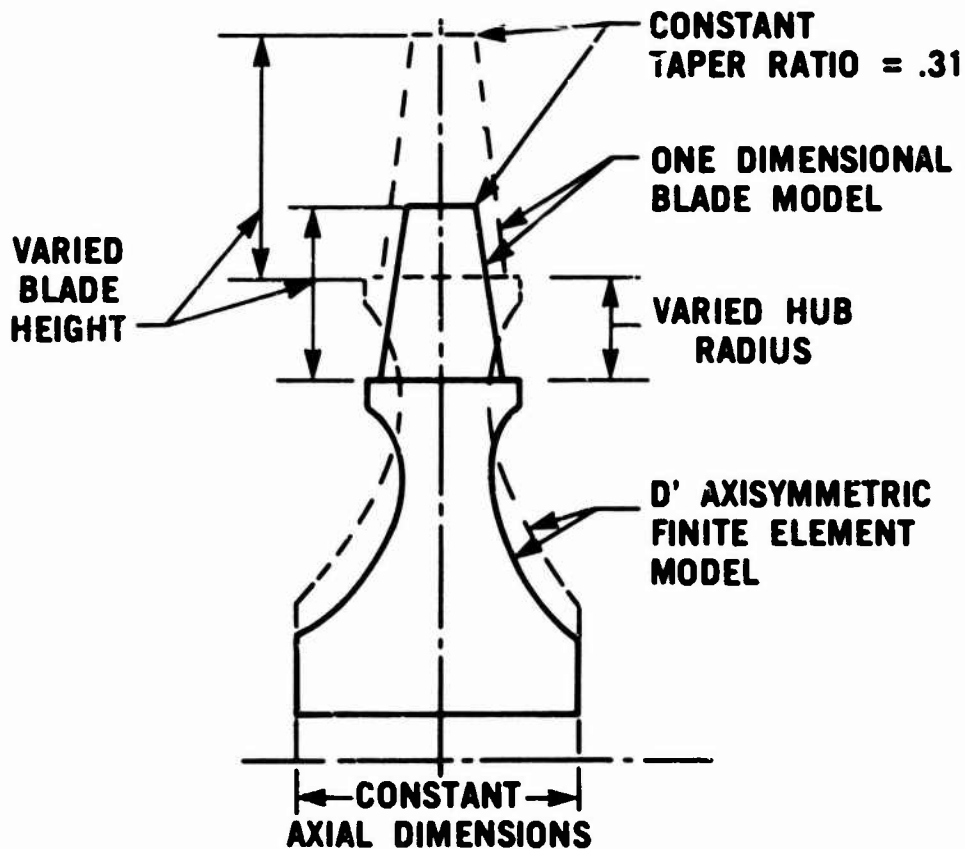
Figure 3.3 — Simplified Turbine Rotor Stress Model

The existing axisymmetric finite element model of the D' first stage disk and its accompanying boundary temperatures was used as the basis for all stages. Use of the same temperature boundaries for all stages is admittedly a simplification, but was considered to be a reasonable alternative to a lengthy heat transfer analysis for a preliminary relative study of this nature. To evaluate the effect cf changing the hub radius, all radial dimensions were varied in proportion to their distance from the bore. Constant platform thickness was maintained.

The blade mechanical stress distribution was determined on a one dimensional basis. Blades in each stage were assumed to have a constant temperature representative of typical relative gas temperatures for that stage.

Weibull failure probability analyses were performed on the disk and blade models separately with existing computer programs. Strength properties used are shown in Table 3.3, and represent current property levels for silicon nitride. The use of the three piece duo-density rotor configuration with the bond ring method of fabrication was assumed.

Figure 3.4 presents the fast fracture probability of failure for the various flow path configurations and rotational speeds studied, plotted as a function of overall turbine mean blade speed squared, the same parameter as used in Figure 3.2 for aerodynamic efficiency. The greater reliability at a given mean blade speed of the two-stage over the three-stage is to be expected because of the extra rotating component in the three-stage design. It should be pointed out that the absolute level of the curves is a strong function of the particular material properties and wheel and blade geometry used. It is felt that apparent correlation of probability of failure with mean blade speed over the limited range studied is attributable in some degree to the fact that for the disk and blade geometries, and material strength properties assumed, the rotors were basically disk strength-limited. That is, the numerical reliability of the disks was in general lower than the blades and was therefore controlling. However, there is evidence to suggest that if the blade is the limiting component, the reliability is still a function of rotational speed, but will become less dependent on blade mean radius.

TABLE 3.3

STRENGTH PROPERTIES

	Temp °F	Weibull Slope m	MOR (psi)
2% MgO Hot-Pressed Si3N4 (Hub)	78	10	109,000
	1700	10	95,000
	2100	10	78,000
	2300	10	63,000
	2500	10	42,000
5% MgO Press-Bonded Si3N4 (Bond Ring)	78	10	90,000
	1700	10	81,900
	2100	10	65,700
	2300	10	52,200
	2500	10	33,300
Injection Molded Si3N4 (Blades and Platform)	78	11.1	36,300
	1700	16.2	33,300
	2100	13.3	31,900
	2300	9.5	33,000
	2500	12.1	31,900
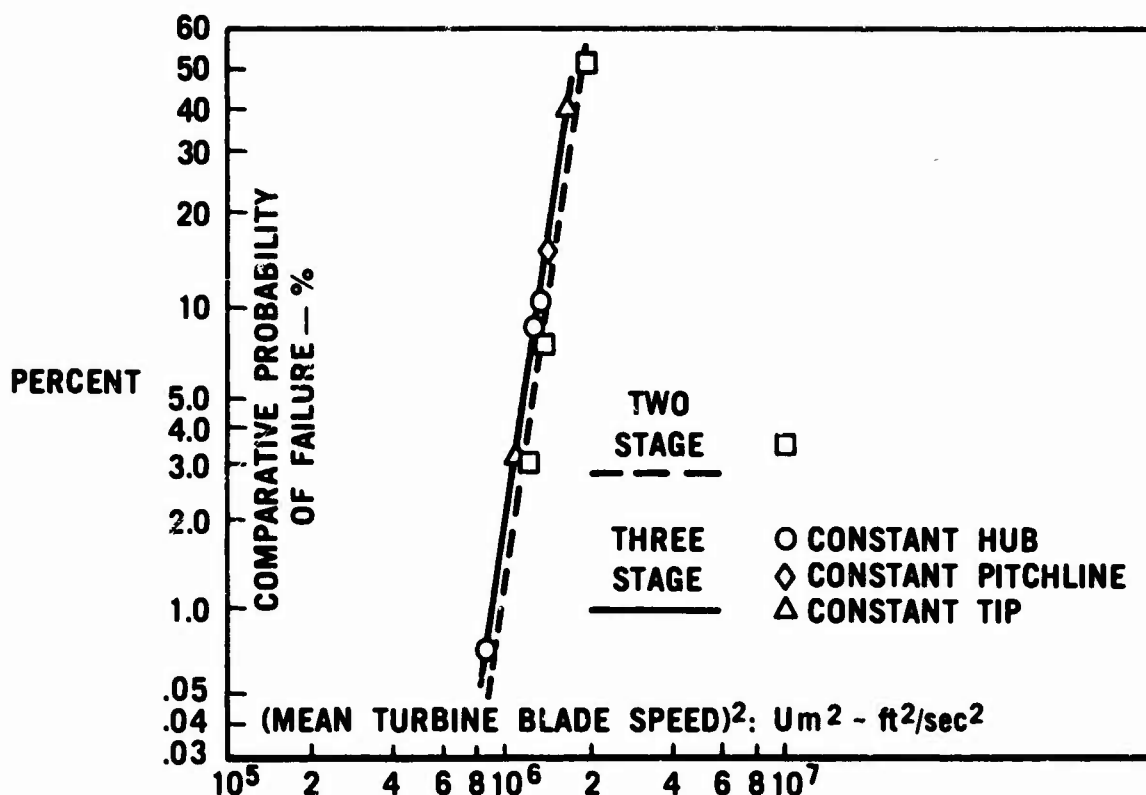
Figure 3.4 — Overall Turbine Rotor Failure Probability at 100 Percent Speed

Discussion

Table 3.4 represents the results of the study in terms of percentage point gain in efficiency of a three-stage turbine over a two-stage turbine for equal levels of overall rotor reliability. It can be seen that the three-stage efficiency is significantly higher than that of the two-stage and should be further considered. Because of the simplified nature of the stress analysis, and because of the particular assumptions regarding material properties and blade-disk geometries, the numerical reliabilities given should be viewed as relative levels rather than as absolute numbers for a particular rotor. If higher strength material properties were assumed, the absolute reliability levels could increase significantly. Similarly, the assumption of a thicker disk or a more tapered blade would be expected to change the absolute reliability level. However, the three stage turbine would still show an efficiency gain relative to the two stage turbine.

TABLE 3.4

EFFECT OF STAGE NUMBER ON AXIAL TURBINE EFFICIENCY AND RELIABILITY

Relative Overall Rotor Reliability*	Aerodynamic Efficiency Increase of Three Stage Over Two Stage Turbine (Percentage Points)
0.970	+5.1
0.950	+4.5
0.90	+3.7

*   Based on Present Disk and Blade Silicon Nitride Properties and Present Disk Design.

This preliminary study has shown that a ceramic three-stage turbine is an attractive alternative to the current two-stage design in terms of increased reliability and/or efficiency. It was shown that, for the same overall level of efficiency, a three stage turbine would have a significantly higher reliability and could operate at 50,000 rpm instead of 64,000 rpm for a two stage design. Alternately, at equal levels of mechanical reliability, a three-stage turbine can be expected to have a 3-5 percentage point efficiency gain relative to a two-stage.

Conclusion

From Figure 3.2, it can be seen that for a given level of efficiency, a three-stage turbine operates at about 80% of the blade speed of a two-stage turbine. This means that, using the same physical size ceramic rotor as is currently under development, the maximum speed for a three-stage turbine would only be about 50,000 rpm as compared to the 64,000 rpm required for the two-stage turbine to reach the same level of efficiency. As a result, the reliability of the three-stage turbine would be significantly higher than the two-stage turbine for comparable efficiencies.

Analysis of Rotor Spin Test Results

In the earlier part of the Vehicular Gas Turbine Program, computer codes were developed and methodology established for designing with brittle materials. The methodology is based on statistical concepts which utilize Weibull's model of brittle fracture. Certain aspects of that methodology have been successfully verified in cold spin tests of ceramic disks and rotor blades. A program is underway to conduct correlative studies in an environment closely simulating engine operating conditions. These studies will be conducted in a hot spin rig described in earlier reports. A ceramic turbine rotor was analyzed in the rig environment to assess the feasibility of using the rig as an evaluation tool and to determine how closely it will simulate the engine conditions.

The hot spin rig described in an earlier report (9) will be used to conduct correlative studies between analytically predicted and experimentally determined failure distributions of ceramic turbine rotors. The test program will be similar to the program previously conducted in the cold spin pit (10), except the tests will be conducted at elevated temperatures.

The proposed test procedure is to first establish a temperature distribution in the rotor at a stable, relatively low speed. The rotor is then accelerated sufficiently rapidly so that only negligible temperature changes occur in the rotor. The failures that occur during acceleration will determine the experimental fast fracture failure distribution. The calculated failure distribution will be determined using finite element computer codes. Temperature and stress distributions in the rotor failure analysis prevailing at the time of failure will be computed and the failure probabilities determined using appropriate strength distribution (Weibull) parameters obtained from MOR tests. Rotors which survive the fast fracture test procedure will be durability tested. The rotor will be operated at steady state temperature and speed conditions for a previously determined period of time. Failures which occur during the durability test will be correlated with life predictions.

The finite element model of the hot spin rig rotor assembly is shown in Figure 3.5. The model is based on the redesigned hot spin rig configuration (10) and will be used to calculate the temperature distributions. The physical parts represented by the finite elements are shaded and labeled. The blade finite element mesh has been previously illustrated (6).

The temperatures in the rotor assembly will be determined by the boundary conditions around the assembly and by the thermal conductivities of the interior of the assembly. Heat is applied to the rotor at the blades with 12 gas burners. The resulting temperatures are measured at the rim and the blades with optical pyrometers. The measured rim temperature forms one boundary condition for the rotor assembly. The assembly bolt is cooled with air, and this air flow is assumed to flow out of the end of the bolt and up over the nut and cap and then up the upstream side of the rotor. This flow is the second boundary condition and is shown as "A" on Figure 3.5.

GAS FLOW →

● ROTOR
● CERAMIC CONE ADAPTOR
● METAL CONE
◐ SHAFT
◑ CAP
◐ NUT
● BOLT
○ AIR
◑ SLEEVE
○◐ COOLING FLOWS
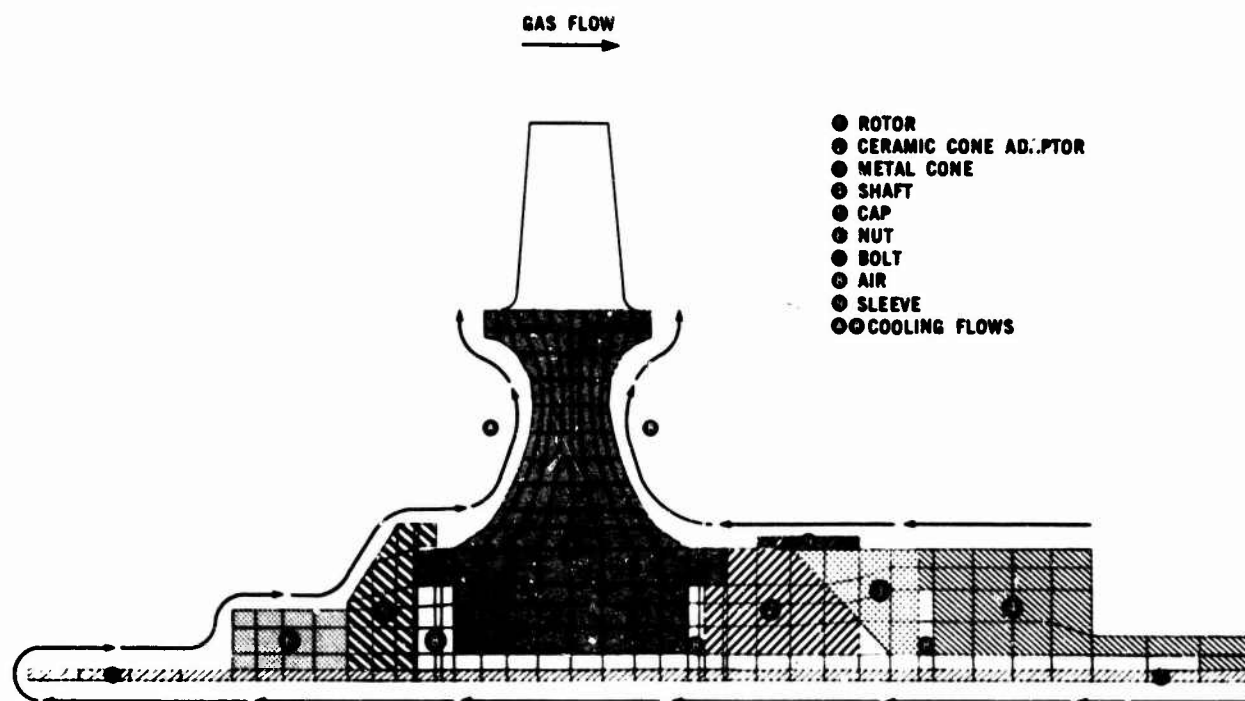
Figure 3.5 — Finite Element Model of Hot Spin Test Rig Rotor and Shaft Assembly

The outer diameter of the shaft is fed with labyrinth discharge air. This flow is assumed to travel across the metal cone and sleeve and up the downstream side of the rotor. This flow is the third boundary condition and is shown as "B" on Figure 3.6. The rim temperature is the source of heat for the assembly, and the two air flows are the heat sinks, resulting in a temperature gradient in the rotor hub.

A sample calculation was done to investigate the feasibility of matching engine temperature distribution in the rotor. The results of this calculation are shown in Figure 3.6 and may be compared to engine results previously published (10). The sample calculation assumed a uniform rim temperature of 2300°F. For the actual test program, the rim temperature will be measured and the measured values will be used as input to the finite element model. The finite element model and the boundary conditions will be checked with the use of thermal paints prior to conducting the correlation study tests. Adjustments will be made in the model, if required, when experimental temperature data become available.
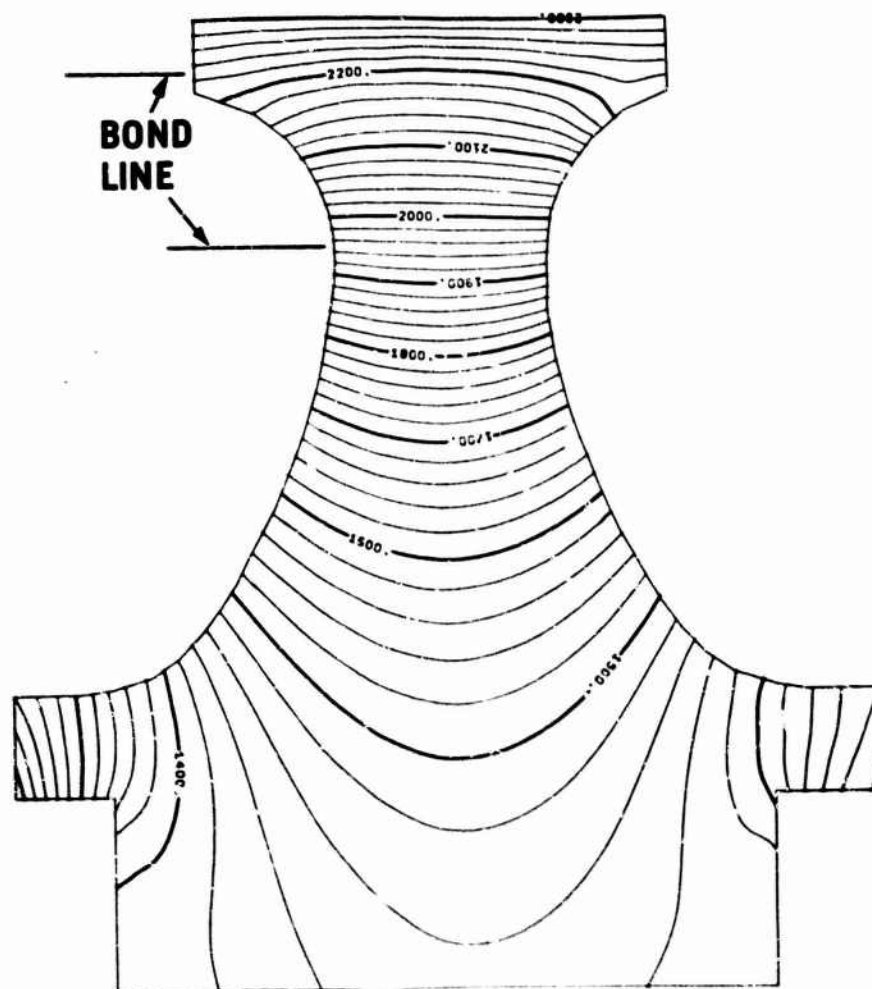
Figure 3.6 — Isotherms (°F) in First Stage Rotor at 24,000 RPM and 2300°F. Rim Temperature Operating Conditions

3.1.2 MATERIALS AND FABRICATION

Introduction

The duo-density process is a multi-step forming procedure beginning with an injection molded reaction sintered silicon nitride blade ring, and ending with a hot pressing operation which forms the hot pressed hub and bonds this hub to the blade ring. Coupled with these operations are the continued use of non-destructive testing techniques both throughout the duo-density process and after finish machining of the hot pressed rotor.

The main thrust of the injection molding effort during this reporting period was 1) the installation of automatic controls on the injection molder; 2) improvements in material mixing techniques; and 3) a reduction in contamination of the injection molding material. Work in hot pressing consisted of 1) the installation of a simplified two piece design rotor assembly; 2) material densification studies; and 3) a continued effort to eliminate hot pressing cracks in the rotor blades and rim.The objective of the NDE program is to concentrate development and application effort on the methods with immediate potential and yet assess other techniques as their development proceeds. In this regard, a preliminary study on the use of a Microfocus x-ray tube was accomplished, and several other new NDE techniques were assessed for long or short term potential.

Molded Blade Ring Fabrication

During injection molding of ceramic turbine components, some variability of molding parameters has been observed. Random variations were experienced in molding material temperature, die temperature, process time, and various other parameters which often exceeded the tolerance limits established for molding acceptable components. These variations led to low yields of good quality molded components and served to point out a need for improved molding controls, with the critical parameters being accurately controlled automatically rather than manually.

In designing a control system to eliminate parametric variations affecting component molding, the variables to be controlled were first defined. It was desired that all material and die temperatures be controlled to within 1°F. Mold release application and compressed air blowout for cleaning the molding tooling were also to be controlled to within 0.1 sec. actuation time. Both the vacuum level in the molding tool and the injection pressure were to be controlled utilizing pressure sensing limit switches. Temperature of the component being formed had previously been measured during the molding process by means of a thermocouple mounted in the die with the bead projecting into an area of the machining stock of the component (Figure 3.7). Utilizing this thermocouple, the die-opening portion of the molding cycle was to be controlled based upon part temperature with a resolution of ±1°F.

Implementation of these concepts into a design for an automatic control system was carried out in-house. The completed control, shown in Figure 3.8, utilized solid state logic to accomplish all control functions as defined in the initial design. CMOS type logic was chosen for its high noise immunity.

In the component molding operations, all time controls are set as desired. Temperature or time mode die opening is selected as are the parameters for mold release, vacuum, and cleaning air. In the fully automatic mode, the power-on button is depressed followed by the cycle start button. The machine molds one component — in this case a rotor blade ring — then stops. After the blade ring is manually unloaded from the tool, the process is repeated. If desired, the machine can also be run in a manual mode. After the power is turned on and cycle start depressed, the control button for each function must be depressed. As each function is completed, the machine returns to standby while awaiting a new command. Any step can be skipped or its sequence altered in the manual mode with the exception of those which would cause machine damage.

Although this system was designed specifically to optimize rotor blade ring molding, it should be equally effective in molding other components.
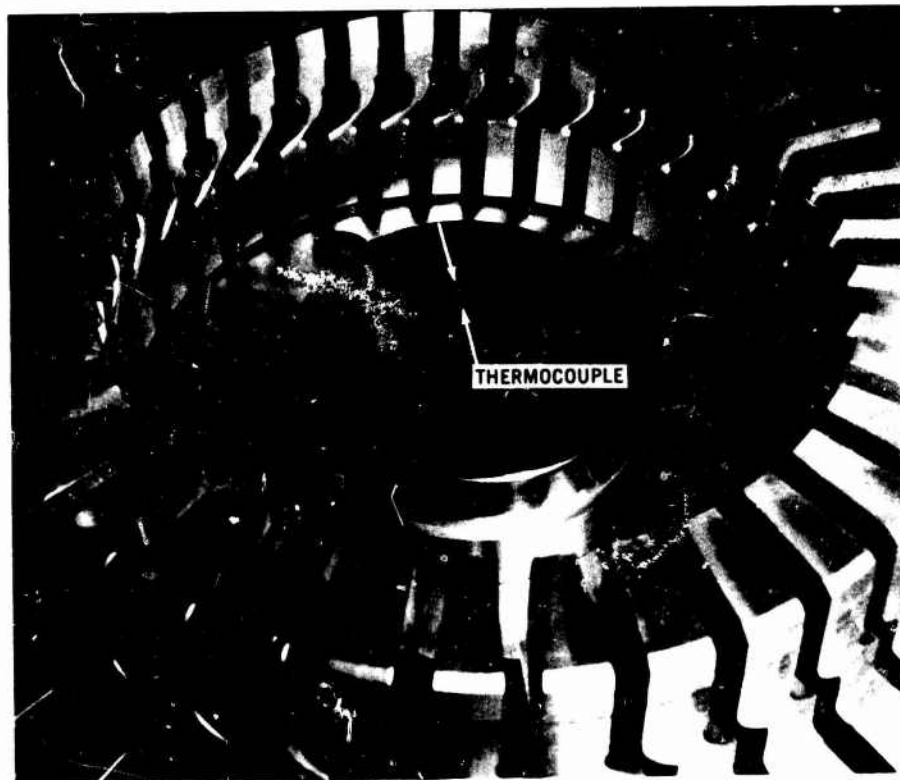
Figure 3.7 — Movable Half of Rotor Blade Ring Tool Showing Thermocouple for Measuring Temperature
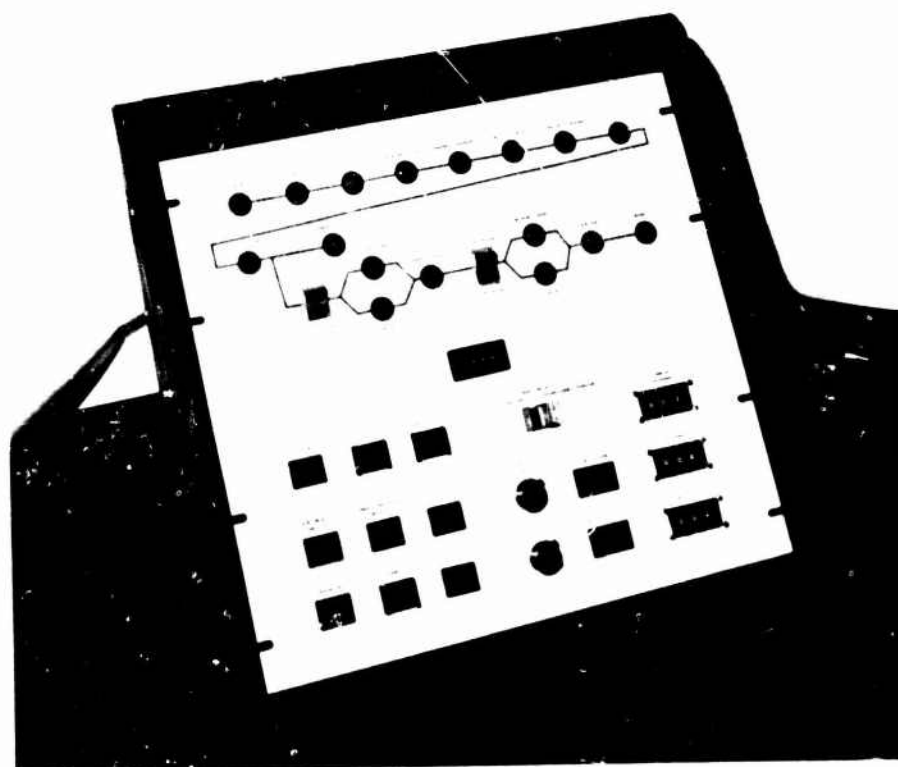
Figure 3.8 — Operator's Controls for Automatic Injection Molding Control Unit

With automatic control to reduce variability of parameters successfully obtained, recording the actual parameter level and correlating its effect on part quality became increasingly important. To record temperature data, two 4 channel strip chart recorders were added to the system. Extra thermocouples were added to the barrel and nozzle, and a temperature comparator was used to provide a signal to the recorders.

Using the recording system during the molding, the effects of process changes were readily seen and analyzed. For example, Figure 3.9 shows that nozzle material temperature drops as the nozzle contacts the tool. This rapid nozzle cooling was found to cause small, solidified inclusions which were visible in the molded component. By adjusting cycle time and nozzle temperature, a critical lower limit of nozzle temperature was determined and henceforth maintained above this level.

DIE & COMPONENT TEMPERATURE   MATERIAL TEMPERATURE
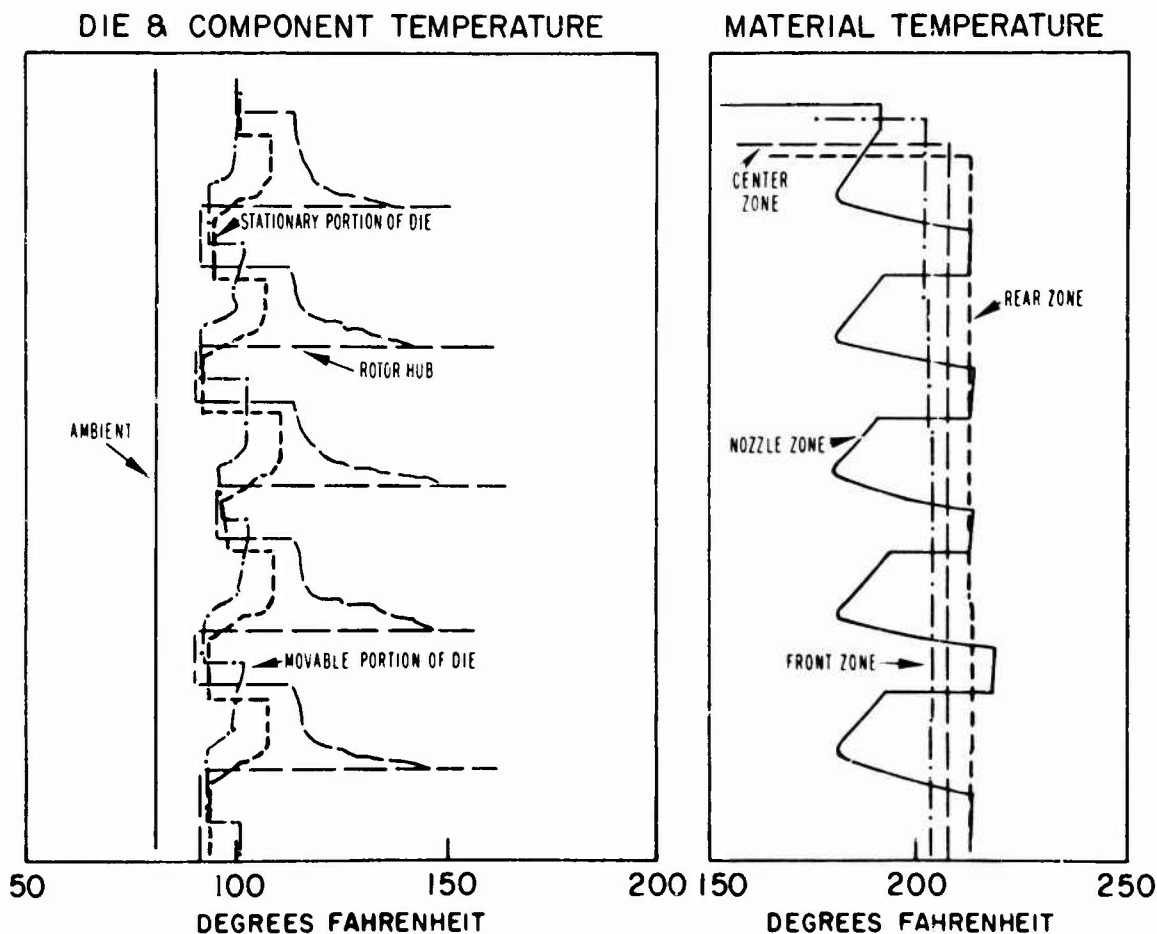
Figure 3.9 — Example of Temperature Recording Charts From Automatic Molding of Rotor Blade Rings

Two improved techniques of molding flaw detection were also employed to more completely characterize the as-molded rotor blade rings. A 70 power stereo microscope with several high intensity fluorescent lamps at oblique angles to the surface being inspected was found to be superior to the 35 power stereo microscope previously used. To more completely examine the blade ring rim for internal voids, an oblique x-ray technique has been instituted. The part is mounted on a 45° angle relative to the x-ray beam and 2 radiographs taken at 90° rotations of the blade ring. These oblique x-rays have allowed increased resolution of rim voids.

Molding of blade rings was continued following installation of the new automatic control system. Due to the previous wide degree of process variations, the exact parameters required to mold acceptable rotor blade rings had to be determined by means of a parametric study, which yielded an initial set

of parameters which produced good rotor blade rings. A quantity of blade rings were molded; however, during processing, vane trailing edge root cracks were discovered, as shown in Figure 3.10.

Investigation of methods of eliminating vane root cracks revealed that they were caused by excessive tool movement during molding. The pressure of the molding material was pushing the tool open slightly during filling. When the pressure was released, the molding machine reclosed the tool, fracturing the vane trailing edge at the root. Die movement was reduced to an acceptable level through clamp adjustment. A Bentley-Nevada proximity probe was installed to measure die movement during molding. Curves of normal (acceptable) die deflection were developed and care taken to maintain clamp adjustment within this limit (>0.0005 inches). A single channel strip chart recorder was added to the control system to record die deflection for each component molded.

Once it was determined that this improvement resulted in rotor blade rings with no trailing edge cracks after processing, additional components were molded. Oblique rim x-ray results for these rotors showed many internal voids in the rim areas, thus necessitating further optimization. A reduction in material temperature of 20°F was found to reduce internal voids to a level undetectable to oblique x-ray. An example of a rim void is shown in Figure 3.11.

A quantity of rotors was molded at the parameters now optimized to give void free rotor blade rings. During this molding run a problem with unmelted inclusions was noted. An example of an inclusion is seen in Figure 3.12. These inclusions have been noted periodically in all rotors molded using the 2.7 g/cc density material. The cause of these inclusions was found to be cooling of the molder nozzle as it contacts the cool tool, as noted earlier in this section. If the temperature dropped below 150°F small inclusions were noted in the rotor blade ring. Raising the initial nozzle temperature maintained nozzle temperature above 150°F, eliminating the inclusion without adversely affecting blade ring quality.

A quantity of rotor blade rings has been molded for processing using all of the improvements discussed in this section.

Figure 3.10 — Trailing Edge Flaw in Injection Molded Rotor Blade Ring

34
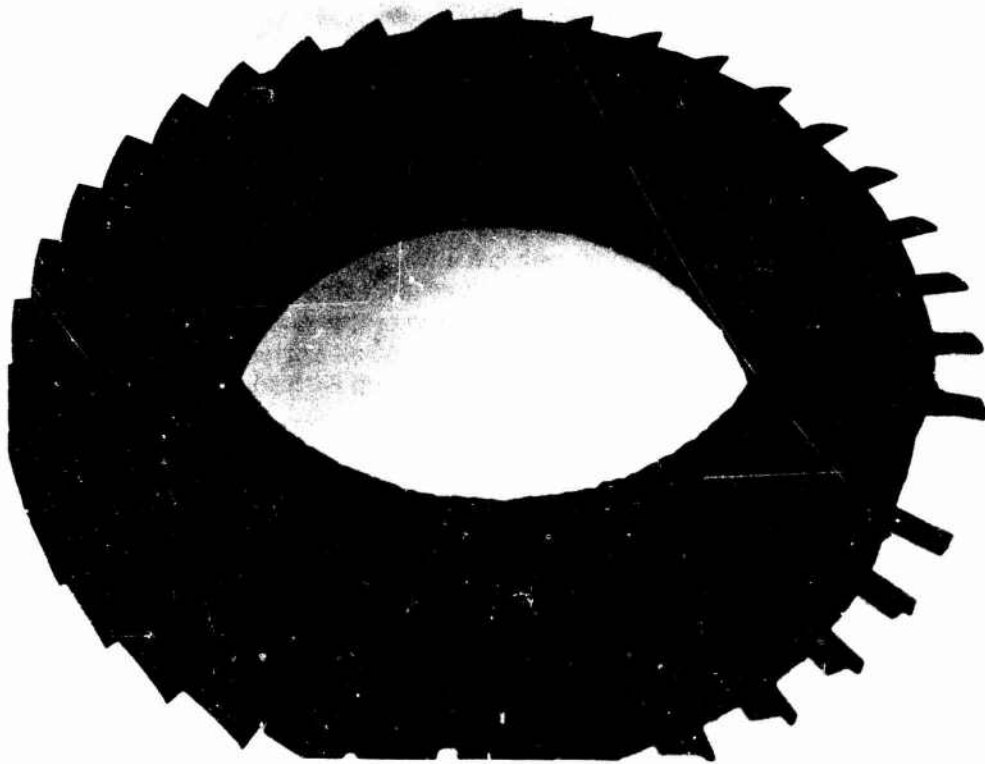
Figure 3.11 — Rim Flaw in Injection Molded Blade Ring

Figure 3.12 — Unmelted Inclusion in Injection Molded Blade Ring

Duo-Density Rotor Fabrication

After the blade ring has been fabricated and nitrided, the next step in the process is to slip-cast the blade fills which completely encapsulate the airfoils and the blade ring rim. This blade filling process was described in detail in the last report (10). The purpose of the blade fill is to provide support for the blades and the rim during the hot press bonding operation when the dense silicon nitride rotor hub is formed and bonded to the blade ring.

Previous to the last report, the primary approach taken was that of hot pressing a fully contoured hub while simultaneously bonding it to the reaction sintered blade ring shown schematically in Figure 3.13. This two piece fully contoured hub required hot pressing pressures of 4000 psi at 1750-1775°C for 3 hours when using silicon nitride powder with two weight percent magnesium oxide. The high axial load resulting from the 4000 psi acting over the entire area beneath the blade ring resulted in cracking
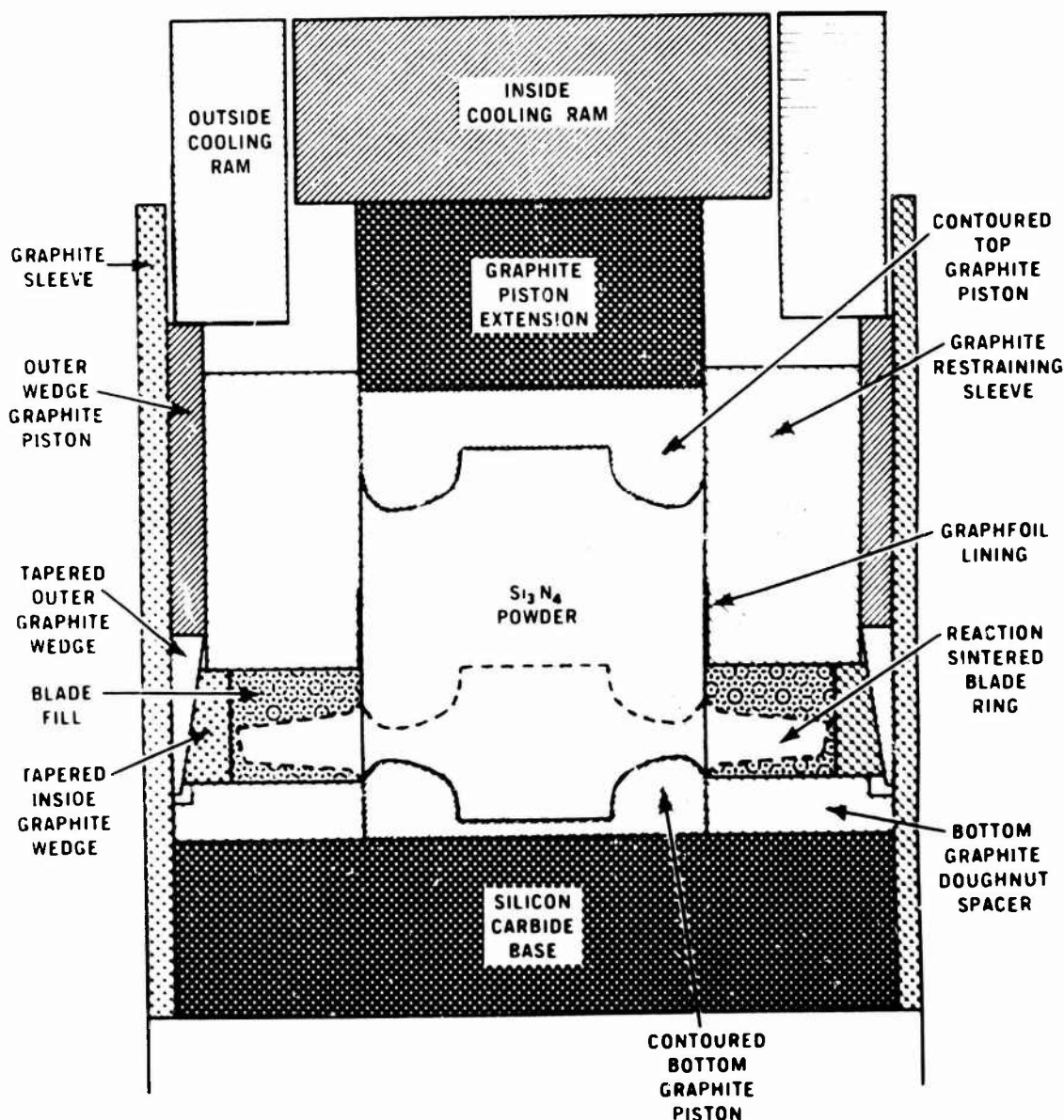
Figure 3.13 — Hot Press Bonding Assembly for Simultaneous Forming and Bonding of a Silicon Nitride Rotor Hub to a Blade Ring

of the blades in the fillet region where the blades join the rim. During the last reporting period (10) a three piece concept, shown in Figure 3.14, was introduced which reduced the axial loading during the bonding process to one-third of that previously used in the fully contoured two piece concept. The three piece concept consisted of hot pressing a hub to theoretical density, machining the outside diameter of the hub and attached graphite pistons, and then hot press bonding this preformed hub to the blade ring using a circular ring of hot pressed silicon nitride.

During this reporting period 46 rotors were fabricated utilizing the three piece concept. The hot pressed rotor hubs were fabricated from silicon nitride powder with 2-5 weight percent magnesium oxide and pressed at 5000 psi for three hours at 1775°C. The bonding ring was formed using 5 weight percent magnesium oxide, which was hot pressed at 1500-2500 psi for 3 hours at 1775°C during the assembly operation. Blade and blade rim cracking was usually minimal, and in some cases no cracking was observed. However, the problem of achieving uniform densification of the bonding ring persisted. Since a modification of the bond ring bottom contoured piston in the hot press (10) reduced the densification problem, both of the pistons were further modified to a flat configuration. The result indicated incomplete densification still occurred, as shown by the circle in Figure 3.15. As mentioned in the previous report (10) another technique was investigated to solve the problem. A preformed bond ring of silicon nitride powder with 5 weight percent magnesium oxide was cold pressed at 8000 psi and then hot press bonded to the hub and blade ring. This approach was taken to insure an even distribution of the silicon nitride powder in the bond ring cavity. However, the results, shown in Figure 3.16, indicated incomplete densification of the lower portion of the bond ring still occurred.

During the time this inconsistent densification problem was being investigated, another problem became apparent. Test bars were cut from several three piece rotors fabricated with systematically varied hot press bonding parameters and tested at elevated temperatures. The results, presented in detail in Section 4.2 of this report, indicated that the strength of the HPSN-to-HPSN joint between the hub and the bond ring was reduced from that of the parent materials. In addition, several rotors exhibited crack-like indications in the HPSN hub-to-HPSN-bond ring joint region which were revealed in an inspection of the rotors during the finish machining process.

As this troublesome bond problem became apparent, a parallel parameter study in hot pressing of Si_3N_4 showed that flat-sided HPSN disks could be made at pressing pressures as low as 500 psi. As a result, a two-piece duo-density Si_3N_4 rotor with a simplified flatter hub profile was considered.

The simplified two piece design, shown in Figure 3.17, eliminated the complex contoured shape of the rotor hub, thereby making possible the densification of the silicon nitride powder at pressures far below those previously required to produce a dense fully contoured hub. As noted above, a study on hot pressing of silicon nitride with various concentrations of MgO and under various pressures, reported in detail in Section 4.1 of this report, indicated adequate strength could be achieved in flat sided disks with hot pressing pressures as low as 500 psi. Ten design D′ duo-density rotors were fabricated in this simplified configuration using pressures of 500 to 1500 psi, with 3-1/2 w/o magnesium oxide added to the silicon nitride powder which was milled with tungsten carbide balls. Blade and rim cracking occurred on all rotors to some degree. A typical leading edge crack is shown in Figure 3.18. Three rotors having no rim cracks and minor blade cracking were selected and are in the process of being machined for rig and engine testing in order to evaluate this design.

Other areas in the rotor fabrication process were also evaluated during this reporting period. The effect of wedge pressure on blade ring deformation was found to be minimized at 1000 pound wedge loading. Below 1000 pounds, the hot pressed rotors exhibit axial cracks in the rim indicating insufficient load was applied to counteract the outward radial pressures exerted by hub densification. Wedge loads above 1500 pounds produced indentations between the blades in the rim as a result of pressure through the first blade fill material.

Another important observation was the significant reduction of blade root cracking problems at the blade fillet with the new design D′ blade ring. Because of the modified blade profile this blade ring design appears to be more compatible with the graphite wedge system fabrication concept.
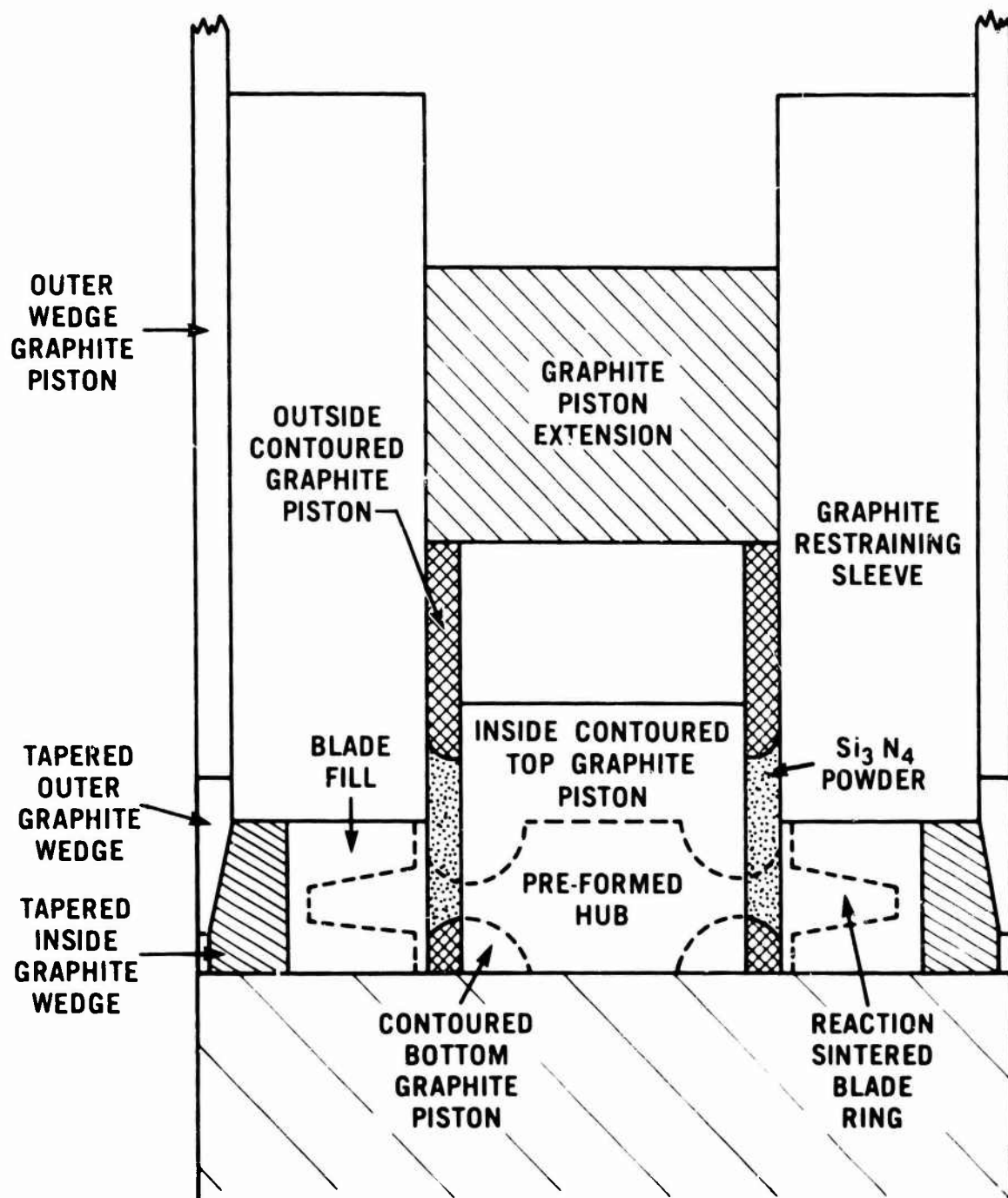
Figure 3.14 — Hot Press Bonding Assembly — Three Piece Duo-Density Concept

Figure 3.15 — Section of Press-Bonded Rotor Made Using Modified Contour Top and Bottom Pistons
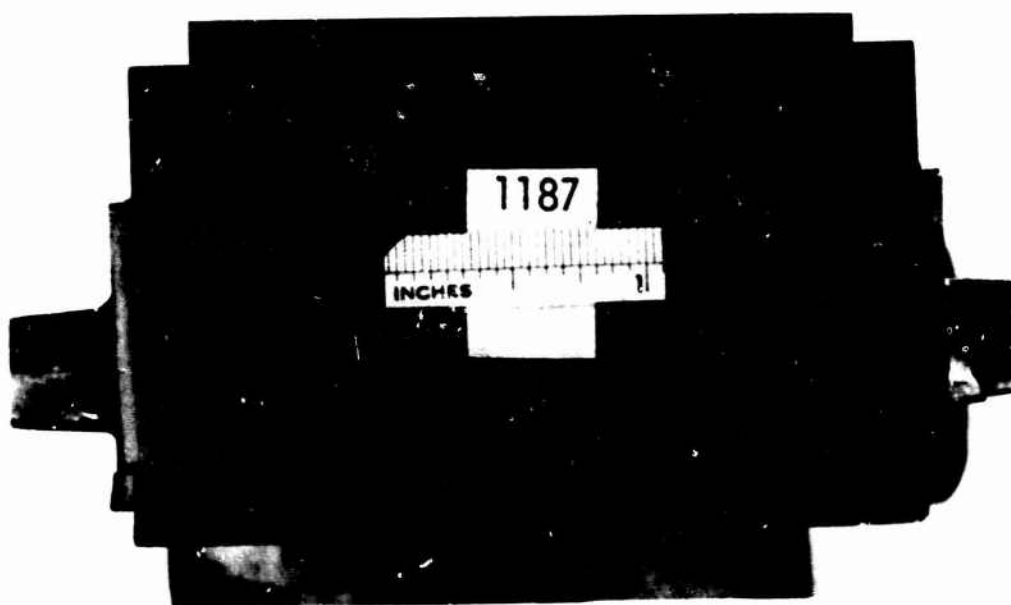
Figure 3.16 — Section of Press-Bonded Rotor Made Using a Dry Pressed Preformed Bond Ring
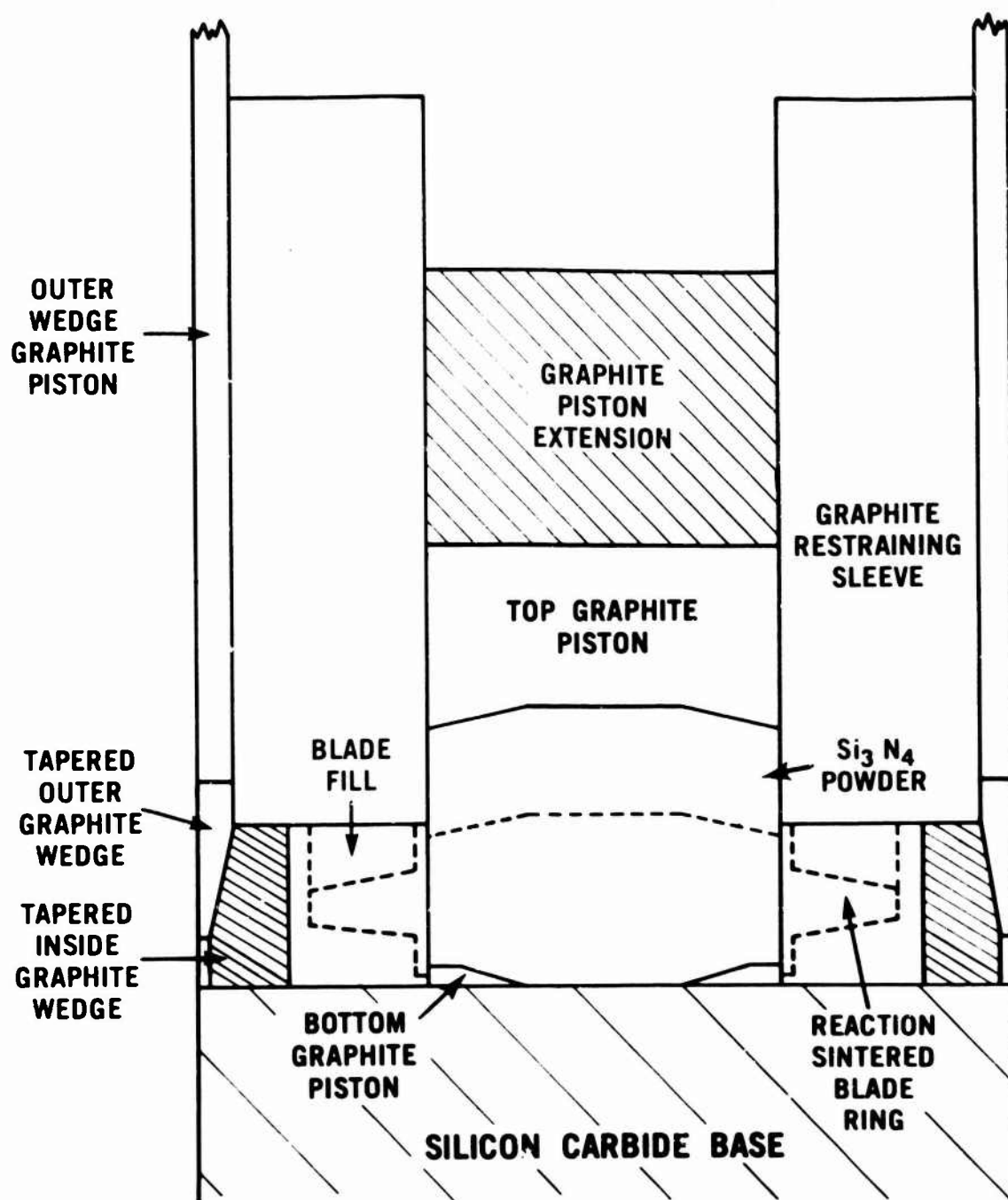
Figure 3.17 — Hot Press Bonding Assembly — Simplified Two Piece-Duo-Density Rotor Concept

TYPICAL LEADING EDGE CRACK
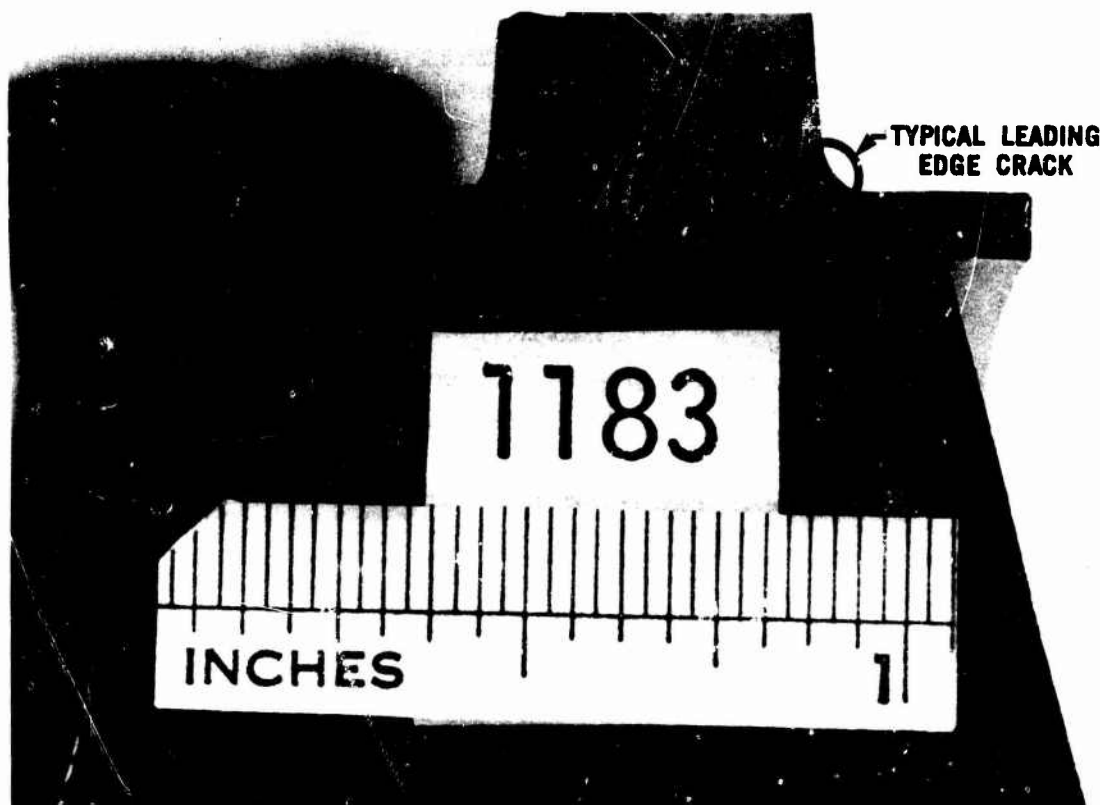
Figure 3.18 — Section of Press-Bonded Rotor Showing a Typical Blade Leading Edge Crack

Non-Destructive Evaluation

A number of Non-Destructive Evaluation (NDE) techniques were considered for the detection of flaws in complex gas turbine components. These techniques are listed in Table 3.5, which shows the current level of development for each of these techniques with respect to 1) their capability of detecting flaws in complex parts; 2) potential for rapid examination of these parts; 3) development time, development costs, and equipment costs, and 4) status or recommendation for future action.

A promising NDE tool, evaluated on a preliminary basis during this reporting period, was the Magnaflux MXK-100M Microfocus x-ray tube. This tube head is portable, weighs about eight pounds, and fits easily into a space less than four inches in diameter. It is particularly advantageous over the conventional x-ray tube because of its small focal spot of 0.05 millimeters which permits 1) film focal distance as low as 3 inches; 2) direct enlargements up to 36x; and 3) extremely fine resolution and geometric sharpness.

Because of these features the MXK-100M x-ray tube would be particularly useful for in-process inspection of duo-density rotor blade rings, where the portable features of the equipment would permit inspection at the molding site. A problem often encountered in the molding of turbine rotor blade rings is the existence of voids directly under the blades in the rim of the rotor. Using conventional x-ray equipment these voids can best be detected using 2 or 3 oblique x-ray views, as noted earlier in this section. A very important feature of the Microfocus x-ray tube is its suitability for design into a panoramic tube. Such a tube would emit a 360° circumferential beam, permitting a single radial shot of a cylindrical object. An example of a simulated panoramic x-ray of a turbine rotor blade ring can be seen in Figure 3.19. This particular film was made using the standard Microfocus tube, and even though the sharpness is not good for all the blades, it is obvious that a circumferential crack exists as well as a void in the rim under one of the blades.

Summarizing the NDE work during this reporting period, activity was concentrated on the immediately useful techniques such as stator vane load testing (Section 3.2.1 of this report) and the preliminary investigation of the Microfocus x-ray tube. As a result the stator vane load test fixture is very nearly operational, and the Microfocus x-ray tube, including the panoramic tube design, is expected to be procured and utilized during 1977. Other techniques such as infrared thermography and the electrostatic method, will be assessed at least through a feasibility study. A third group of N.D.E. techniques include ultrasonics, holosonics, and x-ray tomography. These techniques are considered to require extensive additional development before application could be expected.

TABLE 3.5

CURRENT LEVEL OF DEVELOPMENT FOR NDE TECHNIQUES UNDER CONSIDERATION

CRITERIA	N.D.E. TECHNIQUE						
	Microfocus X-ray	Infra-red Thermography	X-ray Tomography	Electrostatic Method	Holosonic Method	Mechanical Load Testing	High Frequency Ultrasonic
1. Capability of detecting flaws in complex parts	Large flaws	N.D.*	Large flaws	If flaw is put under load	N.D. Feasibility demonstrated only on simpler shapes	Detects flaws through failure. Not a direct indication of flaw	Potentially useful for small flaws, difficult to apply to complex shapes
2. Provides rapid examination of complex parts and gives simple answers	Yes, may be improved with panoramic X-ray tube	N.D.*	Very attractive can store data for pictorial or numerical rapid output	N.D.	N.D.	Yes.	N.D.*
3. Development time and cost estimates	Reasonably short time, low development and equipment cost	N.D.*	Very expensive particularly equipment costs	Short development time, potentially inexpensive	Long development time, high equipment costs	Inexpensive	High development and equipment lists
4. Status or recommendation	Proceed to develop and apply as rapidly possible	Proceed with feasibility study	Proceed on small in-house program. Seek support for larger program	Proceed with feasibility demonstration	Recommend technique for other programs which use hi-frequency equipment	Currently used on stators	Keep abreast of ongoing development work

* N.D. — not determined

Figure 3.19 — Simulated Radial Panoramic View of Turbine Rotor Blade Ring Made
Using Microfocus X-Ray Equipment

Introduction

Rotor testing during this reporting period concentrated on continuing rotor blade bend testing, hot spin rig development, spin pit testing of hot pressed silicon nitride rotor hubs, and lubricant tests for interfacing materials between the ceramic rotor and mating metal components. As reported previously, (9, 10) the blade bend test has been used to evaluate blade strength differences between slip cast and injection molded materials and to evaluate heating and thermal shock effects. The vacuum spin pit was used to evaluate rotor hubs fabricated by a unique hot pressing technique devised by AMMRC. The development of the hot spin rig continued with emphasis placed on improving, the failure detector system, temperature measuring system, and burst absorption capability. The curvic teeth on the rotor shaft and curvic coupling adaptor, used in engine testing of ceramic turbine wheels, have been gold plated to increase the operating temperature capabilities and reduce friction of the ceramic rotor interfaces.

Blade Bend Testing

Blade bending testing of 2.7 gm/cc density D' blade rings and rotors continued during this reporting period. The procedure for this test remained unchanged from that described in the previous report (10).

The blade bend test supplies useful information on the quality of the nitriding cycle For example, comparing the results for blade rings 1773, 1775, 1778, and 1779 versus 1377, 1386 and 1410 as shown in Table 3.6, the characteristic failure loads of the first group nitrided in 100 percent nitrogen are noticeably lower than the second group nitrided in a 4 percent hydrogen — 96 percent nitrogen atmosphere.

Table 3.6 also shows blade failure load test results for a third group (1759, 1747, and 1737) of blade rings nitrided in four percent hydrogen — balance nitrogen. The characteristic failure loads of this group of blade rings are also significantly higher than blade rings nitrided using 100 percent nitrogen. This third group of blade rings also had slightly higher characteristic failure loads than the second group, even though both groups were nitrided under the same conditions. No apparent reason was found for this difference.

TABLE 3.6

SILICON NITRIDE DESIGN D' BLADE BEND TEST RESULTS
Injection Molded 2.7 gm/cc Density Material

Blade Ring Number	Number of Data Points	Weibull Slope	Characteristic Load (lbs.)	Nitriding No. Atmosphere
1773	8	6.5	67	B-56/100% N_2
1775	11	10.0	71	B-56/100% N_2
1778	7	12.2	65	B-56/100% N_2
1779	10	10.0	71	B-56/100% N_2
1377	18	6.6	82	B-48/4% H_2 96% N_2
1386	15	13.8	89	B-48/4% H_2 96% N_2
1410	19	14.1	95	B-48/4% H_2 96% N_2
1759	24	8.9	99	B-54/4% H_2 96% N_2
1747	24	16.3	110	B-54/4% H_2 96% N_2
1737	24	8.0	105	B-54/4% H_2 96% N_2

Cold Spin Testing

The vacuum cold spin pit was used to evaluate four silicon nitride rotor hubs fabricated by the Army Materials and Mechanics Research Center (AMMRC). These hubs consisted of two individually hot pressed halves which were ground flat at the adjoining surfaces and bonded into an integral hub configuration

Figure 3.20 shows a finish machined rotor hub, made by this process, ready for spin testing. The bond interface between the two hot pressed halves is visible as a lighter colored line on the hub outer diameter. The only machining required to prepare the hubs for test was grinding of the axial faces, centerbore, outside hub diameter, and radii on all edges. The rotor hubs were inspected radiographically and by fluoresent dye penetrant. The dye penetrant revealed tight cracks on the inner axial faces of hub A.
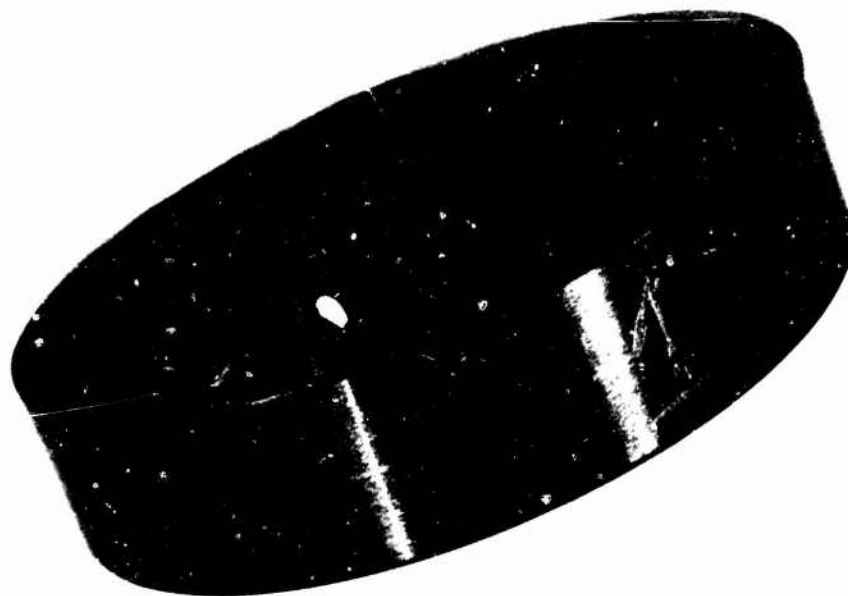
Figure 3.20 — Hot Pressed Silicon Nitride Final Test Hub

Test procedures reported (2,7,8,9,10) were used in cold spin testing these rotor hubs. The test results are shown in Table 3.7.

TABLE 3.7
COLD SPIN TEST RESULTS OF AMMRC ROTOR HUBS

Hub Number	Failure Speed — RPM
A	73,450
1	76,820
5	81,050
6	73,050

A finite element stress analysis was made for rotor hub A, which failed at 73,450 rpm, that showed the maximum principal stress at this speed was 25,250 psi at the center bore. The fragments from these tests have been returned to AMMRC for analysis.

Hot Spin Test Rig

Development of the hot spin test rig continued in preparation for the determination of the correlation between predicted and experimentally determined failure distributions of ceramic turbine rotors. Serveral problem areas in the test rig were identified and modifications in the rig design were evaluated.

Failure Detector

The failure detector system in the hot spin test rig, which was described in the previous report (10), consists of a cylinder of insulating material wound with closely spaced 0.010 inch diameter chromel wire. Figure 3.21 shows the detector mounted in its metal housing. When a turbine rotor fails, the chromel wire is broken by fragments and provides a signal for shut-down of the driving dynamometer by loss of electrical continuity.

A problem with the failure detector developed when failures were signaled, and subsequent examination showed the test rotor to be intact, although a wire in the detector circuit had broken. Examination of the wire revealed that oxidation was occuring and causing the wire to become brittle. Turbine rotor testing in the hot spin test rig subjects the failure detector to many combustor light-offs, wire temperatures to 1800°F, and a cool down before the next light-off. It is believed that the stresses imposed in the chromel wire by expansion and contraction during this cycling were excessive because of the oxidized, brittle condition of the wire. A search was begun to find a new wire with improved high temperature capability and resistance to oxidation. Platinum wire, 0.010 inch diameter, was found to meet these criteria.
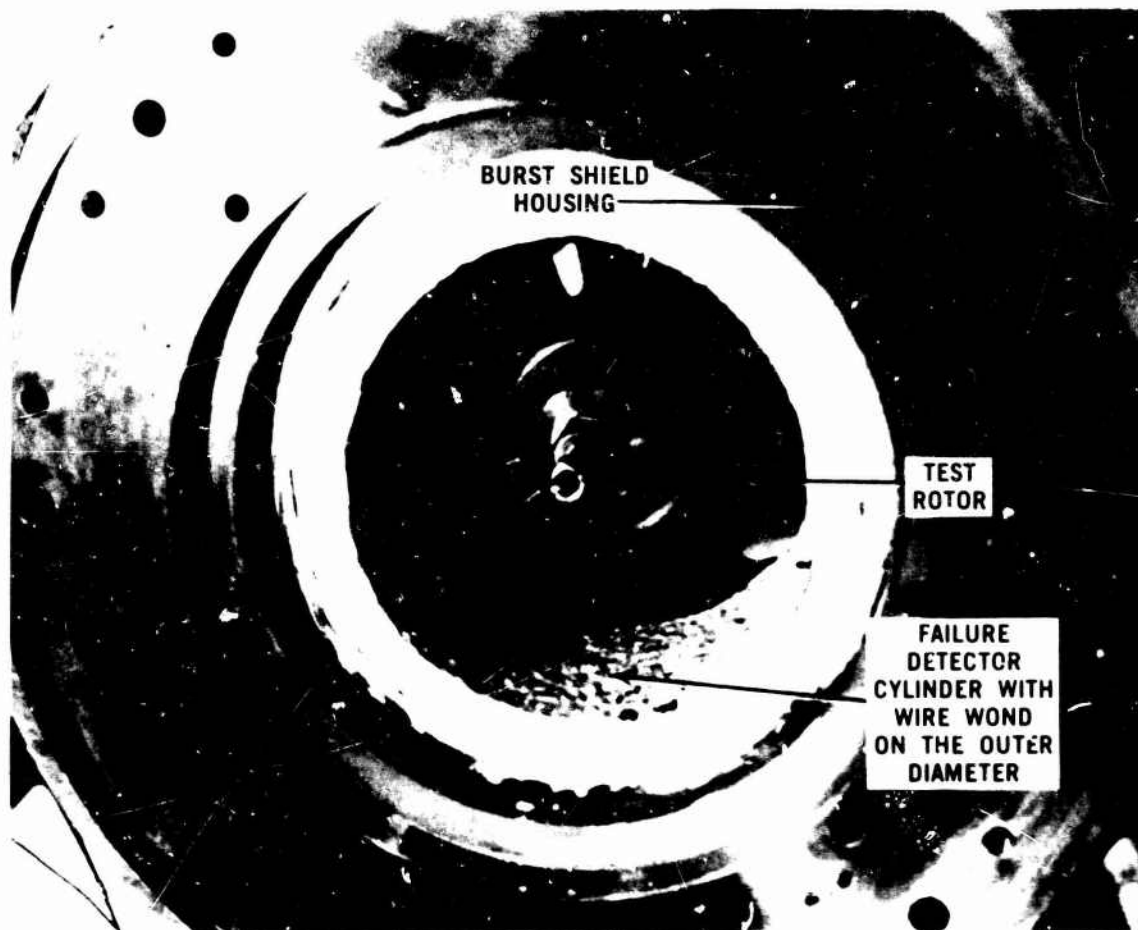
Figure 3.21 — Hot Spin Rig Failure Detector Mounted in the Burst Shield Housing

Another problem which was discovered was that the insulation ring around which the wire was wrapped was drying out and shrinking from the housing during the hot tests. The normally taut wire moves and touchs its neighbor, shorting out the entire assembly and shutting down the test. A procedure has been developed to wrap the insulation ring with wire after the ring has been pre-shrunk in an oven at 1500°F for two days.

Testing of pre-shrunk, platinum wound detectors is in progress and these modifications appear to have solve the problems encountered.

Radiation Pyrometer Mounting

Accurate temperature measurement by a radiation pyrometer requires a clear view of the target object without interference from another object at a different temperature. Until the present reporting period, the radiation pyrometer was mounted on a tripod and focused on the rotor rim by viewing through a hole in the combustor cover between two combustor tubes through a slot in the nose cone insulator. Considerable time was consumed in setting up the pyrometer. Additionally, the pyrometer required resetting each time a temperature measurement at a different radius on the rotor was desired. During this reporting period, a mounting bracket for the pyrometer was designed and built (Figure 3.22) which, when bolted to the hot spin rig adaptor, will automatically align the radiation pyrometer with the rim of the rotor. During rig operation, the bracket arm can be swiveled to record temperature at four radii on the blade, the rotor rim, and four radii on the rotor hub with assurance that the line of vision of the optical pyrometer is unobstructed. This bracket has functioned as designed.
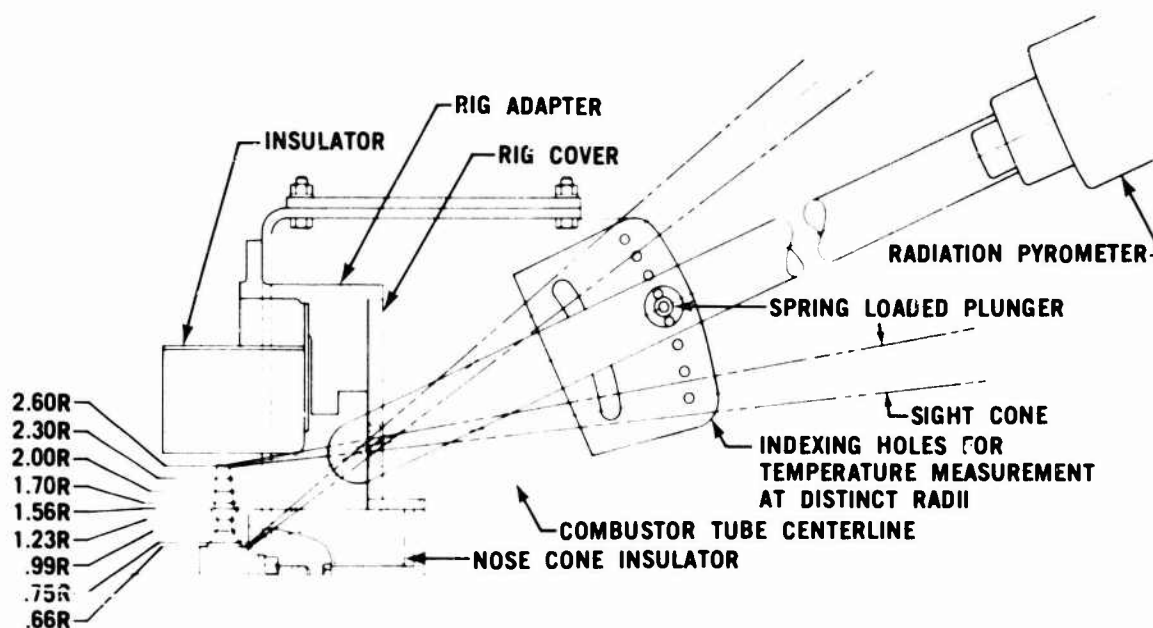
Figure 3.22 — Radiation Pyrometer Mounting in the Hot Spin Rig, Showing Temperature Measurement Locations on a Test Rotor

Hot Spin Rig Burst Absorption Capabilities

Several design changes were previously made in the hot spin rig to reduce turn-around time (10). During this reporting period, further improvements were made which reduce the shaft damage caused by a high speed rotor burst. These include a silver plated turbine shaft labyrinth seal and a silver plated turbine shaft bearing. Thus, contact between the bearing and labyrinth and the turbine shaft at failure should confine the resulting damage to the soft labyrinth seal and bearing and cause minimal damage to the rotor shaft. A bladeless ceramic rotor was accelerated to 64,840 rpm and the temperature

gradient was increased until failure occurred, to assess the burst absorption capability of the test rig and resulted in the following damage:

- The tension member of the bolt fractured as designed and as experienced in previous tests.

- The ceramic fiber insulation and its stainless steel backing absorbed the energy of the burst rotor. Only slight deformation of the insulation backing was noted (Figure 3.23) and this was easily repaired.

- The turbine rotor shaft at the bearing journal was slightly scored (Figure 3.24).

All of the above damage was quickly repaired, which demonstrates relatively fast turn-around time.
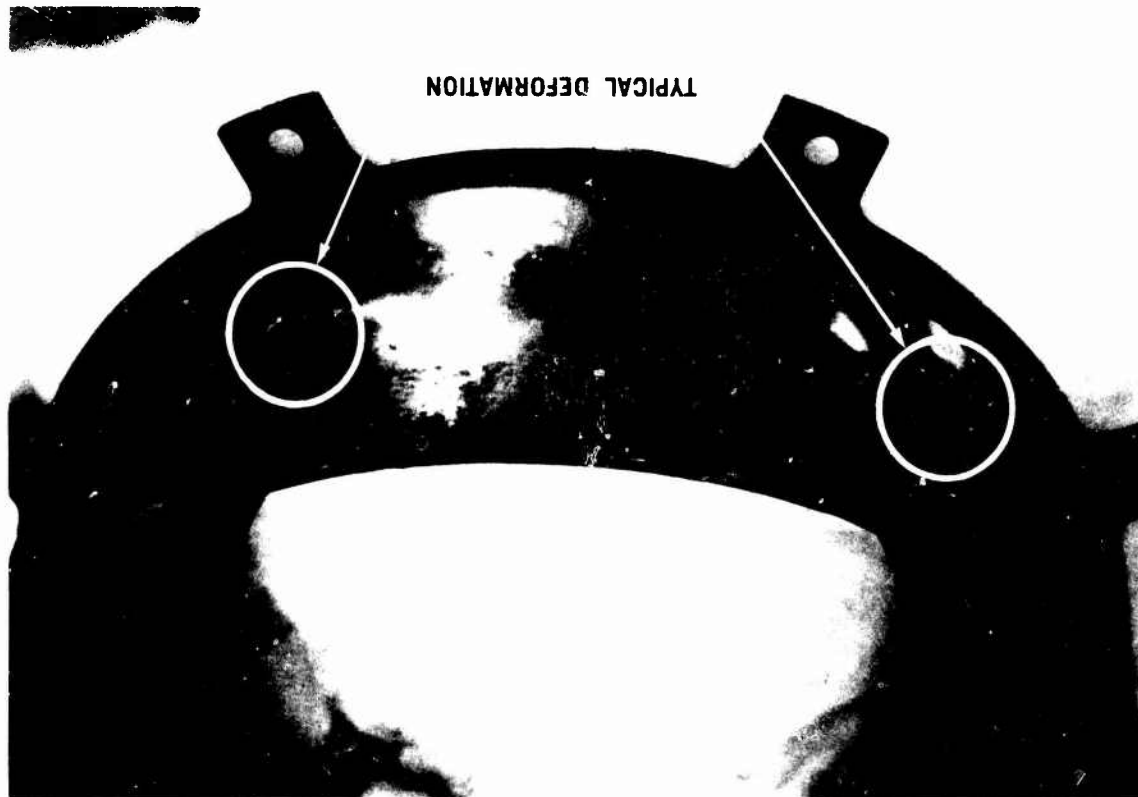
Figure 3.23 — Stainless Steel Insulator Shell After Full Speed Rotor Burst (Ceramic Fiber Insulation Removed)

Rotor Attachment

Investigation of improvements, in the curvic coupling rotor attachment system was continued.

One problem was to reduce the high frictional forces generated when the metal parts expand more than the ceramic parts with which they mate. Some reduction of these forces has been accomplished by two methods:

(1) Separating the ceramic to metal interfaces with a shearable intermediate substance such as Nickel Ease (TM), Molykote (TM), Electrofilm (TM), etc. which would not allow ceramic-to-metal contact which would produce high friction and loads.
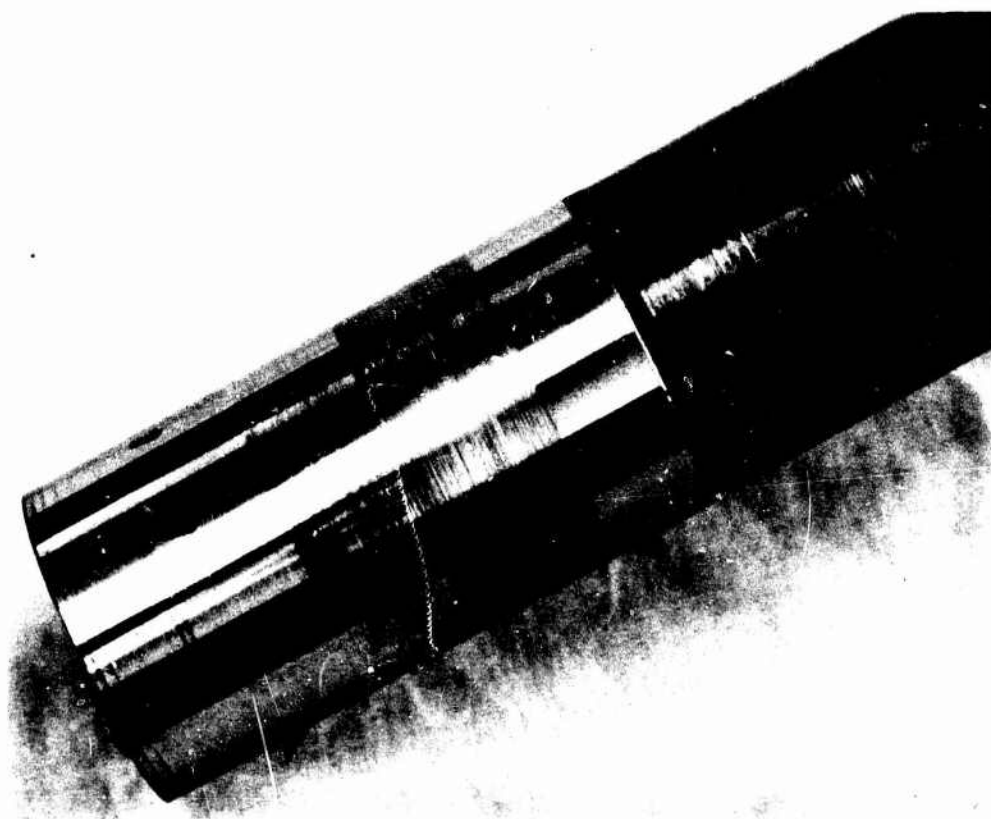
Figure 3.24 — Rotor Shaft Turbine Journal Bearing After Full Speed Rotor Burst

(2) Changing the basic characteristics of one of the two contacting surfaces and hence alter the frictional nature of the interface.

The search for a durable, high temperature lubricant between the ceramic rotor Curvic teeth and metal parts, discussed in previous reports (4, 5, 9, 10), has continued. The best lubricant previously tested (10) was a ceramic-bonded graphite and molydisulfide lubricant called Electrofilm 1000X (TM). This compound has survived three cycles of a simulated engine load and thermal cycle test (10). Observation of the lubricant after test indicated that it has limited life because of the high operating temperature (1400°) required. The manufacturer recommends a maximum operating temperature of only 1000°F.

During this reporting period, the Curvic teeth of a metal Curvic adaptor (10) were coated with 99.5% pure gold to form a permanent layer of shearable material between the ceramic rotor Curvic and the metal Curvic adaptor. The gold coating was electroplated to a thickness of 0.00025 in. over nickel strike on the Inconel 750 adaptor. Only the contacting surfaces of the Curvic teeth were coated. The Curvic adaptor was tested through four simulated engine thermal cycles to 1400°F without failure of the ceramic and without significant deterioration of the gold plate.

Observation of the parts after testing indicates that part of the gold plate transfers to the ceramic material during cycling and lightly bonds the metal Curvic adaptor to the ceramic. However, the parts are easily separated using only a slight force. The frictional character of the interface appears to be changed to that of a gold to gold interface, considerably reducing the frictional loads. This gold coating will be further tested in engine tests of rotors at both the metal Curvic adaptor and main shaft Curvic coupling locations.

SUMMARY

Fabrication of turbine inlet nose cones and stators was resumed on a very limited basis. A 2.7 g/cc density silicon nitride material was utilized for the first time for injection molding of these components.

Two additional test rigs were built for use in pre-engine test evaluations of ceramic stators. One of these rigs, the stator vane mechanical load test fixture, serves a two-fold purpose 1) as a tool to evaluate material and processing variations, and 2) as a screening tool to qualify stator vanes for subsequent engine testing. The other rig, the stator outer shroud pressure test fixture, evaluates the stator outer shroud quality before subsequent engine testing. These new tools were utilized to enhance the qualification of stationary ceramic flow path components. The initial evaluation of the 2.7 g/cc density Si_3N_4 components is underway. In addition, a review of past weight gain data for 2.55 g/cc density Si_3N_4 stators tested at 1930° was completed.

Work continued in a number of areas relating to the operation of the 2500°F flowpath qualification test rig. To date the rig has accumulated 74 lights and 181 hours of hot time above 1900°F. Fifteen of these hours were run at a combustor exit temperature of 2500°F.

3.2.1 MATERIALS AND FABRICATION

Introduction

While the major effort on materials and fabrication development continued to be applied to ceramic turbine rotors blade rings, a very limited fabrication run of nose cones and stators utilizing the recently developed 2.7 g/cc density Si_3N_4 was made.

Stator Fabrication

During this reporting period, initial attempts were made to mold some 2.7 g/cc density silicon nitride stators needed for testing. Using the 2.7 g/cc density material developed for rotor blade rings, attempts were made to optimize the molding conditions. Although it was possible to fabricate stators with no visible molding flaws, fold lines or voids, fillet cracks remained in the stator inner shroud-vane area. The initial composition exhibited shrinkage incompatible with the stator tooling over the range of molding conditions investigated. To reduce shrinkage, the tool temperature was raised, but the material tended to stick in the gate area of the sprue detail. The particular sprue detail utilized was the overflow type which feeds three vanes at the inner shroud inner diameter (Figure 3.25). Sticking in the gate area resulted in fillet cracks in the stator inner shroud-vane area when the tool was opened. The sprue detail was removed to have the gate area teflon coated.

In order to continue development of the stator molding process, an available sprue detail of alternate design was installed in the tool. This detail contains 25 large runners (Figure 3.26). Because of the large runner cross-section, sticking in the gate area was not a problem. Other problems, however, associated with this sprue detail have been previously reported. Molding at the previously established conditions and the higher tool temperature resulted in several crack free stators. The predominance of fabricated parts, however, exhibited fillet cracks attributed to high material shrinkage.

Switching to a different organic molding composition — still at the 2.7 g/cc density level — having a lower shrinkage rate during cooling, was attempted. This composition was previously used successfully at the 2.55 g/cc density level in both the stator and nose cone tooling. The composition was altered to the 2.7 g/cc density level and stator molding attempts initiated with limited success. A sufficient quantity of crack free stators, as evaluated in the as-molded condition, was obtained to warrant further processing. Blade quality was good but outer shroud quality was poor as a result of using the 25 gate sprue detail. Future plans for stator fabrication are to utilize this latest 2.7 g/cc density composition in conjunction with the teflon coated overflow sprue detail.

Nose Cone Fabrication

As was the case with the stator fabrication effort, the new 2.7 g/cc density Si_3N_4 material was utilized in the first attempts to mold turbine air inlet nose cones. This effort was further complicated with the tooling revisions needed to produce the new Design D' nose cone, shown along with the Design C nose cone in Figure 3.27, and the installation of an automated molding control system (Section 3.1.2 of this report).

The low-shrinkage 2.7 g/cc type material developed in the stator fabrication effort was utilized from the onset for these molding trials. Initial problems were encountered with the Design D' tooling. Excessive leakage necessitated rework of the tool. Following this rework, visually good nose cones were molded. However, further processing of nose cones (burnout, argon sintering and nitriding) revealed fine cracks at the fillet between the strut and the inner nose. These cracks have been traced to outer slide movement during withdrawal of the strut core pins in the tool. A system to pull core pins without moving the outer slides has been designed and will be implemented during the next nose cone molding run.

An automated molding control system was installed on the injection molder and evaluated. Its use significantly aided optimization of the nose cone molding parameters and resulted in increased yield from 6/day to 32 visually good nose cones/day in the as-molded condition.
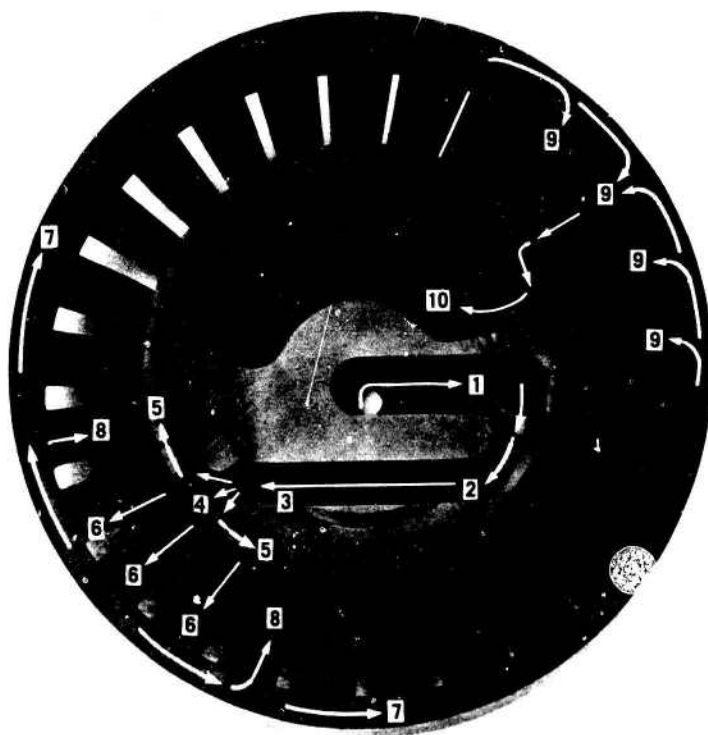
Figure 3.25 — Design D' Stator with Overflow Sprue Detail; Directions of Material Flow Shown by Arrows and Numbers
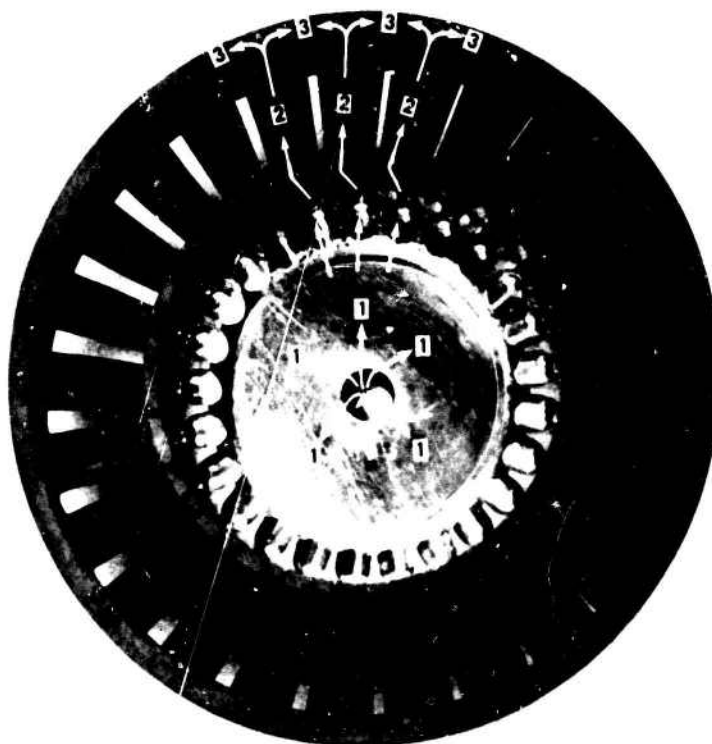
Figure 3.26 — Design D' Stator with 25 Gate Sprue Detail; Directions of Material Flow Shown by Arrows and Numbers
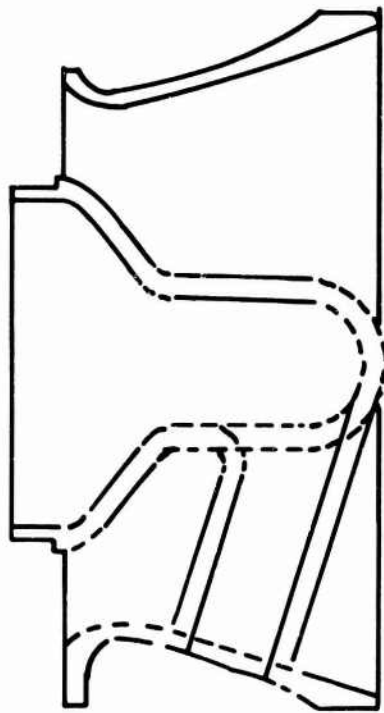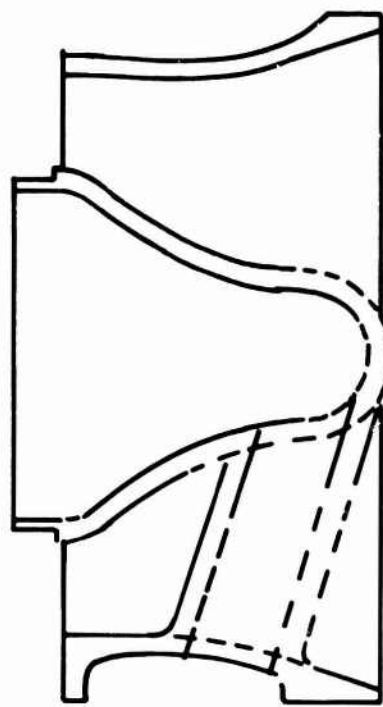
DESIGN C NOSE CONE   **DESIGN D' NOSE CONE**

Figure 3.27 — Cross-Section View of Design C and Design D' Nose Cones

3.2.2   TESTING

Introduction

The Design D' stationary hot flow path components include the combustor, turbine inlet nose cone, common first and second stage stators, and first and second stage rotor tip shrouds. A very limited fabrication effort of turbine inlet nose cones and stators resulted in a few of these parts of imperfect quality being received for testing.

The testing centered on qualification of components for subsequent engine testing. As described in previous reports (6,9,10), stationary ceramic flow path components are initially subjected to a qualification test before being considered acceptable parts for engine testing. This is done in order to screen out parts with fabrication and/or processing defects. This qualification test, in the past, consisted of subjecting the part to 10 cold lights, each followed by a prescribed hold time at temperature and an engine shutdown (10).

However, past testing of components indicated that this 10 light qualification test was successful in eliminating poor quality nose cones and rotor tip shrouds but did not adequately screen out poor quality stators. In order to better evaluate stators prior to engine testing, two additional non-destructive qualification tests are being developed. They are a stator vane bend test and a stator shroud pressure test.

Stator Vane Bend Testing

Stator vane testing was initiated as a basis for establishing a quality control measure to assess material and process improvements (8). For stators to be accepted as engine test candidates, the stator vane bend test must be non-destructive. A need was recognized for a simple test fixture that would permit the proof testing of stators prior to machining. Such a test fixture would not only eliminate poor quality parts at a substantial cost savings, but would also permit rapid correlation between visual inspection data and the mechanical integrity of the stator vane.

During this reporting period such a fixture was built and calibrated, and preliminary testing was initiated. The test fixture, shown in Figure 3.28, consists of a series of twenty-five 0.250 inch diameter pins which independently load the vanes at the inner shroud of each vane. The inner shroud is separated from its neighbors by a thin slot, thus each vane is loaded independently. The part is secured in the fixture by means of six clamps around the outer shroud of the stator. A variable load is applied at the inner shroud by the pins, which places the leading and trailing edges of the vanes in tension. To obtain this variable load, pressure is applied to the pins via a hydraulic system.

Figure 3.29 illustrates the initial calibration results for the stator vane load testing fixture. This curve shows a maximum variation between pins to be about 5 pounds over the 0-700 psi calibration range. Although considered to be acceptable, it is possible that the spread between pins could be improved by reducing friction. This is currently being investigated.

During shake down of the proof test fixture, the fixture was also used as a destructive test device to evaluate the new 2.7 g/cc density Si_3N_4 stators.

Figure 3.30 gives statistical results of data presented in a previous report (9) for stators 829 and 848 along with that from more recently tested stators 1036, 1047 and 1124. The data reveals a marked improvement in stator vane load carrying capability for the more recent stators. Of note is that a significant difference in density exists. Stators 829 and 848 are 2.55 g/cc density while stators 1036, 1047 and 1124 are 2.7 g/cc density. All five of these stators were nitrided in a similar manner.

Figure 3.31 gives statistical results of data from two groups of stators which are all 2.7 g/cc density Si_3N_4 but are processed under different nitriding conditions. Stators 1057, 1083 and 1064 were part of a nitriding run during which a malfunction of the nitrogen gas sensors occurred. The resulting vane load capability shows a deterioration to a level comparable to properly nitrided 2.55 g/cc density parts. The importance not only of density but of close control of the nitriding cycle can be seen from these results.

55

In Section 3.2.1 of this report on stator fabrication, it was noted that initial 2.7 g/cc density stators contained fillet flaws in the outer shroud - vane area. The stator vane bend test was utilized to evaluate the effect of these flaws with regard to vane load capability. Figure 3.32 gives statistical results from two 2.7 g/cc density stators. Stator 1036, previously referred to, yielded results typical of good quantity 2.7 g/cc stator vanes. Stator 1103, without including data from vanes 6, 7, and 8, yielded comparable results. Of note is that vanes 6, 7, and 8 broke at loads less than seven pounds. These low failure loads can be directly attributed to the presence of fillet cracks which extended to the leading edge of the vanes. Work continues towards the determination of the correlation of flaw size and orientation with acceptance for engine testing.

Use of the stator vane bend test as a screening tool required the establishment of a screening load. Based on data contained in a previous report (8), it can be seen that stator vanes capable of greater than 4-5 pounds bend load did not fail under actual engine light offs (0.30 hours and 16 lights). Using this information and the fact that flaw-free vanes typically are capable of greater than 10 pounds bend load, an initial screening bend load of 10 pounds has been selected. To date, five 2.7 g/cc stators have been subjected to the stator vane bend qualification test. Two of the stators, 1055 and 1086, were of extremely poor quality, being from the group of initial 2.7 g/cc density stators which experienced the molding fillet crack problem. Stator 1086 passed, but five vanes on stator 1055 failed. The other three stators successfully passed the 10 pound stator vane bend test.

Figure 3.28 — Stator Vane Mechanical Test Fixture
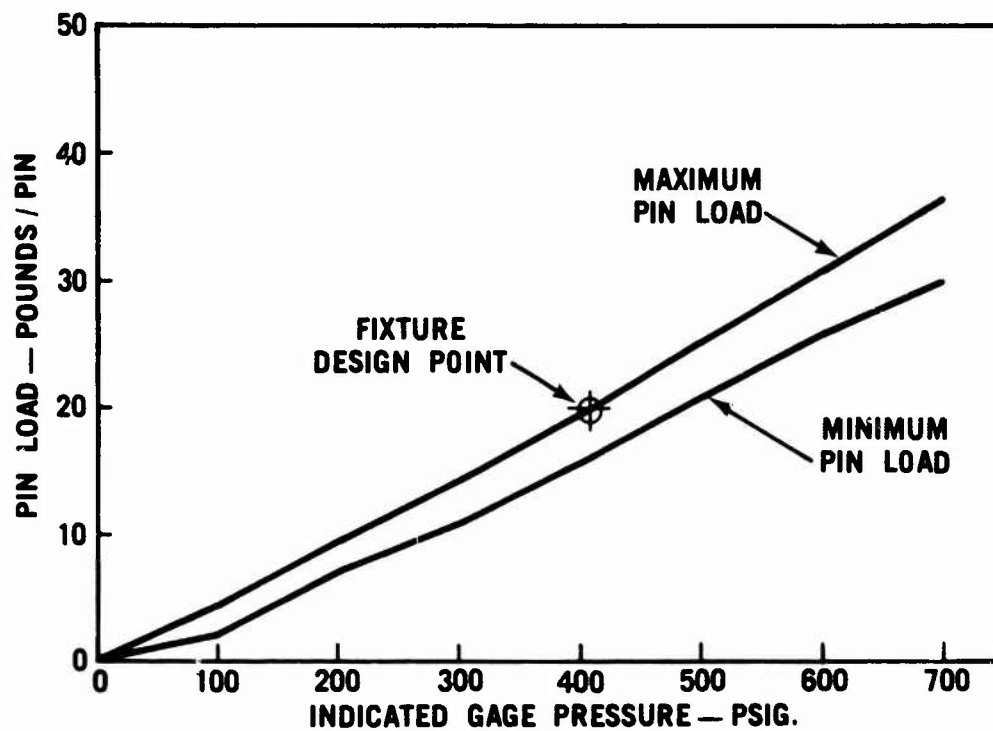
Figure 3.29 — Calibration Curve of Stator Mechanical Test Fixture
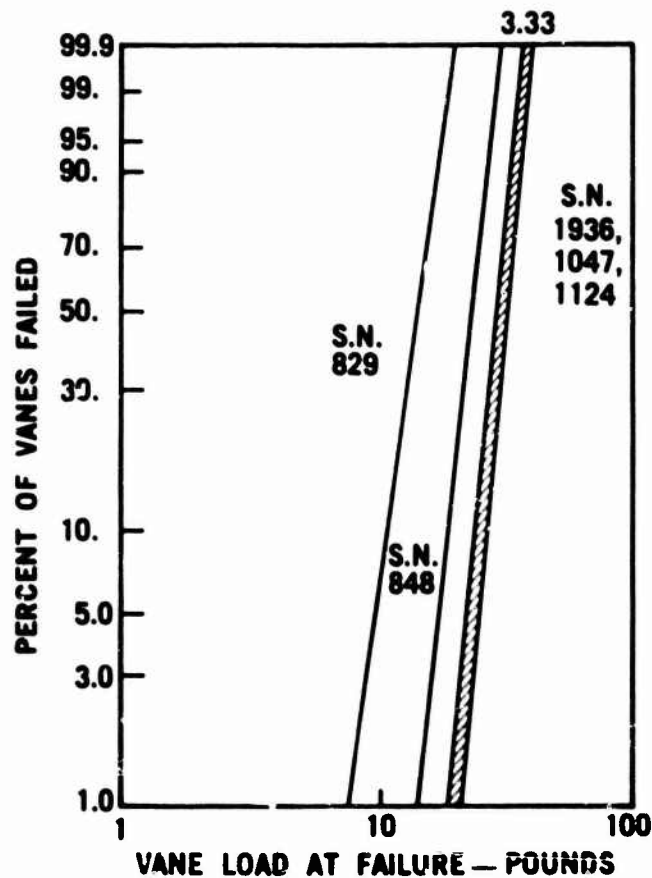
Figure 3.3e — Weibull Distributions of Stator Vane Breaking Loads
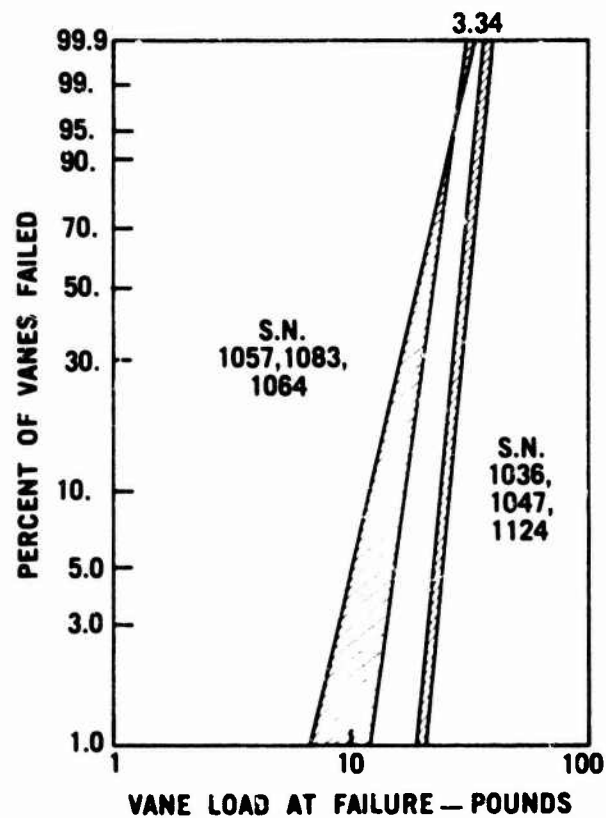
Figure 3.31 — Weibull Distributions of Stator Vane Breaking Loads
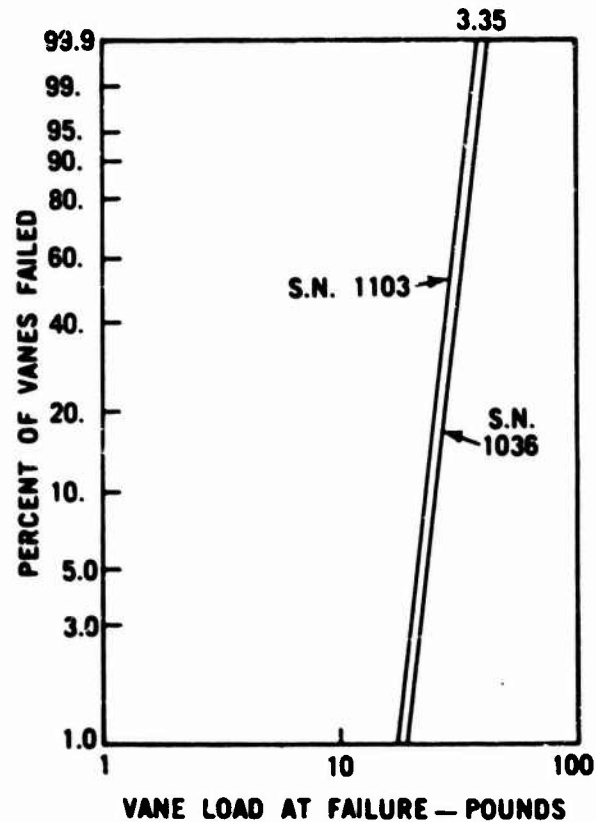
Figure 3.32 — Weibull Distributions of Stator Vane Breaking Loads

Stator Outer Shroud Pressure Test and 10 Light Test

The second of these new qualification tests is the outer shroud pressure test. In this test the stator is supported between two flat steel plates and a pressure is applied to the stator outer shroud inner diameter, putting the stator shroud in tension (Figure 3.33).

As in the case of the vane bend test, it was necessary to establish an appropriate screening stress level. A thermal analysis indicated that the maximum transient thermal stress in the outer shroud is tensile and is approximately 200 psi. This was established as a minimum level for outer shroud qualification. In order to obtain an upper bound on the qualification stress, four good quality 2.55 g/cc density stators were pressure tested to failure. The data was plotted on Weibull paper and yielded a characteristic strength of 11,000 psi and a slope of 7.6. From this data, a maximum level of 9,000 psi was established for outer shroud qualification. For initial 2.7 g/cc stators, the minimum level will be utilized with the intent of modifying it if future data indicates a change is warranted.

During this reporting period, several stators of 2.7 g/cc density were fabricated and finish processed. Although many of these stators contained flaws as discussed in Section 3.2.1 of this report, it was deemed worthwhile to obtain initial data from these components.

Of the 2.7 g/cc stators which passed the bend test, as noted earlier in this section, three have proceeded to the stator outer shroud pressure test. All three stators successfully passed this step in stator qualification prior to engine testing.

The last step in pre-engine test qualification is the 10 light test. Three stators, 1086, 1099 and 1117, have been subjected to the bend test and the 10 light test. Stator 1086 was categorized as poor quality because of the presence of numerous fillet cracks as previously noted. However, these cracks did not extend to either the leading or trailing edges and the part passed the bend test. During the 10 light test, seven vanes failures and one shroud crack were noted. The other two stators, 1099 and 1117, passed the 10 light test.
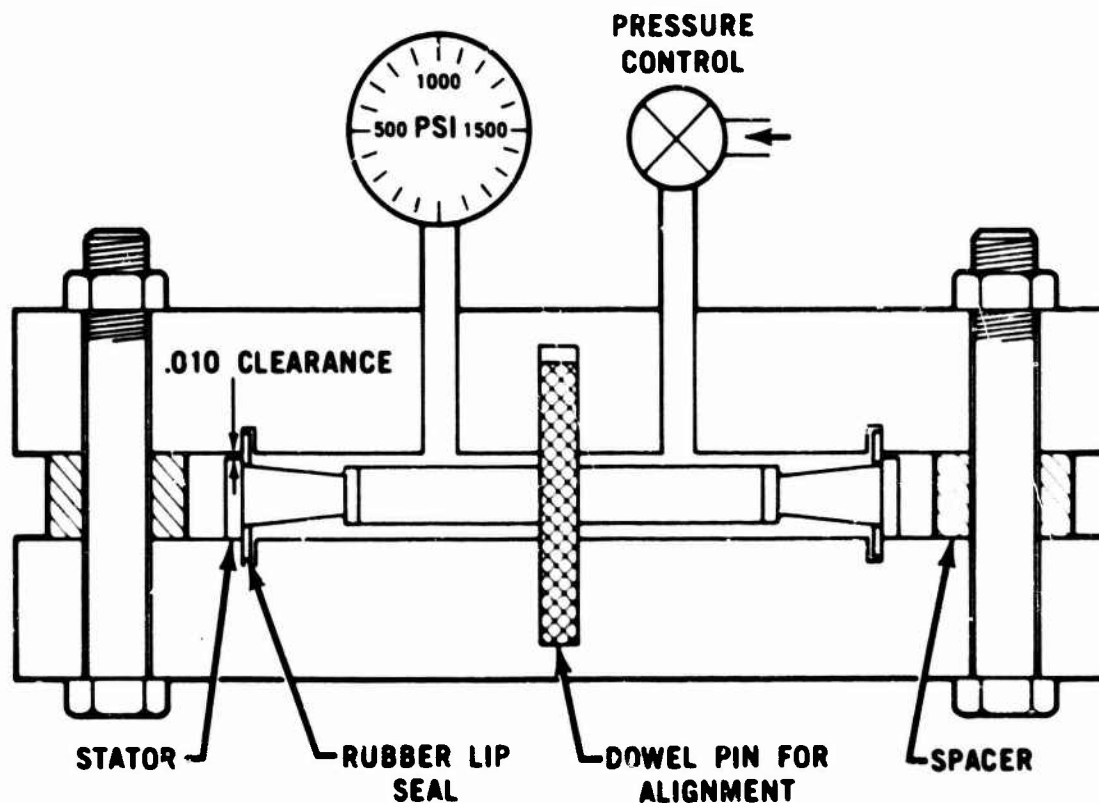
Figure 3.33 — Stator Pressure Test Fixture

Because of the results of testing stator 1086 — the apparent inability of the 10 pound bend test to screen out a part not capable of passing the 10 light test — the stator vane bend test load level specification is being reassessed. To date, the test data indicates a reassessment of the stator outer shroud pressure level specification is not warranted.

In addition to the stators, three 2.7 g/cc density nose cones were finish processed and received for testing. All were subjected to and successfully passed the 10 light test.

Engine and Rig Testing

Limited testing of turbine inlet nose cones and first and second stage stators was conducted in engine test rigs. No testing of combustors and turbine rotor tip shrouds was conducted during this reporting period. Tables 3.8 to 3.10 show the results to date of engine testing on silicon nitride and silicon carbide stationary components.

1930°F Durability

After completion of qualification testing, components may be subjected to static durablity testing in engine test rigs at 1930°F. During the past six months, two nose cones were subjected to this static durability testing. Nose cone 894 has survived 10.25 hours. The first 2.7 g/cc density nose cone, 1018, has successfully accumulated 10 hours.

In addition to this testing, a review of the weight gain data on 2.55 g/cc stators tested at 1930°F in the engine test rig was made. This data has not been previously reported and therefore covers a time span greater than just this reporting period.

TABLE 3.8

SUMMARY OF NOSE CONE TESTING

Serial Number	Static Engine Testing				Cyclic Testing (ARPA)					2500°F Static Testing		Miscellaneous Tests		Component Status	Total Part Time Hours**	Total Part Lights
	Light (Cold)	Shutdowns Cold	Hot	Hours**	Lights Cold	Hot	Shutdowns Cold	Hot	Hours**	Lights	Hours	Lights	Hours**			
Goal	10	6	1	0.2	14	26	–	40	200	4	25					
72												142	16.75	F	16.75	142
102	25	16	7	24.5	44	36	21	56	221.5					F,B	246.00	106
103	16	17	2	0.40	1	2	0	2	50.5					F,O	50.90	22
130					5	3	2	6	24.5					F,H	24.50	8
302	10	8	1	0.20	8	2	8	2	6.5	1	5.0	1	18.30	F,C,O,X	30.00	28
307	60	51	8	37.8	8	10		16	42.8			4	6.6	F,B	90.50	90
304	46	42	4	2.00								15	50.3	F,C,O,X	52.30	61
320												10	1.15	F,X	1.15	10
321	30	27	3	0.50								26	27.50	F,X	26.00	56
906	27	90	7	19.5	1			1	13.25			8	2.50	F,B	34.35	34
907	64	58	6	1.23										F,C,X	1.23	64
914	16	13	6	32.61										F,C	33.61	16
971	14	6	5	62.36										F,B	62.36	14
972	86	61	24	147.15										F,C	147.15	86
975	10	6	1	0.25						3	4.2	2	1.85	F,B	6.3	15
976	16	6	7	55.50										F,B	55.50	16
886*	10	6	1	0.25										6	6.26	16
889	40	36	4	1.00										F,C	1.00	40
890	16	14	5	32.1										F,H	32.1	16
894*	21	0	12	10.4										6	10.4	21
903	10	6	1	0.25										F,C,X	0.25	16
904												7	.5	F,X	.5	7
616	12	11	1	0.25										F,B	6.25	16
616	26	16	6	30.90										F,C	30.61	26
617	10	6	1	0.25										F,C,X	6.25	10
620	12	6	1	0.25										F,H,X	0.25	12
1006*	70	62	7	1.75										8	1.75	70
1011*	10	6	1	0.25										8	6.25	16
1018*	16	11	6	10.2										8	18.2	19

* New entry this reporting period   ** Up to at least 1930°F

Serial Numbers 72–321 are 2.2 g/cc density; 806–904 are 2.55 g/cc density; 1000 series are 2.7 g/cc density.

Key to Component Status
- F - Failed
- O - Failure occurred in other than ARPA duty cycle
- H - Part failed during handling
- S - Serviceable
- C - Cracked shroud
- B - Inner body crack
- X - Internal material flaw involved in failure

TABLE 3.9

SUMMARY OF STATOR TESTING

Serial Number	Static Engine Testing				Cyclic Testing (ARPA)					2500°F Static Testing		Miscellaneous Tests		Component Status	Total Part Time Hours**	Total Part Lights
	Light (Cold)	Shutdowns Cold	Hot	Hours**	Lights Cold	Hot	Shutdowns Cold	Hot	Hours**	Lights	Hours	Lights	Hours**			
Goal	10	9	1	0.2	14	28	–	40	200	4	25					
372	10	9	1	0.20	1	2	0	3	50.5			2	7.9	F,V,I,O	58.80	15
421	10	9	1	0.20								3	2.80	C,X	3.00	13
424	10	9	1	0.25								9	2.75	C,X	3.00	19
428	10	9	1	0.20	17	14	6	25	103					F,C	103.20	41
430	10	9	1	0.20	14	13	6	21	61.5					F,C	81.70	37
525 +	39	15	26	148.75										S	148.75	35
715	10	9	1	0.20								6	0.10	F,V,O	0.30	18
751	11	10	1	0.20								2		C,V,O,X	0.20	13
817	34	31	3	0.75										S	0.75	34
820	14	13	1	0.30										C,X	0.30	14
841	12	11	1	0.20	6	10		16	42.8					F,C	43.00	28
848	11	10	1	0.20										F,H	0.20	11
852	23	20	3	1.70										F,O	1.70	23
858	12	11	1	0.20	6	10		18	42.8					F,C	43.00	28
865	12	11	1	0.25								2	9.50	F,V,I,O	10.15	14
868	12	11	1	0.25								2	9.50	F,V,I,O	10.15	14
879	10	9	1	.25						2	1.0			S	1.25	12
880*	12	9	3	.25								1	5.00	S	7.8	15
884*	28	9	19	20.4										F,H	20.4	28
889*	122	110	12	21.								4	4.88	S	26.2	132
898	10	9	1	0.25										S	0.25	10
910i										1	1.0	4	18.5	F,V,I	19.5	5
911	15	9	6	54.25										F,V	54.25	15
911A	11	10	1	0.25						1	.25	11	21.75	F,V,I,O	22.25	23
921*	19	9	10	8.4										F,H	8.4	19
1066*	10	9	1	0.25										F,C,V	0.25	10
1099*	10	9	1	0.25										S	0.25	10
1117*	10	9	1	0.25										S	0.25	10
824	10	9	1	0.25								1	0.50	F,V,X	0.75	11
927	10	9	1	.25								7	.5	F	.75	17
938	10	9	1	.25										S	.25	10
940	29	15	14	32.75										F,C	32.75	79
943	10	9	1	0.25						3	4.2	1	1.45	F,C	5.9	14
945	11	9	2	.50								1	.03	F,O	.53	12
948	10	9	1	.25										S	.25	10
954	18	9	10	175.00										S	175.00	19
955	12	9	3	23.00										F,C	23.00	12

* New entry this reporting period   ** Up to at least 1930°F
+ Silicon Carbide part
Serial number 372 is 2.2 g/cc density; 421-955 are 2.55 g/cc except fo: 525 which was SiC; 1000 Series are 2.7 g/cc density.

Key to Component Status
  S = Serviceable   C = Cracked shroud
  F = Failed   V = Vane(s) failed
  O = Failure occurred in other than ARPA duty cycle   X = Internal material flaw involved in failure
  H = Part failed during handling   1 = Impact failure from combustor carbon

TABLE 3.10

SUMMARY OF SHROUD TESTING

Serial Number	Static Engine Testing				Cyclic Testing (ARPA)					2500°F Static Testing		Miscellaneous Tests		Component Status	Total Part Time Hours**	Total Part Lights
	Light (Cold)	Shutdowns Cold	Hot	Hours**	Lights Cold	Hot	Shutdowns Cold	Hot	Hours**	Lights	Hours	Lights	Hours**			
Goal	10	9	1	0.2	14	26	–	40	200	4	25					
1	17	9	8	5.33								7	.5	F	5.83	34
24	19	17	2	0.40	1	2	0	2	50.50					C	50.90	22
111	13	12	1	0.30	51	41	54	68	245.30					S	245.30	115
119	15	13	2	0.25										F,C	5.25	15
130	12	11	1	0.25										S	0.25	12
134	10	9	1	0.25										S	0.25	10
2	10	9	1	0.25										F,C	0.25	15
3	12	11	1	0.25						3	2.0	7	34.3	S	36.55	22
4	10	9	1	0.25										F,C	0.25	10
9												2	1.75	V	1.75	2
36	19	17	2	0.40	1	2	0	3	50.5					S	50.90	22
100					1	9	0	10	5.4			30	1.40	S	9.4	40
102					1	9	0	10	5.4					S	5.4	10
104												75	5.10	S	5.10	75
106	10	9	1	0.30	51	41	34	68	245.00					S	245.30	112

** Up to at least 1930°F   Density 2.0-2.7 g/cc

Key to Component Status
  S = Serviceable
  F = Failed
  C = Cracked Shroud

Figure 3.34 summarizes the percent weight gain versus time data gathered on a total of twelve 2.55 g/cc density stators. The curve labeled "minimum observed" is a result of the data from stator 954 (9). Stator 954 achieved 175 hours of test time at 1930°F without failure. Stator 954 weight gain was minimal over the last 125 hours and the total percent weight gain after 175 hours was 0.74%, the lowest achieved to date.

The wide variation in possible weight gain rates for similar density stators is reflected by the data between the maximum and minimum curves. Figure 3.35 offers a possible explanation for this occurrence. In reviewing the numerous variations which have occurred during the 2.55 g/cc density stator fabrication development process, one aspect — the nitriding process — appears responsible for differences in the weight gain versus time data. All but two stators (889 and 955) lent themselves to the process groupings noted as Zones A, B and C. Zone A contains all data from stators nitrided in a 96% N_2/4% H_2 atmosphere (9,10). Zone B contains all data from early stators nitrided at an outside vendor (A) in a 100% N_2 atmosphere. Zone C contains data from two processing variations — stators nitrided at an outside vendor (B), in a 100% N_2 atmosphere and stators partially nitrided at vendor A then renitrided in-house in a 96% N_2/4% H_2 atmosphere. A vendor A furnace malfunction caused this last processing variation which, from weight gain criteria, proved to be undesirable.

The importance of this grouping, from an engine durability viewpoint, is addressed in Figure 3.36. Of the twelve stators from which the data was gathered, nine have failed. Three of the nine failures can be attributed to extraneous circumstances and are not included in the noted failures (F). The data from the remaining six failures indicate that, for 2.55 g/cc density stators of relatively similar strengths, a total percent weight gain to failure relationship may exist. All failures were associated with total weight gains in excess of 1.9%.

Further testing of available 2.55 g/cc density stators and initial testing of 2.7 g/cc density stator is planned.
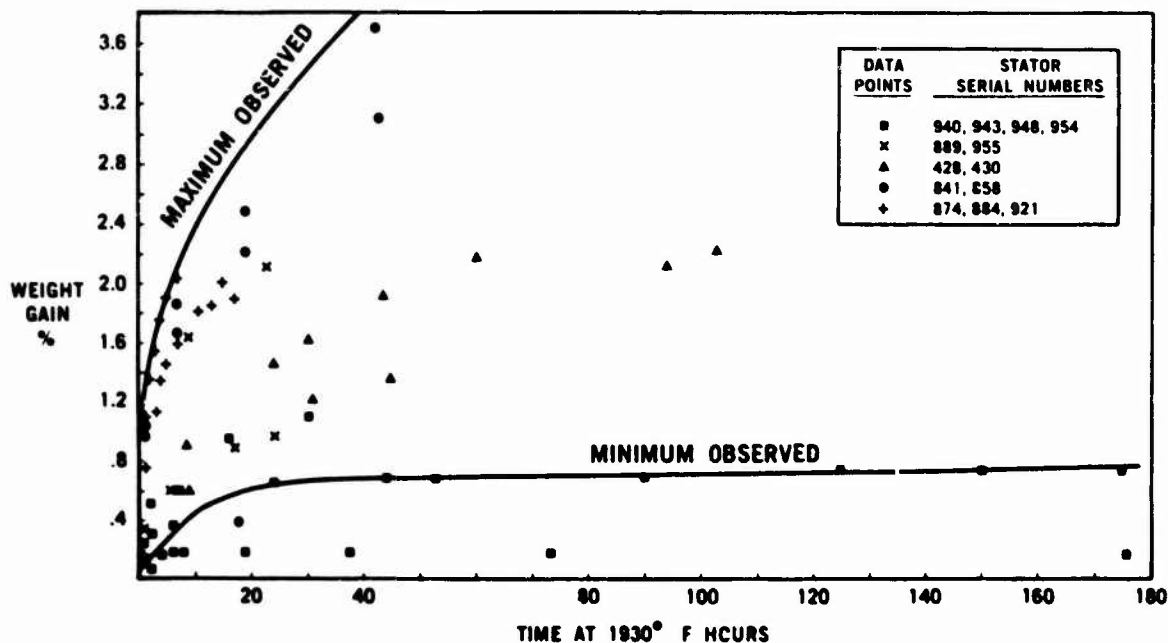
Figure 3.34 — Weight Gain Vs. Engine Test Time at 1930°F for 2.55 gm/cc Density Silicon Nitride Stators
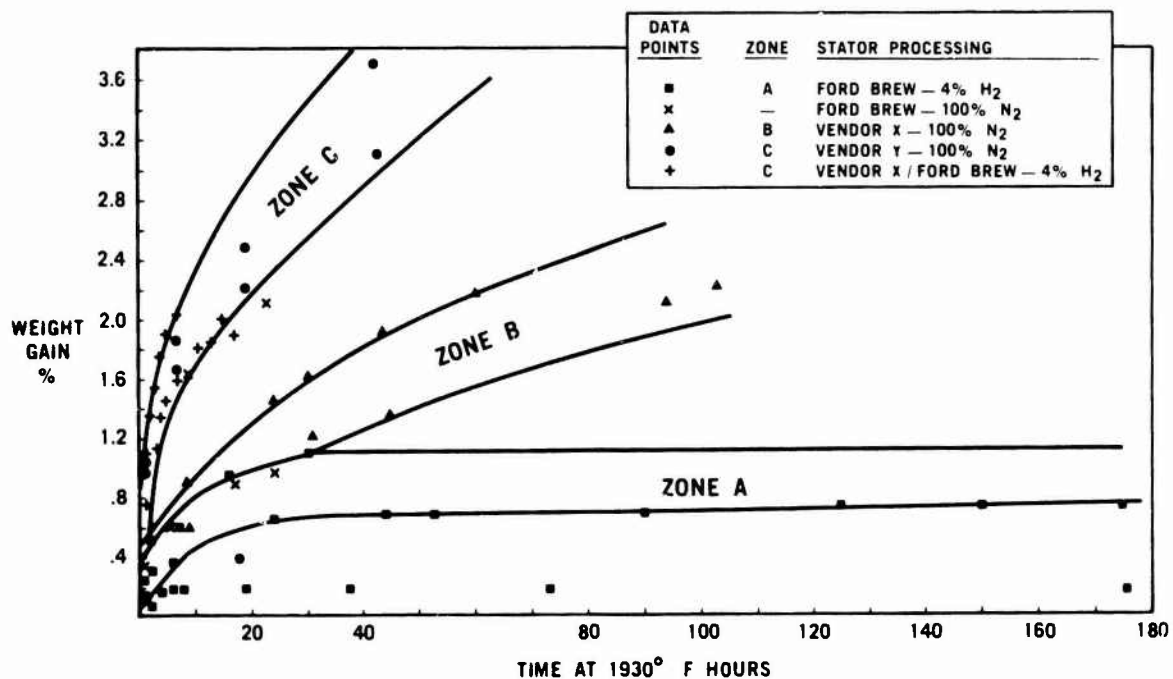
Figure 3.35 — Weight Gain Vs. Engine Test Time at 1930°F for 2.55 gm/cc Density
Silicon Nitride Stators as a Function of Stator Nitriding
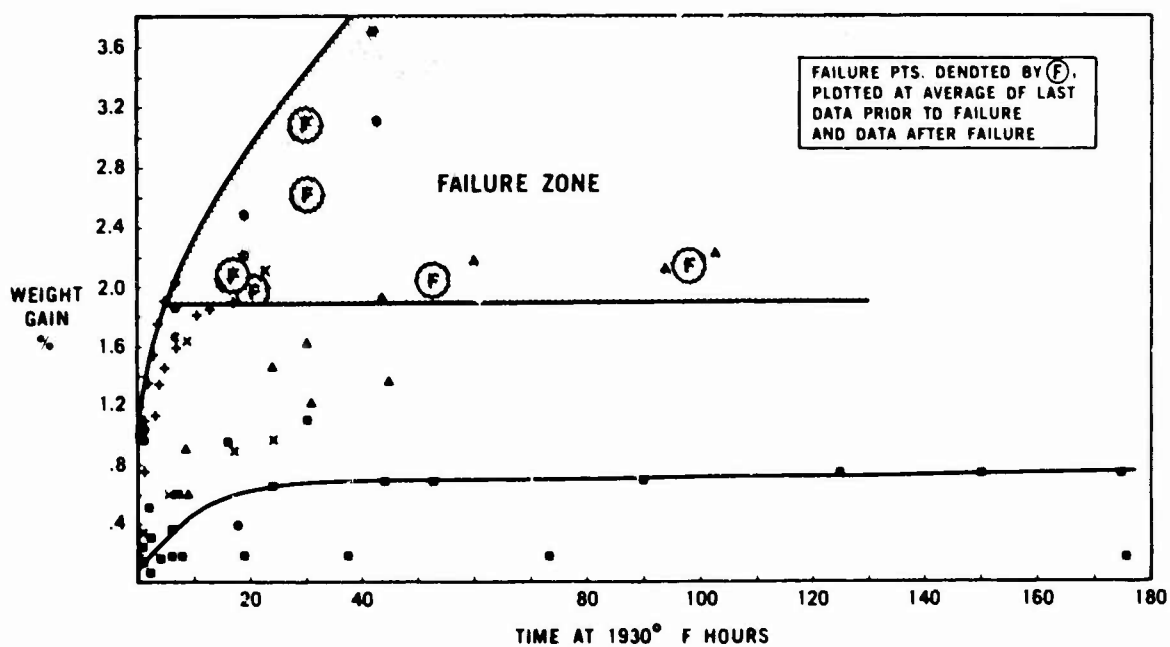
Figure 3.36 — Weight Gain Vs. Engine Test Time at 1930°F for 2.55 gm/cc Density
Nitride Stators Showing Failure Zone

2500°F Durability

Work continued in a number of areas relating to the operation of the 2500°F flowpath qualification test rig. To date the rig has accumulated 74 lights and 181 hours of hot time above 1900°F. Fifteen of these hours were run at a combustor exit temperature of 2500°F.

During this reporting period, work continued on instrumentation and component durability and reliability for the 2500°F test rig. Areas of concentration were as follows:

1. Durability of the ceramic adaptor tube which houses the hot flow path components (Figure 3.37]

2. Procurement of durable and reliable high temperature thermocouples.

3. Determination of the spectral emittance of the ceramic flow path parts under actual test conditions.

4. Further automation of the rig operation.

5. A solution to the problem of carbon build-up in the combustor.
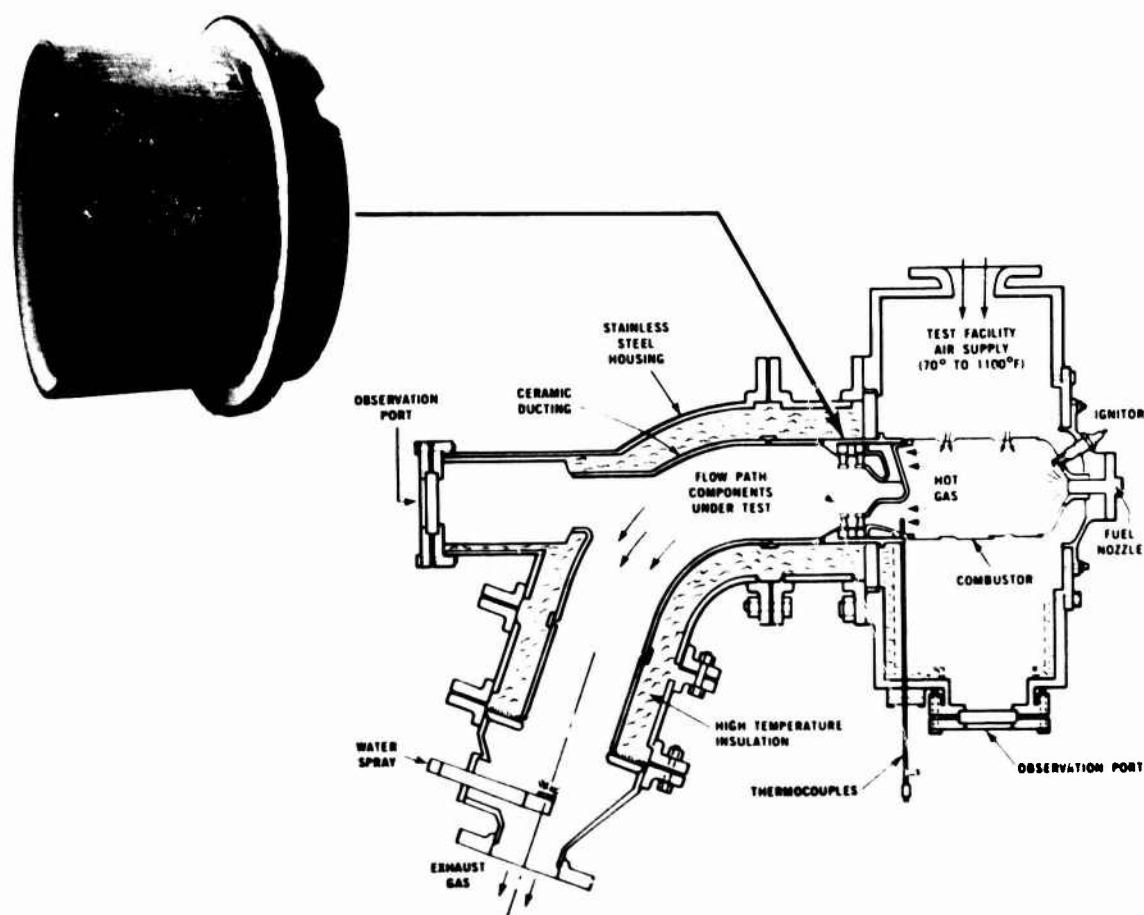
Figure 3.37 — Schematic View of High Temperature Test Rig Showing Location of Ceramic Adaptor Tube

The current status of each of these areas is as follows:

1. The original design slip cast, Si₃N₄ adaptor tube demonstrated limited life (3 lights and 5 hours hot time; and typically cracked as shown in Figure 3.38. An investigation of the problem resulted in a

design modification to the downstream end of the tube (Figure 3.39). A slip cast tube of the redesigned configuration has been successfully tested for 12 lights and 24.2 hours of hot time with five of these hours at gas temperatures of 2500°F.

2. A major effort was made to evaluate vendor-supplied high temperature thermocouples. All thermocouples received are:

   a. Tested in a calibration furnace to check their accuracy.

   b. X-rayed to verify the integrity of the very fine (0.012 dia.) thermocouple wires.

   c. Pressure checked for braze joint leaks.

   d. Flow-tested to determine aspiration air flow rate.

   The above quality checks resulted in the rejection of a major portion of the thermocouples received.

3. In conjunction with the high temperature thermocouples used to measure 2500°F gas temperatures, an Ircon one-color infra red radiation pyrometer is being utilized to determine surface temperatures of the ceramic flow path components. Determination of this data requires that the spectral emittance value of the target surface at each operating conditions be accurately established. For the radiation pyrometer being used, the wavelength band of interest is 2.0 to 2.6 microns. As previously stated, the spectral emittance value for the various ceramic surfaces being tested is not a constant nor is it constant over the full operating range of testing conditions. Influencing factors are material, density, surface finish, degree of surface oxidation, surface contamination, surface temperature, radiation wavelength, etc. Hence, directly applicable data from the literature is not available. However, trend data is available and a testing program has been initiated to enhance the available information. Twenty segments of Ford ceramic components were sent to NASA-Langley Research Center for emittance determination. These specimens were selected to represent several different material densities, surface oxidation, and contamination levels.

Figure 3.38 — Typical Failure of Original Design Adaptor Tube
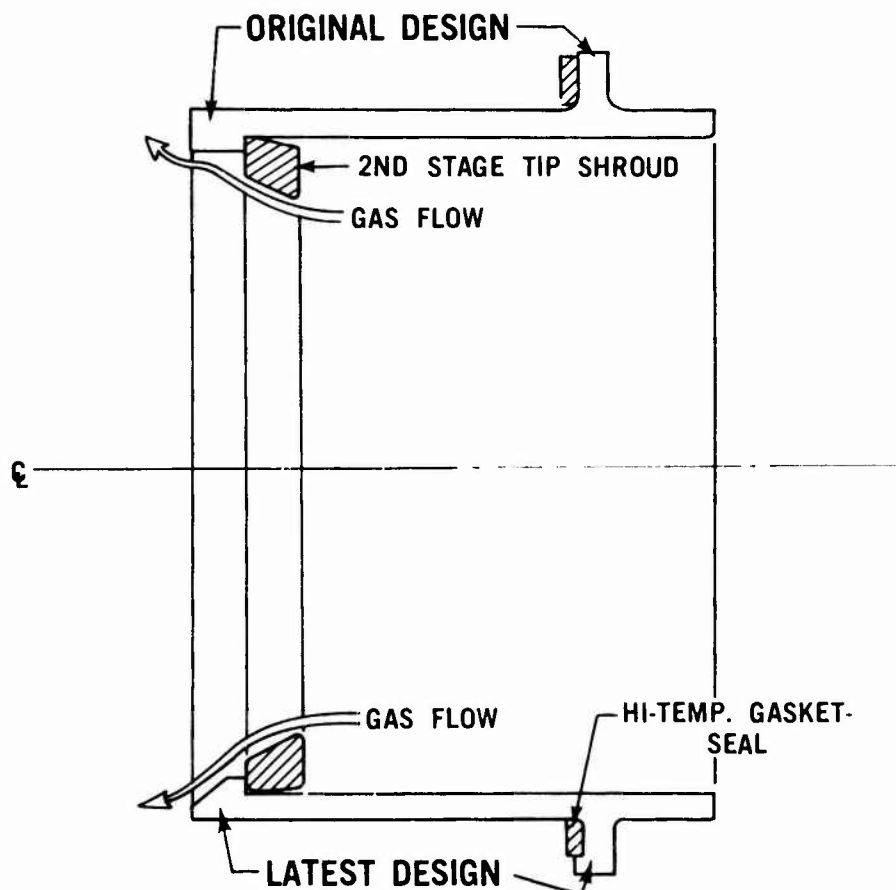
Figure 3.39 — Adaptor Tube Design Modification

The expected Langley data will include:

a. Total emittance.

b. Spectral emittance for wavelengths being used by our two types of radiation pyrometers, i.e. 2.0 to 2.6 micron band for the Ircon one-color pyrometer, and 0.81 & 0.95 microns for the Milletron two-color pyrometer

c. The change of emittance with surface temperature.

Further refinement of the Langley data will be required in order to include the effect of the unique rig enclosure which may result in somewhat higher effective emittance values. The expected data from NASA-Langley Research Center and further data from in-house work should increase the confidence level of using radiation pyrometry for accurate surface temperature measurements.

4. An automatic, closed loop control system was incorporated in the test rig to maintain constant exhaust cooling to 500°F. After considerable development, the system is operating very satisfactorily.

5. The problem of carbon build-up in the combustor dome became apparent as soon as testing at 100% flow conditions began. In the 2500°F flow path qualification rig, the temperature rise requirement of up to 1400°F and the air flow rate of up to 2.14 pounds per second requires a fuel supply rate of up to 165 pounds per hour. This fuel, when being consumed by a standard size engine combustor, creates a rich combustion condition resulting in carbon formation; this does not occur in the engine or in the engine test rigs where the use of regenerators greatly reduces the needed temperature rise. A series of tests were conducted to establish the carbon formation map, and at the present time, a number of combustor design modifications are being evaluated.

4. PROGRESS ON MATERIALS TECHNOLOGY

SUMMARY

Materials technology is a very important portion of the systems approach employed in this project for the development of high temperature gas turbine engines. The generation of ceramic material property data, in progress since the beginning of the project, has been instrumental in component design modifications and failure analysis. As testing and fabrication experience was gained, improvements in materials have also been made. The properties of these improved materials are determined and fed back into design modifications and failure analysis, thus closing the loop. The work on determining material properties and on generating material improvements is reported in this section.

In order to select the best method of processing Si_3N_4 powder, the optimum MgO content and the best hot pressing parameters consistant with the hub forming portion of the duo-density rotor process a processing parametric study was conducted. Strength at two elevated temperatures, along with the Weibull slope, were obtained in a number of hot pressed Si_3N_4 materials. Some of these materials were pressed at pressures as low as 500 psi. Preliminary results of this study shows that the best material would be prepared by ball milling with WC media and would contain 5% MgO.

A major concern with the 3 piece approach to the duo-density rotor has been the degree of bonding and the resultant strength of the bond between the two regions of hot pressed Si_3N_4. Test bars were cut from six duo-density rotors such that the hot pressed to hot pressed bond could be positioned within the zone of maximum stress. Test results showed a strength variation at different locations, with higher strengths obtained at the center region and lower strengths found at the outer regions.

Strength measurements were performed on Refel reaction silicon carbide, the material used most recently for ceramic combustors. Statistical bend strength distributions were measured at room temperature and at five elevated temperatures. In addition, tensile strength was measured at room temperature.

A process for producing complex shapes of silicon carbide by injection molding and reaction sintering has been under development in recent years. Principles of the process and strength data are given. Both one piece stators and monolithic rotors have been fabricated.

Previous results obtained from nitriding of large loads of silicon metal powder shapes, such as molded stators and rotor blade rings, have shown that the nitriding reaction was not under control. Undesired exothermic reactions could cause silicon melting before nitriding was completed, with subsequently reduced mechanical properties and degraded microstructure. A technique is described which essentially allows the furnace to control the nitriding rate dependent upon the nitrogen gas consumption rate. Data are given which show that this type of nitriding improves the material structure for a wide range of furnace loads.

The work on developing Sialon materials has been terminated as a result of funding reductions. The effort to develop high strength, stable Sialon materials by sintering is summarized in this section.

Work was undertaken to evaluate the use of hot isostatic pressing to further densify reaction sintered Si_3N_4 preforms, using Vycor encapsulation. Additives were evaluated and some densification and strengthening were obtained. Attempts to densify complex shaped parts were not successful.

4.1 PROPERTIES OF HOT PRESSED SILICON NITRIDE

In order to obtain the best Weibull strength and resulting rotor hub reliability, a parametric study was initiated which considered the following variables:

1. Material purity: "CP85" versus "KBI" Si_3N_4 powders. The powder designated CP85 was the as-received powder purchased from A.M.E. The KBI powder refers to the CP85 after (1) magnetic separation to remove 0.3% of magnetic material and (2) air classification at 50 microns at the rate of 9.07-11.33 kg/hr (20-25 lbs./hr.). Starting with 136 kg (300 lbs.) of CP85, 0.45 kg (one lb.) was removed by magnetic separation, 43.5 kg (96 lbs.) were classified as plus 50 microns, 7.7 kg (17 lbs.) were classified as dust collector fines (ultrafine material), 1.81 kg (4 lbs.) were used for cleanout run, 0.45 kg (one lb.) was used to make screen size distribution analysis, and 78.9 kg (174 lbs.) were classified as minus-50 microns. The minus-50 micron powder was designated "KBI". "KBI" is Kawecki Berylco Incorporated, a supplier of silicon powder and recently also licensed by AME to manufacture and sell Si_3N_4 powder in the U.S.; they conducted the separation and classification of the powder.
2. Hot pressing additive content: 2 to 7 weight % MgO.
3. Powder milling conditions.
   a. Milling balls: WC versus Al_2O_3
      WC balls were 0.95 cm size and Al_2O_3 balls were 1.9 cm size. In a gallon size milling jar, 30,000 gm. WC were used with 800 gm. Si_3N_4 in dry milling, and with 2000 gm. Si_3N_4 in wet milling; 6000 gm. Al_2O_3 balls were used with 800 gm. Si_3N_4 in dry milling and with 2000 gm. Si_3N_4 in wet milling.
   b. Wet versus dry milling. Wet milling was done with methanol.
   c. Milling time: 24-72 hours.
4. Hot pressing pressure: 3.45-34.5 MPa (500-5000 psi)

Approximately 60 hot pressings were made over several months with a combination of variables based mainly on past experience. Towards the middle part of the program, a factorial analysis plan was started. Table 4.1 shows the processing conditions used and Table 4.2 shows the Weibull parameters obtained for those billets.

The billets were flat discs 7.6 cm. in diameter by 2.5 cm. thick. Approximately 40 "A" size (14) MOR test bars were machined from each billet. Generally, half of the bars were tested at 871°C (1600°F) and the balance were tested at 1204°C (2200°F) in four-point bending using 0.953 cm. upper span and 1.905 cm. lower span at a stress rate of 2200 MPa/min. The two test temperatures were selected because they represent the temperatures at the bore and at the bond ring of the rotor.

From the MOR data such as shown in Table 4.3 for billet t019, Weibull strength parameters of characteristic MOR ($\sigma\theta$) and Weibull modulus (m) were calculated by a maximum-likelihood (t5, t6) program and are tabulated in Table 4.2. Evaluation of the results in Table 4.2 shows that, within the conditions investigated:

1. Wet milling with Al_2O_3 balls produced low strengths.
2. Little difference was apparent among dry WC, dry Al_2O_3, and wet WC milling.
3. Surprisingly, the extensive powder cleaning did not show significantly superior results.
4. High strengths were obtainable even at as low as t500 psi pressing pressure. This is important since the use of high pressure in rotor hub fabrication tends to damage the delicate blade ring.
5. Within the range investigated, milling time had no significant effect on the results.

In order to evaluate the effect of each variable in a more quantitative manner, a factorial analysis experiment was initiated halfway through the project. Because of the large number of variables involved, a full factorial to evaluate six variables plus a possible unknown variable at four levels each would require t6,384 experiments. Even then, each experiment, to be truly significant, would involve approximately 20 billets for proper sampling. Thus, the task would be horrendous. Instead, a saturated fractional factorial analysis for six variables, plus an unknown variable, at two levels each, was made as an initial effort, and without statistical billet-to-billet sampling, as shown in Table 4.4.

TABLE 4.1
PROCESSING CONDITIONS FOR VARIOUS DISCS

			WET						DRY					
			WC			Al₂O₃			WC			Al₂O₃		
			24 Hrs.	48 Hrs.	72 Hrs.	24 Hrs.	48 Hrs.	72 Hrs.	24 Hrs.	48 Hrs.	72 Hrs.	24 Hrs.	48 Hrs.	72 Hrs.
		14.5 MPa		1036R						1000T, 1015N					1017T
		10.3 MPa		1037N						1144T, 1015N					1143T
		13 MPa								1001N					
		14.5 MPa		1019T, 1026N				1016N, 1013N		1031N					1033T
		10.3 MPa		1020N				1013N		1032N					
		13 MPa													
		14.5 MPa		1004T											
		10.3 MPa		1026T											
		13 MPa													
		14.5 MPa	996N	997N	994R 1011N,1012N		1020T	1006N		995N					1000T,1009T
		10.3 MPa	1025N	1021R	1011N,949R			1027T, 990T		993N				977T	
		13 MPa		1003R				1007T							
		14.5 MPa									1010T			1030N	
		10.3 MPa													
		13 MPa													
		14.3 MPa		1039B											
		10.3 MPa		1040B											
		13 MPa													
		14.3 MPa			1042B										
		10.3 MPa			1043B									•	
		13 MPa													
		14.3 MPa			1101B										
		10.3 MPa			1100B										

TABLE 4.2
WEIBULL PARAMETERS

Disc No.	871°C		1204°C	
	$\sigma\theta$, MPa (ksi)	m	$\sigma\theta$, MPa (ksi)	m
977	519 (75.2)	8.5	431 (62.5)	18.6
989			412 (59.7)	11.1
990			237 (34.4)	11.9
993			394 (57.2)	14.6
995	554 (80.3)	16.2	435 (63.1)	20.5
996			370 (62.5)	11.2
997			377 (54.7)	12.4
998			418 (60.6)	12.6
1000			359 (52.1)	11.0
1001			371 (53.8)	10.2
1003			385 (55.8)	11.1
1004			357 (51.7)	9.8
1006			224 (32.5)	6.2
1007			237 (34.4)	12.4
1008			408 (59.1)	13.2
1009	564 (81.8)	10.3	428 (62.1)	17.4
1010	639 (92.6)	21.7	368 (53.3)	11.2
1011			375 (54.4)	22.3
1012	509 (73.8)	8.7	360 (52.2)	16.7
1013			340 (49.3)	11.3
1014	450 (65.3)	4.8	299 (43.3)	17.2
1015			288 (41.7)	19.0
1016	485 (70.3)	6.2	290 (42.1)	14.9
1017	593 (86.0)	11.6	421 (61.1)	15.6
1018	541 (78.4)	11.6	381 (55.2)	19.1
1019	724 (105.0)	9.4	420 (60.9)	12.7
1020	458 (66.4)	8.9	390 (56.5)	11.7
1021			399 (57.9)	20.6
1025			394 (57.2)	19.6
1026			408 (59.1)	13.2
1027				
1028	505 (73.2)	8.3	367 (53.2)	13.1
1030	470 (68.2)	5.0	345 (50.1)	21.1
1031	535 (77.6)	7.7	414 (60.1)	10.7
1032	506 (73.4)	5.8		
1033	679 (98.5)	11.3	372 (54.0)	15.6
1035			339 (56.4)	11.3
1036			395 (57.3)	12.1
1037			360 (52.2)	14.5
1039	605 (87.8)	7.1	432 (62.6)	14.6
1040	569 (82.5)	11.3	419 (60.7)	15.5
1042	445 (64.5)	8.0	390 (56.6)	71.0
1043	454 (65.8)	7.9	354 (51.3)	16.5
1100	586 (85.0)	9.9	354 (51.3)	10.4
1101	641 (93.0)	10.1	439 (63.6)	13.0
1133	599 (86.9)	12.9	425 (61.6)	12.3

TABLE 4.3
SAMPLE MOR DATA (BILLET 1019)

871°C (1600°F)				1204°C (2200°F)			
MPa	ksi	MPa	ksi	MPa	ksi	MPa	ksi
667	96.8	745	108.0	373	54.1	453	65.7
703	102.0	618	89.6	389	56.4	409	59.3
710	103.0	645	93.6	440	63.8	356	51.6
508	73.7	717	104.0	413	59.8	437	63.4
663	96.2	772	112.0	350	50.7	399	57.9
689	99.9	681	98.8	415	60.2	415	60.2
800	116.0	582	84.4	458	66.4	389	56.4
710	103.0	696	101.0	397	57.6	405	58.8
841	122.0	601	87.1	454	65.8	389	56.4
758	110.0			318	46.1	429	62.2

TABLE 4.4
FACTORIAL ANALYSIS MATRIX

EXPERIMENT	DISC NUMBER	POWDER	%MgO	BALL TYPE	WET/DRY	TIME	MACHINING SOURCE*	DUMMY VARIABLE**
1A	1011	CP85	5	WC	WET	72	B CO.	+
1B	1012	CP85	5	WC	WET	72	B CO.	+
2	1029	CP85	5	Al_2O_3	WET	48	T CO.	−
3	1010	CP85	2	WC	DRY	72	T CO.	−
4	1030	CP85	2	Al_2O_3	DRY	48	B CO.	+
5	1018	KBI	5	WC	DRY	48	B CO.	−
6	1017	KBI	5	Al_2O_3	DRY	72	T CO.	+
7	1019	KBI	2	WC	WET	48	T CO.	+
8A	1014	KBI	2	Al_2O_3	WET	72	B CO.	−
8B	1016	KBI	2	Al_2O_3	WET	72	B CO.	−

* MACHINING SOURCE: NAME OF SHOP WHICH MACHINED THE MOR TEST BARS.

** DUMMY VARIABLE: A FICTITIOUS VARIABLE TO INDICATE WHETHER THERE IS A STRONG INTERACTION AMONG THE REAL VARIABLES OR WHETHER THERE IS A STRONG VARIABLE WHICH HAS NOT BEEN CONSIDERED.

Because the strength data might be influenced by subtle differences in test bar machining quality, a variable called the "machining source" was included to indicate whether the machining source would have a strong influence on the results. The dummy variable was included to indicate if any strong interaction or unknown variable existed. Duplicate runs were made in experiments 1 and 8 to evaluate the reproducibility of results. The matrix as shown represents the very minimum amount of experimental data in this initial work for factorial analysis, and should be considered preliminary information.

Since the ultimate objective is highest reliability of the rotor hub, reliability numbers were used as the basis for comparing the billet qualities. The method used for the calculation of reliability was discussed by Swank and Uy (17). A sample data base for calculating reliability is shown in Table 4.5. The characteristic MOR and Weibull modulus m measured at 871°C (1600°F) and 1204°C (2200°F) were used to estimate the values at the other temperatures by assuming straight line functions. These strength parameters plus thermal and elastic properties measured elsewhere in the program were used in conjunction with the calculated mechanical and thermal stress contours to calculate reliability values by means of the Weibull equation. The rotor blade ring was considered to be fixed in material to be 2.7 g/cc injection molded Si_3N_4 (IMSN) which was calculated to have a reliability of 0.99190. The Weibull parameters for the various billets and the calculated rotor reliabilities assuming those billets were made into rotor hubs are shown in Table 4.6. Using these reliability numbers, the factorial analysis matrix of Table 4.4 was evaluated as follows: Taking each variable at a time, the average effect of each level of that variable was calculated. For example, consider the powder variable: the average reliability in using CP85 powder is

$$1/4(0.94617 + 0.89297 + 0.99097 + 0.11273) = 0.73571$$

while the average reliability in using KBI powder is

$$1/4(0.98775 + 0.98987 + 0.98826 + 0.16247) = 0.79209$$

Therefore, the KBI powder is superior by

$$0.78209 - 0.73571 = 0.04638$$

This procedure is repeated for all the other variables at each of their two levels, including the dummy (+) and dummy (−) levels.

As shown in Table 4.7, the strengths of the variables were ranked from 1 to 7. As it turned out, the milling ball type had the strongest effect on reliability while the wet/dry milling variable had a weak effect. Fortunately, the dummy variable had the least effect, which means that there was not a strong interaction among the variables considered and there was no other significant variable which needed to be taken into consideration. The significance of the effect of each variable was next evaluated at the bottom of Table 4.7 by comparing the strength of each effect with the average irreproducibility of reliability in experiments 1a, 1b, and 8a, 8b. Since the irreproducibility in reliability was 0.19299, all the effects smaller than this number would be considered insignificant or within the irreproducibility limits. In Table 4.7, only the variables consisting of ball type, machining source, and % MgO showed effects larger than the irreproducibility range. The best material would therefore be WC milled and would contain 5% MgO. The results also indicate that the machining source did have a strong influence on the results and that company "T" would be preferred over company "B".

All of the above evaluation assumed, of necessity, that the material sampling was large enough to be significant, which it really was not, as previously pointed out. This analysis was taken as an initial step towards a logical parametric study and is presented here to illustrate the approach.

There is however, a definite conclusion to be drawn from the above study, and that is assuming the calculated reliabilities are correct, it is possible to utilize CP85 powder, under proper processing conditions, to achieve the required short term rotor reliabilities of over 0.9 in this program. Included in the above statement is the additional assumption that the MOR data on test bars of 2.7 IMSN represent the properties of the rotor blade ring as it goes into the engine. Both above assumptions are currently being evaluated experimentally for accuracy. In the meantime, it is also obvious from these results that tightening rotor fabrication quality control to ensure better reproducibility of properties is helpful in improving the reliability picture.

TABLE 4.5
TYPICAL DESIGN PROPERTIES FOR ROTOR HUB MATERIAL

Material: Hot Pressed Silicon Nitride
Designation: Billet 1018
Density: 3.17 g/cc
Composition: 2.2 Mg, 0.8 Al, 0.6 Fe, 0.2 Ca

	PROPERTY	UNIT	TEMPERATURE, °K					
			300	530	810	1090	1370	1640
WEIBULL	MOR_0	MPa	617	617	617	566	429	303
STRENGTH	m_w	—	11.6	11.6	11.6	11.6	11.6	22.9
	a	10^{-6} / °K	1.84	2.39	2.87	3.20	3.46*	3.66*
THERMAL	k	WATTS m x°K	29.4	25.9	22.5	19.0	15.9	13.8
PROPERTIES	C_p	JOULES kg X °K	745	950	1100	1209	1372	1360
	E	GPa	294	294	294	292	291*	286*
ELASTIC	v	—	0.256	0.254	0.251	0.246	0.239*	0.221*
PROPERTIES	G	GPa	117	117	117	117	117*	117*

* EXTRAPOLATED VALUE OR CALCULATED FROM EXTRAPOLATED VALUES

TABLE 4.6
WEIBULL PARAMETERS AND CALCULATED RELIABILITIES

BILLET NO.	CHARACTERISTIC MOR, MPa		WEIBULL SLOPE		ROTOR RELIABILITY			
	871°C	1204°C	871°C	1204°C	RING	HUB	ROTOR	
1011	500	375	16.3	22.3	0.99190	0.99970	0.99160	
1012	509	360	8.7	16.7	0.99190	0.90810	0.90074	AVERAGE 0.94617
1029	449	324	10.5	16.5	0.99190	0.90027	0.89297	
1010	639	368	21.7	11.2	0.99190	0.99917	0.99097	
1030	471	346	5.0	21.1	0.99190	0.11365	0.11273	
1018	541	381	11.6	19.1	0.99190	0.99542	0.98775	
1017	593	422	11.6	15.6	0.99190	0.99796	0.98987	
1019	725	420	9.4	12.7	0.99190	0.99833	0.98826	
1014	451	299	4.8	17.2	0.99190	0.01513	0.01491	
1016	485	290	6.2	14.9	0.99190	0.31256	0.31003	AVERAGE 0.16247

TABLE 4.7
FACTORIAL ANALYSIS

LEVEL	VARIABLE						
	POWDER	% MgO	BALL TYPE	WET/DRY	TIME	MACHINING SOURCE	DUMMY VARIABLE
CP85	0.73571						
KBI	0.78209						
KBI	0.04638						
2% MgO		0.56361					
5% MgO		0.95419					
5% MgO		0.39058					
WC			0.97829				
Al_2O_3			0.53951				
WC			0.43878				
WET				0.74747			
DRY				0.77033			
DRY				0.02286			
48 HOURS					0.74543		
72 HOURS					0.77237		
72 HOURS					0.02694		
B CO.						0.55228	
T CO.						0.96552	
T CO.						0.41324	
DUMMY (+)							0.75926
DUMMY (−)							0.75854
DUMMY (+)							0.00072

RANKING OF STRENGTH OF VARIABLES AT THEIR INDICATED LEVEL CHANGES:

RANK:	1	2	3	4	5	6	7
VARIABLE:	BALL TYPE	MACHINING SOURCE	% MgO	POWDER	TIME	WET/DRY	DUMMY
EFFECT:	0.43878	0.41324	0.39058	0.04638	0.02694	0.02286	0.00072

AVERAGE REPRODUCIBILITY IN EXPERIMENTS 1 AND 8 = 1/2(0.99160-0.90074) + 1/2(0.31003-0.01491) = 0.19299

4.2 STRENGTH OF THE HPSN/HPSN BOND IN THREE-PIECE DUO-DENSITY ROTORS

In the three-piece rotor fabrication approach, one of the major concerns has been the quality of the HPSN/HPSN bond at the neck region of the hub. Therefore, six rotors made under varying conditions of bonding were evaluated for bond strength. All the hubs and bond rings were made from CP85 powder. Four rotors had 2% MgO in the hub and 5% MgO in the bond ring, one rotor had 5% MgO in the hub and 7% MgO in the bond ring. The pre, pressures varied slightly from 1500 to 2000 psi. The milling conditions also were varied, as shown in Table 4.8. It can be noted that wet alumina milling was excluded.

TABLE 4.8
ROTOR PROCESSING CONDITIONS AND SUMMARY DATA

	ROTOR NUMBER					
	1114	1118	1165	1159	1161	1157
HUB:	2% W72D	2% W48W	2% A48D	2% A48D	5% A48D	5% A48D
BOND RING:	5% W72W	5% W144W	5% A48D	5% A48D	5% A48D	7% A48D
BONDING PRESSURE, MPa (PSI):	10.3 (1500)	10.3 (1500)	10.3 (1500)	13.8 (2000)	13.8 (2000)	13.8 (2000)
FLAT CUT BARS, SURFACES IN TENSION						
θMPA (ksi) CHARACTERISTIC STRENGTH	283 (41.1)	394 (57.2)	206 (29.9)	207 (39.1)	343 (49.8)	230 (33.4)
m WEIBULL MODULUS	3.7	8.0	5.5	3.0	5.0	1.5
n NUMBER OF BARS	8	8	6	8	7	6
EDGE CUT BARS						
θH	243 (35.3)	328 (47.5)	215 (31.2)	246 (35.7)	412 (59.7)	345 (50.1
m	5.3	6.1	4.2	3.9	11.7	14.7
n	8	6	6	7	6	7
FLAT CUT BARS, CENTER IN TENSION						
θ	363 (52.6)	406 (58.9)	285 (41.3)	348 (50.5)	441 (63.9)	374 (54.3)
m	5.4	7.3	7.9	3.1	16.6	7.7
n	6	6	6	6	5	6
TYPE OF BREAK						
FOLLOWS BOND COMPLETELY	9	6	18	9	5	11
STARTS AT BOND, SHIFTS TO HUB	5	6	—	8	8	8
NOT AT BOND LINE	6	6	—	2	5	
BARS CUT FROM CURVIC (i.e., HUB)						
θ	389 (53.5)	424 (61.5)	448 (64.9)	414 (60.1)	464 (87.3)	447 (64.8)
m	12.8	9.2	13.7	6.4	14.8	15.1
n	8	9	8	8	6	8

Code for compositions:
2%; 5% = percent MgO added
W; A = WC or Al_2O_3 milling balls
48; 72; 144 = hours of milling
W;D = wet or dry milling

The six rotors tested represented six different compositional or forming conditions. The center section of the bond ring, (determined on bars tested with the leading and trailing edges in compression) consistently showed higher characteristic MOR and Weibull moduli than the outer section of the bond (leading and trailing edges in tension). This is probably due to lower density near the surface and to voids remaining after the skin was removed during machining. Variation in bond quality existed from leading edge surface to trailing edge surface, most noticeably with rotor 1157 in which the leading edge strengths were four times those of the trailing edge. In other cases, such as rotor 1159, a variation about the circumference of the rotor occurred.

By grouping the data, with rotors based on 2% MgO bond rings, hubs and 5% MgO mixes using S_3N_4 ground with WC balls (1114 and 1118) were stronger than mixes based on material ground with Al_2O_3 balls (1165 and 1159). Using the same MgO content (5% in rotor 1161) in both hub and bond appeared advantageous.

In summarizing the bond strength evaluation, the numerical data obtained from this series of rotors, combined with visual observation of this group and numerous other rotors, demonstrated that considerable variation existed from pressing-to-pressing and within the individual rotor. When the bond was properly formed, it approached the strength of the basic HPSN materials. These results have pointed

out the difficulty of obtaining consistently uniform, high strengths under current methods of fabrication.

Bond strength was evaluated by cutting MOR test bars across the HPSN/HPSN bonds in different orientations and locations according to Figure 4.1 and testing the bars in different orientations at 1204°C (2200°F) according to the sketches in Tables 4.9 to 4.14. This particular test temperature was chosen because it represented the bond joint conditions at 100% speed and 100% turbine inlet temperature.

The test bars were cut from the hubs in the radial direction and included material from the blade ring, the bond ring, and the inner hub. This technique permitted the HPSN/HPSN bond line to be
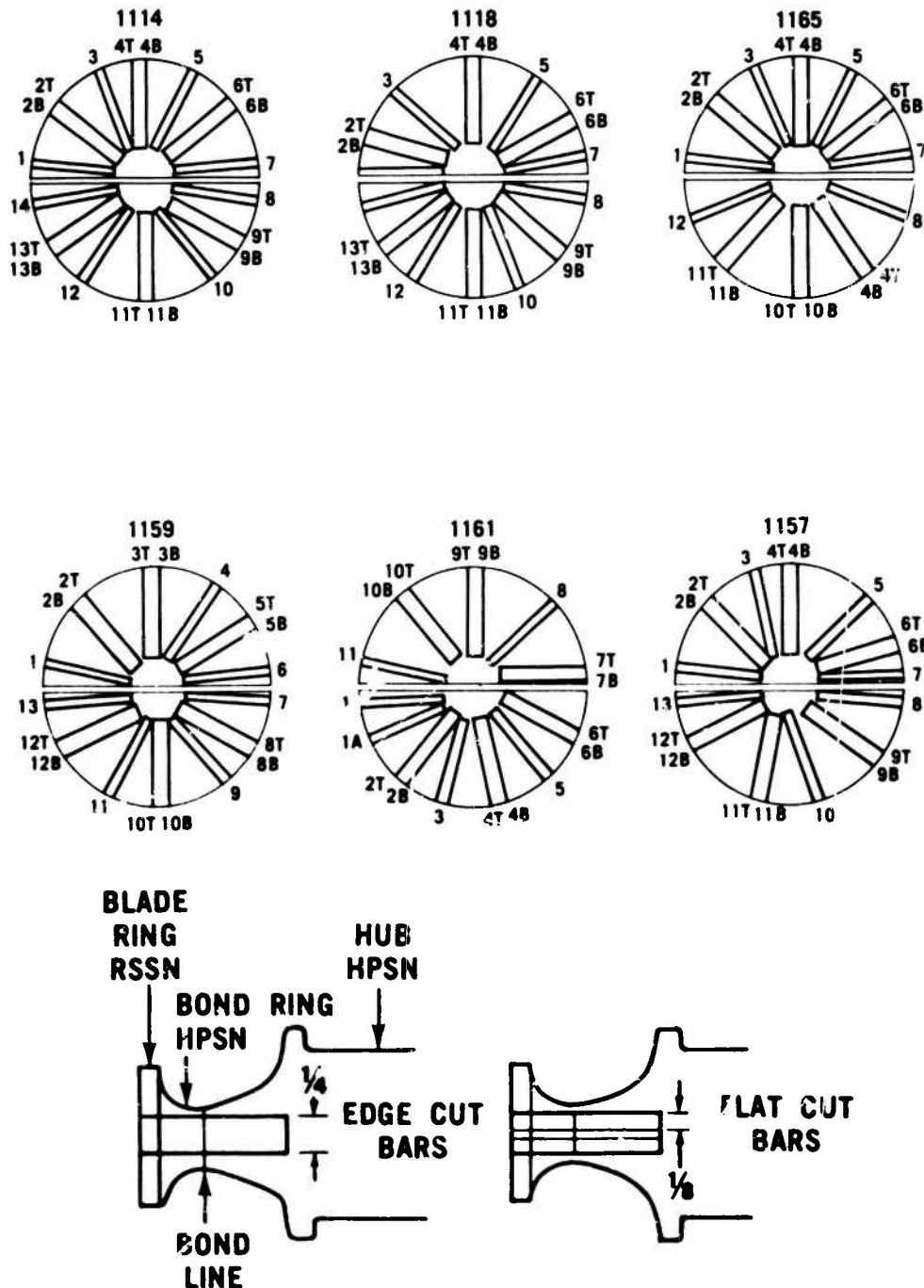

Figure 4.1 — Location of Test Bars within Rotor Hubs

positioned within the upper span of the test jig, and therefore within the zone of uniform maximum stress. The dimensions of the hub permitted cutting bars with two orientations: "on edge" in which the 0.635 cm (1/4-inch) width of the test bar was parallel to the pressing direction or axis of the rotor, and "flat" in which the 0.318 cm (1/8-inch) thickness was parallel to the pressing direction. The edge-cut bars therefore represented the center portion of the bond, since most of the material at the surfaces of the hub as formed was removed during cutting and finishing. The flat-cut bars were cut in two layers so that, with reference to the pressing direction, the top surface of the upper bar, and the bottom surface of the lower bar represented material close to the machined surfaces of the rotor. The lower surface of the top bar and the top surface of the lower bar would be typical of the material in the center of the bond. The bars were broken with either surface or interior portions of the bond in tension in order to determine if differences in strength occurred across the bond width. The data obtained are summarized in Table 4.9, and the individual values are shown in Tables 4.9 through 4.14.

TABLE 4.9
ROTOR 1114 BOND STRENGTHS

Hub (#1080) Material: KBl-1 powder, milling GR-2, dry milled 72 hours with WC balls. Two percent MgO, pressed at 34.5 MPa (5000 psi).

Bond Material: CP-85-B powder, milling GQ-5, wet milled 72 hours with WC balls. Five percent MgO, pressed at 10.3 MPa (1500 psi).

Bars Cut on Edge

Bars#				
1	240 MPa	34,800 psi	(3)	θ = 243 (211-282) MPa
3	190	27,500	(3)	= 35,390 (30,800-40,900) psi
5	171	24,800	(1)	m = 5.28 (2.62-7.33)
7	192	27,800	(3)	
8	270	39,200	(3)	
10	285	41,300	(3)	
12	260	37,700	(3)	
14	203	29,400	(3)	
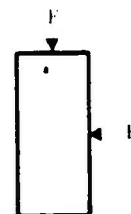
Bars Cut Flat

Leading Edge in Tension

2B	192 MPa	27,800 psi	(1)	
6B	154	22,300	(1)	θ = 286 (221-375) MPa
11B	338	49,000	(2)	= 41,400 (32,100-54,400) psi
				m = 3.69 (1.51-5.29)

Trailing Edge in Tension

2T	282 MPa	40,900 psi	(2)
6T	318	46,100	(2)
11T	280	40,600	(2)
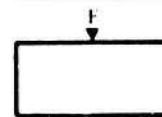
Leading Edge in Compression

4B	345 MPa	50,100 psi	(3)	
9B	416	60,300	(2)	θ = 363 (305-437) MPa
13B	397	57,600	(3)	= 52,600 (44,200-63,300) psi
				m = 5.42 (2.23-7.78)
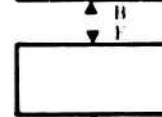
Trailing Edge in Compression

4T	306 MPa	44,400 psi	(1)
9T	284	41,200	(1)
12T	290	42,000	(2)
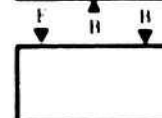
Bars from Curvic

15	339 MPa	49,200 psi	
16	331	48,000	
17	379	54,000	
18	393	57,000	
19	368	53,400	
20	322	46,700	
21	385	55,900	
22	334	48,400	

θ = 369 (348-392) MPa
= 53,500 (50,400-56,800) psi
m = 12.8 (6.34-17.8)

F is direction of forming.
B is direction of breaking

Notes:
(1) Break initiated at bond line but moved into bonding material.
(2) Break in hub material, away from bond line.
(3) Break followed bond line.
(4) Break initiated outside upper knife edges.

Numbers in parentheses following θ and m are the 90% confidence limits

79

TABLE 4.10
## ROTOR 1118 BOND STRENGTHS

Hub (#1055) Material: KBI-1 powder, milling GC-2. Wet milled 48 hours with WC balls. Two percent MgO, pressed at 34.5 MPa (5000 psi).

Bond Material: CP85B powder, milling GU-5. Wet milled 144 hours with WC balls. Five percent MgO, pressed at 10.3 MPa (1500 psi).

Bars Cut on Edge

Bar #					
5	291 MPa	42,200 psi	(3)	θ = 328 (286-379) MPa
7	260	37,700	(1)	= 47,500 (41,500-54,900) psi
8	260	37,700	(3)	m = 6.09 (2.79-8.58)
10	361	52,300	(3)	
12	330	47,800	(3)	
14	375	54,400	(3)	
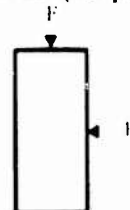
Bars Cut Flat

Leading Edge Tension

2B	392 MPa	56,900 psi	(1)	θ = 394 (337-466) MPa
6B	442	64,100	(2)	= 57,200 (48,900-67,600) psi
11B	410	59,500	(1)	m = 5.98 (2.46-8.59)
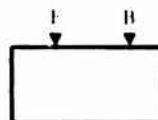
Trailing Edge Tension

2T	248 MPa	36,000 psi	(2)
6T	387	56,200	(2)
11T	336	48,700	(2)
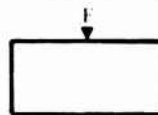
Leading Edge Compression

4B	440 MPa	63,800 psi	(2)	θ = 406 (357-487) MPa
9B	423	61,300	(3)	= 58,900 (51,800-67,700) psi
13B	427	61,900	(1)	m = 7.27 (2.98-10.4)

Trailing Edge Compression

4T	370 MPa	53,700 psi	(2)
9T	282	40,900	(1)
13T	364	52,800	(1)
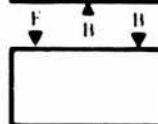
Bars From Curvic

15	390 MPa	56,700 psi	θ = 424 (387-466) MPa
16	387	56,200	= 61,500 (56,200-67,800) psi
17	476	69,100	m = 9.17 (4.20-12.9)
18	368	53,400	
19	422	61,200	
20	417	60,500	
21	392	56,900	

F is direction of forming.
B is direction of breaking.

Notes. (1) Break initiated at bond line, but moved into bonding material.

(2) Break in hub material, away from bond line.

(3) Break followed bond line.

(4) Break initiated outside upper knife edges.

Numbers in parenthesis following θ and m are the 90% confidence limits.

TABLE 4.11
ROTOR 1165 BOND STRENGTHS

Hub (#1158) Material: CP-85-B powder, milling HB-2. Dry milled 58 hours with
Al$_2$O$_3$ balls, two percent MgO. Pressed at 34.5 MPa (5000 psi).

Bond Material: CP 35-B powder milling HD-5. Dry milled 48 hours with
Al$_2$O$_3$ balls, five percent MgO. Pressed at 10.3 MPa (1500 psi).

Bars Cut on Edge

Bar #				
1	282 MPa	40,900 psi	(3)	θ = 214 (189-302) MPa
3	189	27,400	(3)	= 31,000 (27,400-43,800) psi
5	179	25,900	(3)	m = 4.2 (1.7-8.0)
7	197	28,500	(3)	
8	273	39,600	(3)	
12	194	28,200	(3)	

Bars Cut Flat

Leading Edge Tension

2T	210 MPa	30,500 psi	(3)	
6T	108	15,600	(3)	θ = 206 (176-248) MPa
10T	221	32,000	(3)	= 29,900 (25,200-35,900) psi
				m = 5.5 (2.3-7.9)

Trailing Edge Tension

2B	224 MPa	32,500 psi	(3)
6B	185	26,800	(3)
10B	203	29,500	(3)

Leading Edge Compression

4T	226 MPa	32,800 psi	(3)	
9T	310	44,900	(3)	θ = 285 (253-324) MPa
11T	250	36,300	(3)	= 41,300 (36,700-47,900) psi
				m = 7.9 (3.2-11.3)

Trailing Edge Compression

4B	307 MPa	44,600 psi	(3)
9B	263	38,20⁻	(3)
11B	272	39,⁻00	(3)

Bars From Curvic

F is direction of forming
B is direction of breaking

13	433 MPa	62,800 psi	
14	467	67,700	θ = 441 (423-474) MPa
15	389	56,400	= 64,000 (61,400-68,700) psi
16	390	56,600	m = 13.7 (6.81-19.1)
17	462	67,000	
18	453	65,700	
19	467	67,600	
20	399	57,900	
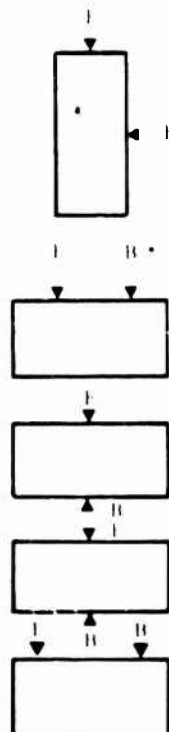
Notes: (1) Break initiated at bond line, but moved into bonding material.
(2) Break in hub material, away from bond line.
(3) Break followed bond line.
(4) Break initiated outside upper knife edges.

Numbers in parenthesis following θ and m are the 90% confidence limits.

TABLE 4.12
ROTOR 1159 BOND STRENGTHS

Hub (#1155) Material: CP-85-B powder, milling HB-2. Dry milled 48 hours with Al_2O_3 balls, two percent MgO. Pressed at 34.5 MPa (5000 psi).

Bond Material: CP-85-B powder, milling HD-5, dry milled 48 hours with Al_2O_3 balls, five percent MgO. Pressed at 13.8 MPa (2000 psi).

Bars Cut on Edge

Bar #			
1	164 MPa	23,800 psi	(3)
4	253	36,700	(1)
6	260	37,700	(3)
7	308	44,600	(3)
9	248	35,700	(1)
11	192	27,800	(3)
13	155	22,500	(1)

$\theta = 246$ (199-308) MPa
  $= 35,700$ (28,900-44,600) psi
m $= 3.92$ (1.80-5.53)
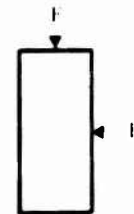
Bars Cut Flat

Leading Edge Tension

2B	253 MPa	36,700 psi	(1)
5B	217	31,400	(3)
10B	181	28,200	(3)

$\theta = 270$ (198-376) MPa
  $= 39,100$ (28,700-54,500) psi
m $= 3.03$ (1.25-4.35)
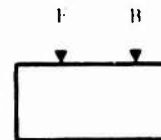
Trailing Edge Tension

2T	154 MPa	22,300 psi	(3)
5T	320	46,400	(1)
10T	339	49,200	(1)
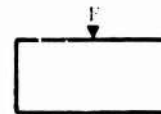
Leading Edge Compression

3B	248 MPa	36,000 psi	(1)
8B	429	62,200	(2)
12B	233	33,800	(3)

$\theta = 348$ (256-483) MPa
  $= 50,500$ (37,200-70,000) psi
m $= 3.07$ (1.26-4.41)
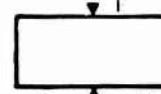
Trailing Edge Compression

3T	323 MPa	46,700 psi	(1)
8T	427	61,900	(3)
12T	232	33,700	(2)
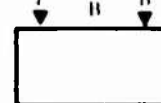
F is direction of forming.
B is direction of breaking.

Bars Cut From Curvic

14	397 MPa	57,600 psi
15	356	51,600
16	435	63,100
17	483	70,400
18	328	47,500
19	409	59,300
20	417	60,500
21	293	42,500

$\theta = 414$ (369-468) MPa
  $= 60,100$ (53,500-67,900) psi
m $= 6.44$ (3.19-8.94)

Notes: (1) Break initiated at bond line, but moved into bonding material.
(2) Break in hub material, away from bond line.
(3) Break followed bond line.
(4) Break initiated outside upper knife edges.

Numbers in parenthesis following θ and m are the 90% confidence limits.

TABLE 4.13
ROTOR 1161 BOND STRENGTHS

Hub (#1156) Material: CP85B powder, milling HC-5. Dry milled 48 hours with Al$_2$O$_3$ balls, five percent MgO. Pressed at 34.5 MPa (5000 psi).

Bond Material: CP85B powder, milling HD-5. Dry milled 48 hours with Al$_2$O$_3$ balls, five percent MgO. Pressed at 13.8 MPa (2000 psi).

Bars Cut on Edge

Bar #		MPa	psi		
	1	397 MPa	57,600 psi	(1)	θ = 412 (379-448) MPa
	1A	415	60,200	(2)	= 59,700 (55,000-65,000) psi
	3	439	63,600	(2)	m = 11.7 (4.8-16.7)
	5	352	51,000	(2)	
	8	361	52,400	(3)	
	11	419	60,800	(2)	

Bars Cut Flat

Trading Edge Tension

		MPa	psi		
	7T	293 MPa	42,500 psi	(3)	θ = 343 (290-409) MPa
	10T	350	50,700	(1)	= 49,800 (42,100-59,300) psi
					m = 5.0 (2.3-7.0)

Trailing Edge Tension

		MPa	psi	
	7B	421 MPa	61,100 psi	(1)
	10B	339	49,200	(1)
	2T	246	35,700	(3)
	4B	308	44,600	(3)
	6T	286	41,500	(1)
				(4)

Leading Edge Compression

		MPa	psi		
	9B	429 MPa	62,200 psi	(1)	θ = 441 (412-475) MPa
	2B	423	61,300	(2)	= 63,900 (59,700-68,900) psi
	4T	437	63,400	(3)	m = 16.6 (6.0-24.3)
	6B	462	67,000	(1)	

Trailing Edge Compression

		MPa	psi	
	9T	405 MPa	58,800	(1)

Bars From Curvic

	MPa	psi	
12	458 MPa	66,400 psi	θ = 464 (435-497) MPa
13	456	66,200	= 67,300 (63,100-72,100) psi
14	494	71,700	m = 14.6 (5.99-20.9)
15	459	66,500	
16	422	61,200	F is direction of forming
17	427	61,900	B is direction of breaking

Notes: (1) Break initiated at bond line, moved into bonding material
      (2) Break in hub material, away from bond line
      (3) Break followed bond line
      (4) Break initiated outside upper knife edges.

Numbers in parenthesis following θ and m are the 90% confidence limits.
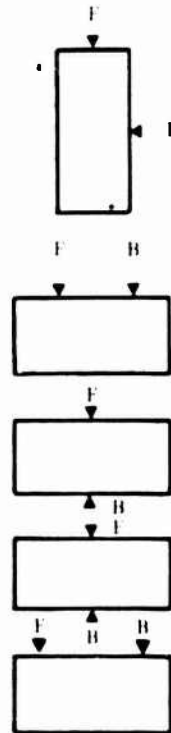
TABLE 4.14
ROTOR 1157 BOND STRENGTHS

Hub (#1154) Material: CP85B powder, milling HC-5. Dry milled 48 hours with
Al_2O_3 balls. Five percent MgO, pressed at 34.5 MPa (5000 psi).

Bond Material: CP85B powder, milling HE-7. Dry milled 48 hours with
Al_2O_3 balls. Seven percent MgO, pressed
at 13.8 MPa (2000 psi).

Bars Cut on Edge

Bar #					
1T	338 MPa	49,000 psi	(3)	θ = 345 (327-387) MPa
3	356	51,600	(3)	= 50,100 (47,400-53,200) psi
5	365	53,000	(3)	m = 14.7 (8.72-20.7)
7	302	43,800	(3)	
8	308	44,600	(3)	
10	348	50,400	(3)	
13	332	48,200	(3)	
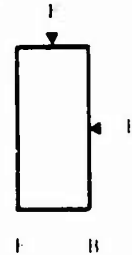
Bars Cut Flat

Leading Edge Tension

2B	302 MPa	43,800 psi	(3)	θ = 230 (121-460) MPa
6B	318	45,800	(3)	= 33,400 (17,500-66,700) psi
11B	325	47,100	(3)	m = 1.48 (0.60-2.09)

Trailing Edge Tension

2T	84 MPa	12,200 psi	(1)
6T	81	11,600	(1)
11T	111	16,100	(1)
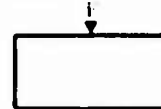
Leading Edge Compression

4B	389 MPa	56,400 psi	(1)	θ = 374 (331-427) MPa
9B	266	38,600	(1)	= 54,300 (48,000-61,900) psi
12B	361	52,300	(1)	m = 7.69 (3.15-11.0)

Trailing Edge Compression

4T	383 MPa	55,600 psi	(1)
9T	323	46,900	(3)
12T	406	58,900	(1)
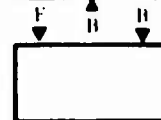
Bars Cut From Curvic

14	388 MPa	56,400 psi	
15	479	69,400	
16	435	63,100	θ = 447 (425-470) MPa
17	450	65,200	= 64,800 (61,600-68,200) psi
18	421	61,100	m = 15.1 (7.47-20.9)
19	417	60,500	
20	428	62,100	
21	456	66,200	

F is direction of forming.
B is direction of breaking.

Notes: (1) Break initiated at bond line, but moved into bonding material.
      (2) Break in hub material, away from bond line.
      (3) Break followed bond line.
      (4) Break initiated outside upper knife edges.

Numbers in parenthesis following θ and m are the 90% confidence limits.

84

The six rotors tested represented six different compositional or forming conditions. The center section of the bond ring, (determined on bars tested with the leading and trailing edges in compression) consistently showed higher characteristic MOR and Weibull moduli than the outer section of the bond (leading and trailing edges in tension). This is probably due to lower density near the surface and to voids remaining after the skin was removed during machining. Variation in bond quality existed from leading edge surface to trailing edge surface, most noticeably with rotor 1157 in which the leading edge strengths were four times those of the trailing edge. In other cases, such as rotor 1159, a variation about the circumference of the rotor occurred.

By grouping the data, with rotors based on 2% MgO hubs and 5% MgO bond rings, mixes using Si_3N_4 ground with WC balls (1114 and 1118) were stronger than mixes based on material ground with Al_2O_3 balls (1165 and 1159). Using the same MgO content (5% in rotor 1161) in both hub and bond appeared advantageous.

In summarizing the bond strength evaluation, the numerical data obtained from this series of rotors, combined with visual observation of this group and numerous other rotors, demonstrated that considerable variation existed from pressing-to-pressing and within the individual rotor. When the bond was properly formed, it approached the strength of the basic HPSN materials. These results have pointed out the difficulty of obtaining consistently uniform, high strengths under current methods of fabrication.

4.3 PROPERTIES OF REACTION SINTERED SIC

Introduction

As previously reported (10), Refel reaction sintered SiC has proven to be a suitable material for the gas turbine combustor. During this reporting period, the statistical strength distributions at room temperature, in both four-point bending and tension, were determined for a batch of the material. In addition, the statistical bend strength distributions at five elevated temperatures were also measured in order to provide Weibull strength parameters for design and for correlation of bend strength distribution with tensile strength distribution.

Material Testing

Bend strength testing was conducted according to the Proposed Military Standards for Testing of Structural Ceramics (14).The MOR vs. temperature data for Refel SiC are presented in Table 4.15. The MLE (Maximum Likelihood Estimator — see Section 5 of this report) Weibull parameters are plotted in Figure 4.2 as a function of temperature. The 90% confidence bands are also shown.

TABLE 4.15

FOUR POINT BEND STRENGTH, KSI, OF REFEL SILICON CARBIDE

Test Temperature

78°F(26°C	47.2	68.3	68.4	66.2	62.1	56.1
	64.0	65.5	51.0	66.1	73.3	71.4
	64.1	64.8	59.1	67.1	47.2	52.6
	64.6	50.3	74.4	56.5	52.6	72.1
	57.6	52.7	54.0	66.4	53.7	54.3
932°F(500°C):	64.4	72.4	61.0	62.2	61.4	69.5
	41.7	61.9	60.6	75.4	84.3	72.3
	66.1	61.6	61.3	68.2	72.8	67.5
	61.6	57.3				
1832°F(1000°C):	64.1	60.6	61.6	59.4	64.8	51.1
	65.8	60.4	43.0	60.3	57.6	53.9
	61.9	66.9	55.4	57.3	50.4	54.4
	58.9	61.7				
2191°F(1200°C):	74.9	84.3	63.5	71.7	80.0	62.4
	64.3	74.5	56.6	68.9	71.9	72.5
	82.0	79.1	57.5	61.1	70.7	69.1
	76.6	60.9				
2372°F(1300°C):	59.9	51.3	70.6	52.9	51.7	80.6
	58.4	66.0	55.9	67.6	67.4	70.6
	68.7	72.1	67.6	74.7	70.5	71.7
	70.2	63.0				
2462°F(1350°C):	60 5	53.3	59.1	57.1	66.4	70.4
	73.1	57.8	58.3	68.1	66.3	53 9
	70.7	63.0	62.5	65.0	64.8	63.5
	65.1	56.2				

The tensile testing was carried out at Pennsylvania State University by Dr. H. Eugene Shull according to a method he developed (18). Figure 4.3 shows a sketch of the tensile specimen. Samples were

finish ground in the longitudinal direction using a 200 grit diamond wheel. Crosshead speed was (0.02) in./min. (0.05 cm./min.).

Fifty nine samples were tested. Eight broke on shoulders where the load was transferred to them by carbide balls. Table 4.16 shows the tensile strength data.Table 4.17 shows the different statistical summaries based on:

(1) All 59 values — Group 1.

(2) All values in Group 1 excluding the two lowest ones regarded as outlyers without quantative justification — Group 2.

(3) All values in Group 2 excluding the eight tests involving shoulder fractures — Group 3.

It can be seen that there is little difference among the three ways of grouping.

Correlation Between MOR and Tensile Strength Distribution

By converting the MOR strength distribution into tensile strength distribution through the Weibull equation, one can compare the converted tensile strength distribution with the experimental distribution.
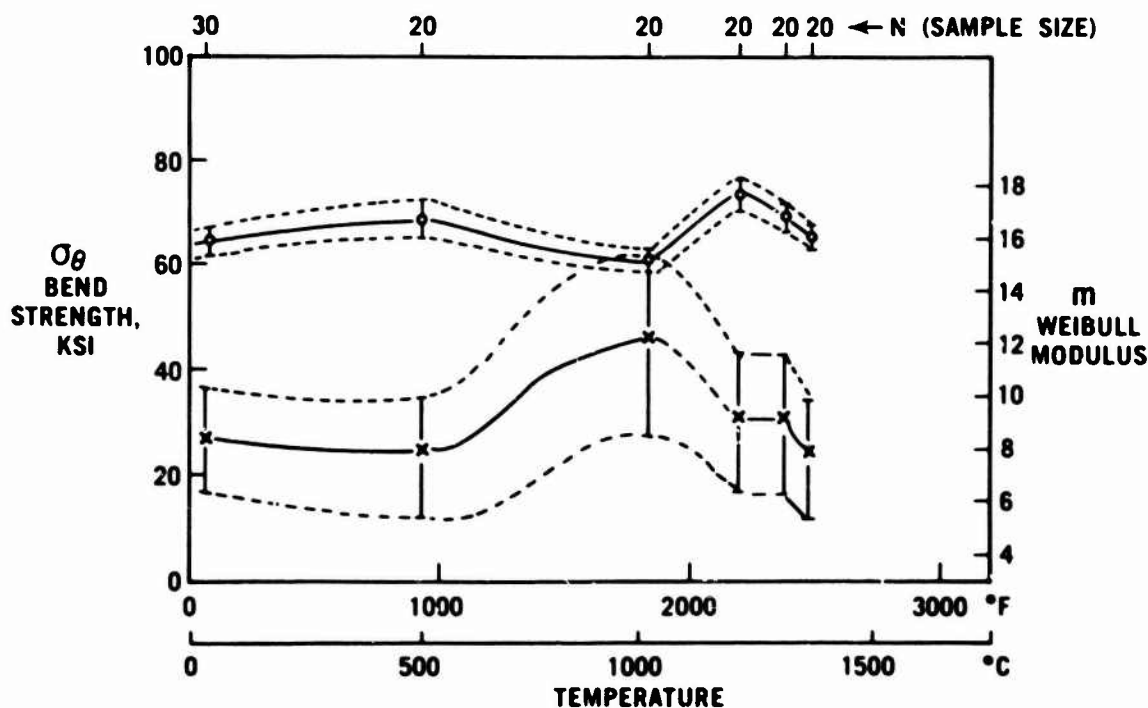
Figure 4.2 — Bend Strength and Weibull Modulus of Refel SiC Vs. Temperature (90% Confidence Limits)
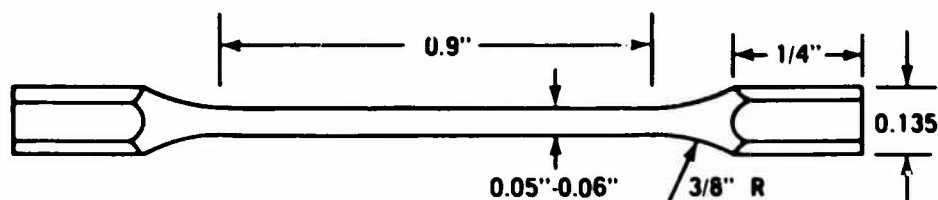
Figure 4.3 — Tensile Test Specimen

TABLE 4.16

ROOM TEMPERATURE REFEL TENSILE DATA, KSI

35.8	46.0	43.7	42.7	27.8	37.4	38.5+
40.6	40.2	39.6	46.1	37.3	39.9	44.0
44.9	40.6	46.6	46.4	33.1	44.2	32.6
45.3	52.1	33.9	51.4	43.3	35.9	47.1
46.6	47.2+	33.3+	47.2	30.1	34.8+	48.4
34.4	44.8	32.2	25.2	36.0+	32.8	41.6+
32.1	42.8	45.7	39.0	42.3+	46.6	46.1+
41.8	31.8	44.9	52.7	47.4	53.4	41.9
37.4	19.7	13.3				

+ Shoulder Fracture.

TABLE 4.17

STATISTICAL SUMMARY OF TENSILE TEST RESULTS

Group	Sample Size	Characteristic Tensile Strength, psi	Weibull Slope m
1	59	43,200 (41,600 - 44,800)	6.3 (5.2 - 7.4)
2	57	43 700 (42,300 - 45,200)	7.3 (6.0 - 8.4)
3	49	44,000 (42,400 - 45,600)	7.1 (5.7 - 8.3)

See text for explanation of grouping.
Based on MLE Weibull program.
Numbers in parenthesis are 90% interval estimates.

Comparison of the calculated and experimental tensile strength distributions is shown in Figure 4.4. It can be seen that the distribution calculated from the MOR data is outside the 90% confidence limits of the experimental tensile strength distribution.

The higher characteristic strength and slightly higher Weibull modulus of the calculated distribution suggests that there may still be significant parasitic stresses and/or inadequate specimen surface quality in the experimental tensile testing.
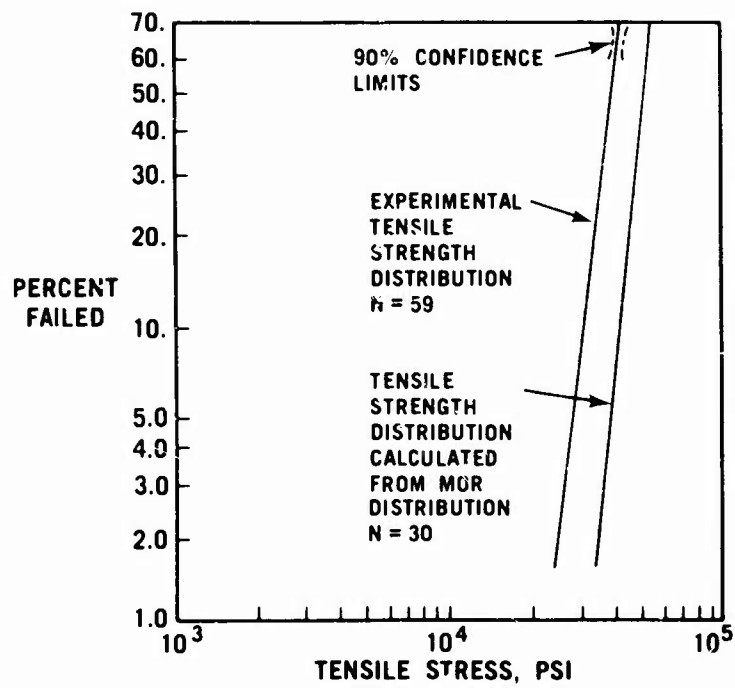
Figure 4.4 — Weibull Distribution of Refel SiC Tensile Strength Measured at 78°F

Introduction

A process for preparing complex shapes of silicon carbide by injection molding and reaction sintering has been developed in-house over the last several years and has been reported in some detail. (19, 20, 21, 22). Briefly, the process consists of three steps:

1. A molding step in which a thermoset polymer filled with SiC particles is injection molded into the desired shape.

2. A carbonization step in which the polymer is pyrolyzed to carbon and a pore structure is formed.

3. A reaction sintering step in which the porous body is infiltrated with molten silicon and the carbon phase is converted to silicon carbide.

The final microstructure and the behavior of the material in each of the processing steps is influenced by the particle size, particle size distribution, and volume fraction of silicon carbide filler. These parameters were investigated to permit optimization of the entire process.

Mechanical Properties

The mechanical properties determined by transverse rupture testing on a brittle solid such as SiC are closely related to the sample surface preparation, gross flaws within the sample, volume of sample under maximum stress, and rate of stress application. Strength normally measured in 4-point loading of SiC samples 1/4 x 1/8 x 1 inch with both as-molded and diamond ground surfaces ranged from values of 30 Kpsi $(21 \times 10^7 N/m^2)$ to 70Kpsi $(48 \times 10^7 N/m^2)$, and examination of fractured pieces indicated that flaws in molding or in surface preparation were strength controlling.

Complex Turbine Parts

To obtain early experience in processing complex shaped parts, several turbine stators have been fabricated. Silicon carbide rotors, as shown in Figure 4.5, have also been substituted as part of an in-house program.

Testing of stators was performed in a modified turbine engine with special provision for securing the stator. The modified engine was alternately ignited and cooled for 10 cycles, after which the stator was examined for damage. After successful completion of this 10-light test, the stator was further tested in a modified engine under controlled heating and cooling conditions, with the maximum stator temperature of 1900°F.

Several SiC stators have been molded and silicided. Figure 4.6 is a photograph of a stator which passed the 10 light test described earlier as well as 147 hours of engine testing without apparent change or deterioration. Further testing of this stator is planned.
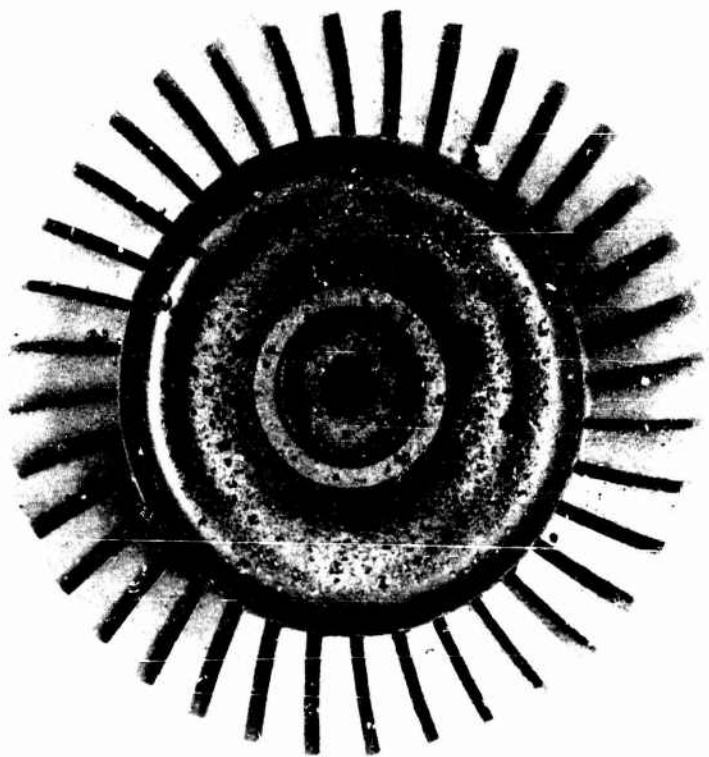
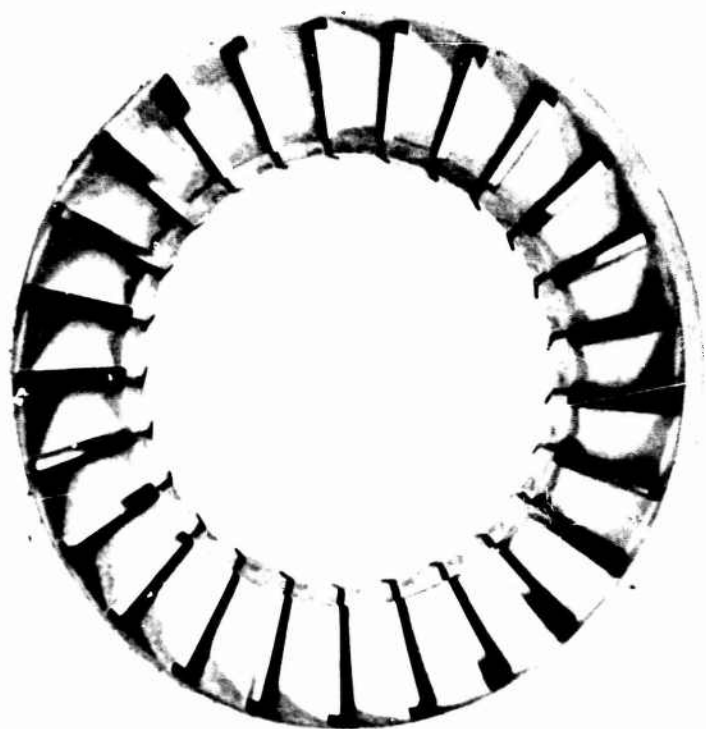Figure 4.5 — Molded Reaction Sintered Silicon Carbide Rotor

Figure 4.6 — Molded Reaction Sintered Silicon Carbide Stator

NITRIDING OF REACTION BONDED SILICON NITRIDE

Introduction

In the previous report (10) it was concluded that a microstructure of uniform fine porosity yielded the best physical properties for 2.7 g/cc density injection molded reaction bonded Si_3N_4. It was also concluded that the nitriding exotherm must be controlled in order to obtain a uniform microstructure. A time-temperature cycle was proposed that accomplished these goals for small furnace loads. However, when this cycle was used with large furnace loads, typical of loads used for nitriding of turbine engine components, a microstructure characteristic of an uncontrolled exotherm resulted.

This section will describe work on a control system to nitride large furnace loads without encountering the exotherm. Typical microstructures will be presented to show that this system does control the nitriding exotherm and can produce components with optimum microstructure.

Background

The furnace used for nitriding large loads of silicon was a cold wall vacuum furnace with molybdenum heat shields and tungsten heating elements. The furnace was equipped with a temperature controller, programmer and recorder. The nitridings were performed in a static atmosphere controlled at 3 psi positive pressure. It was observed that during the course of a nitriding run, the furnace pressure would frequently drop below the desired control pressure. When the pressure falls below the control pressure, a solenoid is automatically opened and gas is admitted to the furnace to bring the furnace pressure back to the control pressure. An event marker was installed in the temperature recorder which indicated when the gas inlet solenoid opened. Over a large number of runs, the pressure fluctuations seemed to correlate with temperature increases. As temperature holds were encountered, the fluctuations decreased with time. This indicated that there seemed to be a correlation between the pressure behavior of the furnace chamber and the nitriding reaction.

The Nitrogen Demand Cycle

The nitriding and microstructure data indicate that the nitriding reaction cannot be controlled when a programmed temperature cycle is employed. In order to control the exothermic behavior of the reaction, it seemed reasonable to allow the reactants to control the rate of reaction. This was accomplished by monitoring the reaction rate at one temperature and allowing the reaction to reach completion at that temperature before allowing the temperature to increase. This reasoning forms the basis of the nitrogen demand cycle.

The schematic of the nitrogen demand control system is shown in Figure 4.7. The components are the same as previously described, except that a logic system has been added. This nitrogen demand control behaves in a manner such that when a pressure fluctuation occurs, the temperature program is instructed to hold and a timer is activated. Every additional pressure fluctuation resets this timer to its starting position. The timer must operate for a prescribed period of time (Tc) before the temperature programmer is allowed to advance. The temperature will then increase until another pressure fluctuation is noted and the sequence repeats itself until the maximum temperature of 1400°C is reached. The purpose of the time constant, Tc, is to insure the reaction has reached equilibrium before the temperature is increased. In practice, Tc is between 7 and 12 minutes.

Other control techniques have been employed in attempts to implement this basic concept. Lumby [23] has used thermocouples imbedded in the silicon in conjunction with temperature comparator circuitry to measure the difference between part temperature and furnace temperature. When the temperature difference becomes too large, the partial pressure of nitrogen in the furnace is decreased, thereby retarding the reaction. Messier [24] has employed mass flow meters to detect increased demand for nitrogen by monitoring changes in gas flow. When the flow exceeds predetermined limits, temperature holds would occur. The closed loop pressure control system just described has the advantages of being easy to instrument and allowing the nitriding to be carried out in a quasi static environment, which a number of investigators [25, 26] deem desirable.

Nitriding Results

The nitriding information discussed in this section consists of the temperature cycle, percent nitrogen consumption and typical microstructure. The percent gas consumption was calculated based on the number of pressure fluctuations recorded. During the course of this nitriding development program, the quality of the test bars in terms of molding flaws varied to a large extent, making the resulting modulus of rupture values questionable. Consequently, only the microstructure was presented because it was felt that it formed the most reliable basis for evaluating material quality.

Figure 4.8 shows the results for three nitriding runs which were performed using a fixed temperature program. Two runs, B-36 and B-45, consisted of two temperature hold periods followed by a
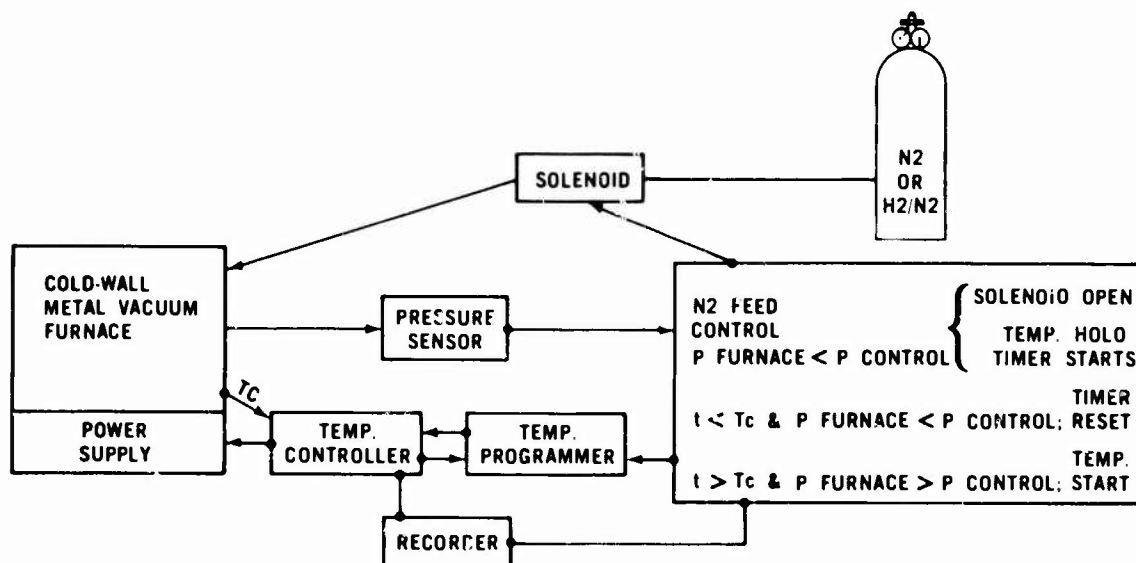

Figure 4.7 — Schematic of the Nitrogen Demand Cycle
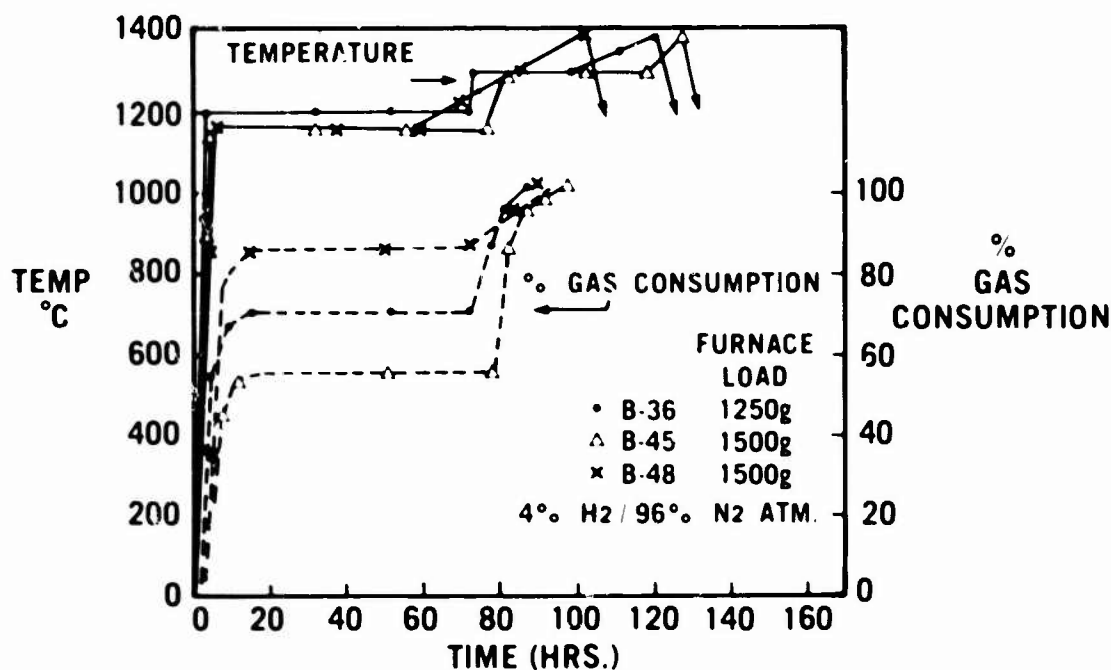
Figure 4.8 — Time Vs. Temperature and Gas Consumption Vs. Time Profiles of
Three Programmed Nitridings

94

constant ramp rate up to the maximum nitriding temperature of 1400°C. One run, B-48, was a constant rate cycle as defined in the last report (10). The gas consumption curves were similar in that a large portion of the nitriding occurred during the first 20 hours of the cycle, with no appreciable nitriding being performed over the long initial hold period. For the B-36 and B-45 cycles a second large gas consumption region corresponds to the second temperature ramp and hold period. For the constant-rate cycle B-48, the gas consumption rate in the second "use" region is lower than for the other cycles. This corresponds to the slower temperature ramp rate.

The microstructures of the silicon nitride (Figure 4.9) from these three cycles are all similar in that there are regions of large grains (see arrows) which have been identified with the nitriding exotherm and the temperature exceeding the melting point of silicon (10). This type of microstructure has been associated with low strength RBSN, and is considered undesirable.

Figure 4.10 shows the results of three nitrogen demand cycles. The input for the temperature programmer is shown to be a linear increase (10°C/hr) from 1000°C to 1400°C. However, the demand cycle logic extends this cycle from 40 hours to as much as 160 hours with the actual cycle time depending on the number and frequency of occurance of the pressure fluctuations. The gas consumption curves are approximately linear with time, showing that the nitriding proceeds at a continous, constant rate.

Examination of the microstructures from these nitridings, Figure 4.11, yields no evidence that the melting point of silicon (1420°C) was exceeded. The structure is uniform with no apparent large porosity or grains, which could act as defects. The structures obtained with the nitrogen demand cycle also appear to be nitrided more completely. There is very little evidence of free silicon in these structures as compared with structures from the temperature programmed cycles. This structure is typical of high strength material (10).

Discussion

In the last report (10), data was presented concerning the nitriding of 2.7 g/cc density RBSN at a constant temperature of 1177°C. This data is compared to the gas consumption data from run B-36 in Table 4.18. It shows that there is good agreement between the weight gain data and the gas consumption data. The shape of the gas consumption curves are also very similar to the nitriding kinetic curves presented by consumption data (27). This indicated that the gas consumption data is a good approximation of the nitriding behavior of the material.
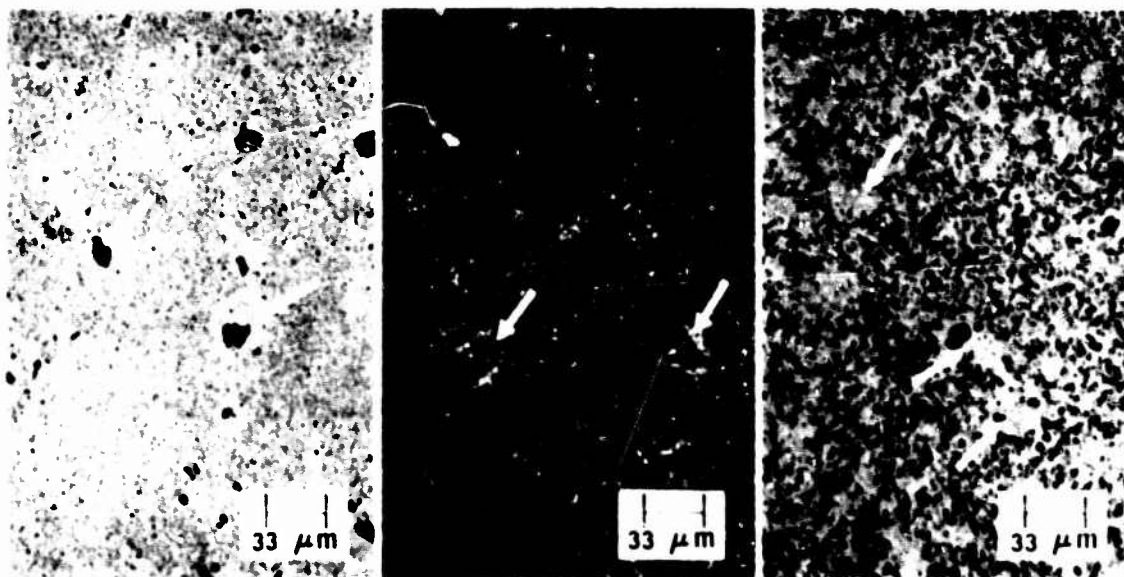
Figure 4.9 — Typical Microstructure of 2.7 gm/cc Density Silicon Nitride from Programmed Nitridings
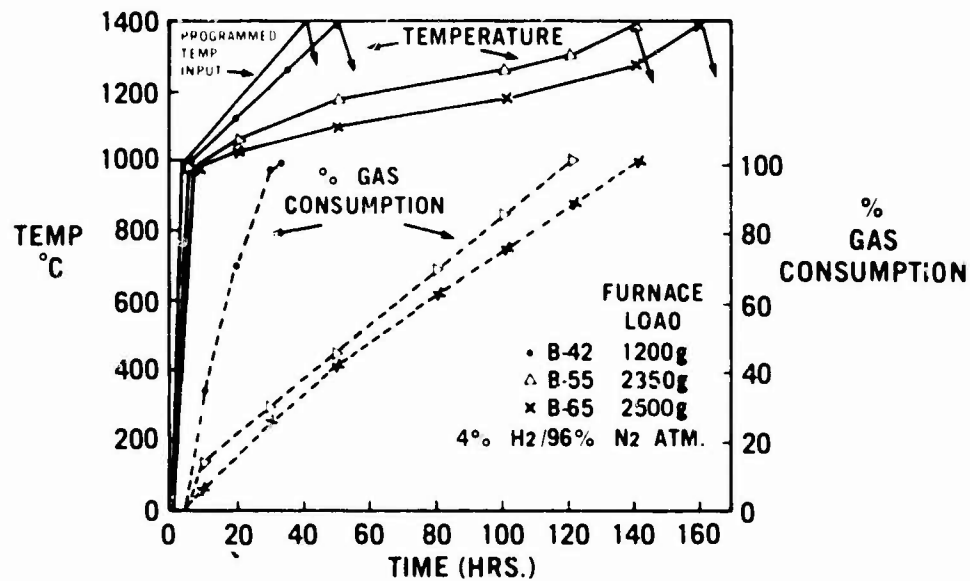
Figure 4.10 — Time Vs. Temperature and Gas Consumption Vs. Time Profiles of
Three Nitrogen Demand Nitridings
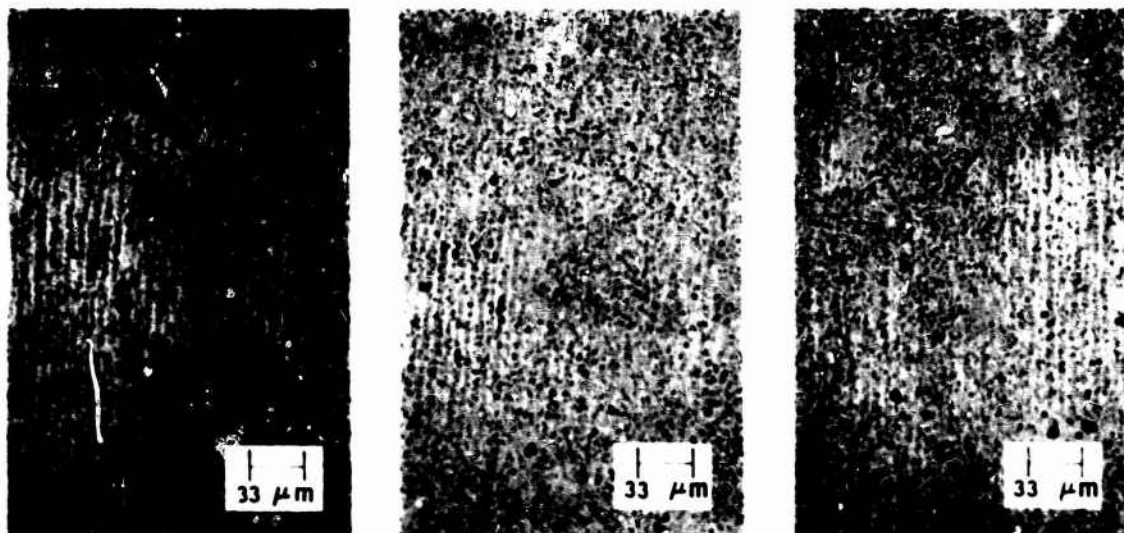
Figure 4.11 — Typical Microstructure of 2.7 gm/cc Density Silicon Nitrides from
Nitrogen Demand Nitridings

TABLE 4.18

NITRIDING BEHAVIOR AT 1177°C

(4% H$_2$/96% N$_2$ Atmosphere)

Weight Gain Results		Gas Consumption Data from Run B-36	
Time at 1177°C	% Nitrided	Time at 1177°C	% Gas Consummed
0	19.2	0	25
24	60.8	24	70
72	59.2	72	70

The gas consumption data from the nitrogen demand cycle shows that the nitriding kinetics have been drastically changed. With the demand cycle, the nitriding rate is approximately linear with time over the entire temperature cycle. Table 4.19 shows that the gas consumption rate (or nitriding rate) seems to vary with increasing furnace load. Because of the nature of the nitrogen demand cycle, the nitriding times are also dependent on the furnace load.

TABLE 4.19

SUMMARY OF NITRIDING DATA

Run No.	Cycle Time	Nitriding ATM	Furnace Pressure (Pc)	Time Constant (Tc)	Furnace Load	Cycle Time	Gas Consumption Rate (Nitriding Rate)
B 36	Temp. Programmed	4% H$_2$/96% N$_2$	3 psig	N.A.	1250g	100 hr	N. A.
B 45	Temp. Programmed	4% H$_2$/96% N$_2$	3 psig	N.A.	1500g	120 hr	N. A.
B 48	Temp. Programmed	4% H$_2$/96% N$_2$	3 psig	N.A.	1500g	125 hr	N. A.
B 42	N$_2$ Demand.	4% H$_2$/96% H$_2$	3 psig	10 Min.	1200g	45 hr	3.0 %/hr
B 55	N$_2$ Demand	4% H$_2$/96% N$_2$	3 psig	10 Min.	2350g	140 hr	0.87%/hr
B 65	N 2 Demand	4% H$_2$/96% N$_2$	3 psig	7 Min.	2500g	160 hr	0.75%/hr

Previous experience shows that the furnace load affects the severity of the nitriding exotherm [10]. It is desirable, therefore, to have a cycle which is dependent upon the furnace load. This system does effectively control the nitriding exotherm.

Summary

Nitriding results from temperature programmed cycles have been presented which show that, for large furnace loads, the microstructure of the resulting 2.7 g/cc density Si$_3$N$_4$ is undesirable. The data also shows that the gas consumption for these cycles occurs over a very small period of time. This implies that the nitriding reaction is not under control.

A control system was developed which allows the furnace load to effectively control the nitriding cycle. The results of this type of nitriding shows the microstructure, for a wide range of furnace loads, does not vary appreciably. When compared to previous results (10), this microstructure is typical of high quality material. The gas consumption data shows that nitriding proceeds in a continous fashion, with the nitriding occurring uniformly over the complete cycle time.

4.6   SIALON RESEARCH

Further work on Sialon research has been terminated by the agencies supporting the overall program. Therefore, this section of the report will review the work which was performed in an effort to develop stable, high strength, sintered Sialon materials.

Summary of Work to Date

When Sialon work was initiated [7], the original Oyama-Jack formulation [28,29] had not yet been shown to be improbable. Therefore, early efforts were concentrated on the pressureless sintering of silicon nitride-alumina mixtures [7,8]. It was discovered [8] that high room temperature strengths [80-90 kpsi in four-point bending] could be obtained by the pressureless sintering of slip cast bars of such mixtures with 3-6% yttria additive, in an argon atmosphere at relatively low temperatures [1600-1650°C] for long times [8-24 hours]. As long as the bars were prepared with not more than 16% by weight alumina, they contained only Sialon as a crystalline phase. Materials prepared with higher or lower yttria contents were not as strong, and those with 16-25% yttria additive showed a glass halo in their x-ray diffraction patterns.

The strengths of all the Si_3N_4-Al_2O_3 and Si_3N_4-Al_2O_3-Y_2O_3 Sialons started to decrease at about 1000°C. This behavior, coupled with the glass halo observed in the x-ray diffraction patterns of the high yttria materials, strongly suggested the presence of a glassy phase whether or not yttria was present. Attempts to crystallize the glass in the yttria-containing Sialons by heat treatment resulted in an additional crystalline product which was predominantly Y_2O_3-$2SiO_2$ [8]. After the crystallization treatment, the room temperature strength was less than before but with little further decrease in strength at elevated temperature.

In the course of some thermal shock tests, it was discovered [10] that those materials containing more than a very small amount of yttria melted to some extent at about 1200°C. The extent of melting increased with increasing yttria in the Sialon, and appeared to be independent of crystallization treatment. The discovery of this melting phenomenon discouraged further work on yttria-containing Sialons.

Continuing studies of additive-free Si_3N_4-Al_2O_3 Sialons showed that room temperature strengths could be increased to the 60 kpsi range [MOR in four-point bending] by suitable selection of sintering conditions, but that strength still decreased at elevated temperature, although only one crystalline phase was present. Presumably these materials still contained a glassy phase.

While these studies of Si_3N_4-Al_2O_3 and Si_3N_4-Al_2O_3-Y_2O_3 materials were in progress, considerable evidence [30,31] was being collected to the effect that Sialon was really the vacancy-free material Si_3N_4-XAl_2O_3-$XAlN$, rather than Si_3N_4-XAl_2O_3. This being the case, it was not surprising that an additional phase was formed in trying to prepare it from just Si_3N_4 and Al_2O_3.

In efforts to prepare single phase Sialons by pressureless sintering of Si_3N_4, Al_2O_3 and AlN or equivalent combinations in the Si_3N_4-Al_2O_3-AlN-SiO_2 system, difficulties were encountered in maintaining the desired composition. Although samples were buried in powders of the same composition, with an intervening thin boron nitride powder layer and placed inside a covered boron nitride crucible, the bars tended to lose weight during sintering, the loss being least for the bars nearest the center of the crucible. In addition, it was found that considerable contamination of the starting powders occurred during milling. Since the powders were milled with high alumina balls, the contaminant was mostly alumina. However, the results of analysis for alumina were markedly dependent upon the analytical technique employed, so that the compositions of starting powders milled in this manner were uncertain.

In order to control weight loss, a sealable boron nitride crucible was fabricated and proved successful. Since contaminant alumina could not be accurately compensated for, work was begun on reducing particle size with an air jet mill. In addition, some fine particle starting powders were obtained. A

number of Sialon specimens have been prepared from unmilled, coarse silicon nitride and aluminum nitride (325 mesh) powders and nominally 0.3 μm alumina as well. Attempts to deal with the silica contamination from the silicon nitride were made by compensating for this contaminant in preparations from SiO_2, Si_3N_4, Al_2O_3 and AlN.

In general, the results obtained, in terms of the phase composition of products, were in good agreement with predictions made from the product diagram of Land, Wimmer, Burns and Chandbury [32]. This particular product diagram was especially convenient for comparison because the x-ray diffraction patterns of all phases were given. Specimens prepared from alumina-rich starting materials which lost little or no weight on sintering contained "J" phase as well as Sialon. Specimens which lost weight generally contained phases near the aluminum nitride corner of the diagram, a reasonable observation if the weight loss resulted from the formation and subsequent decomposition of silica.

Preparations from four-component starting materials tended to contain silicon as well as Sialon, suggesting that some of the silica decomposed before it could react. Materials prepared from SiO_2, AlN, and Al_2O_3 generally contained Si and Al_2O_3, indicating incomplete reaction as well as silica decomposition. A possible consequence of SiO_2 contamination was the frequent finding of a trace of Si materials prepared at relatively high temperatures (1760°C) from Si_3N_4, Al_2O_3 and AlN. The Si was absent from lower temperature preparations.

Sialon specimens prepared at 1760°C from slightly alumina-rich starting materials which contained a trace of "J" phase were of moderate room temperature strength (about 40 kpsi in four-point bending) and remained so at 1200°C. Specimens prepared from stoichiometric but coarse mixtures of Si_3N_4, Al_2O_3 and AlN, buried in powders of the same composition in sealed crucibles, reached theoretical apparent densities whether sintered for one hour at 1650°C under argon or nitrogren, or for one hour at 1760°C under argon. The open porosities were about 27% for the materials prepared at 1650°C and 25% for the 1760° material, not surprising in view of the coarse starting powders. The 1650° materials were single phase, while those prepared at 1760°C contained traces of silicon.

It appears that these two sets of compositions, slightly alumina rich and stoichiometric, bear further investigation with a view toward optimizing materials preparation and sintering conditions.

Introduction

The objective of this effort was to explore methods of forming Si_3N_4 turbine rotors by forming the entire part of RBSN and then hot pressing to densify the areas requiring high strength. This subsequent hot pressing can be unidirectional if the region to be densified is simple in shape, or isostatic if it is complex. Because of the large movements required in hot pressing powder into fully dense material, it is difficult to find a suitable encapsulant which can produce an accurate geometry. In densification of a RBSN part of much greater density than powder, there is not only less movement involved but it is also much easier to seal off the surface contours.

Process Development

Coupons 1-1/4 x 1-1/4 x 1/4 inch and individual rotor blades were made by injection molding of silicon with an organic binder. The chemical analysis of the silicon powder used was: 98.56% Si, 0.04% Ca, 0.82% Fe, and 0.20% Al. After burn-out of the binder, the silicon coupons were then nitrided into Si_3N_4 of 2.46-2.76 g/cc density. The variability of starting microstructures from batch-to-batch was not considered in this feasibility study.

To prepare these coupons for further densification under a hot, high-pressure gaseous environment, the porous surfaces had to be sealed off. Sealing consisted of a coating of boron nitride followed by encapsulation in a vacuum tight Vycor casing. Without the boron nitride barrier, the low viscosity of the Vycor glass at the high temperatures used would permeate the surface layers of the RBSN and pose a differential thermal expansion problem. Figure 4.12 shows a coated and an uncoated Si_3N_4 rotor blade; Figure 4.13 shows an encapsulated specimen.

Hot isostatic pressing was accomplished at Ceramic Systems, Inc., by subjecting the glass encapsulated coupon to argon gas at temperatures of 1730 - 1760°C (3150-3200°F) and pressures of 3000 - 7700 psi for intervals from 15 to 200 minutes at maximum temperature and pressure. The hot isostatic furnace is shown in Figure 4.14.

Hot pressing additives, when used, were introduced into the silicon molding mixture. The nominal additive contents mentioned in this paper refer to the weight percent additive with reference to the silicon powder. These additives improved the plasticity of the Si_3N_4 during densification and reduced the tendency for local cracking. Another way to introduce the densification aids into the RBSN was to soak the RBSN in a salt solution containing the proper metal cation. However, this latter procedure was not employed in the major portion of this project.

Results and Discussion

A total of thirty runs were made, four of which had more than one sample in the furnace. Eight runs were repetitions of the same conditions in order to generate more material for strength evaluation. The effects of additives, hot pressing time, and specimen geometry are presented and discussed below.

Effect of Additives

Under the experimental conditions used, the need for additives to enhance the degree of densification was indicated. Without any additives at all, a slip cast Si_3N_4 sample of 2.05 g/cc density, after being isostatically pressed at 3000 psi and 3150°F for 60 minutes, broke readily during removal of the glass. Its final density was only 2.15 g/cc. In addition, as shown in Figures 4.15 and 4.16, the degree of densification increases with MgO content at constant Fe_2O_3 contents and vice versa. In Figures 4.15 and 4.16, the degree of densification was calculated as:

$$\% \text{ Densification} = \frac{\delta f - \delta o}{\delta t - \delta o} \times 100$$

where δ_f is the final density, δ_0 the initial density, and the theoretical density δ_t of Si_3N_4 is 3.18 g/cc. Although no experiments were made to specifically evaluate the effect of increasing Fe_2O_3 content, Figure 4.16 shows that, at 3.7% MgO, increasing the Fe_2O_3 content from zero to 3% despite shorter pressing times and lower pressing pressures improved the degree of densification. Or, going back to Figure 4.15, one can also see that at constant 0.5% MgO, 60 minutes pressing time, and 7000 psi pressing pressure, the addition of 3% Fe_2O_3 improved the densification from 38% to 85%.
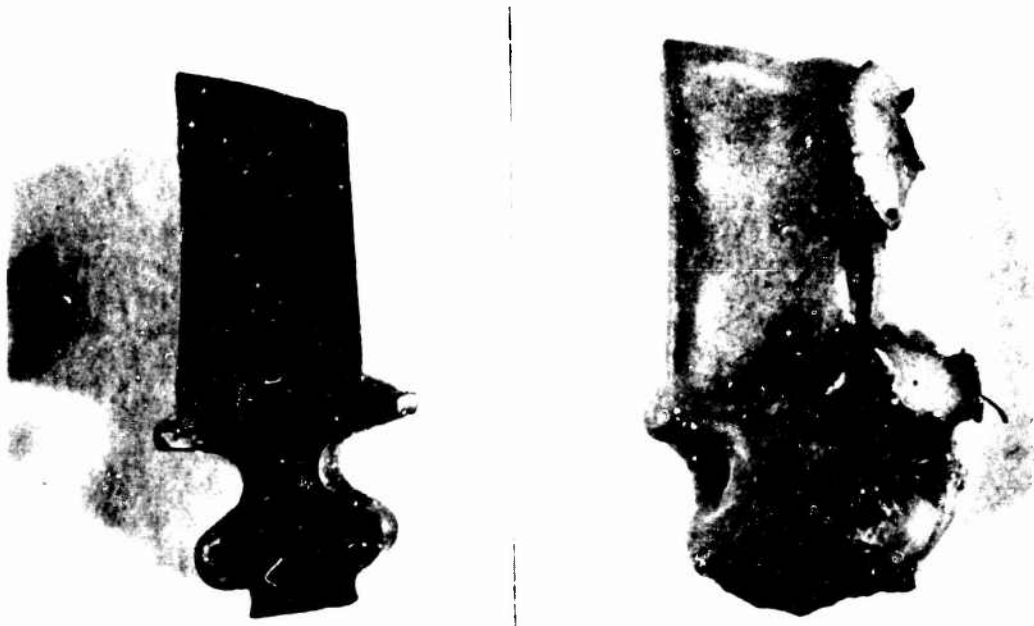
Figure 4.12 — Reaction Sintered Silicon Nitride Before (Left) and After (Right) Boron Nitride Coating
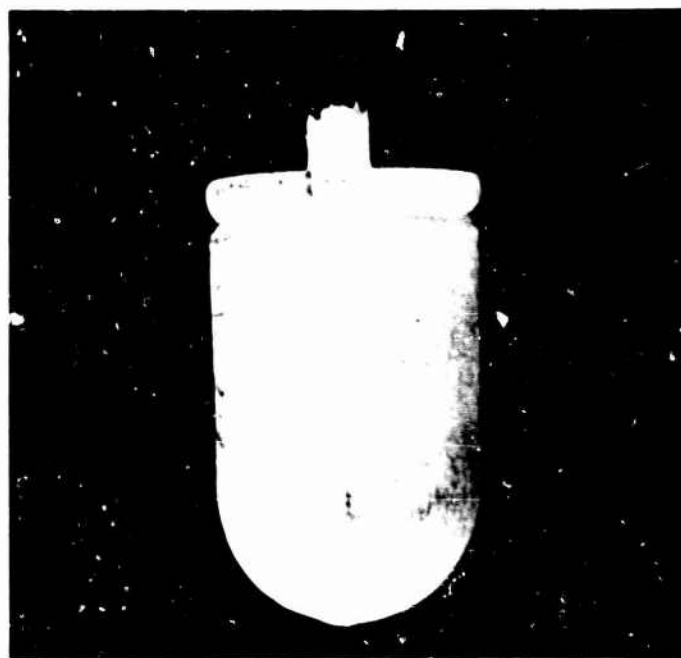
Figure 4.13 — Glass-Encapsulated Specimen Ready for Hot Isostatic Pressing
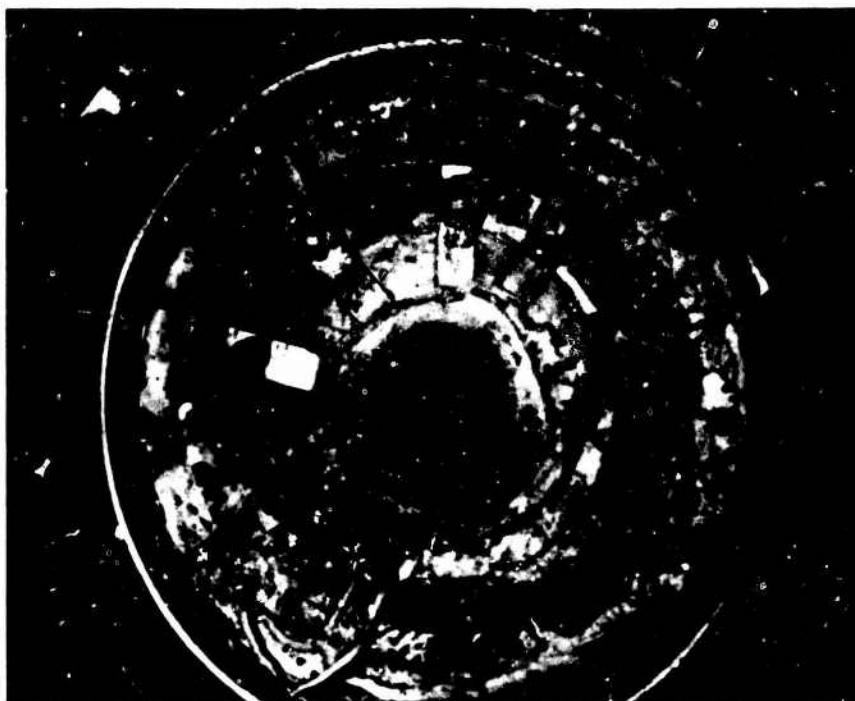
Figure 4.14 — Interior of Hot Isostatic Furnace
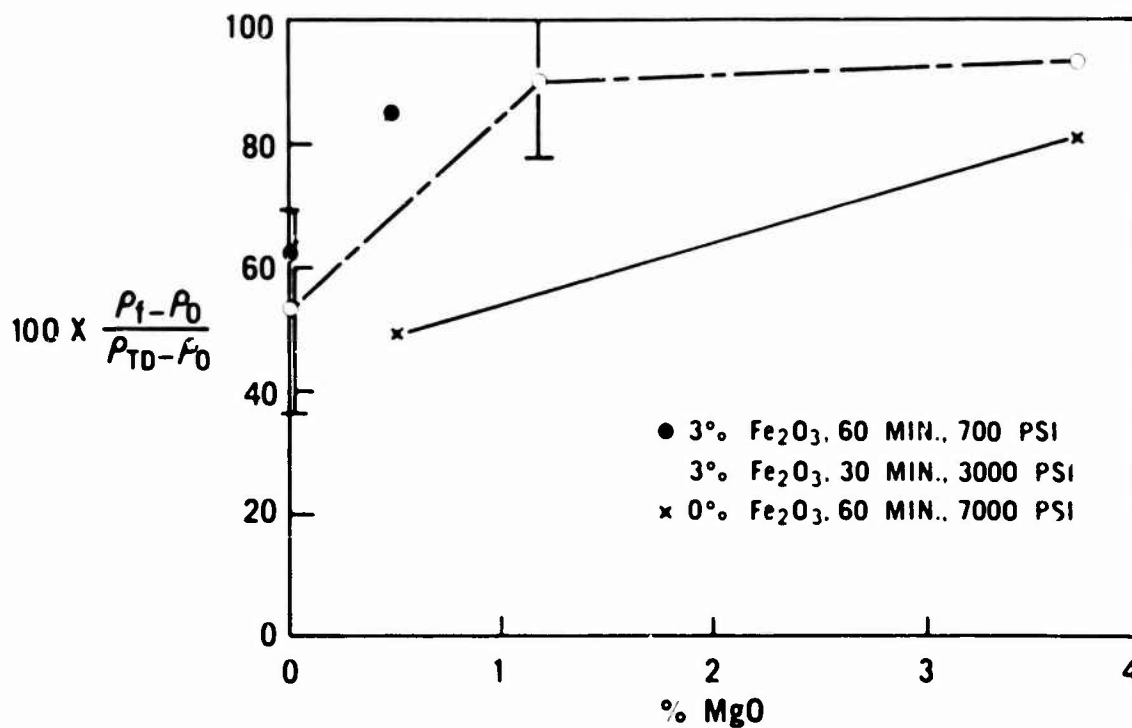
Figure 4.15 — Effect of MgO Content Upon Silicon Nitride Densification

$$100 \times \frac{\rho_f - \rho_0}{\rho_{TD} - \rho_0}$$

Legend:

× 3.7% MgO, 0% Fe$_2$O$_3$, 7000 PSI
● 3.7% MgO, 3% Fe$_2$O$_3$, 3000 PSI
○ 1.2% MgO, 3% Fe$_2$O$_3$, 3000 PSI
▲ 0% MgO, 3% Fe$_2$O$_3$, 7000 PSI
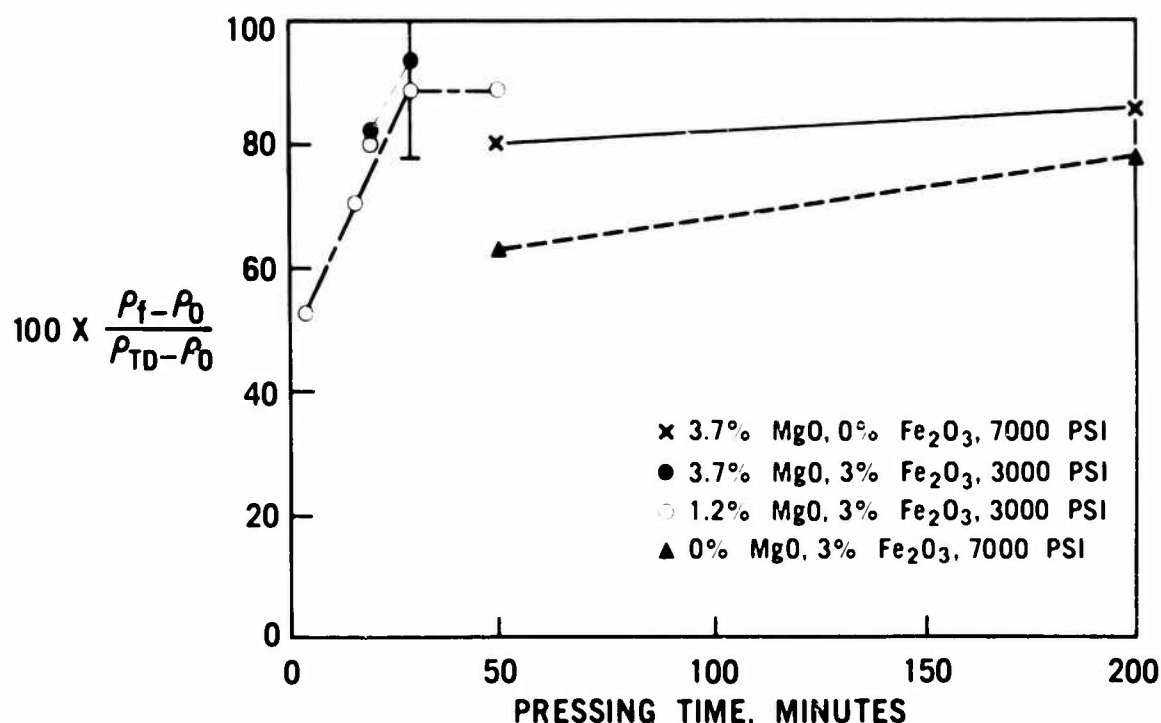
Figure 4.16 — Effect of Pressing Time Upon Silicon Nitride Densification

The data show also that there are various experimental conditions by which one can achieve approximately 90% densification, i.e., 3.14 g/cc final density if starting density were 2.60 g/cc. These conditions include:

1. 3.7% MgO, 0% Fe$_2$O$_3$, 7700 psi, 60 minutes pressing time,

2. 3.7% MgO, 3% Fe$_2$O$_3$, 3000 psi, 20 minutes pressing time,

3. 1.2% MgO, 3% Fe$_2$O$_3$, 3000 psi, 30 minutes pressing time.

All the above parameters are minimum values. In other words, exceeding them should not detract from densification.

Because of the presence of silicides and free silicon in the material, the theoretical density is less than 3.18 g/cc. As shown in Figure 4.17, the isostatically hot pressed material on the right side has nearly zero porosity, but because of the presence of silicides and silicon, its final density measured only 3.15 g/cc. The reason for not using 3.15 g/cc as the theoretical density instead of 3.18 g/cc in computing the percent densification was the variability in the amount of silicides and silicon from sample-to-sample. For more accurate calculations, each sample could be individually measured on a quantative metallograph for % silicides and silicon, and individual density values could be calculated and assigned to each starting RBSN material.

Without any additives at all, some voids crushed leaving localized cracks within the part. This usually occurred in conjunction with a low degree of densification.

Strengthening

Eight coupons made under similar conditions of 3.7% MgO, 0% Fe$_2$O$_3$, 7700 psi, and 60 minutes pressing time were machined into 1/8 x 1/8 x 1 inch bend test bars and tested in four-point bending (3/8 inch top span, 3/4 inch bottom span) at a loading and of 320 lbs/min. to assess the change in the strength-temperature curve due to this densification. Seven coupons made under varying other processing conditions were also evaluated for the degree of strength improvement.

Figure 4.18 shows a comparison of the strengths of several hot isostatically densified (VIP) materials with strengths of various popular classes of Si₃N₄. It can be seen that the VIP materials fall somewhere between RBSN and HPSN. If the starting material had no extraneous silicides and silicon, higher strengths might be expected of the VIP material.

AS — NITRIDED RSSN
250X

AFTER HOT ISOSTATIC PRESSING
500X
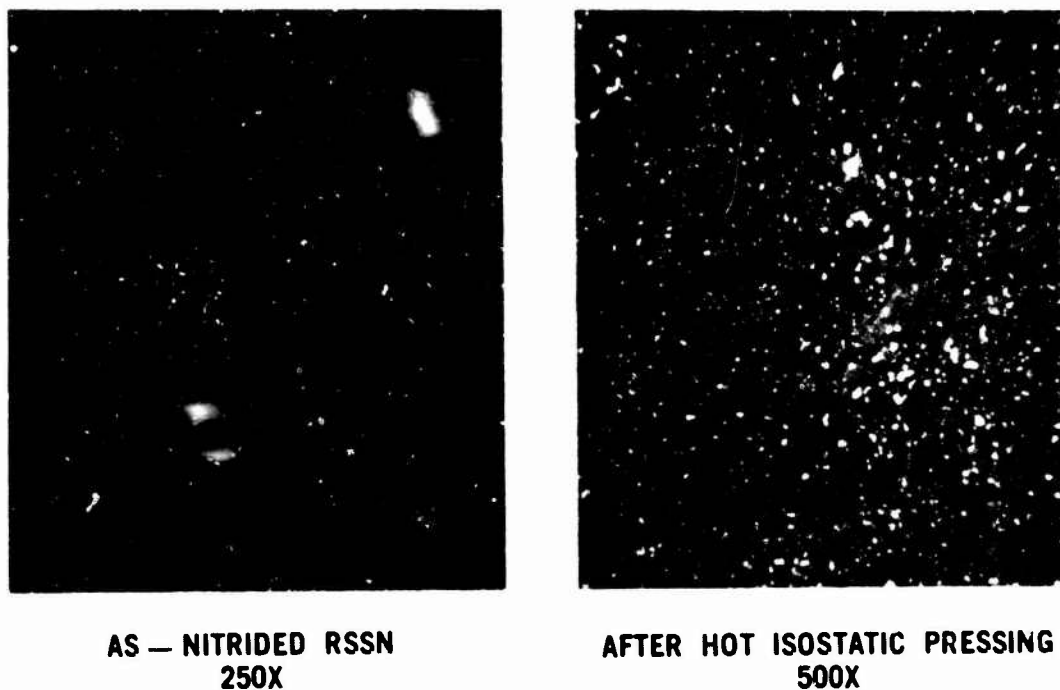
Figure 4.17 — Microstructure of Reaction Sintered Silicon Nitride Before and After Hot Isostatic Pressing
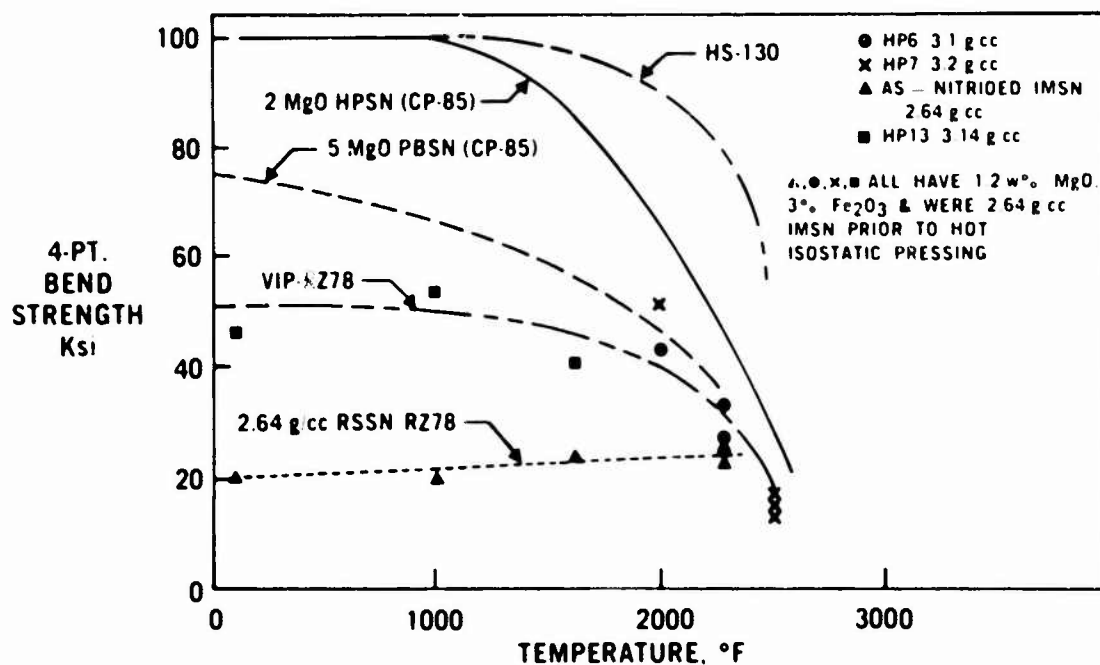
Figure 4.18 — Comparison of Strengths of a Hot Isostatically Densified Silicon Nitride Versus Other Types of Silicon Nitride

The alpha/beta content of the starting material could also play a part in the final strength obtainable, since it has been well known in the hot pressing of Si_3N_4 that starting with alpha powder produces stronger hot pressed Si_3N_4 than starting with beta powder.

It is interesting to note in Figure 4.18 that the RBSN, which contained 3.7% MgO and 3% Fe_2O_3, did not show a strength drop-off up to 2500°F. This is similar to regular RBSN of the same composition made without MgO. Apparently the presence of MgO did not degrade the high temperature strength (beyond 2200°F) until the material had been subjected to the hot isostatic pressing conditions. This is probably due to the formation of the silicate.

Bonding

Two attempts were made to determine the feasibility of diffusion bonding RBSN to HPSN employing hot isostatic pressing. In the first attempt, a bar of RBSN containing no MgO and 3% Fe_2O_3 was encapsulated in intimate contact with a bar of the commercial NC-132 HPSN. After hot isostatic pressing at 7700 psi and 30 minutes, the RBSN showed very little densification and the bond broke easily during machining.

In the second attempt, the RBSN bar contained 3.7% MgO and no Fe_2O_3 and the HPSN bar was made from the commercial CP85 powder with 5% MgO. This pair was hot isostatically pressed at 7700 psi for 60 minutes. A good diffusion bond was obtained, as shown in Figure 4.19. The shrinkage of the RBSN bar also caused a pull on the HPSN bar resulting in a bowed bi-ceramic couple as shown in Figure 4.20. To reduce residual stresses, a long hold time at the pressing temperature may be required to ensure completion of plastic flow. In addition, a stress relief treatment may be essential at lower temperatures to reduce the differential thermal contraction stresses.

Complex Parts

Four attempts were made at various times during the course of this work to extend the densification technique to a rotor blade, which represented a part having complex geometry. All the samples were
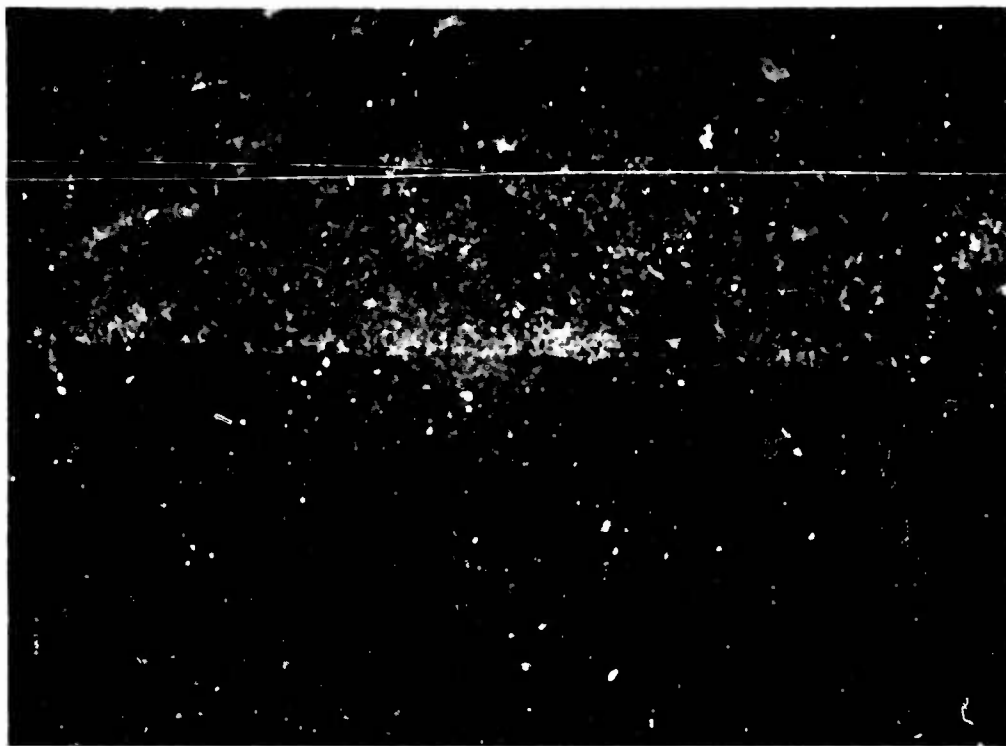
Figure 4.19 — Interface Between Reaction Sintered and Hot Pressed Silicon Nitrides After Hot Isostatic Pressing

broken, such as shown in Figure 4.21. It is believed that the differential thermal expansion between Vycor and the Si₃N₄ caused the breakage. One contributing factor is believed to be the use of a thick, 1/4 inch glass encapsulant relative to the thin 1/8 inch rotor blade.
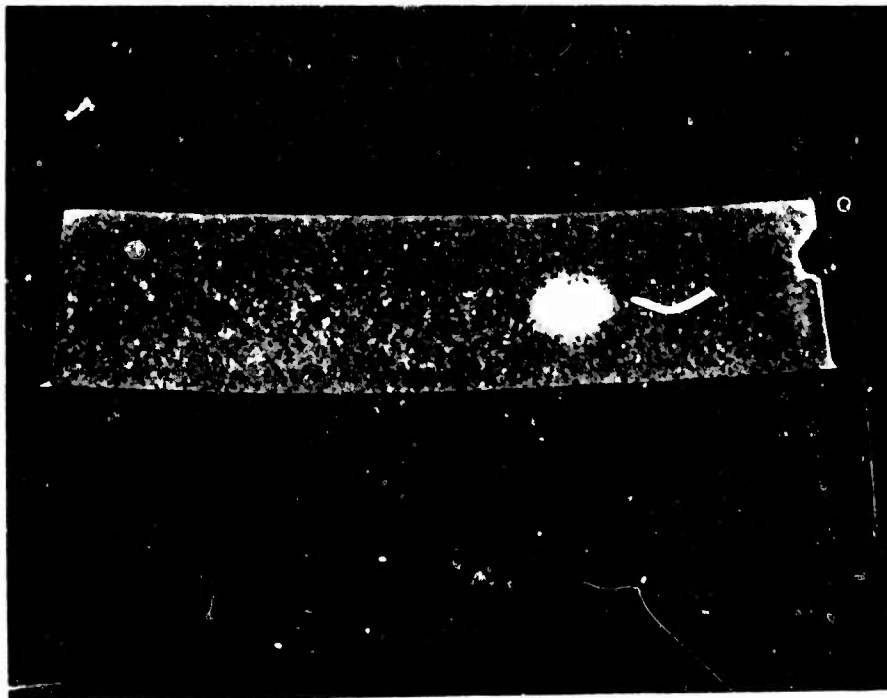
Figure 4.20 — Deflection of Bonded Reaction Sintered and Hot Pressed Silicon Nitrides After Hot Isostatic Pressing

Figure 4.21 — Broken Rotor Blade and Ring After Hot Isostatic Pressing

Conclusions

The feasibility of hot isostatically pressing reaction sint... Si_3N_4 to high density has been shown, along with the effect of densification agents. Higher densities and improvements in low temperature (below 2200°F) strength have been achieved over that of the reaction sintered material. The feasibility of simultaneously diffusion bonding RBSN to HPSN while densifying the RBSN has also been demonstrated. However, further investigation is needed to reduce the resulting residual stresses which may be set up across the interface.

The current encapsulation system is not suitable for isostatic densification of complex parts such as thin rotor blades.

5.   ANALYTICAL CODES

Summary

The maximum-likelihood method was selected as the procedure for the estimation of the parameters of the Weibull Distribution. This result was based on extensive literature surveys and Monte Carlo investigations. The maximum-likelihood method provides the desirable properties for estimations which are exact for small sample sizes and yields a basis for hypothesis testing. The effect of sample size on the confidence of estimation has also been determined.

Analytical relations are developed for computing time-dependent reliability for ceramic structures which exhibit the phenomenon of delayed fracture or static fatigue. The equations are derived from the subcritical crack growth model using fracture mechanics relations which are combined with Weibull's statistical model of strength and the time to failure is described probabilistically.

5.1   STATISTICAL DATA ANALYSIS

The reliability of ceramic structures as a function of stress and/or time and the strength of ceramic materials are random variables which are widely accepted to follow the Weibull distribution (3-10, 33, 34). The three-parameter Weibull probability density function is give by

$$
w(x; m, \theta, \mu) = \begin{cases} \dfrac{m}{\theta} \left(\dfrac{x-\mu}{\theta} \right)^{m-1} \exp\left[-\left(\dfrac{x-\mu}{\theta} \right)^{m} \right], & x \geq \mu, \\ 0, & x < \mu; \ m, \theta > 0; \ \mu \geq 0. \end{cases}
$$

The distribution parameters are m, the shape parameter or Weibull slope; θ, the scale parameter or characteristic value; and μ, the location or threshold parameter. It has been commonly assumed that, for ceramic materials and components, the threshold parameter is zero. The cumulative distribution function of the two-parameter Weibull distribution is give by

$$
W(x; m, \theta) = \begin{cases} 1 - \exp\left[-\left(\dfrac{x}{\theta} \right)^{m} \right], & x \geq 0 \\ 0, & x < 0. \end{cases}
$$

The previous report (10) shows the effect of Weibull slope on the material characteristic MOR strength requirement for a specified component reliability. A 20 percent increase in Weibull slope from a nominal slope of 10 produces a 16 percent decrease in the strength requirement; a 20 percent decrease in slope causes a 27 percent increase in the strength requirement.

The Weibull parameters used in reliability analyses are estimates of the true distribution parameters based on a finite sample. Many different estimation techniques exist and, in general, they will produce somewhat different results. During the preliminary analysis of material strength data, two statistical methods had been used: the method of moments, MOM (34), and the method of pseudo-least-squares, PLE (35,36,37). One example of the differences in the methods follows. Table 5.1 contains the failure stresses of 26 "A"-size MOR bars (14) taken from hot-pressed Si_3N_4 billet 989, tested at 2200°F in quarter-point four-point bending.

TABLE 5.1

MOR STRENGTH VALUES
HOT PRESSED SILICON NITRIDE BILLET 989

51800.0	52000.0	52100.0	52600.0	53000.0	53300.0
53600.0	53700.0	54700.0	55600.0	56600.0	57300.0
57900.0	58200.0	58200.0	58300.0	58800.0	59000.0
59800.0	60200.0	60800.0	60800.0	61100.0	62800.0
63600.0	71100.0				

The point estimates of the Weibull slope and the characteristic values are given in Table 5.2 for each method.

TABLE 5.2

WEIBULL PARAMETER ESTIMATES

Method	$\hat{m}$	$\hat{\theta}$
MOM	16.16	59468
PLE	14.41	59648

The estimates of the characteristic value are very close while the Weibull slope estimates vary and would yield considerable differences in the component strength requirements. These differences prompted an investigation to determine what method should be used for the estimation of the Weibull parameters and to establish uniform statistical procedures for the entire program.

An extensive literature survey of estimation techniques was conducted and discussions were held with numerous statisticians. Chou [35] discusses the criteria by which the quality of a classical estimator may be judged. These criteria include unbiasedness, consistency, efficiency and sufficiency. Berger and Lawrence [37] point out that modern estimators are available which are not only efficient but also provide confidence intervals. Mann, Schafer and Singpurwalla [15] discuss moment estimators, least-square estimators, best linear invariant estimators and maximum-likelihood estimators. They state that the last two of these should be used for hypothesis testing because they have the smallest mean-squared error.

Mann and Fertig [38] indicate that it has been shown that a Bayesian approach to the estimation of confidence bounds offers no particular improvement over classical methods. Thoman, Bain and Antle [16] discuss the method of maximum-likelihood and present exact confidence intervals, unbiasing factors, tests of hypotheses and asymptotic methods.

The maximum-likelihood estimators (MLE), $\hat{m}$ and $\hat{\theta}$ of the Weibull parameters m and θ, satisfy the equations:

and

$$\frac{n}{\hat{m}} - n \frac{\sum x_i^{\hat{m}} \ln x_i}{\sum x_i^{\hat{m}}} + \sum \ln x_i = 0$$

$$\hat{\theta} = \left[\sum \frac{x_i^{\hat{m}}}{n} \right]^{\frac{1}{\hat{m}}}$$

These equations may be solved by the Newton-Raphson iterative procedure [39] which will require the use of a computer. Thoman, et. al. [16] conducted a Monte Carlo study of the MLE and compared their results to Menon's estimator [40]. Comparison of the MLE to other methods may be made through the comparisons with Menon's estimator given in Bain and Antte [41]. The maximum-likelihood estimator was shown to be the most efficient of the methods studied and, although it is highly biased for small samples, the bias may be removed.

A Monte Carlo study was conducted to compare the maximum-likelihood method to the methods of moments and of pseudo-least squares which were recently being used. Approximately 5000 samples each of size 5, 10 and 20 were used. The expected value and the variance of each parameter for each method was calculated and a goodness of fit test based on the Kolmogorov-Smirnov statistic was conducted. At each sample size the maximum-likelihood estimators were unbiased, showed the least variance and most often provided the best fit. Because this method will provide for significance tests

and confidence intervals for the parameters and the distribution, and because this method is highly respected in the literature, the maximum-likelihood method was selected as the single Weibull parameter estimation technique for this program.

The maximum-likelihood estimate for billet 989, mentioned earlier, for the Weibull slope is 11.07 and for the characteristic value 59707 psi. A Fortran computer program (see Appendix A) was written to calculate the maximum-likelihood estimates. The program calculates the point and 90 percent interval estimates for the parameters and the distribution B_{10}, the distribution mean and standard deviation. A nonparametric Kolmogorov-Smirnov goodness of fit test is conducted and the test statistic D_2 was printed. An example based on the data of Thoman et. al. (16) is provided in Appendix B.

The exact confidei ne intervals for the parameters are based on the distributions obtained by Monte Carlo methods presented in Thoman et. al. (16). It is not unexpected that the uncertainty in the estimation of a parameter will increase as the sample size decreases. This uncertainty, however, has rarely been quantified. The width of the confidence intervals for the parameters is a measure of the uncertainty and aids in the selection of the sample size of a test. Figures 5.1 and 5.2 are drawn from Tables 1 and 4 of Thoman et. al. (16) and show the 90 percent confidence bounds for the Weibull slope and the characteristic value. The bounds for the Weibull slope are a function of sample size only while, for the characteristic value, they are a function of both the sample size and the Weibull slope. As can be seen from the graphs, the error or uncertainty in estimates from small sample sizes is very large. Important judgments and significant analysis should not be based on small samples. Sample sizes of at least 30 should be used for all but the most preliminary investigations. An uncertainty of ± 10 percent in Weibull slope requires more than 120 samples. This uncertainty is not peculiar to just ceramics but is intrinsic to the statistical analysis of data whether that data be material strength or the life of some electronic component. The choice of sample size depends on many factors including the cost and timing of testing and the degree of conservation which is acceptable, but erroneous judgments may be made and unacceptable designs pursued if the sample sizes are too small.
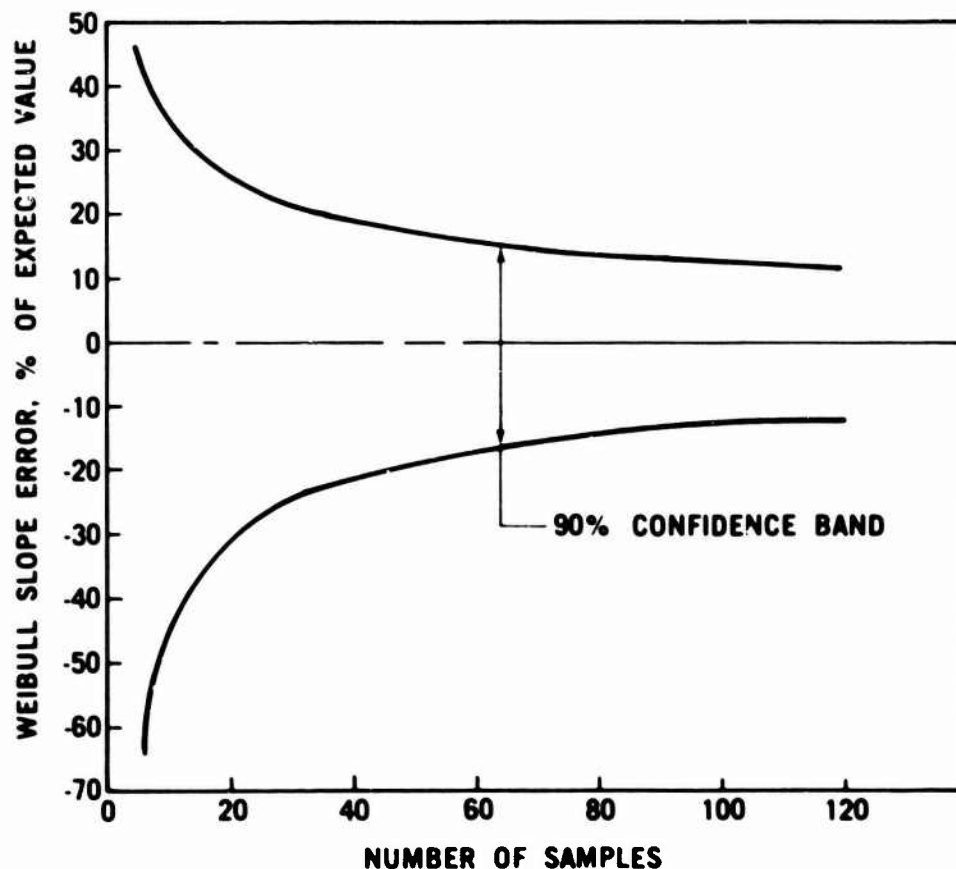

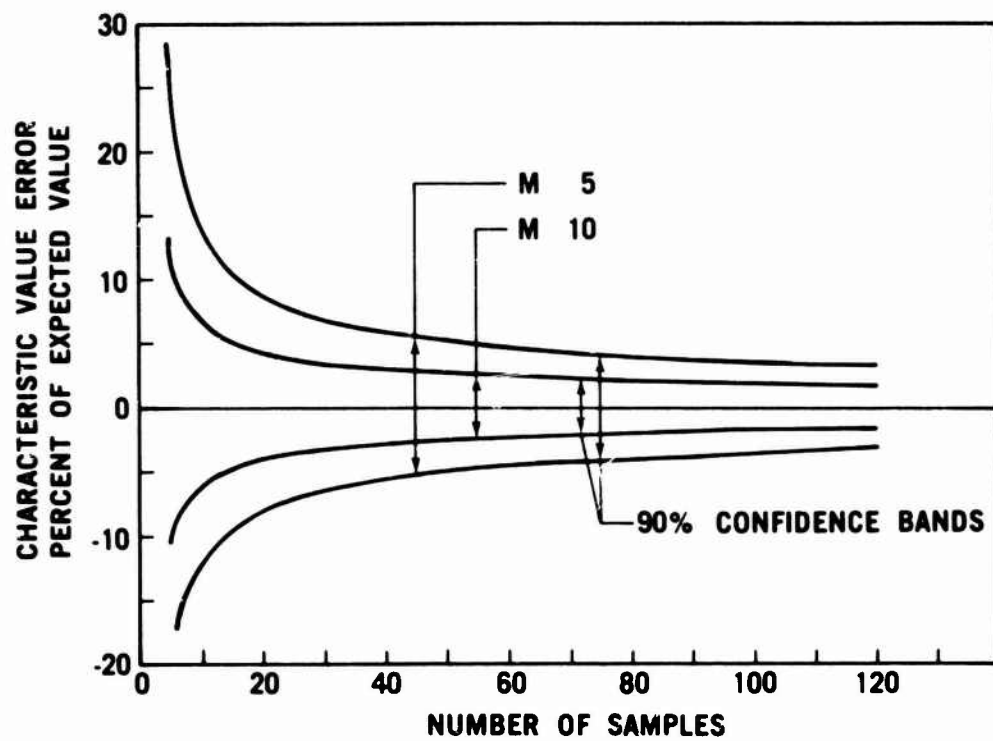Figure 5.1 — Weibull Slope Error Vs. Sample Size

Figure 5.2 — Characteristic Value Error Vs. Sample Size

Introduction

Certain ceramics that are being considered for the highly stressed turbine rotor exhibit the phenomenon of delayed fracture or static fatigue. While under stress, the material experiences degradation of strength with time and fails at a stress less than that necessary to induce fast fracture. This strength degradation and the resulting time-dependent failures are attributed to the subcritical crack growth which, in ceramics in question, is usually associated with higher operating temperatures (> 1000°C).

Since the turbine rotor is expected to operate in that temperature regime, the subcritical crack growth is of concern and the time-dependence of strength must be considered when estimating safe loads, strength requirements, reliability, etc.

The method originally developed by Evans and Wiederhorn (11,42) for predicting time-to-failure of simple uniaxially-stressed structures has been extended in this work to complex, multiaxially-stressed ceramic components, notably turbine rotors.

In order to facilitate a subcritical crack growth analysis of such complexly stressed structures, the following simplifying assumptions are necessary:

1. Insofar as the effects of creep on high temperature crack propagation are concerned, Evans and Wiederhorn (11) have indicated that the use of conventional fracture mechanics relations will provide adequate approximations as long as the high temperature plastic deformations accompanying creep are linearly visco-elastic. This qualification has been shown to be true of the hot pressed varieties of Si_3N_4, which are prime candidates for the turbine disks.

2. It is assumed that only the normal stress crack propagation, i.e., the opening mode (K_i) is operating; shearing modes II and III are neglected.

3. In the case of the time-dependent load ($\sigma(t)$), the orientation of principal stresses throughout the structure is assumed to remain constant with time, which generally is far from reality but should lead to conservative results.

4. The time to failure is treated probabilistically using Weibull's statistical model of fracture. Previous in-house work has shown considerable success with this model in treating fast fracture failures of ceramic materials that are being considered for turbine rotor application. Since the flaws that control strength are usually identical for both the fast fracture and the time-dependent failure modes, it was thought logical to continue with the Weibull model.

5. It is assumed that the effects of subcritical growth can be neglected at temperatures below 1000°C. In actuality, subcritical crack growth does occur at much lower temperatures. However, the rate of crack propagation is so slow at these temperatures that measurements are extremely difficult if at all possible.

Presently, the full implications of all these simplifying assumptions cannot be assessed. However, the time to failure equations, as derived in this work, are being applied to turbine rotors in preparation for life-testing in hot-spin and engine test rigs, where the validity of these assumptions will be evaluated.

Analysis

In line with the assumption that only the normal stress crack propagation (opening) mode is being considered, one can take advantage of the relations derived for the uniaxial state of stress case by treating a multiaxially-stressed ceramic structure as an assembly of uniformly stressed finite elements and applying these relations to the individual elements. An assumption is here made that the subcritical crack growth occurs independently in each element, so that a failure of any one element constitutes

the failure of the entire structure. This assumption is justified because the critical flaw size at the time of fracture is expected to be smaller than the typical dimensions of an individual element.

A stress condition of an element of a structure is completely defined by three principal stresses σ_{1i}, σ_{2i}, σ_{3i} and their respective direction cosines. A normal stress is related to the principal stresses by a known equation

$$\sigma_{ni} = \sigma_{1i} \left[\left(\cos^2 \psi + \left(\frac{\sigma_2}{\sigma_1} \right)_i \sin^2 \psi \right) \cos^2 \phi + \left(\frac{\sigma_3}{\sigma_1} \right)_i \sin^2 \phi \right] = \sigma_{1i} \beta_i (\psi, \phi) \tag{1}$$

ψ and θ are the position angles of the normal stress σ_{ni} with respect to the maximum principal tensile stress σ_{1i}. In a most general case, both σ_{1i} and β_i will be functions of time. β_i is defined by the expression in the square bracket.

For ceramics which exhibit subcritical crack growth, the crack velocity has been shown [11,42] to be related to the stress intensity factor K_I by a power law

$$v = \frac{da}{dt} = A K_I^n \tag{2}$$

where the parameters A and n are determined experimentally -- either in double torsion or similar fracture mechanics tests — or in MOR-tests conducted at several different strain rates (11).

Upon application of a normal stress σ_{ni} to an element of the structure, the stress intensity factor at the fracture controlling flaw becomes

$$K_{Ii} = \sigma_{ni} Y_i a^{\frac{1}{2}} \tag{3}$$

Y_i being a geometric factor [43] for the element. As the normal stress approaches the fast fracture strength of the material, the stress intensity factor reaches its critical value, as follows:

$$K_{ICi} = \sigma_{nci} Y_i a^{\frac{1}{2}} \tag{4}$$

Since only the normal stress crack propagation mode (I) is considered here, the time-to-failure for an uniformly-stressed element is obtained by combining equations (2) and (3), separating variables and integrating:

$$\int_0^{t_{fi}} A_i Y_i^n \sigma_{ni}^n (t) \, dt = \frac{2}{(n-2)} \left[\left(\frac{1}{a_a} \right)_i^{\frac{n-2}{2}} - \left(\frac{1}{a_c} \right)_i^{\frac{n-2}{2}} \right] \tag{5}$$

116

t_{fi} is the time to failure. In a typical finite element model of a turbine rotor, the dimensions of the strength controlling flaw are generally small, even at fracture, compared to the controlling dimension of an element so that the geometric factor Y_i can be considered constant up to fracture and can be taken out from under the integral sign:

$$\int_0^{t_{fi}} A_i \, \sigma_{ni}^n \,(t)\, dt = \frac{2}{(n-2)\,Y_i^n} \left[\left(\frac{1}{a_a}\right)_i^{\frac{n-2}{2}} - \left(\frac{1}{a_c}\right)_i^{\frac{n-2}{2}} \right] \tag{6}$$

Once the time-function $A_i(t)$ and $\sigma_{ni}(t)$ are determined for each element from the load history of the structure, equation (6) can be solved for the time to failure, provided, both the initial (a_{ai}) and the final (a_{ci}) flaw sizes are known.

The initial size of the strength-controlling flaw will be usually determined in Non-Destructive Evaluation (NDE) tests. However, the resolution of currently available NDE techniques for ceramic materials is still far from adequate in identifying the sizes of flaws that are commensurate with the stress levels found in the highly stressed ceramic turbine components, notably, turbine rotors. In cases like this, an indirect method has been suggested in which the initial size of the strength-controlling flaw, as well as it's distribution are inferred, by way of fracture mechanics relations, from the fast fracture strength measurements. The premise is that the flaws which control the strength are identical for both the fast fracture and the time-dependent fracture. In this method, the analysis of failure probabilities (P) for the fast fracture is combined with analysis of subcritical crack growth and the time to failure is described statistically.

The fast fracture strength of a multiaxially-stressed element is expressed in terms of maximum principal tensile stress σ_{1fi} in the element and is associated with a reliability level R_{fi} by way of characteristic strength $\sigma_{\theta i}$:

$$\sigma_{1fi} = \sigma_{ui} + \sigma_{\theta i}(\ell_n \frac{1}{R_f})_i^{\frac{1}{m}} \tag{7}$$

The threshold strength σ_{ui} is customarily set equal zero for most structural ceramics.

The initial flaw size is related to the fast fracture strength according to equation (4)

$$a_{ai} = \left(\frac{K_{IC_0}}{\sigma_{nf}\,Y}\right)_i^2 \tag{8}$$

σ_{nf_i} being the fast fracture strength of an element measured normal to the strength controlling flaw in the absence of crack propagation and $K_{IC_{oi}}$ is the corresponding value of the critical stress intensity factor, both measured at the same temperature.

Similarly the critical size of the flaw at the time of the fracture is

$$a_{ci} = \left(\frac{K_{IC}}{\sigma_{nc}\,Y}\right)_i^2 \tag{9}$$

where σ_{nci} is the value of the applied stress normal to the strength controlling flaw at the time of fracture, and K_{IC_i} the value of critical stress intensity factor corresponding to the environmental conditions (temperature) prevailing at fracture. K_{IC_i} usually varies with temperature, so that generally $K_{IC_i} \neq K_{IC_{oi}}$.

For a specific loading (stress distribution), the relation between the normal stress and the maximum principal tensile stress remains constant regardless of the stress level, i.e.,

$$\left(\frac{\sigma_{nf}}{\sigma_{1f}}\right)_i = \left(\frac{\sigma_{nc}}{\sigma_{1c}}\right)_i = \beta_i\,(\psi, \phi) \leq 1.0 \tag{10}$$

Let R_{ai} be the desired survival probability of a ceramic structure subjected to some load history $\sigma(t)$ for which the time to failure is being sought and R_{ai} the corresponding reliability required of an individual element. On the basis of (7), (8) and (10), the initial size of the strength-controlling flaw which corresponds to a survival probability R_{ai} at some reference loading condition, denoted here with subscript 'o' and assumed for convenience to be the maximum loading of the element is

$$a_{ai} = \left(\frac{K_{ICo}}{\beta_o\,\sigma_{\theta o}\,Y}\right)_i^2 \left(\ell_n\frac{1}{R_{ai}}\right)^{-\frac{2}{m}} \tag{11}$$

$\sigma_{\theta oi}$ being the characteristic fast fracture strength of the element at the reference loading condition in the absence of slow crack growth. The critical size of the same flaw at fracture $(t = t_{fi})$ is similarly

$$a_{ci} = \left(\frac{1}{Y}\right)_i^2 \left(\frac{K_{ICi}}{\beta_i\,\sigma_{1i}}\right)_{t\,=\,t_{fi}}^2 \tag{12}$$

Generally, the stress distributions corresponding to the maximum (reference) loading condition (σ_{1oi}) and the loading condition at fracture $(\sigma_{1i})_t = t_{fi}$ will be different so that $\beta_{oi} = (\beta_i)_t = t_{fi}$. Substituting (11) and (12) into (6)

$$\int_o^{t_{fi}} A_i\,\beta_i^n\,\sigma_{1i}^n\,dt = \frac{2}{(n-2)\,Y_i^2}\left[\left(\frac{\beta_o\,\sigma_{\theta o}}{K_{ICo}}\right)_i^{n-2}\left(\ell_n\frac{1}{R_{ai}}\right)^{\frac{n-2}{m}} - \left(\frac{\beta_i\,\sigma_{1i}}{K_{ICi}}\right)_{t\,=\,t_{fi}}^{n-2}\right] \tag{13}$$

Normalizing both sides of (13) with the reference load parameters $(\beta_o, \sigma_{1o}^n$ and $A_o)$ and rearranging terms

$$\int_o^{t_{fi}} H_i\,(t)\,dt = \frac{2a_{\theta o1}}{(n-2)\,V_{co1}}\left(\frac{\sigma_{\theta o}}{\sigma_{1o}}\right)_i^2\left(\frac{\beta_i\,\sigma_{1i}\,K_{ICo1}}{\beta_{o1}\,\sigma_{1o1}\,K_{ICi}}\right)_{t\,=\,t_{fi}}^{n-2}\left[\left(\frac{\beta_{o1}\,\sigma_{\theta o1}\,K_{IC1}}{\beta_i\,\sigma_{1i}\,K_{ICo1}}\right)^{n-2}\left(\ell_n\frac{1}{R_{ai}}\right)^{\frac{n-2}{m}} - 1.0\right] \tag{14}$$

where

$$H_i\,(t) = \left(\frac{A\,\beta^n\,\sigma_1^n}{A_o\,\beta_o^n\,\sigma_{1o}^n}\right)_i \tag{15}$$

is the ratio of the instantaneous to the reference load parameters,

$$a_{\theta o1} = \left(\frac{K_{ICo}}{\beta_o\,Y\,\sigma_{\theta o}}\right)_i^2 \tag{16}$$

is the characteristic size of the strength controlling flaw in an element, associated with the reference load condition and having the probability of occurrence of $P = 0.632$ and

$$V_{coi} = A_{oi} K_{ICoi}^{n} \tag{17}$$

is the critical rate (at fracture) of crack propagation at reference conditions. V_{coi} can be either calculated from equation (17) or obtained directly from the V-K_I — diagram.

For materials such as the hot pressed Si_3N_4 which is being considered for the turbine disk, the crack propagation exponent $n = 10$ and the Weibull slope $m = 10$ to 16. Since a necessary condition for an element to have a practical life span is that $R_{ai} \ll R_{fi}$, the unit term in the square bracket can be generally neglected. In such a case equation (14) simplifies to

$$\int_0^{t_{fi}} H_i(t)\,dt = \frac{2 a_{\theta oi}}{(n-2)\,V_{coi}} \left(\frac{\sigma_{\theta o}}{\sigma_{1o}}\right)^2_i \left(\frac{\ell_n \frac{1}{R_{ai}}}{\ell_n \frac{1}{R_{foi}}}\right)^{\frac{n-2}{m}} \tag{18}$$

or on the basis of (11) and (7)

$$\int_0^{t_{fi}} H_i(t)\,dt = \frac{2 a_{oi}}{(n-2)\,V_{coi}} \left(\frac{\ell_n \frac{1}{R_{ai}}}{\ell_n \frac{1}{R_{foi}}}\right)^{\frac{n-2}{m}} \tag{19}$$

a_{oi} being the size of the strength-controlling flaw in an element associated with a fast fracture reliability of R_{foi} at maximum (reference) loading condition.

In the special case, when both the stress distribution (β_i and $\sigma_{\theta i}$) and the stress amplitude (σ_{1i}) are constant with time, we have

$$H_i(t) = 1.0$$

and equation (14) is solved directly for the time to failure t_{fi}

$$t_{fi} = \frac{2 a_{oi}}{(n-2)\,V_{coi}} \left[\left(\frac{\ell_n \frac{1}{R_{ai}}}{\ell_n \frac{1}{R_{fi}}}\right)^{\frac{n-2}{m}} - 1.0\right] \tag{20}$$

Since $\left(\frac{a_o}{V_c}\right)$ has a dimension of time (it is the time necessary to traverse the initial length of crack at a critical crack propagation rate) we denote

$$t_o = \frac{2 a_{oi}}{(n-2)\,V_{ci}}.$$

and introduce

$$t_{\theta i} = t_{oi} \left(\ell_n \frac{i}{R_{fi}}\right)^{-\frac{(n-2)}{m}} \tag{21}$$

119

the characteristic time to failure of an element ($R_{ai} = P_{\theta i} = 36.8\%$). Using Weibull's notation the time to failure at a survival probability of R_{ai} is then

$$t_{fi} = t_{\theta i} \left(\ell n \; \frac{1}{R_{ai}} \right)^{\frac{n-2}{m}} - t_{oi} \tag{22}$$

or

$$R_{ai} = \exp\left\{ - \left(\frac{t_f + t_o}{t_\theta} \right)_i^{\frac{m}{n-2}} \right\} \tag{23}$$

Equation (23) plotted on Weibull paper becomes a straight line with slope of $\left(\frac{m}{n-2}\right)$ and intersecting the ordinate ($t_{fi} = 0$) at R_{fi}. In most practical cases t_o will be small compared to t_f and would be omitted.

Equations 18 and 22 will be applied to turbine rotors at a later date when material data becomes available to assess if the calculated survival probability of rotors correlates with the results from the hot spin rig.

6. REFERENCES

1. McLean, A. F., Fisher, E. A., Harrison, D. E., "Brittle Materials Design, High Temperature Gas Turbine". AMMRC-CTR-72-3, Interim Report, March, 1972.

2. McLean, A. F., Fisher, E. A., Bratton, R. J., "Brittle Materials Design. High Temperature Gas Turbine". AMMRC-CTR-72-19, Interim Report, September, 1972.

3. McLean, A. F., Fisher, E. A., Bratton, R. J., "Brittle Materials Design, High Temperature Gas Turbine". AMMRC-CTR-73-9, Interim Report, March, 1973.

4. McLean, A. F., Fisher, E. A., Bratton, R. J., "Brittle Materials Design, High Temperature Gas Turbine". AMMRC-CTR-73-32, Interim Report, September, 1973.

5. McLean, A. F., Fisher, E. A., Bratton, R. J., "Brittle Materials Design, High Temperature Gas Turbine". AMMRC-CTR-74-26, Interim Report, April, 1974.

6. McLean, A. F., Fisher, E. A., Bratton, R. J., "Brittle Materials Design, High Temperature Gas Turbine". AMMRC-CTR-74-59, Interim Report, September, 1974.

7. McLean, A. F., Fisher, E. A., Bratton, R. J. Miller, D. G., "Brittle Materials Design, High Temperature Gas Turbine". AMMRC-CTR-75-8, Interim Report, April, 1975.

8. McLean, A. F., Fisher, E. A., Bratton, R. J., Miller, D. G., "Brittle Materials Design, High Temperature Gas Turbine". AMMRC-CTR-75-28, Interim Report, September, 1975.

9. McLean, A. F., Baker, R. R., Bratton, R. J., Miller, D. G., "Brittle Materials Design, High Temperature Gas Turbine". AMMRC-CTR-76-12, Interim Report, April, 1976.

10. McLean, A. F., Baker, R. R., "Brittle Materials Design, High Temperature Gas Turbine". AMMRC-CTR-76-31, Interim Report, October, 1976.

11. Evans, E. G., Wiederhorn, S.M., "Crack Propagation and Failure Prediction in Silicon Nitride at Elevated Temperature," Journal of Material Science (9). 1974, p. 270-278.

12. Ainley, D. C. and Mathieson, G. C. R., "A Method of Performance Estimation for Axial Flow Turbines", Reports and Memoranda No. 2974, December 1951, Her Majesty's Stationary Office.

13. Dunham J. & Came, D. M., "Improvements to the Ainley Mathieson Method of Turbine Performance Prediction", ASME Paper 70-GT-2, 1970.

14. Proposed Military Standard, "Test Methods for Structural Ceramics," Army Materials and Mechanics Research Center, October 15, 1973.

15. Mann, N. R., Schafer, R. E. and Singpurwalla, N. D., "Methods for the Statistical Analysis of Reliability and Life Data", John Wiley, 1974.

16. Thoman, D. R., Bain, L. J. and Antle, C. E., "Inferences on the Parameters of the Weibull Distribution", Technometrics, 11, 445-460.

17. Swank, L. R., and Uy, J. C., "Ceramic Turbine Rotor Reliability Testing and Failure Analysis in the Hot Spin Test Rig", Ceramics for High Performance Applications, March, 1977. To be published.

18. Shull, H. E., "Design and Use of a Tensile Test Device for Small Brittle Material Specimens", Bulletin of The American Ceramic Society, Vol. 55, No. 2 (1976), p. 202-204.

19. Willermet, A, Pett, R. A. and Whalen, T. J., "Injection Moldable Reaction Sintered Silicon Carbide", Paper 6-52-74, April 24, 1974, Annual Meeting, American Ceramic Society, Chicago, Illinois.

20. Whalen, T. J., Willermet, P. A. and Noakes, J., "Injection Moldable SiC", 3rd Materials Conference - Turbine Applications, Ann Arbor, Michigan, November 1, 1974.

21. Noakes, J. E., Terner, L. and Whalen, T. J., November 1, 1974. "Reaction Sintered - Silicon Carbide" Paper 34-BE-75F., September 23, 1975, Fall Meeting, American Ceramic Society, Indianapolis, Indiana.

22. Whalen, T. J., Noakes, J. E. and Terner, L., "Processing and Properties of Injection-Mold Reaction-Sintered SiC". Paper 29-BEN-76P., November 1, 1976, Fall Meeting, American Ceramic Society, San Francisco, California.

23. Lumby, R. J., Horsley, R. F., British Patent 1,431,780, September, 1973.

24. Wong, P., Messier, D. R., "Fabrication of Si_3N_4 by Rate Controlled Reaction Sintering" Bulletin Amer. Ceram. Soc., Vol. 54, No. 8 (1975).

25. Lindley, M. W., Jones, B. F., "Reaction Sintered Silicon Nitride", J. Material Science, 11, (1976).

26. Richmond, M. H., Jennings, H. M., "Structure, Formation Mechanisms and Kinetics of Reaction Bonded Silicon Nitride", J. Materials Science, 11, (1976).

27. Messier, D. R., Wong, P., "Kinetics of Formation and Mechanical Properties of Reaction Sintered Si_3N_4", Ceramics for High Performance Applications, Editors J. J. Burke et. al., Metals and Ceramics Information Center, Columbus, Ohio, 1974, p. 181.

28. Oyama, Y. and Kamigaito, O., "Hot-Pressing of Si_3N_4-Al_2O_3", Journal of the Ceramic Association of Japan 80. (8), (1972), p. 327.

29. Jack, K. H. and Wilson, W. I., "Ceramics Based on the Si-Al-O-N and Related Systems", Nature Physical Sciences 238, (1972), p. 20.

30. Lumby, R. J., North, B. and Taylor, A. J., "Chemistry and Creep of Sialons", Special Ceramics 6, 283 (1975), p. 283.

31. Gaukler, L. J., Lukas, H. L. and Petzow, C., "Contribution to the Phase Diagram Si_3N_4-AlN-Al_2O_3-SiO_2", J. Am. Ceramic Soc. 58 (7-8), (1975), p. 346.

32. Land, P. L., Wimmer, J. M., Burns, R. W. and Choudhury, N. S., "Compounds and Properties of the Si-Al-O-N System", Air Force Materials Laboratory Report AFML-TR-209 (1976).

33. Dukes, W. H., "Some Principles of Brittle Material Design,", ASME 75-GT-112.

34. DeSalvo, G. J., "Theory and Structural Design Applications of Weibull Statistics", WANL-TME-2688, 1970.

35. Chou, Ya-Lun, "Probability and Statistics for Decision Making", Holt, Rinehart and Winston, 1972.

36. Ford Motor Company Internal Computer Program, "CRE".

37. Berger, R. W. and Lawrence, K., "Estimating Weibull Parameters by Linear and Nonlinear Regression," Technometrics, 16, p. 617-619.

38. Mann, N. R. and Fertig, F. W., "Simplified Efficient Point and Interval Estimators for Weibull Parameters", Technometrics, 17, p. 361-368.

39. Kunz, K. S., Numerical Analysis, McGraw Hill, 1957.

40. Menon, M. V., "Estimation of the Shape and Scale Parameters of the Weibull Distribution", Technometrics, 5, p. 175-182.

41. Bain, L. J. and Antle C. E., "Estimation of Parameters in the Weibull Distribution", Technometrics, 9, p. 621-627.

42. Wiederhorn, S.M., "Fracture Mechanics of Ceramics," edited by R. C. Bradt, D. P. Hasselman, and F. F. Lange, (Plenum, New York 1974), p. 613-646.

43. Paris, P. C., Sih, G. C., "Stress Analysis of Cracks," ASTM STP 381 (1964), p. 52.

44. Miller, D. G., Bratton, R. J., Lange, F. F., Singhal, S. C., Booker, Jr., C. R., "Brittle Materials Design, High Temperature Gas Turbine," AMMRC-CTR-76-32, Westinghouse Final Report, December, 1976.

APPENDIX A

FORTRAN LISTING OF MAXIMUM-LIKELIHOOD
ESTIMATION PROGRAM AND DATA FILES

```
*S.MLE :

1*#FTN S.MLE=H.MLE(OPTZ,NOGO,CORE=24K,ULIB)LIB/FORD
20C     PROGRAM WRITTEN BY RICHARD A. JERYAN, FORD MOTOR COMPANY
30C     GAS TURBINE ENGINEERING DEPARTMENT, DEARBORN, MI 48121
35C     (REF: THOMAN, BAIN AND ANTLE; TECHNOMETRICS, V.11, P.455)
40C     LAST REVISION 4/11/77
50 DIMENSION X(200),BN(196),ELM(2,116),ELO(2,116)
60 DIMENSION AMRANK(20,20),AMR(200),D2CR(25)
70 DIMENSION U05(30),U95(30)
75C     POLYNOMIAL APPROXIMATION FOR GAMMA FUNCTION. REF: EQN. 6.1.36,
76C     'HANDBOOK OF MATHEMATICAL FUNCTIONS,' NBS AMS 55
80 F(AX)=1.-0.577191652*AX+0.988205891*AX^2-0.897056937*AX^3
90%+0.918206857*AX^4-0.756704078*AX^5+0.482199394*AX^6
100%-0.193527818*AX^7+0.035868343*AX^8
120 CALL YOPEN(02,'QK051509/BNFORMLE$BRUCE,R;')
130 CALL YOPEN(03,'QK051509/INTFORM$BRUCE,R;')
140 CALL YOPEN(04,'QK051509/INTFORO$BRUCE,R;')
150 REAL MO,M,LBM,LBO,LBXB10
160 PRINT,
170 PRINT,
180 PRINT,'THIS PROGRAM WILL CALCULATE THE UNBIASED MAXIMUM LIKELIHOOD ESTIMATOR'
190 PRINT,'FOR THE WEIBULL SHAPE PARAMETER AND CHARACTERISTIC VALUE'
200 READ(02,500) BN
210 READ(03,500) (ELM(1,I), ELM(2,I),I=1,116)
220 READ(04,500) (ELO(1,I),ELO(2,I), I=1,116)
230 8 CONTINUE
240 READ(01,500,END=5000) N,(X(I), I=1,N)
250 500 FORMAT (V)
260 IF (N.LT.5) GO TO 4000
270 IT=50
280CFIRST ESTIMATE OF THE SLOPE IS CALCULATED AS THE SLOPE OF THE
290C LINE BETWEEN THE FIRST AND THE LAST DATA POINTS.
300 CALL SORTS(X,N,'A',ERR)
310 MO=(ALOG(ALOG((N+.4)/.7))-ALOG(ALOG((N+.4)/(N-.3))))/
320%(ALOG(X(N))-ALOG(X(1)))
330 A=0.
340 ERROR=0.001
350 A=X(N)
360 DO 10 I=1,N
370 X(I)=X(I)/A
380 10 CONTINUE
390 S1=0.
400 S2=0.
410 S3=0.
420 S4=0.
430 DO 100 I=1,N
440 S1=S1+ALOG(X(I))
450 S2=S2+X(I)^MO
460 S3=S3+ALOG(X(I))*(X(I)^MO)
470 S4=S4+((ALOG(X(I)))^2)*(X(I)^MO)
480 100 CONTINUE
490 DO 200 I=1,IT
500 M=((1./MO)+(S1/N)-(S3/S2))/((1./MO^2)+((S4/S2)-((S3/S2)^2)))
510 M=M+MO
520 S2=0.
530 S3=0.
540 S4=0.
550 DO 300 J=1,N
560 S3=S3+ALOG(X(J))*(X(J)^M)
570 S4=S4+((ALOG(X(J)))^2)*(X(J)^M)
580 S2=S2+X(J)^M
590 300 CONTINUE
600 DLDM=(N/M)-M*(S3/S2)+S1
610 MO=M
620 IF(ABS(DLDM)-ERROR) 250,250,200
```

```
630 200 CONTINUE
640 WRITE (6,2000)
650 2000 FORMAT('NO SOLUTION FOUND')
660 GO TO 5000
670 250 THETA=0.
680 DO 400 I=1,N
690 THETA=THETA + X(I)^MO
700 400 CONTINUE
710 WRITE (6,2001)
720 2001 FORMAT (//'SAMPLE VALUES:'//)
730 WRITE (6,2002) (A*X(I), I=1,N)
740 2002 FORMAT (1X,6F10.1)
750 THETA = A*(THETA/N)^(1./MO)
760C MULTIPLY BY UNBIASING FACTOR
770 MO = MO*BN(N-4)
775C   IF (N.LE.120) CALCULATE PARAMETER INTERVAL ESTIMATES
780 IF (N.GT.120) GO TO 2005
790 WRITE (6,2003)
800 2003 FORMAT(/37X,'POINT',15X,'90 PERCENT',/35X,'ESTIMATES',
810% 9X,'INTERVAL ESTIMATES')
820 UBM = MO/ELM(1,N-4)
830 LBM = MO/ELM(2,N-4)
840 UBO = THETA/EXP(-ELO(1,N-4)/MO)
850 LBO = THETA/EXP(ELO(2,N-4)/MO)
860 WRITE (6,2004) MO,LBM,UBM
870 2004 FORMAT(/'WEIBULL SHAPE PARAMETER=',9X,F10.5,6X,
880% '(',F10.5,',',F10.5,')')
890 WRITE (6,2006) THETA,LBO,UBO
900 2006 FORMAT('WEIBULL CHARACTERISTIC VALUE= ',F10.2,
910% 9X,'(',F10.2,',',F10.2,')')
920 GO TO 2025
930 2005 WRITE (6,2010) MO
940 2010 FORMAT (//'WEIBULL SHAPE PARAMETER=          ',F10.5)
950 WRITE (6,2020) THETA
960 2020 FORMAT ('WEIBULL CHARACTERISTIC VALUE= ',F10.2)
970C   DISTRIBUTION MEAN=
980 2025 AAX= 1./MO
990 AAF=1.0
995C   RECURSION FORMULA FOR GAMMA FUNCTION
1000 2026 IF (AAX.LE.1.00) GO TO 2027
1010 AAF = AAF*AAX
1020 AAX = AAX - 1.00
1030 GO TO 2026
1040 2027 AMEAN = THETA*AAF*F(AAX)
1050C   DISTRIBUTION VARIANCE AND STANDARD DEVIATION
1060 AAAX=2./MO
1070 AAAF=1.0
1080 2028 IF (AAAX.LE.1.00) GO TO 2029
1090 AAAF = AAAF*AAAX
1100 AAAX = AAAX - 1.00
1110 GO TO 2028
1120 2029 VARI= (THETA^2)*(AAAF*F(AAAX)-((AAF*F(AAX))^2))
1130 STDDEV= SQRT(VARI)
1140C VALUE OF X AT W(X;M,0)=0.10; ( B10 )
1150 XB10 = THETA*(0.10536052^(1./MO))
1160 WRITE (6,2030) AMEAN
1170 2030 FORMAT (/'DISTRIBUTION MEAN=               ',F10.2)
1180 WRITE (6,2040) STDDEV
1190 2040 FORMAT ('DISTRIBUTION STANDARD DEVIATION= ',F10.2)
1195C   IF (N.LE.30) CALCULATE B10 INTERVAL ESTIMATES
1200 IF (N.GT.30) GO TO 2045
1210 DATA U05/1.,1.,1.,1.,-1.422,-1.125,-1.015,-.955,-.915,-.8794,-.852,
1220% -.826,-.802,-.78,-.7648,-.741,-.722,-.706,-.69,-.674,-.662,
1230% -.648,-.637,-.626,-.616,-.605,-.596,-.597,-.578,-.5672/
1240 DATA U95/1.,1.,1.,1.,4.4453,3.76,3.10,2.64,2.24,2.1304,1.95,1.82,1.7,
1250% 1.6,1.5091,1.44,1.38,1.32,1.27,1.2262,1.18,1.14,1.1,1.07,1.04,1.01,
1260% .99,.96,.94,.9147/
1270 LBXB10 = XB10/(EXP(U95(N)/MO))
1280 UBXB10 = XB10*(EXP(-U05(N)/MO))
1290 WRITE(6,2051) XB10,LBXB10,UBXB10
1300 2051 FORMAT('B10 VALUE=',23X,F10.2,6X,'(',F10.2,',',F10.2,')')
1310 GO TO 2052
```

```
1320 2045 WRITE(6,2050) XB10
1330 2050 FORMAT ('B10 VALUE=                          ',F10.2)
1340 2052 CONTINUE
1350C      K-S GOODNESS OF FIT TEST
1360C      .20 SIGNIFICANCE LEVEL (NONPARAMETRIC)
1370 IF(N.GT.25) GO TO 2055
1380 DATA D2CR/.900,.684,.585,.494,.446,.410,.381,.358,.339,.322,
1390$ .307,.295,.284,.274,.266,.258,.250,.244,.237,.231,
1400$ .227,.223,.218,.214,.21/
1410 D2CRIT = D2CR(N)
1420 GO TO 2060
1430 2055 D2CRIT = 1.07/SQRT(N)
1440 2060 IF(N.GT.20) GO TO 3500
1445C   READ MEDIAN RANK TABLE
1450 CALL YOPEN(05,'QK051509/MRDATA$BRUCE,R;')
1460 DO 3000 I=1,20
1470 DO 3000 J=1,20
1480 3000 AMRANK(I,J) = 0.000
1490 DO 3010 I=1,20
1500 READ (05,500) (AMRANK(I,K),K=I,20)
1510 3010 CONTINUE
1520 DO 3020 I=1,N
1530 AMR(I)=AMRANK(I,N)
1540 3020 CONTINUE
1550 GO TO 3600
1560 3500 DO 3030 I=1,N
1570 AMR(I)=(I-.3)/(N+.4)
1580 3030 CONTINUE
1590 3600 CONTINUE
1600 D2=0.0
1610 DO 3620 I=1,N
1620 3610 FF = 1.-EXP(-(((A*X(I))/THETA)^MO))
1630 D1 = ABS(FF-AMR(I))
1640 IF(D1.LE.D2CRIT) GO TO 3616
1650 WRITE (6,3615)
1660 3615 FORMAT('****',/,'****THE DATA EXCEEDS THE GOODNESS-
1661$ OF-FIT LIMITS OF THE',/,'KOLMOGOROV-SMIRNOV TEST AT THE
1662$ 20% SIGNIFICANCE LEVEL',/,'****')
1663 D2=D1
1665 GO TO 3625
1670 3616 IF(D1.LE.D2) GO TO 3620
1680 D2 = D1
1690 3620 CONTINUE
1700 3625 WRITE (6,3630) D2
```

$BNFORMLE:

```
.70,.752,.792,.820,.842,.859,.872,.883,.893,.901,.908,.914,.9185
.923,.927,.931,.9345,.938,.9405,.943,.945,.947,.949-.951,.953,.955
.9565,.958,.959,.960,.961,.962,.963,.964,.965,.966,.967,.968
.969,.670,.9705,.971,.9715,.972,.9725,.973,.9735,.974,.9745,.975
.9755,.976,.9765,.977,.9775,.978,.9785,.979,.9795,.980,.980,.980
.9805,.981,.981,.981,.9815,.982,.982,.982,.9825,.983,.983,.983,.9835
.984,.9842,.9844,.9846,.9848,.985,.9852,.9854,.9856,.9858,.986
.9861,.9862,.9863,.9864,.9865,.9866,.9867,.9868,.9869,.987
.9872,.9873,.9875,.9876,.9878,.9879,.9881,.9882,.9884,.9885
.9887,.9888,.9890,.9891,.9893,.9894,.9896,.9897,.9899,.9900
.9901,.9901,.9902,.9903,.9903,.9904,.9904,.9905,.9906,.9906
.9907,.9908,.9908,.9909,.9909,.9910,.9911,.9911,.9912,.9913
.9913,.9914,.9914,.9915,.9916,.9916,.9917,.9918,.9918,.9919
.9919,.9920,.9921,.9921,.9922,.9923,.9923,.9924,.9924,.9925
.9926,.9926,.9927,.9928,.9928,.9929,.9929,.9930,.9931
.9931,.9932,.9933,.9933,.9934,.9934,.9935,.9936,.9936,.9937
.9938,.9938,.9939,.9939,.9940,.9941,.9941,.9942,.9943,.9943
.9944,.9944,.9945,.9945,.9946,.9947,.9948,.9948,.9949,.9949
.9950
```

*INTFORM:

```
.683,2.779,.697,2.436,.709,2.183,.720,2.015,.729,1.896,.738,1.807,.745,1.738
.752,1.682,.759,1.636,.764,1.597,.770,1.564,.775,1.535,.779,1.510,.784,1.487
.788,1.467,.791,1.449,.795,1.434,.798,1.418,.802,1.405,.805,1.392,.808,1.381
.810,1.370,.813,1.361,.815,1.351,.818,1.343,.820,1.334,.822,1.327,.824,1.319
.826,1.313,.828,1.306,.830,1.300,.832,1.294,.834,1.288,.835,1.283,.837,1.278
.839,1.273,.841,1.269,.842,1.265,.844,1.261,.845,1.256,.846,1.253,.847,1.249
.849,1.246,.850,1.242,.851,1.239,.852,1.235,.853,1.232,.854,1.229,.856,1.227
.857,1.224,.858,1.221,.859,1.218,.860,1.216,.861,1.213,.862,1.211,.863,1.208
.864,1.206,.864,1.204,.865,1.203,.866,1.200,.867,1.198,.868,1.196,.869,1.194
.869,1.192,.870,1.190,.871,1.188,.872,1.187,.872,1.185,.873,1.184,.874,1.182
.875,1.181,.875,1.179,.876,1.178,.876,1.176,.877,1.175,.878,1.173,.879,1.172
.879,1.170,.880,1.169,.880,1.167,.881,1.166,.881,1.165,.882,1.164,.882,1.162
.883,1.161,.863,1.160,.884,1.159,.884,1.158,.885,1.157,.885,1.156,.886,1.155
.886,1.154,.887,1.153,.887,1.152,.888,1.151,.888,1.150,.889,1.149,.889,1.148
.890,1.147,.890,1.146,.891,1.146,.891,1.145,.892,1.144,.892,1.143,.693,1.142
.893,1.141,.893,1.140,.894,1.139,.894,1.139,.895,1.138,.895,1.137,.895,1.136
.896,1.135,.896,1.135,.897,1.134,.897,1.133
```

*INTFORO:

```
1.247,1.107,1.007,.939,.874,.829,.784,.751,.717,.691,.665,.644,.622,.605
.587,.572,.557,.544,.532,.520,.509,.499,.489,.480,.471,.463,.455,.447
.441,.433,.428,.421,.416,.410,.404,.398,.394,.389,.384,.379,.376,.371
.367,.362,.360,.355,.352,.347,.345,.341,.338,.334,.332,.329,.326,.323
.321,.318,.315,.312,.310,.307,.305,.302,.301,.298,.296,.293,.292,.289
.288,.285,.284,.282,.280,.278,.277,.275,.273,.271,.270,.268,.266,.264
.263,.261,.260,.258,.257,.256,.254,.253,.252,.250,.249,.247,.247,.245
.244,.243,.242,.241,.239,.238,.237,.236,.234,.233,.232,.231,.230,.229
.228,.227,.226,.225,.224,.223,.222,.221,.220,.220,.218,.218,.217,.216
.215,.214,.213,.213,.211,.211,.210,.210,.208,.208,.207,.207,.205,.205
.204,.204,.202,.202,.201,.201,.199,.199,.198,.198,.197,.197,.196,.196
.194,.194,.193,.193,.191,.191,.190,.190,.189,.189,.188,.188,.186,.187
.185,.186,.184,.185,.183,.184,.182,.183,.181,.181,.180,.180,.179,.179
.178,.178,.177,.177,.176,.177,.175,.176,.174,.175,.173,.174,.172,.173
.171,.172,.170,.171,.170,.171,.169,.170,.168,.169,.167,.168,.166,.167
.165,.166,.164,.165,.164,.165,.163,.164,.162,.163,.162,.163,.161,.162
.160,.161,.159,.160,.159,.160,.158,.159
```

MRDATA:

```
.5,.2929,.2063,.1591,.1294,.1091,.0943,.083,.0741,.067,.0611,.0561
.0519,.0483,.0452,.0424,.04,.0378,.0358,.0341
.7071,.5,.3864,.3147,.2655,.2295,.2021,.1806,.1632,.1489,.1368,.1266,.1178
.1101,.1034,.0975,.0922,.0874,.0831
.7937,.6136,.5,.4218,.3648,.3213,.2871,.2594,.2366,.2175,.2013
.1873,.1751,.1644,.155,.1465,.139,.1322
.8409,.6853,.5782,.5,.4404,.3935,.3557,.3244,.2982,.276,.2568,.2401
.2254,.2125,.2009,.1905,.1812
.8706,.7345,.6352,.5596,.5,.4519,.4122,.3789,.3506,.3263,.3051
.2865,.27,.2553,.2421,.2302
.8909,.7705,.6787,.6065,.5481,.5,.4596,.4253,.3958,.37,.3475,.3275,.3097
.2937,.2793
.9057,.7979,.7129,.6443,.5878,.5404,.5,.4653,.435,.4085,.385,.3641
.3453,.3283
.917,.8194,.7406,.6756,.6211,.5747,.5347,.5,.4695,.4425,.4184,.3968
.3774
.9259,.8368,.7634,.7018,.6494,.6042,.565,.5305,.5,.4718,.4484,.4264
.933,.8511,.7825,.724,.6737,.63,.5915,.5575,.5272,.5,.4755
.9389,.8632,.7987,.7432,.6949,.6525,.615,.5816,.5516,.5245
.9439,.8734,.8127,.7599,.7135,.6725,.6359,.6032,.5736
.9481,.8822,.8249,.7746,.73,.6903,.6547,.6226
.9517,.8899,.8356,.7875,.7447,.7063,.6717
.9548,.8966,.845,.7991,.7579,.7207
.9576,.9025,.8535,.8095,.7698
.96,.9078,.861,.8188
.9622,.9126,.8678
.9642,.9169
.7659
```

APPENDIX B
EXAMPLE OF MAXIMUM-LIKELIHOOD
ESTIMATION PROGRAM

```
*LIST YBULDATA

10  23
20  17.88,28.92,33.00,41.52,42.12,45.60,48.48,51.84,51.96,54.12
30  55.56,67.80,68.64,68.64,68.88,84.12,93.12,98.64,105.12
40  105.84,127.92,128.04,173.40

*MLE
08/24/77  08:14:06


THIS PROGRAM WILL CALCULATE THE UNBIASED MAXIMUM LIKELIHOOD ESTIMATOR
FOR THE WEIBULL SHAPE PARAMETER AND CHARACTERISTIC VALUE


SAMPLE VALUES:

        17.9      28.9      33.0      41.5      42.1      45.6
        48.5      51.8      52.0      54.1      55.6      67.8
        68.6      68.6      68.9      84.1      93.1      98.6
       105.1     105.8     127.9     128.0     173.4
```

	POINT ESTIMATES	90 PERCENT INTERVAL ESTIMATES	
WEIBULL SHAPE PARAMETER=	1.97695	(1.40708,	2.46502)
WEIBULL CHARACTERISTIC VALUE=	81.88	(67.25,	99.94)
DISTRIBUTION MEAN=	72.58		
DISTRIBUTION STANDARD DEVIATION=	38.34		
B10 VALUE=	26.23	(15.04,	36.20)
D2=	0.119588		
END OF DATA			

```
*
```

No. of Copies	To
	Advanced Research Projects Agency, 1400 Wilson Boulevard, Arlington, Virginia 22209
2	ATTN: Director
1	Deputy Director
1	Director of Materials Sciences - Dr. A. L. Bement
1	Deputy Director Materials Sciences - Dr. E. C. van Reuth
1	Technical Information Office - Mr. F. A. Koether
1	Air Force Aeropropulsion Laboratory Wright-Patterson Air Force Base, Dayton, Ohio 45433
	Aerospace Research Laboratory, ATTN: ARL-LL, Wright-Patterson Air Force Base, Dayton, Ohio 45433
1	ATTN: Dr. Henry Graham
1	Mr. Larry Hjelm
1	Major L. Jacobson
1	Dr. James Wimmer
	Air Force Materials Laboratory
1	Major Roger Austin, Wright-Patterson Air Force Base, Dayton, Ohio 45433
1	Dr. Mike Buckley, LLP, Wright-Patterson Air Force Base, Dayton, Ohio 45433
1	Mr. Gail Eichelman, Manufacturing Processes Division, Wright-Patterson Air Force Base, Dayton, Ohio 45433
1	Mr. S. Lyons, Wright Patterson Air Force Base, Dayton, Ohio 45433
1	Dr. R. Ruh, LLM, Wright-Patterson Air Force Base, Dayton, Ohio 45433
1	Capt. Smyth, Wright-Patterson Air Force Base, Dayton, Ohio 45433
1	Air Force Research and Development Dr. A. Lovelace, Deputy Assistant Secretary (R&D) Office of Assistant Secretary of the Air Force (Research and Development), Room 4E973, Pentagon, Washington D.C. 20330
1	Air Force Systems Command Major Jose Baca, Headquarters, DLFP, Propulsion and Power Branch, Andrews Air Force Base, Washington D. C. 20034

D1

ARMY MATERIALS AND MECHANICS RESEARCH CENTER
WATERTOWN, MASSACHUSETTS 02172

TECHNICAL REPORT DISTRIBUTION

No. of Copies	To
	Argonne National Laboratory
1	Dr. Paul G. Shewmon, D212, 9700 South Cass Avenue, Argonne, Illinois 60439
1	Mr. R. N. Singh, Materials Science Division, 9700 South Cass Avenue, Argonne, Illinois 60439
	U. S. Army Air Mobility Research and Development Laboratory
2	J. Accurio, Director, Lewis Directorate, NASA, Lewis Research Center, 21000 Brookpark Road, Cleveland, Ohio 44135
1	R. Berrisford, Chief, Structures Division, Eustis Directorate, Ft. Eustis, Virginia 23604
1	T. Coleman, Director, Langley Directorate, Langley Research Center, Langley Field, Virginia 23365
2	F. Immen, J. Wheatly, Advanced Systems Research Office, Ames Research Center, Moffett field, California 94035
1	J. White, Assistant Technical Director, Eustis Directorate, Fort Eustis, Virginia 23604
1	U. S. Army Aviation Material Laboratories Commanding Officer, Fort Eustis, Virginia 23604
1	U. S. Army Aviation School Library Librarian, Fort Rucker, Alabama 36360 ATTN: Bldg. 5907
1	U. S. Army Aviation Systems Command Commanding General, ATTN: R. Long, Deputy Director RD&E, P. O. Box 209, St. Louis, Missouri 63166
1	U. S. Army Engineers Commanding Officer, Waterways Experiment Station, Vicksburg, Mississippi 39180 ATTN: Research Center Library
	U. S. Army Material Command Commanding General, Washington D. C. 20315
1	AMCRD-TC (Dr. El-Bisi)
1	ANCDL (Dr. Dillaway)
1	Army Materials Command Headquarters Dr. Donald Weidhuner, Chief, Power Division, Research Development and Engineering Directorate, 5001 Eisenhower Avenue, Alexandria, Virginia 22304

TECHNICAL REPORT DISTRIBUTION

No. of Copies	To
	Director, Army Materials and Mechanics Research Center
	Watertown, Massachusetts 02172
2	ATTN: AMXMR-PL
1	AMXMR-PR
1	AMXMR-CT
1	AMXMR-AP
1	AMXMR-X (Dr. Wright)
1	AMXMR-EO (Dr. Katz)
2	AMXMR-TM (Dr. Lenoe)
2	AMXMR-D (Dr. Priest)
1	AMXMR-EO (Dr. Messier)
2	AMXMR-P (Dr. Burke)
1	AMXMR-MS (Mr. MacDonald)
1	AMXMR-E (Dr. Larson)
1	AMCMR-E (Lt. Col. E. E. Chick)
	U.S. Army MERDEC
	Commanding Officer, Fort Belvoir, Virginia 22060
1	ATTN: STSFB-EP (Mr. Frank Jordan)
1	STSFB-EP (Mr. W. McGovern)
1	AMCPM-FM (Mr. Allen Elkins)
1	AMXFB-EM (Mr. George F. Sams)
1	Army Missile Command
	Commanding General, ATTN: AMCRD-F. J. Beebe, Washington D.C. 20315
1	Commanding General, Redstone Arsenal, Alabama 35809 ATTN: Technical Library
1	Commanding General, ATTN: AMCDL, Webb Taylor, 5001 Eisenhower Avenue, Alexandria, Virginia 22304
	USACDC Ordnance Agency, Aberdeen Proving Ground
1	Commanding Officer, Maryland 21005, ATTN: Technical Library Building 313
1	Commanding Officer, Maryland 21005, ATTN: Library, Building 350
	Army Research and Development
1	Office, Chief Research and Development, Department of the Army, ATTN: R. Ballard, Physical and Engineering Sciences Division, Washington, D.C. 20315
1	Office Chief Research and Development, Department of Army, ATTN: Col. J. Barnett, Physical and Engineering Sciences Division, Washington, D.C. 20315

ARMY MATERIALS AND MECHANICS RESEARCH CENTER
WATERTOWN, MASSACHUSETTS 02172

TECHNICAL REPORT DISTRIBUTION

No. of Copies	To
1	Commanding Officer, Army Research Office (Durham), Bx CM, Duke Station Durham, North Carolina 27006 ATTN: Dr. H. M. Davis
8	Lt. Col. James Kennedy, Chief, Materials Branch, European Research Office U.S. Army R & D Group, (FUR), Box 15, FPO New York 09510
1	Mr. H. Morrow, Eustis Directorate, AMRDL, Fort Eustis, Virginia 23604
5	U.S. Army Tank-Automotive Command Commanding General, Warren, Michigan 48090, ATTN: AMSTA-BSL, Research Library Br, ATTN: AMSTA-RKM (Mr. C. Green), ATTN: AMSTA-PGR (Mr. Engel), ATTN: AMSTA (Dr. Banks), ATTN: AMSTA (Mr. L. Barnett)
1	U.S. Army Weapons Command Commanding General, Research and Development Directorate, Rock Island, Illinois 61201, ATTN: AMSWE-RDR
1	U.S. Atomic Energy Commission Dr. Joseph Griffo, Space Nuclear Systems Division, Century XXI Building, Mail Station F-309, Washington D.C. 20545
1	Dr. Alan Womack, Assistant Director, Gas Cooled Reactors, Washington D.C. 20545
1	British Embassy Dr. R. Warren, Contract Officer, Defense Research and Development Staff, 3100 Massachusetts Avenue N.W., Washington D. C. 20008
1	Bureau of Mines Dr. E. P. Flint, Room 4513, Interior Building, Washington D. C. 20240
1	Mr. Ron Lowrey, P. O. Box 70, Albany, Oregon 97321
1	Mr. M. A. Schwartz, Tuscaloosa Metallurgy Research Laboratory, P. O. Box 1, University, Alabama 35486
12	Defense Documentation Center Commander, Cameron Station, Building 5, 5010 Duke Street, Alexandria, Virginia 22314
1	Department of Transportation Mr. Michael Lauriente, 400 Seventh Street, S. W., Washington, D. C. 20590
1	Directorate for Energy .. C. Christensen, Assistant for Resources, OASD (I & L), Room 2B341 Pentagon, Washington, D. C. 20301

ARMY MATERIALS AND MECHANICS RESEARCH CENTER
WATERTOWN, MASSACHUSETTS 02172

TECHNICAL REPORT DISTRIBUTION

No. of Copies	To
1	Office of the Director of Defense Mr. R. M. Standahar, Research and Engineering, Room 3D1085, Pentagon, Washington, D. C. 20301
4	Energy Research and Development Administration Division of Transportation, 20 Massachusetts Avenue, N.W. Washington D. C. 20545 ATTN: Mr. George Thur (TEC) Mr. Frank Moore (CLNRT) Mr. Robert Schulz (TEC) Mr. John Neal (CLNRT)
1	Mr. E. N. C. Dalder, Materials and Radiation Effects Branch, Division of Magnetic Fusion Energy, MSG-234, Washington D.C. 20545
1	Dr. C. Martin Stickley, Division of Laser Fusion, Mail Station A-364, Washington, D.C. 20545
1	Mrs. Patricia Mooney, Office of Management and Budget, Coordination Branch, Room 8001, New Executive Office Bldg., Washington, D. C. 20503
1	Mr. Steve Wander, Division of Fossil Fuels, Washington, D. C. 20545
1	Dr. S. M. Wolf, Division of Physical Research, Mail Station J-309, Washington, D. C. 20545
1	Federal Energy Office Mr. Thomas Gross, Staff Member, Office of Energy Conservation, Room 4234, Columbia Plaza Bldg., Washington, D. C. 20461
1	Federal Power Commission Dr. Charles Berg, Chief Engineer, Room 2100 825 North Capital Street, N. E., Washington, D. C. 20426
1	USA Foreign Science and Technology Center Commander, ATTN: AMXST-SD3, Mr. C. Petschke, 220 7th Street NE, Charlottesville, Virginia 22901
1	National Academy of Sciences Mr. Donald G. Groves, Staff Engineer, National Materials Advisory Board, 2101 Constitution Avenue, N. W., Washington, D.C. 20418
2	National Aeronautics and Space Administration Ms. Bolick, Goddard Space Flight Center, Greenbelt, Maryland 20771
1	Dr. G. C. Deutsch, Assistant Director of Research (Materials), Code RR-1, NASA, Washington, D.C. 20546

No. of Copies	To
1	Mr. James J. Gangler, Advanced Research and Technology Division, Code RRM, Room B556, Headquarters, Washington, D.C. 20546
1	Mr. P. R. Miller, NASA Headquarters, Code RPD, 600 Independence Avenue, S.W., Washington, D.C. 20546
	NASA Lewis Research Center, 21000 Brookpark Road, Cleveland, Ohio 44135
8	ATTN: Mr. W. Saunders Dr. S. K. Dutta Dr. Hubert Probst Mr. C. Blankenship Dr. Robert C. Bill Mr. M. Krasner Mr. Donald Guentert Mr. Neil T. Saunders
	National Bureau of Standards
1	Dr. Robb Thomson, Senior Research Scientist, Room B109, Bldg. 225, Washington, D.C. 20234
1	Dr. Donald Vieth, Administration Bldg., Room A1002, Washington, D.C. 20234
1	Dr. John B. Wachtman, Jr., Division Chief, Inorganic Materials Division, Room A359, Materials Building, Washington, D.C. 20234
1	Dr. S. Wiederhorn, Physical Properties Section, Institute for Materials Research, Washington, D.C. 20234
	National Science Foundation
1	Dr. Raymond Bisplinghoff, Deputy Administrator, 1300 G. Street, N.W., Washington, D.C. 20550
1	Mr. R. Reynik, Director, Division of Materials Research, 1800 G. Street, N.W., Washington, D.C. 20550
1	Dr. Leonard Topper, Office of Energy R & D Policy, Room 537, 1800 G. Street, N.W., Washington, D.C. 20550
	U. S. Naval Air Propulsion Test Center
1	Mr. Robert Benham, AEP-22, (AE), Philadelphia, Pennsylvania 19112
1	Mr. Joe Glotz, Department of the Navy, Trenton, New Jersey 08628
	Naval Air Systems Command
1	Mr. Irving Machlin, High Temperature Materials Divsion, Materials and Processes Branch, (NAIR-52031D), Department of the Navy, Washington, D.C. 20360
1	Mr. Charles F. Bersch, Department of the Navy, Washington, D.C. 20360

TECHNICAL REPORT DISTRIBUTION

No. of Copies	To
	Office of Naval Research
1	Dr. A. M. Diness, Metallurgy Branch, Code 471, 800 N. Quincy Street, Arlington, Virginia 22217
1	Mr. Keith Ellingsworth, Power Program, Arlington, Virginia 22217
1	Mr. R. Rice, Washington, D.C. 20390
1	**Naval Ships Engineering** Mr. John Fairbanks, Prince George Center, Hyattsville, Maryland 20782
1	**Naval Ships Research and Development Center** Mr. George A. Wacker, Head Metal Physics Branch, Annapolis, Maryland 21402, ATTN: Code 2812
1	Mr. W. Wheatfall, Code 2812, Annapolis, Maryland 21402
1	**Naval Ship Systems Command Headquarters** Mr. Roy Peterson, Chief, Pollution Abatement and Gas Turbine Research, Ship Research and Technology Division, 2531 Jefferson Davis Highway, Arlington, Virginia 20362
1	**Naval Underwater System Center** Mr. John Miguel, Newport, Rhode Island
1	**Naval Weapons Center** Dr. W. Thielbain, Code 4061, China Lake, California 93555
2	Dr. James I. Bryant, Office of the Chief of Research, Development and Acquisition, ATTN: DAMA-CSS, the Pentagon, Washington, D.C. 20310
1	Mr. Tyler Port, Special Assistant, OASA, (I&L), Room 3E620, Pentagon, Washington, D.C. 20301
1	**Aerojet Liquid Rocket Company** Mr. O. I. Ford, Technical Manager, Combustor Systems, P. O. Box 18222, Sacramento, California 95813
1	**The Aerospace Corporation** Mr. Donald Lapades, P. O. Box 92957, Los Angeles, California 90009
1	**AiResearch Manufacturing Company** Dr. Robert F. Kirby, Materials Engineering Dept. 93-393M, Sky Harbor Airport, 402 South 36th Street, Phoenix, Arizona 85034
1	Mr. McCoy, Materials Engineering, Dept. 93-393M, 402 South 36th Street, Phoenix, Arizona 85034

TECHNICAL REPORT DISTRIBUTION

No. of Copies	To
1	Supervisor, Propulsion Engine Advanced Technology Dept., 93-12M Sky Harbor Airport, 402 South 36th Street, Phoenix, Arizona 85034
1	Mr. Dennis W. Swain, Department 93-19M, P. O. Box 5217, Phoenix, Arizona 85010
1	American Lava Corporation Dr. J. T. Bailey, Chattanoga, Tennessee 37405
1	Arthur D. Little, Incorporated Mr. D. William Lee, Acorn Park, Cambridge, Massachusetts 02140
	Avco Corporation
1	Mr. Louis J. Fiedler, Materials and Process Technology Lab., 550 S. Main Street, Stratford, Connecticut 06497
1	Dr. T. Vasilos, Applied Technology Division, Lowell Industrial Park, Lowell, Massachusetts 01851
1	Babcock and Wilcox Dr. A. W. Illyn, Technical Director, Refractories Division, Old Savannah Road, Augusta, Georgia 30903
	Battelle Columbus Laboratories
1	Mr. Winston Duckworth and Mr. Lewis E. Hulbert, 505 King Avenue, Columbus, Ohio 43201
1	Mr. James Lynch, Metals and Ceramics Information Center, 505 King Avenue, Columbus, Ohio 43201
1	Battelle Memorial Institute Mr. William Combs, 2030 M Street N. W. Washington, D. C. 20036
	Bell Aerospace Company
1	Dr. Wilfred H. Dukes, Assistant Director Engineering for Development, P.O. Box 29307, New Orleans, Louisiana 70139
1	Mr. A. E. Leach, Manager, Process Development Engineering, Mail Zone C-33, P. O. Box 1, Buffalo, New York 14240
1	Mr. Nelson R. Roth, P.O. Box #1, Department V70, Buffalo, New York 14240

TECHNICAL REPORT DISTRIBUTION

No. of Copies	To
1	Cabot Corporation Mr. S. T. Wlodek, Stellite Division, 1020 West Park Avenue, Kokomo, Indiana 46901
3	The Carborundum Company Dr. John A. Coppola, Mr. C. H. McMurty, Mr. William D. Long, Research and Development Division, Niagara Falls, New York 14302
2	Caterpillar Tractor Company Mr. A. R. Canady, Mr. John M. Bailey, Technical Center, Building F, Peoria, Illinois 61602
1	Ceradyne Incorporated Mr. J. A. Rubin, P. O. Box 11030, 303 South Red Hill Avenue, Santa Ana, California 92705
1	Ceramic Finishing Company Dr. H. P. Kirchner, P. O. Box 498, State College, Pennsylvania 16801
1	Ceramic Systems Incorporated Mr. Eldor R. Herrmann, 11402 Schaefer Highway, Detroit, Michigan 48227
1	Chrysler Corporation Mr. C. E. Wagner, Senior Research Staff Engineer, CIMS: 418-37-18, P. O. Box 1118, Detroit, Michigan 48231
1	Mr. Philip J. Willson, Chemical Research, Box 1118, CIMS: 418-19-18, Detroit, Michigan 48231
1	Colt Industries Mr. E. J. Dulis, President, Materials Research Center, Box 88, Pittsburgh, Pennsylvania 15230
1	Coors Porcelain Company Research Department, 17750 West 32nd Avenue, Golden, Colorado 80401
1	Corning Glass Works Mr. John C. Lanning, Manager, Erwin Plant, Advanced Engine Components Department, Corning, New York 14830
1	Creare Incorporated Ms. Sharon Wright, Technical Library, Hanover, New Hampshire 03755

ARMY MATERIALS AND MECHANICS RESEARCH CENTER
WATERTOWN, MASSACHUSETTS 02172

TECHNICAL REPORT DISTRIBUTION

No. of Copies	To
1	Curtis-Wright Corporation Mr. S. Walosin, One Passaic Street, Woodridge, New Jersey 07075
2	Cummins Engine Company, Incorporated Mr. R. Kamo, Mr. K. J. Mather, Columbus, Indiana 47201
1	Deposits and Composites, Incorporated Mr. Richard E. Engdahl, 1821 Michael Faraday Drive, Reston, Virginia 22090
1	Dow Corning Corporation Mr. G. Kookootsedes, Market Development, Resins and Chemicals, Midland, Michigan 48640
1	Mr. Donald E. Weyer, Midland, Michigan 48640
1	Eagle-Picher Industries Dr. J. J. Stiglich, 200 9th Avenue N.E. Miami, Oklahoma 74354
1	Eaton Corporation Mr. William E. Gurwell, Research Center 26201 Northwestern Highway, Southfield, Michigan 48076
1	EF Industries, Incorporated Mr. J. D. Mote, 1301 Courtesy Road Louisville, Colorado 80027
1	Electric Power Research Institute Dr. Richard E. Balzhiser, P. O. Box 10412, 3412 Hillview Avenue Palo Alto, California 94304
1	Dr. Arthur Cohn, P.O. Box 10412, 3412 Hillview Avenue, Palo Alto, California 94304
1	Energy Research Corporation Bethel, Connecticut 06801
1	Esso Research and Engineering Company Dr. John V. Milewski, Government Research Laboratory, P. O. Box 8, Linden, New Jersey 07036
1	Ferro Corporation Mr. Y. Baskin, Manager Inorganic Chemical Research, Technical Center, 7500 East Pleasant Valley Road, Independence, Ohio 44131

No. of Copies	To
1	Fiber Materials Mr. Paul F. Jahn, Vice President, Broadway and Main Street, Graniteville, Massachusetts 01829
1	Garrett Corporation Mr. H. R. Schelp, 9851 Sepulveda Boulevard, Los Angeles, California 90009
1	Gas Turbine International Mr. Jack W. Sawyer, 4519 Eighteen Street North Arlington, Virginia 22207
1	Gas Turbine World Mr. Victor de Biasi, Editor, P. O. Box 494, Southport, Connecticut 06490
	General Atomics Corporation
1	Mr. N. B. Elsner, Box 81608, San Diego, California 92138
1	Mr. Karl Koyama, Box 81608, San Diego, California 92138
1	Dr. Robert K. Thomas, FA4-4, Reactor Engineering, P. O. Box 81608, San Diego, California 92138
	General Electric
1	Dr. C. A. Bruch, Manager, Advanced Studies, Aircraft Engine Group, Cincinnati, Ohio 45215
1	Dr. J. E. Burke, Corporate Research and Development, P. O. Box 8, Schenectady, New York 12301
1	Dr. H. von E. Doering, Manager, Fuels/Corrosion Unit, Gas Turbine Products Division, Building 53-311, Schenectady, New York 12345
1	Dr. Soloman Musikant, Manager, Metallurgy and Ceramics Lab General Electric Valley Forge, Valley Forge, Pennsylvania
1	Dr. Michael J. Noone, Space Sciences Laboratory, Box 8555, Philadelphia, Pennsylvania 19101
1	Mr. Arthur L. Ross, Valley Forge Space Center, P. O. Box 8555, Philadelphia, Pennsylvania 19101
1	Mr. Chester T. Sims, Manager, Advanced Materials, Gas Turbine Products Division., Schenectady, New York 12301

No. of Copies	To
	General Motors Corporation
1	Dr. Morris Berg, AC Spark Plug Division, Flint, Michigan 48556
1	Dr. John S. Collman, Head, Power Systems Development, Research Laboratories, Warren, Michigan 48090
1	Dr. Robert W. Gibson, Jr., Head, Library Department GM Technical Center, Warren, Michigan 48090
1	Mr. M. Herman, Detroit Diesel Allison Division, Indianapolis Operations, P. O. Box 894, Indianapolis, Indiana 46206
1	Mr. Michael E. Naylor, General Motors Technical Divsion, Passenger Car Turbine Division, Warren, Michigan 48090
1	Mr. O. Prachar, Passenger Car Turbine Department, Engineering Staff, General Motors Technical Center, Warren, Michigan 48090
1	Dr. Edward Reynolds, General Motors Technical Center, Passenger Car Turbine Division, Warren, Michigan 48090
	GTE Sylvania
1	Dr. Richard Kliener, Tonawanda, Pennsylvania 18848
1	Dr. William H. Rhodes, GTE Laboratories, Waltham Research Center, 40 Sylvan Road, Waltham, Massachusetts 02154
1	**Howmet Corporation** Mr. Wm. R. Freeman, Jr., Vice President and Technical Director, Superalloy Group, One Misco Drive, Whitehall, Michigan 47461
1	**Industrial Materials Technology** Dr. Robert Widmer, President, 19 Wheeling Avenue, Woburn, Massachusetts
1	**Institut fur Werkstoff-Forshung** Dr. W. Bunk, DFVLR, 505 Porz-Wahn, Linder Hohe, Germany
1	**International Harvester Company** Mr. A. R. Stetson, Chief, Process Research Laboratories, Mail Zone R-1, Solar Division of Int. Harvester Company, 2200 Pacific Highway, San Diego, California 92112
1	Mr. M. J. Klein, Research Staff Specialist, Mail Zone R-1, Solar Division of International Harvester, 2200 Pacific Highway, P. O. Box 80966, San Diego, California 92138

No. of Copies	To
1	The International Nickel Company, Incorporated Mr. Gaylor D. Smith, 1 New York Plaza, New York, New York 10004
2	Kawecki-Berylco Industries, Incorporated Mr. E. Laich, Mr. R. J. Longenecker, P. O. Box 1462, Reading, Pennsylvania 19603
1	Kaman Sciences Corporation Garden of the Gods Road, Colorado Springs, Colorado 80907
	Lawrence Livermore Laboratory
1	Mr. C. F. Cline, L-503, Box 808, Livermore, California 94550
1	Dr. Michael Guinan, B. Div./L-24, P.O. Box 808, Livermore, California 94550
1	Dr. Mark Wilkins, B Div./L-24, P. O. Box 808, Livermore, California 94500
1	Lawrence Radiation Laboratory Mr. R. L. Lormand, P. O. Box 808, Livermore, California 94550
1	Manlabs, Incorporated Dr. L. Kaufman, Project Director, 21 Erie Street, Cambridge, Massachusetts 02139
1	Materials Consultants, Incorporated 2150 South Josephine Street Denver, Colorado 80210
1	Materials Research and Computer Simulation Mr. William Oldfield, 634 Berkeley Place, Westerville, Ohio 43081
1	Materials Science Corporation Technical Library, Blue Bell Office Campus, Merion Towle Building, Blue Bell, Pennsylvania 19422
1	Mechanical Technology, Incorporated Mr. D. W. McLaughlin, Research and Development Division, 968 Albany-Shaker Road, Latham, New York 12110
1	National Beryllia Corporation Dr. Peter L. Fleischner, Haskell, New Jersey 07420
1	Northern Research and Engineering Corporation Ms. Rayna Lee Caplan, Librarian, 219 Vassar Street, Cambridge, Massachusetts 02139

ARMY MATERIALS AND MECHANICS RESEARCH CENTER
WATERTOWN, MASSACHUSETTS 02172

TECHNICAL REPORT DISTRIBUTION

No. of Copies	To
	Norton Company
1	Mr. M. Blake, One New Bond Street, Worcester, Massachusetts 01606
1	Mr. E. W. Hauck, Market Manager, Engine Components, One New Bond Street, Worcester, Massachusetts 01606
1	Dr. M. L. Torti, One New Bond Street, Worcester, Massachusetts 01606
1	Owens-Corning Fiberglass Corporation Mr. P. E. McConnell, Technical Center, Granville, Ohio 43023
	Owens Illinois Glass
1	Mr. L. M. Donley, 1900 North Westwood Avenue, Toledo, Ohio 43601
1	Mr. Y. K. Pei, 1020 North Westwood Avenue, Toledo, Ohio 43607
	PPG Industries, Incorporated
1	Mrs. Jane Bookmyer, Information Services Division, P. O. Box 11472 Pittsburgh, Pennsylvania 15238
1	Mr. F. G. Stroke, Asst. Manager Market Development, 1 Gateway Center, Pittsburgh, Pennsylvania 15222
	Pratt and Whitney Corporation
1	Mr. James F. Holloway, Materials Project Engineer, 400 Main Street, E. Hartford, Connecticut 06108
1	Mr. M. Allen Magid, Materials Marketing Engineer, Florida R & D Center P. O. Box 2691, West Palm Beach, Florida 33402
1	Mr. Francis L. VerSnyder, Manager, Materials Engineering and Research Lab, 400 Main Street, E. Hartford, Connecticut 06108
1	Program Development Consultant Dr. Robert A. Harmon, 25 Schalren Drive, Latham, New York 12110
1	The Rand Corporation Dr. Eugene C. Gritton, Physical Sciences Department, 1700 Main Street, Santa Monica, California 90406
	Raytheon Company
1	Ms. Madaleine Bennett, Librarian, Research Division Library, Foundry Avenue, Waltham, Massachusetts 02154
1	Dr. Stanley Waugh, Research Division, 28 Seyon Street, Waltham, Massachusetts 02154

No. of Copies	To
1	R. I. A. S. Mrs. R. J. Benacquista, 3808 Acosta Road, Fairfax, Virginia 22030
1	Rockwell International Corporation Mr. F. E. Krainess, D/391-204 AB70, 12214 Lakewood Boulevard, Downey, California 90241
1	Dr. Don Thompson, Science Center, 1049 Camino Dos Rios, Thousand Oaks, California 91360
1	Rohr Industries, Incorporated Mr. Joseph Simpson, Technical Library, P. O. Box 1516, Chula Vista, California 92012
2	SKF Industries, Incorporated Mr. Warren Jameson, Mr. Harish Dalal, Engineering and Research Center, 1100 1st Avenue, King of Prussia, Pennsylvania 19406
1	Southern Research Institute Mr. H. Stuart Starrett, Head, Mechanics Section, 2000 Ninth Avenue South, Birmingham, Alabama 35205
1	Special Metals Corporation Mr. Willard H. Sutton, Manager, Ceramics Projects, New Hartford, New York 13413
1	Stackpole Carbon Company Mr. P. W. Parsons, Manager, Commercial Research Department, St. Marys, Pennsylvania 15857
1	Stone and Webster Engineering Corporation Mr. David Cormier, Nuclear Planning Division, 87 Nash Memorial, Road, Abington, Maryland 02351
	Teledyne
1	Mr. Robert Beck, Department Head, Development Materials 1330 Laskey Road, Toledo, Ohio 43601
1	Dr. Eli Benstien, Director of Engineering, 1330 Laskey Road, Toledo, Ohio 43601
1	Mrs. Marlene S. Dowdell, Librarian, 1330 Laskey Road, Toledo, Ohio 43601
	TRW Incorporated
1	Mr. J. A. Alexander, Manager, Materials Research Department, 23555 Euclid Avenue, Cleveland, Ohio 44117

TECHNICAL REPORT DISTRIBUTION

No. of Copies	To
1	Dr. John S. Foster, Jr., Vice President for Energy Research and Development, One Space Park, Redondo Beach, California 90278
1	Technical Library, TRW Equipment, 23555 Euclid Avenue, Cleveland, Ohio 44117
1	Dr. Neal Richardson, One Space Park, Redondo Beach, California 90278
1	Turbodyne Corporation Ms. Diane Konsor, 711 Anderson Avenue North, St. Cloud, Minnesota 56301
1	Mr. Donald J. Legacy, Wellsville, New York 14895
1	Mr. John Polyansky, Gas Turbine Design Engineering, 626 Lincoln Avenue S.E., St. Cloud, Minnesota 56301
1	Turbo Power and Marine Systems, Incorporated Mr. Carl Merz, Farmington, Connecticut 06032
1	Mr. C. A. Vassilakis, New Britain Avenue, Farmington, Connecticut 06032
1	Union Carbide Corporation Dr. O. Conrad Trulson, Carbide Products Division, 270 Park Avenue, New York, New York 10017
1	United Aircraft Research Laboratories Dr. Frank Galasso, East Hartford, Connecticut 06108
1	United Technologies Research Center Dr. J. J. Brennan, East Hartford, Connecticut 06108
1	Whittaker Corporation Mr. V. A. Chase, Chief of Development Laboratory, Research and Development Division, 3540 Aero Court, San Diego, California 92123
1	Williams Research Corporation Mr. R. Barry Strachan, Walled Lake, Michigan 48088
1	Wyman-Gordon Company Mr. Wayne Everett, Research and Development, North Grafton, Maine 01536

ARMY MATERIALS AND MECHANICS RESEARCH CENTER
WATERTOWN, MASSACHUSETTS 02172

TECHNICAL REPORT DISTRIBUTION

No. of Copies	To
1	Brown University Professor Marc Richman, Engineering Division, Providence, Rhode Island 02912
1	California Institute of Technology Mr. Thomas J. Ahrens, Assoc. Prof. of Geophysics, Seismological Laboratory, 295 San Rafel Avenue, P. O. Bin 2, Arroyo Annex, Pasadena, California 91109
1	Dr. William A. Edminston, Jet Propulsion Laboratory - Bldg 157, 4800 Oak Grove Drive, Pasadena, California 91103
1	Carnegie-Melion University Professor M. C. Shaw, Head, Department of Mechanical Engineering, Pittsburgh, Pennsylvania 15213
1	Georgia Tech. Mr. J. D. Walton, Jr., EES, Atlanta, Georgia 30332
1	Harvard University Professor Michael F. Ashby, Gordon McKay Professor of Metallurgy, Pierce Hall, Cambridge, Massachusetts 02138
1	Illinois Institute of Technology Mr. Seymour Bortz, IIT Research Institute, 10 West 35th Street, Chicago, Illinois 43601
1	Dr. Keith E. McKee, Director of Research Engineering Mechanics Div., IIT Research Institute, 10 West 35th Street, Chicago, Illinois 60616
1	Iowa State University Dr. Thomas D. McGee, Professor of Ceramic Engineering, Ames, Iowa 50010
1	Lehigh University Dr. R. M. Spriggs, Assistant to the President, Bethlehem, Pennsylvania 18015
1	Massachusetts Institute of Technology Professor Merton Flemings, Cambridge, Massachusetts 02139
1	Professor D. W. Kingery, Room 13-4090, Cambridge, Massachusetts 02139
1	Professor Frank S. McClintock, Department of Mechanical Engineering, Cambridge, Massachusetts 02139

TECHNICAL REPORT DISTRIBUTION

No. of Copies	To
1	Dr. Donald R. Uhlmann, Associate Professor of Ceramics, Department of Metallurgy and Materials Science, Cambridge, Massachusetts 02139
1	North Carolina State University Professor Robert F. Davis, Department of Materials Science, Box 5427, Raleigh, North Carolina 27607
1	Northwestern University Professor Morris E. Fine, The Technological Institute, Dept. of Materials Science, Evanston, Illinois
1	Stanford University Dr. Paul Jorgensen, Associate Director, Materials Laboratory, Menlo Park, California 94025
1	Ms. Lucille Steelman, Order Librarian, ATTN: G-037 Library, Menlo Park, California 94025
1	Southern Methodist University Professor T. L. Chu, Institute of Technology, Electronic Sciences Center, Dallas, Texas 75222
1	University of Bridgeport Dr. Joseph E. Motherway, Bridgeport, Connecticut 06602
1	University of California Professor Earl R. Parker, Department of Materials Science and Engineering, 286 Hearst Mining Building Berkeley, California 94720
1	University of Illinois Dean Daniel C. Drucker, Engineering College, Urbana, Illinois 61801
1	University of Michigan Professor Edward E. Hucke, Materials and Metallurgical Engineering, Ann Arbor, Michigan 48104
1	Dr. Maurice J. Sinnott, Department of Chemical and Metallurgical Engineering, Ann Arbor, Michigan 48104
1	University of Pennsylvania Professor R. P. Kroon, Philadelphia, Pennsylvania 19104

TECHNICAL REPORT DISTRIBUTION

No. of Copies	To
1	Dr. Charles J. McMahon, Jr., Assoc. Prof. Materials Science, School of Metallurgy and Materials Science, Philadelphia, Pennsylvania 19104
1	Professor Burton Paul, Department of Mechanical Engineering, Philadelphia, Pennsylvania 19104
1	University of Utah Professor I. B. Cutler, College of Engineering, Division of Materials Science and Engineering, Salt Lake City, Utah 84112

2 Authors

311 Total Copies Distributed

ABSTRACT

The demonstration of uncooled brittle materials in structural applications at 2500°F is the objective of the Brittle Materials Design, High Temperature Gas Turbine program. Ford Motor Company, the contractor is utilizing a small vehicular gas turbine comprising an entire ceramic hot flow path including the highly stressed turbine rotors. Westinghouse, the subcontractor originally planned to evaluate ceramic first stage stator vanes in an actual 30 MW test turbine engine however the objective was revised to demonstrate ceramic stator vanes in a static test rig. Both miniature had in-house research programs in the area prior to this contract.

In the stationary gas turbine project the use of ceramic stator vanes in a static rig for 100 cycles up to temperatures of 2500°F has been completed. This accomplishment meets the revised objectives for the stationary turbine project and therefore the project was completed. The report of the last six months progress will be included in the final report for the project and subsidiary materials were fabricated and all of these three are being prepared for testing.

ABSTRACT

The demonstration of uncooled brittle materials in structural applications at 2500°F is the objective of the Brittle Materials Design, High Temperature Gas Turbine program. Ford Motor Company, the contractor is utilizing a small vehicular gas turbine comprising an entire ceramic hot flow path including the highly stressed turbine rotors. Westinghouse, the subcontractor was originally planned to evaluate ceramic first stage stator vanes in an actual 30 MW test turbine engine, however, that objective was revised to demonstrate ceramic stator vanes in a static test rig. Both companies had in-house research programs in this area prior to this contract.

In the stationary gas turbine project, the test of ceramic stator vanes in a static rig for 180 cycles up to temperatures of 2500°F has been completed. This accomplishment meets the revised objectives for the stationary turbine project and therefore this project will be included in the final report for the project and published separately.

Fabrication of duo-density silicon nitride turbine rotors continued during this reporting period. Due to persistent bonding problems between the hot pressed materials in the three-piece design, the fabrication concept was altered to a simplified two-piece design with the only bond being between hot pressed Si3N4 and reaction bonded Si3N4. This change was also made possible by the results of a hot pressing parameters study, which showed that good strength and density could be achieved at reduced hot pressing pressures. Ten two-piece rotors were fabricated and all of these there are being prepared for testing.

The reaction molding of duo-density rotor blade rings has been improved by the addition of a mild state automatic control system which was installed on the injection molding machine. A problem of unresolved delamination was discovered and solved by the use of material extrusion and increased nozzle temperature during molding. Microfocus X-ray equipment has been evaluated and found advantageous for blade ring flaw detection.

Fabrication of turbine inlet nose cones and stators was resumed on a limited basis. A silicon metal powder organic system yielding 2.7 g/cc density reaction bonded silicon nitride material was utilized for the first time for injection molding of these components. Two additional test fixtures were built for use in pre-engine test evaluation of ceramic stators. One of these fixtures, the stator vane mechanical load test fixture was utilized in a NDE test to evaluate material and processing variations and (2) as a screening tool to qualify stator vanes for subsequent engine testing. The other rig, the stator vane abradal pressure test fixture, evaluates the stator outer abradal quality before subsequent engine testing. In the testing area, the primary emphasis was placed on the utilization of these new fixtures to enhance the qualification of stationary ceramic flow path components. The initial evaluation of the best quality 2.7 g/cc density Si3N4 components is underway. In addition, a review of past weight gain data for 2.55 g/cc density stators, tested at 1930°F, was completed.

In order to select the best method of processing Si3N4 powder the optimum high content and the best hot pressing parameters consistent with the hub forming portion of the duo-density rotor process, a parametric processing study was conducted. Strength at two elevated temperatures, along with the Weibull slope were obtained for a number of hot pressed Si3N4 materials. A major concern with the three-piece approach to the duo-density rotor has been the degree of bonding and the resultant strength of the bond between the two regions of hot pressed Si3N4. Test bars were cut from an duo-density rotors such that the hot pressed to hot pressed bond could be positioned within the zone of maximum stress. Test results showed a strength variation at different locations being higher at the center region and lower at the leading and trailing edges. Strength measurements were performed on Refel reaction bonded silicon carbide. The material tested for comparison purposes, showed best strength distributions were measured at room temperature and at five elevated temperatures. In addition, tensile strength was measured at room temperature.

Previous results obtained from nitriding of large loads of silicon metal powder shapes such as molded stators and rotor blade rings have shown that the nitriding reaction was not under control. A technique was developed which allows the furnace to control the nitriding dependent upon the nitrogen gas consumption rate resulting in improved material structure. The task originally planned to evaluate ceramic first stage stator vanes in an actual 30 MW test turbine engine however, that objective was revised to demonstrate ceramic stator vanes in a static test rig. Both companies had in-house research programs in this area prior to this contract.

Work on analytical codes resulted in the development of relationships for comparing time-dependent reliabilities of ceramics in the presence of delayed fracture or static fatigue. These equations are derived from the statistical crack growth model and combined with Weibull strength statistics to determine failure probabilities.

(4) Interim rept. no 11, 1 Jul-
31 Dec 76.

REPORT DOCUMENTATION PAGE	READ INSTRUCTIONS BEFORE COMPLETING FORM

1. REPORT NUMBER (19) (18) AMMRC CTR-77-20	2. GOVT ACCESSION NO.	3. RECIPIENT'S CATALOG NUMBER
4. TITLE (and Subtitle) (6) Brittle Materials Design, High Temperature Gas Turbine.		5. TYPE OF REPORT & PERIOD COVERED Interim Report Number 11 7-1-76 to 12-31-76
		6. PERFORMING ORG. REPORT NUMBER
7. AUTHOR(s) (10) A. F. McLean, Ford Motor Company E. A. Fisher, Ford Motor Company		8. CONTRACT OR GRANT NUMBER(s) (15) DAAG 46-71-C-0162, ARPA Order-1849
9. PERFORMING ORGANIZATION NAME AND ADDRESS Ford Motor Company, Dearborn, MI 48121		10. PROGRAM ELEMENT, PROJECT, TASK AREA & WORK UNIT NUMBERS D/A Project: ARPA Order 1849 AMCMS Code: Agency Accession: DA OD 4733
11. CONTROLLING OFFICE NAME AND ADDRESS Army Materials and Mechanics Research Center Watertown, Massachusetts 02172		12. REPORT DATE (11) August 1977
		13. NUMBER OF PAGES 129 (12) 136 p.
14. MONITORING AGENCY NAME & ADDRESS(If different from Controlling Office)		15. SECURITY CLASS. (of this report) Unclassified
		15a. DECLASSIFICATION/DOWNGRADING SCHEDULE

16. DISTRIBUTION STATEMENT (of this Report)

Distribution limited to U.S. Government agencies only; Test Evaluation data; August, 1977. Other requests for this document must be referred to the Director, Army Materials and Mechanics Research Center, ATTN: AMXMR-PL, Watertown, Massachusetts 02172.

17. DISTRIBUTION STATEMENT (of the abstract entered in Block 20, if different from Report)

18. SUPPLEMENTARY NOTES

19. KEY WORDS (Continue on reverse side if necessary and identify by block number)

Gas Turbine Engine	Silicon Nitride
Brittle Design	Silicon Carbide
Ceramics	Non-Destructive Test
High Temperature Materials	Mechanical Properties

20. ABSTRACT (Continue on reverse side if necessary and identify by block number)

(See reverse side)

141250

ABSTRACT

The demonstration of uncooled brittle materials in structural applications at 2500°F is the objective of the "Brittle Materials Design, High Temperature Gas Turbine" program. Ford Motor Company, the contractor, is utilizing a small vehicular gas turbine comprising an entire ceramic hot flow path including the highly stressed turbine rotors. Westinghouse, the subcontractor, originally planned to evaluate ceramic first stage stator vanes in an actual 30 MW test turbine engine; however, this objective was revised to demonstrate ceramic stator vanes in a static test rig. Both companies had in-house research programs in this area prior to this contract.

In the stationary gas turbine project, the test of ceramic stator vanes in a static rig for 100 cycles up to temperatures of 2500°F has been completed. This accomplishment meets the revised objectives for the stationary turbine project and, therefore, this project was completed. The report of the last six months progress will be included in the final report for the project and published separately.

Fabrication of duo-density silicon nitride turbine rotors continued during this reporting period. Due to persistent bonding problems between the hot pressed materials in the three-piece design, the fabrication concept was altered to a simplified two-piece design with the only bond being between hot-pressed Si_3N_4 and reaction bonded Si_3N_4. This change was also made possible by the results of a hot pressing parametric study, which showed that good strength and density could be achieved at reduced hot pressing pressures. Ten two-piece rotors were fabricated, and of these, three are being prepared for testing.

The injection molding of duo-density rotor blade rings has been improved by the addition of a solid state automatic control system which was installed on the injection molding machine. A problem of unmelted inclusions was discovered and solved by the use of material extrusion and increased nozzle temperature during molding. Microfocus X-ray equipment has been evaluated and found advantageous for blade ring flaw detection.

Fabrication of turbine inlet nose cones and stators was resumed on a limited basis. A silicon metal powder/organic system yielding 2.7 g/cc density reaction bonded silicon nitride material was utilized for the first time for injection molding of these components. Two additional test fixtures were built for use in pre-engine test evaluations of ceramic stators. One of these fixtures, the stator vane mechanical load test fixture, serves a two-fold purpose (t) as an NDE tool to evaluate material and processing variations, and (2) as a screening tool to qualify stator vanes for subsequent engine testing. The other rig, the stator outer shroud pressure test fixture, evaluates the stator outer shroud quality before subsequent engine testing. In the testing area, the primary emphasis was placed on the utilization of these new fixtures to enhance the qualification of stationary ceramic flow path components. The initial evaluation of the best quality 2.7 g/cc density Si_3N_4 components is underway. In addition, a review of past weight gain data for 2.55 g/cc density stators, tested at 1930°F, was completed.

In order to select the best method of processing Si_3N_4 powder, the optimum MgO content and the best hot pressing parameters consistent with the hub forming portion of the duo-density rotor process, a parametric processing study was conducted. Strength at two elevated temperatures, along with the Weibull slope, were obtained for a number of hot pressed Si_3N_4 materials. A major concern with the three-piece approach to the duo-density rotor has been the degree of bonding and the resultant strength of the bond between the two regions of hot pressed Si_3N_4. Test bars were cut from six duo-density rotors such that the hot pressed to hot pressed bond could be positioned within the zone of maximum stress. Test results showed a strength variation at different locations, being higher at the center region and lower at the leading and trailing edges. Strength measurements were performed on Refel reaction silicon carbide, the material used for ceramic combustors. Statistical bend strength distributions were measured at room temperature and at five elevated temperatures. In addition, tensile strength was measured at room temperature.

Previous results obtained from nitriding of large loads of silicon metal powder shapes, such as molded stators and rotor blade rings, have shown that the nitriding reaction was not under control. A technique was developed which allows the furnace to control the nitriding dependent upon the nitrogen gas consumption rate, resulting in improved material structure. The task on developing high strength, stable sintered Sialon materials was terminated as a result of funding reductions; the results of this work are summarized. Work was undertaken to evaluate the use of hot isostatic pressing to further densify reaction sintered Si_3N_4 performs, using glass encapsulation. Additives were evaluated and some densification and strengthening were obtained. As yet, attempts to densify complex shaped parts were not successful.

Work on analytical codes resulted in the development of relationships for computing time-dependent reliability of ceramics in the presence of delayed fracture or static fatigue. These equations are derived from the subcritical crack growth model and combined with Weibull strength statistics to determine failure probabilities.